Cyprus University of Technology

Faculty of Engineering and Technology

Doctoral Dissertation

A DESIGN TOOL FOR A PARABOLIC TROUGH COLLECTOR INDUSTRIAL PROCESS HEAT SYSTEM BASED ON DYNAMIC SIMULATION

Panayiotis K. Ktistis

Limassol, January 2022

CYPRUS UNIVERSITY OF TECHNOLOGY

FACULTY OF ENGINEERING AND TECHNOLOGY

DEPARTMENT OF MECHANICAL ENGINEERGIN AND MATERIALS SCINECE AND ENGINEERING

Doctoral Dissertation

A DESIGN TOOL FOR A PARABOLIC TROUGH COLLECTOR INDUSTRIAL PROCESS HEAT SYSTEM BASED ON DYNAMIC SIMULATION

Panayiotis K. Ktistis

Limassol, January 2022

Approval Form

Doctoral Dissertation

A DESIGN TOOL FOR A PARABOLIC TROUGH COLLECTOR INDUSTRIAL PROCESS HEAT SYSTEM BASED ON DYNAMIC SIMULATION

Presented by

Panayiotis K. Ktistis

Supervisor: Soteris Kalogirou, Professor

Signature _____

Member of the committee: Adolfo Palombo, Professor

Signature _____

Member of the committee: Tasos Georgiades, Associate Professor

Signature _____

Cyprus University of Technology

Limassol, January 2022

Copyrights

The approval of the dissertation by the Department of Mechanical Engineering and Materials Science and Engineering does not imply necessarily the approval by the Department of the views of the writer.

Acknowledgements

I would like to thank my supervisor Dr. Soteris Kalogirou for the continuous support, advices and patience during my Ph.D. It was a pleasure to work with one globally academic excellent in the field of solar energy. His advanced knowledge and experience have encouraged me in my research.

Additionally, I would like to express my sincere gratitude to my wife and my family for their encouragement and continuous support through my studies. My appreciation also goes to all my colleagues and project partners for the collaboration and knowledge exchange.

Finally, I would like to thank the Research Promotion Foundation of the Republic of Cyprus for the foundation of my Ph.D. studies.

Abstract

The most effective way to reduce the use of fossil fuels for energy production is by employing renewable energy systems. From the various types of renewable energy sources, the mostly used one is solar energy. Especially for Cyprus, the ratio of direct to diffuse solar radiation is 70:30, and thus a parabolic trough collector system (PTC) would be the perfect system for thermal energy production for high temperatures. It is very important to focus on renewable energy systems for the industrial sector specifically since the industrial sector is the second largest fuel consumer in Cyprus. Thus, PTC systems for low temperature steam production can be used in several industries to reduce fuel consumption.

In this work, initially, an investigation of PTC systems used worldwide has been carried out, discussing also how this technology has been improved through the years. Next, an extensive literature review is carried out, which is classified into two sections; in the first one, an investigation has been done of PTC prototypes, thermal energy storage and Transient System Simulation (TRNSYS) simulation models which are mainly used for industrial process heat (IPH) applications, and in the second section, an overview of the Cyprus energy status is presented in order to investigate the potential of using this technology for IPH by the Cyprus industries. Subsequently the novel PTC system installed in an industry in Cyprus is described and analyzed through experimental and numerical investigation. A dynamic simulation model is built in TRNSYS simulation tool to investigate the performance of the system which is then validated using the monitoring data from the real PTC system installed at the factory.

The novelty of this study is the development of a design tool based on a scaled-up model built in TRNSYS, which allows the potentially interested industries to identify the suitable system that fits their needs. All data are provided in the form of graphs and allow anyone to use as input data the thermal energy demand and required steam temperature of the industry to retrieve information about the size of a suitable system that satisfies these requirements depending on each case. The payback period for all cases examined varies from 2 to 6 years, depending on the size of the system.

TABLE OF CONTENTS

LIST OF TABLES

LIST OF FIGURES

LIST OF NOMENCLATURE

A	Area (m^2)
Cp	Specific heat (kJ/kg·K)
Eq	Equation
FF	Friction Factor
$F_R(\tau\alpha)_n$	The efficiency with which solar radiation is absorbed by the tube and removed by fluid flowing through the PTC (kJ/hr·m^2)
$F_R U_L$	The collector loss rate (W/m^2·K)
$F'U_L$	Modified loss coefficient (W/m^2·K)
H	Enthalpy (kJ/kg·K)
h	Hours of storage
k	Effective thermal conductivity of the concrete in the axial direction (kJ/m·h·K)
L	Length (m)
$\dot{m}$	Mass flow rate (kg/s)
m	Mass (kg)
N	Number of collectors
Nu	Nusselt number
P	Power (W)
Pr	Pressure (Bar_g)
p	Perimeter (m)
$\dot{Q}_u$	Useful energy gain rate of the collector (kJ/hr)
R	Modifier for other flow rates and more than one collector in series
Re	Reynolds number
T	Temperature (°C)
t	Time (hour)
U	Loss coefficient (kJ/h·K)
V	Volume (m^3)
w	Width (m)

Subscripts

a	ambient

av	Average
c	Concrete
cs	Cross sectional
destr.	Destruction
ene	Energy
exe	Exergy
i	Inlet
j	Time step
o	Outlet
opt	Optical
p	Plant
r	Receiver
st	Steam
sim	Simulated
th	Thermal Energy
w	water
y	Payback years

Greek Symbols

η	Efficiency
ρ	Density (kg/m^3)

LIST OF ABBREVIATIONS

CFD	Computational Fluid Dynamics
CR	Concentration ratio
CPC	Compound Parabolic Collectors
CSP	Concentrated Solar Power
CTES	Concrete Thermal Energy Storage
CUT	Cyprus University of Technology
DSG	Direct Steam Generation
DHW	Domestic Hot Water
DISS	Direct Solar Steam
DLR	German Aerospace Center
DNI	Direct Normal Irradiation (W/m^2)
EU	European Union
FVM	Finite Volume Method
HTF	Heat transfer fluid
IAM	Incidence Angle Modifier
IEA	International Energy Agency
IPH	Industrial Process Heat
LCCA	Life Cycle Cost Analysis
LFC	Linear Fresnel Collectors
LMTD	Log Mean Temperature Difference
MCRT	Monte Carlo Ray Tracing
PRE	Percentage Relative Error (%)
PSA	Plataforma Solar de Almeria
PTC	Parabolic Trough Collectors
PV	Photovoltaic
PWF	Present Worth Factor
ORC	Organic Rankine Cycle
RES	Renewable Energy Systems
SEGS	Solar Energy Generating Systems

SF	Solar Field
SG	Steam Generator
TES	Thermal Energy Storage
TMY	Typical Meteorological Year
TRNSYS	Transient System Simulation Tool

CHAPTER 1

1 Introduction

After the 20th century, many countries have focused on renewable sources for thermal and electricity production. The general objective is to minimize the environmental impact caused by the increased use of fossil fuels. Globally, the dominant renewable source is solar energy and many technologies were developed to exploit this resource such as thermal plants and photovoltaics (PVs).

Different types of solar thermal collectors are used for the exploitation of solar energy. In general, the role of a solar thermal collector is to absorb the sun's rays and convert the solar radiation energy in a highly efficient manner to thermal energy with the use of a heat transfer fluid (HTF). The HTF could be air, water, oil, or other organic solvents. The solar collectors, which are applicable, could be divided into two broad categories according to their operating temperature (Kalogirou, 2004). The first category comprises the flat plate collectors, vacuum tubes, and compound parabolic collectors (CPC), which produce thermal energy at a temperature up to 120 °C. These are commonly used for domestic water heating, space heating, solar cooling, and low-temperature process heat applications. The second category is the concentrated collectors, which include: the parabolic trough collectors (PTCs), Linear Fresnel Collectors (LFC), solar dishes and central receiver systems. The medium temperature solar concentrating

collectors can produce thermal energy from 110 to 250 °C for industrial process heat (IPH) applications. Large concentrating solar collectors are used for utility-scale power generation and can produce thermal energy from 300 to 500 °C. The applications of solar thermal energy concerning the operating temperature are shown in Figure 1.

Figure 1: Technology choice depends on application temperature.

In this study PTCs are used, which is the most matured technology from all concentrating systems. A PTC consists of an absorber tube and a parabolic trough reflector. The absorber tube, which is coated with a selective coating of high absorptance and low emittance, is placed in the focal line surrounded by a glass envelope. Vacuum is usually maintained in the space between the tube and the glass to reduce heat losses, to increase the thermal efficiency, and protect the absorber coating from the ambient conditions. It is important to note that the PTC must track the sun with high accuracy to achieve higher thermal power. As can be seen in Figure 2, the incident rays of the sun fall on the trough reflector, and the Direct Normal Irradiance (DNI) is concentrated on the absorber tube where the HTF is circulating. By doing so, the temperature of the HTF increases, thus the solar energy is converted to thermal energy. The HTF is then circulated to the steam generator (SG) or to the thermal energy storage system (TES), depending on the needs.

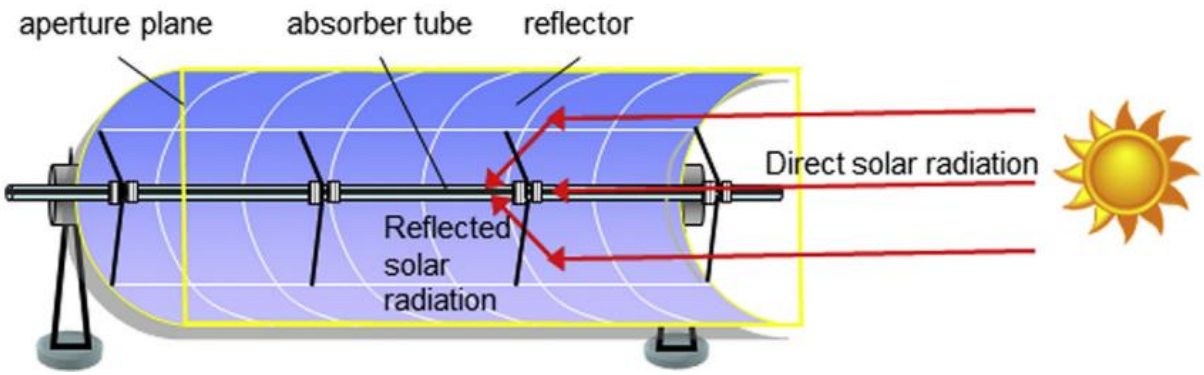

Figure 2: PTC structure (Anzazu et al., 2015).

1.1 Progress steps of Parabolic Trough Collector Systems

The first system using concentrated solar power (CSP) collectors and in particular PTCs is established in 1880 for heating air and upgraded throughout the years for different processes, according to the needs, mainly for steam generation. The most important progress steps of PTC systems that helped to improve the PTC technology are shown in Figure 3.

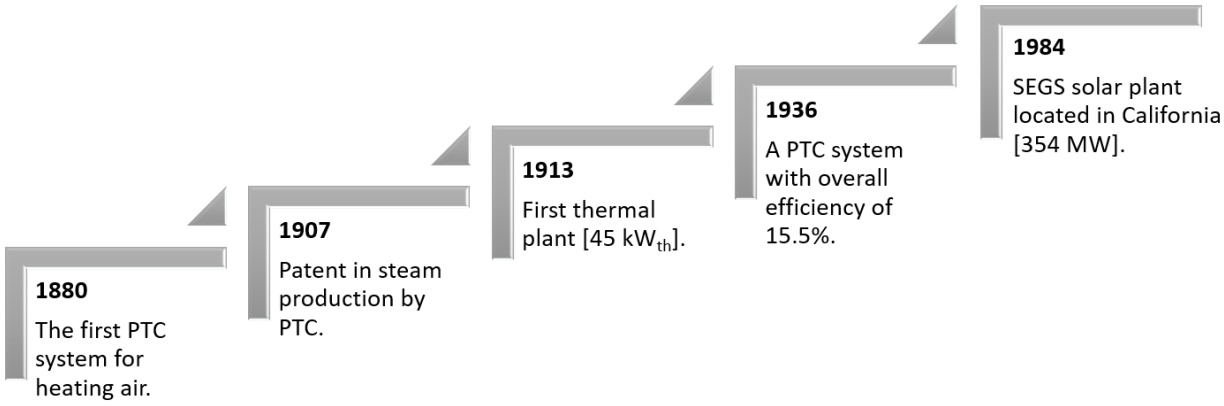

Figure 3: Important system progress steps of PTC system throughout the years.

After the 20th century, the PTCs, due to their higher efficiency, have been utilized first in the USA, Africa, and later to the southern European countries. Historically, in 1880, John Ericsson has used the first PTC system for heating air (Günther et al., 2015). After 27 years, in 1907, the German Wilhelm Meier and Adolf Remshardt acquired a patent for steam production by PTC (García et al., 2010). In 1913, in Mendi of Egypt, F. Shuman and C.V Boys had constructed the first thermal plant with a nominal power of 45 kW_{th} for steam production (Spencer, 1989). The collectors used, shown in Figure 4 were 62 m in length and 4 m in width (Ragheb, 2011).

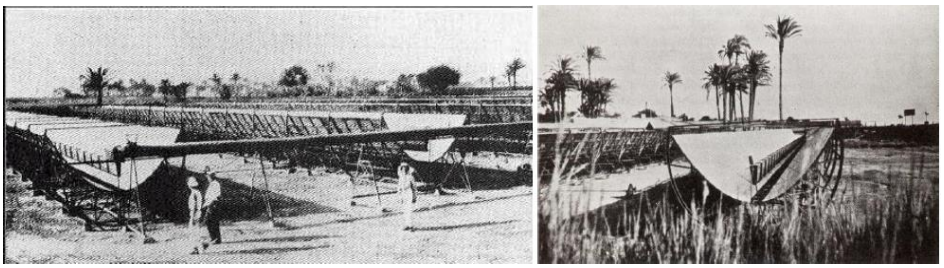

Figure 4: The first thermal Plant in Egypt (Ragheb, 2011).

A PTC system with an overall efficiency of 15.5% is developed in 1936 by C.G. Abbot. The PTC system was producing steam at 374 °C for mechanical power processes with the aim of 0.5 hp steam engine (Pytilinski, 1978).

Due to several reasons mainly because of the first and second world wars and the low cost of fuels, limited the exploitation of this technology for 60 years. However, after 1977, the continuous increase in fuel cost had forced the governments to invest in renewable solar energy systems (García et al., 2010). At that time the American and German Departments of Energy decided to release funds for the production of thermal energy and pumping of water by PTCs. Some years later, modern thermal plants were developed in the states of Arizona, California in the USA, and Almeria in Spain, mainly for electricity production. The Solar Energy Generating Systems (SEGS) solar plants located in California (in three different locations) from 1984, is now one of the biggest solar thermal PTC applications in the world with a total power of 354 MW (Figure 5).

Figure 5: SEGS Thermal plant in California (Sandia National Laboratories: Exceptional Service in the National Interest, 2020).

The knowledge and experience earned from the construction and operation of the PTCs in California were crucial for the future development of this technology. In 2007, this technology is

also adopted in Southern European countries with the leading country being South Spain (Granada) (2008), which is the first country that constructed a PTC plant of 50 MW_e power (Página Não Encontrada, 2010). Considering all the functional impacts of this technology, the governments of Spain, the USA, India, China, Egypt, Algeria, Morocco, and Australia have motivated organizations to invest and develop PTC plants. It is estimated that up to the year 2030, the electricity capacity by solar thermal power plants will be 800,000 MW_e compared to 13,402 MW_e in 2014 (Jebasingh and Herbert, 2016).

1.2 Industrial process heat applications

A big consumer of thermal power worldwide is the industry. As the PTC systems can produce thermal energy, they can satisfy the thermal needs of a wide range of industries. These systems can produce steam or hot water efficiently at a temperature of up to 300 °C. Consequently, depending on the type of industry, the thermal needs and the required temperature are different. The advantage of this system is that it can be adapted and operate efficiently according to the needs of a particular industry.

In most European countries, the most significant fuel consumer (after transportation) is the industrial sector. According to the International Energy Agency (IEA), in 2008, 30% of the global energy needs is due to the industrial sector (Guerrero-Quijano et al., 2011). Many types of industries, such as chemical, food and beverage, fabrics, textiles and laundries, have a thermal energy demand of steam or hot water at the middle to high temperatures of about 110 °C to 250 °C for different operation processes. Due to the higher operating temperatures, the flat plate collectors, which is the broadest spread technology for thermal energy production, could not satisfy these thermal energy needs. The higher temperature the flat plate collectors can achieve is maximum 100 °C. The use of PTC systems for this purpose is the most appropriate, and during the last few years is applied mostly for pilot systems in Europe.

Furthermore, the thermal needs of the industries are determined by the final process (steam or hot water and target temperature). The thermal processes of the industries are drying, evaporating, sterilizing, boiling, cooling, freezing purposes (Table 1). According to Kalogirou (2003) and Jebasingh et al. (2016) the milk and dairy, food and beverage, wood, textile, paper,

chemical, metal, plastic, brick, and automotive painting, are the industries where PTC systems could be applied effectively as the thermal output meets the thermal needs of these industries.

Table 1: Solar thermal energy for industrial uses (Farjana et al., 2017).

Sector	Process	Temperature Range (°C)	Process	Temperature Range (°C)
Chemicals	Biochemical reaction	20–60	Cooking	80–100
	Distillation	100–200	Thickening	110–130
	Compression	105–165		
Foods & beverages	Blanching	60–100	Cleaning	60–90
	Scalding	45–90	Sterilization	100–140
	Evaporating	40–130	Tempering	40–80
	Cooking	70–120	Drying	40–200
	Pasteurization	60–145	Washing	30–80
	Smoking	20–85		
Paper	Bleaching	40–150	Cooking	110–180
	De-inking	50–70	Drying	95–200
Fabricated Metal	Pickling	40–150	Phosphating	35–95
	Chromaing	20–75	Purging	40–70
	Degreasing	20–100	Drying	60–200
	Electroplating	30–95		
Rubber&Plastic	Drying	50–150	Preheating	50–70
Machinery& Equipment	Surface treatment	20–120	Cleaning	40–90
Textiles	Bleaching	40–100	Washing	50–100
	Coloring	40–130	Fixing	160–180
	Drying	60–90	Pressing	80–100
Wood	Steaming	70–90	Cooking	80–90
	Pickling	40–70	Drying	40–150
	Compression	120–170		
Dairy	Pressurization	60–80	Concentrates	60–80
	Sterilization	100–120	SG feedwater	60–90
	Drying	120–180		
Tinned food	Sterilization	110–120	Cooking	60–90
	Pasteurization	60–80	Bleaching	60–90
Meat	Washing,	60–90	Cooking	90–100
	Sterilization	60–90		
Flour & By-products	Sterilization	60–80	-	-
Timber By-products	Thermo diffusion beams	80–100	Pre-heating water	60–90
	Drying	60–100	Preparation pulp	120–170
Bricks & Blocks	Curing	60–140	-	-
Plastics	Preparation	120–140	Extension	140–160
	Distillation	140–150	Drying	180–200
	Separation	200–220	Blending	120–140
Automobile	Water heating	~90	Other processes	~50
	Cleaning	~120		
Pharmacy	Different processes	7–180	-	-
Mine	Cleaning	~60	-	-

Moreover, up to now there are three existing types of technologies that can be used to satisfy the thermal needs of the industries (Kalogirou, 2014a):

i. Unified boiler steam generation concept

The heated HTF (most common: thermal oil) circulates from the PTC array to the steam generator or steam boiler. Then, feedwater enters the SG at a high temperature, where steam is generated by heat exchange. Thus, superheated steam is produced and delivered to the factory at the required temperature and pressure as shown in Figure 6.

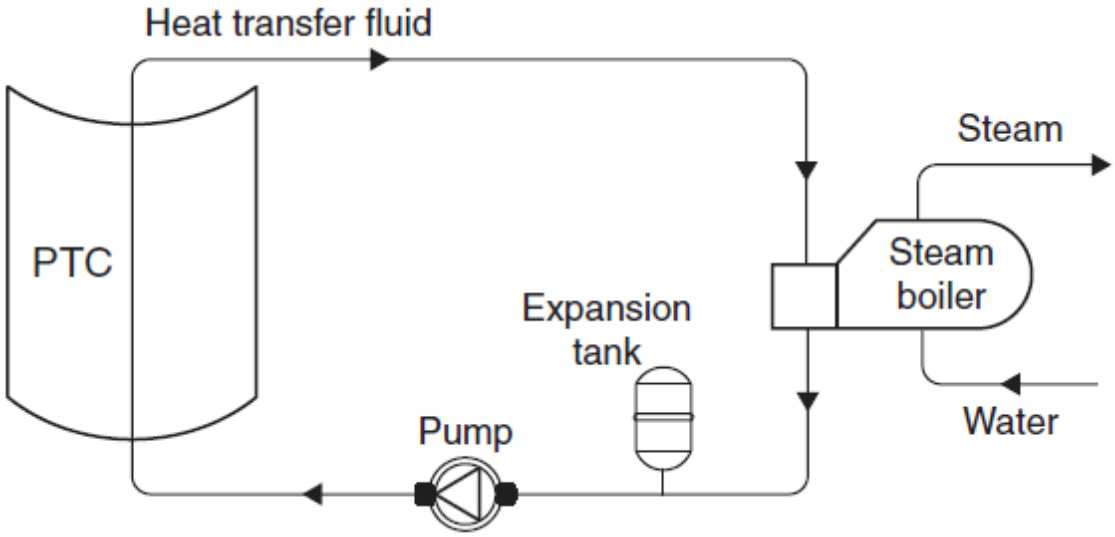

Figure 6: The unified boiler steam generation concept (Kalogirou, 2014a).

ii. Flash steam generation concept

A flash SG shown schematically in Figure 7 can be used to produce steam at the required temperature and pressure. Water is circulating through the PTC array at a high temperature to prevent steam production in the absorber tubes. The heated water enters the flash SG, and due to the differential pressure, steam is produced and delivered to the process. The remaining subcooled water circulates back to the collector field. A water tank is required in the system (not shown in Figure 7) because makeup water needs to be supplied to keep the level in the flash vessel constant.

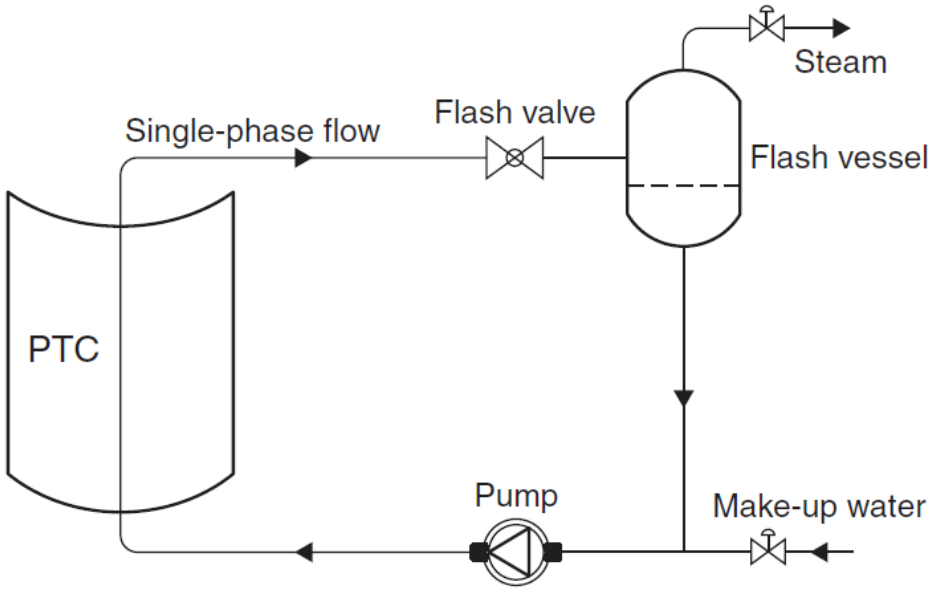

Figure 7: The steam-flash steam generation concept (Kalogirou, 2014a).

iii. Direct Steam Generation (DSG).

Finally, the newest technology of DSG shown schematically in Figure 8, could also be used for IPH applications. The steam is allowed to be produced in the absorber tube and delivered to the process. The makeup water could feed directly to the collector field inlet or the steam drum or mixed with the recirculated water. At the moment this design suffers from pressure stability problems.

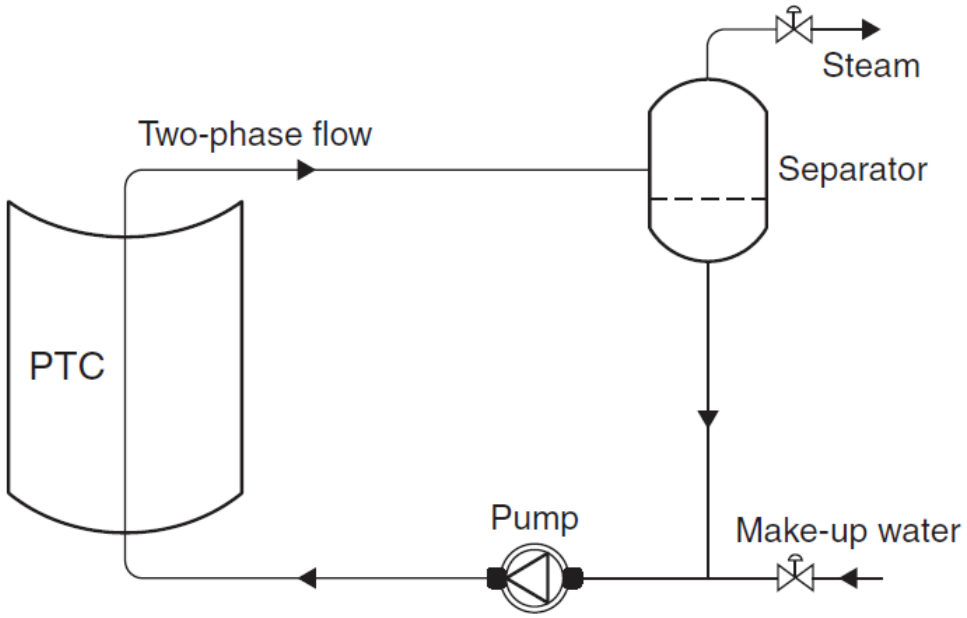

Figure 8: The DSG concept (Kalogirou, 2014a).

1.3 Discussion

Applying PTC systems in industries to contribute to their thermal energy demand, could have significant economic, environmental, and social impacts. Particularly, the factories would be independent of the fuel cost fluctuation, and it could stabilize the final product prices at a lower level. The energy safety that results from the lower dependence on the fuel suppliers is the most significant motivation for this kind of investment. In addition to the short payback times of these systems for various industries, the adoption of this technology will also help the global reduction of climate change phenomena that will lead to less environmental pollution, and thus a healthier environment. Several industries in different countries have realized these facts in their environmental impact and have set targets for their thermal production strategies.

This work aims to prove the profits that could arise from an installation of a PTC system for IPH applications, focusing on Cyprus industries. From the broad literature review on the PTC field and the status of the Cyprus energy, the roadmap of this study will be identified to achieve the ultimate target and objectives. The general objective is to investigate, evaluate and optimize a real PTC system installed in the Cyprus industry under different operation strategies and modes with experimental and simulation analyses. Additionally, the overall scope is to develop a validated simulation model which could adapt to the demands of other industries' and provide useful information. An experimental and simulation analysis of the installed system will be done to achieve that.

CHAPTER 2

2 Literature review

The literature review is classified into two sections. Firstly, an investigation has been done on the PTC technology, and secondly, an overview of the Cyprus energy situation is examined. This work aims to understand the technology of PTC and the related research fields. Additionally, an extensive survey of the Cyprus energy situation has been done in order to investigate the potential of using this technology for IPH by the industries of Cyprus.

The PTC system consists of the collectors, the TES, the SG and the auxiliary equipment (valves, pipelines). To ensure a highly efficient PTC system, these parameters have to be combined effectively. In this literature review, the PTC prototypes used for IPH after 1980 are described. Moreover, the TES technologies are identified and TES prototypes are presented, especially for concrete thermal energy storage (CTES) and several solar thermal plants that are now in operation. Subsequently, the use of PTC systems for IPH applications is reported, listing the systems installed worldwide and their performance. Besides, many researches have focused on simulation programs and their validation with real experimental data. Using this method is more effective for researchers to investigate the performance of a PTC system by changing various parameters, the system's optimization is achieved. Additionally, in the second part, an overview of the current energy situation in Cyprus has been performed identifying the industrial sectors of

Cyprus which have the potential for installing PTC systems. Finally, considering the literature review and what has been done so far, the aim of this work is established.

2.1 Parabolic Trough Collector Systems

2.1.1 Parabolic Trough Collector prototypes for Industrial Process Heat applications

Many researchers and R&D companies after 1980, tried to construct PTC prototypes for IPH applications. The main objective was to develop an economically attractive solution, simple design, which need to be durable in the long term when operating under various environmental conditions. The overall scope is to design a high efficient PTC which is reliable, sustainable and must satisfy the thermal demands of the industry.

Acurex Solar corporation has constructed two collectors, PTC 3001 and 3011. The materials used were a glaverbel thin glass with second-surface silvered reflector and a black-chrome coated steel absorber tube. The absorber is placed in a non-evacuated borosilicate glass outer tube with anti-reflective coating. The collector structure was a steel-tube backbone with steel-sheet ribs, and four photo-detectors were used to control the tracking system. This collector was installed at the Plataforma Solar de Almeria (PSA) in Spain. Other collectors were also constructed by other companies such as Solar Kinetics T-700 and T-800, the IV collector from Suntec System Inc, and the IND-300 PTC by Solel Solar Systems in Israel. It is important to indicate that the reflector of T-700 and T-800 was made from an aluminized acrylic film that has much lower cost achieving 94% reflectance. The IV collector maintains a vacuum inside the glass envelope to minimize the heat losses.

Additionally, a two-axis-tracking collector was tested, achieving higher efficiency; however, the high construction, maintenance, and operating costs are a serious disadvantage of this idea and this may be the reason that is not adopted by the industry. There are three well-known commercial collectors used to produce heat for industries. The American company Industrial Solar Technologies, from 1985 produced the PT1 for ground and RMT for roof mounting. The PTC-1800 from Solitem company and the Poly trough 2300 of NEP Solar are also in the market for a number of years (García et al., 2010).

Research and Development efforts are focused on investigations to improve the collector structure and avoid the degradation of its materials and trough shape through the years. These investigations, over the years, lead to better PTC performance, and achieved increased reliability and sustainability of the overall collector system. Moreover, many ways of improving the optical efficiency and minimize thermal losses are suggested to keep the effectiveness of the collectors at a high level. Several modifications are proposed mainly on the absorber and the reflective materials. Most of the research carried out focused on achieving a high performance collector at the lowest possible cost.

At the early stages of this technology, Thomas and Guven (1993) have tried to calculate the thermal losses of a PTC. They have reached three solutions to reduce the losses:

1. Maintain vacuum in the absorber to glass gap:
    - The collector efficiency increased by 11-12%; however, the vacuum in the long-term period is lost.
2. Fill the gap with a low thermal conductivity gas:
    - The collector efficiency increased by 4-5% and reduce thermal losses by 50%.
3. Increase the gap between the absorber and the glass:
    - Reduce the convection losses.

Kalogirou (1994) designed and constructed a novel and innovative PTC with a low cost, high accuracy, stiffness, and easy to build. The overall target was to create from the economic side an attractive mass-produced PTC collector. Fiberglass material has used with plastic pipes achieving resistance in humidity and stiffness and high optical efficiency as the structure was very accurate. In a test under wind speed of 90 mph, the structure remained stable. The cost was estimated to be 30 US$/m^2. The innovative use of fiberglass in the construction of the trough was a base for other researches in the field.

As the PTCs are concentrating the sun rays on the focal line, a deformation of the shape of the structure could have negative impacts on the thermal and optical efficiencies. The accuracy with which the collectors are tracking the sun also has a significant role on the overall efficiency of the system. A perfect tracking system ensures that the maximum energy collected from the sun is achieved. As part of European Union (EU) funded project, Eurotrough collector was constructed

which achieved the lowest structure deformation, compared with other prototypes. With this collector, a significant reduction of the thermal losses, an increase of the optical efficiency, and resistance to the air deformation were achieved (Coccia et al., 2014). Arasu et al. (2007), relying on Kalogirou (1994) suggestion used fiberglass for their parabolic structure with a reduced production cost of 48 US$/m^2. The collector was tested at a wind speed of 34 m/s, and the deformation was found to be insignificant.

In 2014 a UNIVPM.01 designed a PTC prototype based on fiberglass material, and although the concentration ratio (CR) was low 9.25 the thermal efficiency was close to other PTCs (Figure 9). The absorber was constructed from aluminum with low-iron glass envelope that increased the transmittance. The PTC has a low cost, low weight, and high mechanical resistance (Coccia et al., 2015).

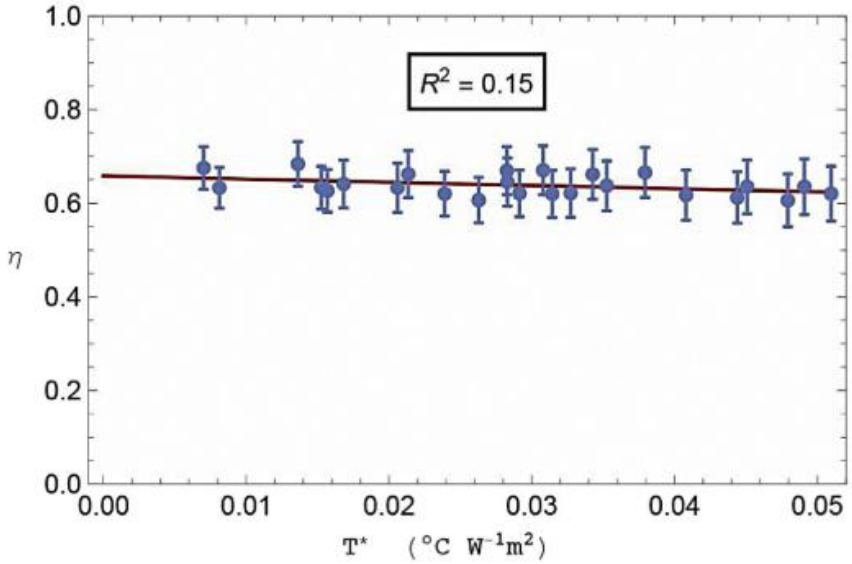

Figure 9: Thermal efficiency of UNIVPM.01 collector – experimental data (Coccia et al., 2015).

Fernández-García et al. (2015) investigated three types of PTCs for IPH applications. Three different cases were tested with the same geometry shown in Figure 10:

Case 1: Collector with glass cover on the absorber and without glass cover of the collector (Figure 10a).

Case 2: Collector without glass cover on the absorber but with glass cover of the collector. Two variations were tested:

a. No thermal insulation on the reflector back (Figure 10b)
b. Thermal insulation on the reflector back (Figure 10c)

Case 3: Collector with glass cover on the absorber and the collector. Two variations were tested:

a. No thermal insulation on the reflector back (Figure 10d)
b. Thermal insulation on the reflector back (Figure 10e).

They concluded that the cases 2.a and 2.b are not useful as they had significant thermal losses from the receiver and low thermal efficiency. A low-cost solution with high thermal efficiency was case 1. Comparing cases 1, 3.a and 3.b; it is observed that there are no significant changes to their thermal energy efficiency and losses. The cover on the reflector has several advantages (if the cost is not substantial), such as more extended durability, lower demand for maintenance and protection from environmental conditions. It also concluded that the case 2.b is useless compared to the cost.

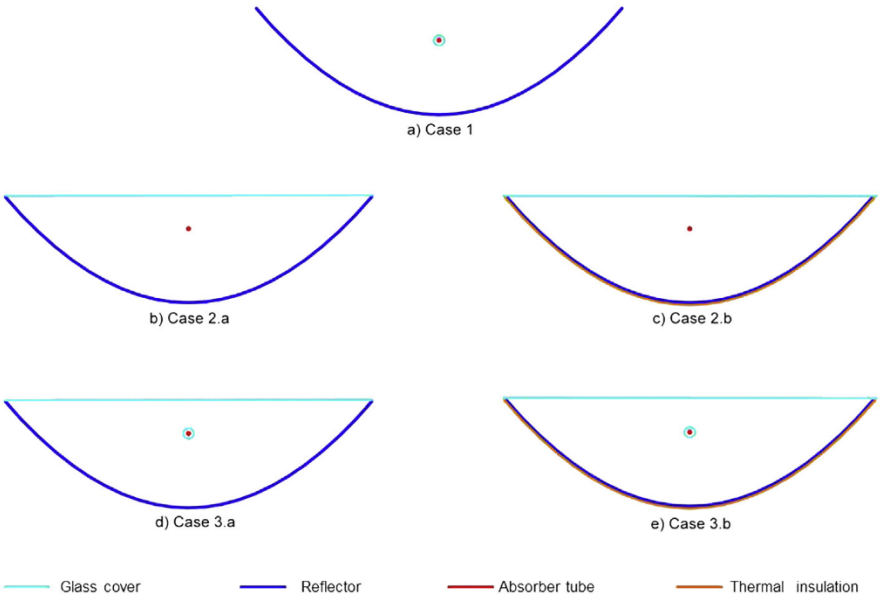

Figure 10: Geometric configurations studied (a) Case 1, (b) Case 2.a, (c) Case 2.b, (d) Case 3.a (e) Case 3.b (Anzazu et al., 2015).

Qu et al., (2017) investigated the case of rotating two rows of three LS-3 PTC prototypes with nominal thermal power of 300 kW_{th}. They can rotate 14° from north to east or north to west depending on the season variation with the advantage of cosine loss reduction. The authors concluded, when the incidence angle is larger (autumn and winter period), the PTC array will

operate in the optimum north-south axis angle. On the contrary, during the summer and spring periods, the incidence angle is smaller and can operate in a north-south axis tracking. The authors observed a 30.6% decrease in cosine losses (Figure 11a) and a 14.6% increase of PTC efficiency (Figure 11b) compared to north-south axis tracking in autumn and winter.

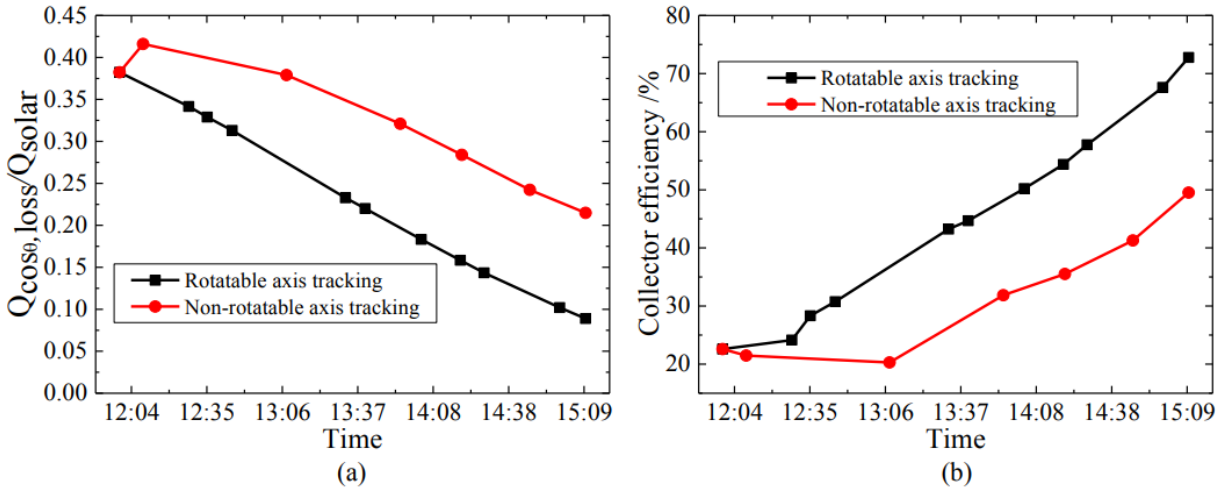

Figure 11: (a) Compare the experimental results of the amount ratio of the cosine loss ($Q_{cos0,\ loss}$) to solar energy (Q_{solar}) for rotatable and non – rotatable axis tracking (b) Compare the experimental results of the PTC efficiency for rotatable and non – rotable axis tracking Qu et al. (2017).

The most challenging field of the PTC is the enhancement of the overall efficiency which is related to the optical and thermal efficiency of the systems. Many researches have focused on optical efficiency enhancement by proposing various selective coatings on the receiver tubes. The overall scope was to maximize the absorber properties and reduce the emissive properties. A significant parameter for a high-quality selective coating is to achieve these targets and propose a stable selective coating at the operating temperatures and at outdoor conditions for a long period. Additionally, they need to maximize the transmissivity of the glass envelope around the receiver.

The optical errors which lead to thermal errors also occur due to the rays which are not focused on the absorber tube. This phenomenon is happening due to the geometrical characteristics of the PTC (mirror reflectivity, rim angle, surface errors), the tracking accuracy of the mechanism, and structural stability (on wind and self-load). Several designs have been tested with a second reflector incorporated; however, the overall thermal efficiency was not increased more than 1.6% (Manikandan et al., 2019). Additionally, the end loss effect also affects the overall performance.

Researches have suggested different solutions to reduce the end loss and cosine effect. Some researches suggest extending the absorber tube (Li et al., 2015), changing the orientation from east-west to north-south direction (Xu et al., 2014), increasing the trough length, and dual-axis tracking mode (Bakos, 2006).

Furthermore, the design and operation parameters have a significant role in the overall system performance. Based on Ghazouani et al. (2020a), the aperture area has a significant role in overall performance. As the collector width is increasing and the collector length is decreasing, the cost of energy produced by a PTC system and the thermal and exergy efficiency are improved. Moreover, by decreasing the PTC inlet temperature and increasing the mass flow rate, the cost of thermal energy and thermal efficiency is improved.

However, one of the most challenging fields of the PTC is the heat flux distribution that occurred on the absorber tube. The rays are mostly concentrated at the bottom of the absorber. At the top, the absorber receives just the rays coming from the sun. As a result, the heat flux is not uniform. Halimi et al. (2018) experimentally examined under Morocco climate conditions the effects of solar flux distribution for a U-pipe exchanger in positions according to the aperture (Figure 12a) perpedicular, inclined (Figure 12b) and parallel (Figure 12c) position. It was concluded that for a focal distance of 0.19 m the optimum position is the parallel.

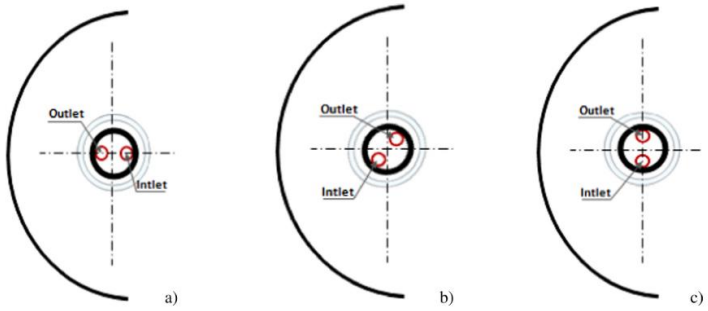

Figure 12: U-pipe absorber tube positions according to the aperture of the collector: (a) Perpendicular, (b) Inclined, (c) Parallel (Halimi et al., 2018).

Additionally, the effects of solar flux distribution for different focal lengths, rim angles, and diameters for a u-pipe exchanger is also examined. The heat flux distribution is measured at different circumferential points on a PTC prototype using an unfixed solarimeter for 10^{o} step from 0° to 360°. The results are shown in Figure 13 and the more uniform heat fluxes occurred at a focal point of 0.19 m and an absorber tube diameter of 0.042 m.

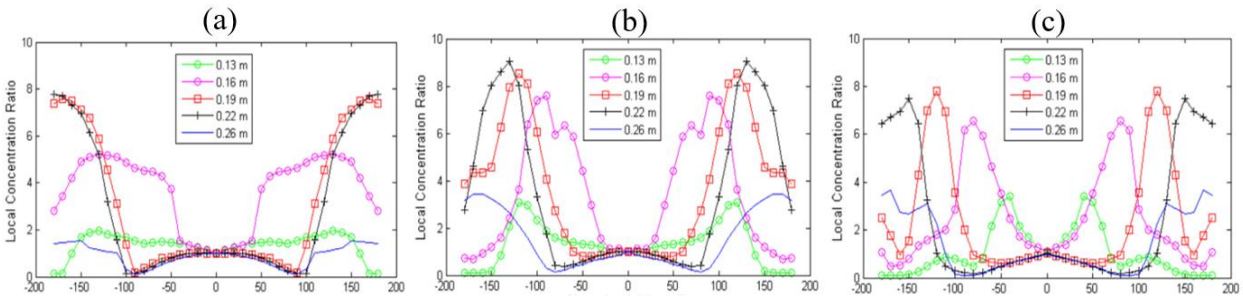

Figure 13: Solar distribution on the outer surface of the absorber, for various focus point distances: (a) D=0.222 m, (b) D=0.042 m and (c) D=0.062 m (Halimi et al., 2018).

The non-uniform heat flux distribution on the absorber also has a significant role in the thermal performance of the system. Many researchers investigated ways to improve the heat transfer characteristics inside the absorber, by inserting vortex generators, fins, and metal foams. Some of them are shown in Figure 14. A general conclusion is that a more uniform heat flux distribution on the absorber tube significantly influences the temperature distribution and the transfer coefficient inside the absorber tube (He et al., 2019). However, all these techniques are increasing the pressure drop of the system and leads to a higher cost.

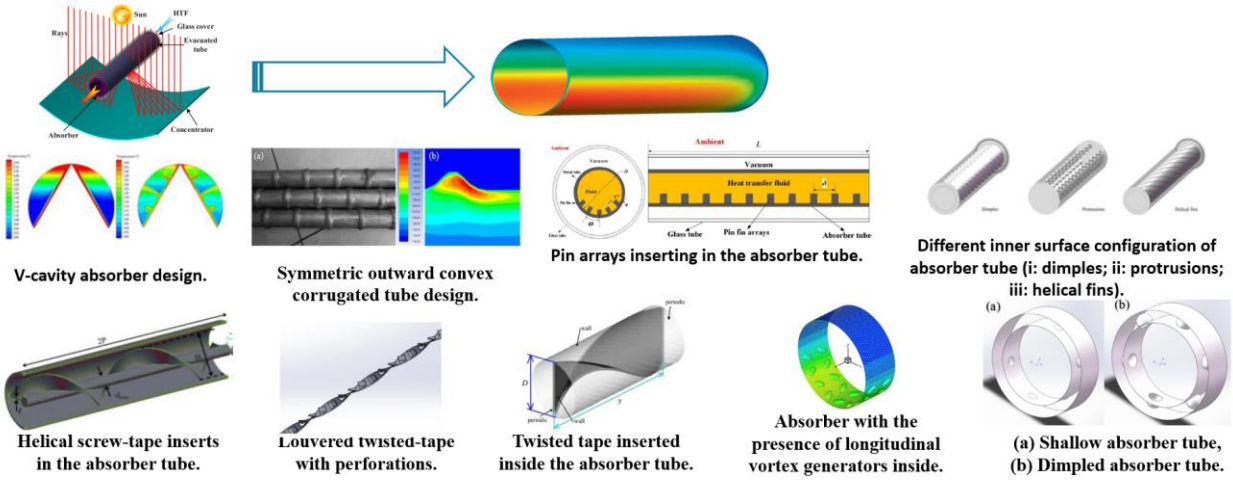

Figure 14: Ways to improve the heat transfer characteristics inside the absorber tube.

Cheng et al. (2012) tried to improve the heat transfer characteristics with the presence of longitudinal vortex generators inside the absorber tube. An absorber tube model is developed using Computational Fluid Dynamics analysis (CFD) and Monte Carlo Ray Tracing (MCRT) method to predict the non uniform heat flux distribution and to be applied on the absorber outer wall as a heat source (boundary condition). The numerical computational results were compared

with the case of a smooth absorber. The authors concluded that by changing the Reynolds number (Re), the average wall temperature and thermal loss decreased by 1.35% - 12.10%. The average wall temperature and thermal losses increased as the HTF temperature increased but was at a lower level compared to the smooth absorber by 2.23 -13.62%. In conclusion, because the longitudinal vortex generators were inserted, as the Direct Normal Irradiation (DNI) increased, the thermal performance was more stable, and the thermal losses were reduced (0.11% - 13.39%).

The addition of metal foams in the absorber tube was carried out by Wang et al. (2013). They developed a numerical model and concluded that by the use of metal foam, the optimum thermo-hydraulic performance increased. The temperature distribution on the wall of the absorber tube had high uniformity (45% lower temperature difference than that of a smooth absorber), so the thermal stresses reduced drastically. Consequently, the new absorber tube with inserted metal foams is applied more effectively in a Direct Steam Generation (DSG) process where the steam has low viscosity, and so the pressure drop is smaller. Furthermore, the length of the superheated section could decrease to improve the heat transfer characteristics and achieve higher overall performance.

Moreover, a symmetric outward convex corrugated tube is proposed by Fuqiang et al. (2016). The symmetric outward convex corrugated in the longitude direction is used, which improves the heat transfer characteristics. With an MCRT method, the outer heat flux is determined and used as a boundary condition in a CFD analysis. A numerical model is developed to analyze the optical and thermal behavior of the absorber tube and the results are compared with a smooth absorber tube. It revealed that the temperature distribution is much uniform, so the thermal deformation is minimized up to 13.1%. A turbulence flow is generated due to the outer convex shape of the pipe, so the heat transfer characteristics improved, with an effective heat transfer coefficient of more than 8.4%. Thus, the effectiveness of the absorber tube (and the glass envelope) is highly improved.

Xiangtao et al. (2017) managed to set better heat transfer characteristics in an absorber tube by using five-pin fin arrays inserted in the inner bottom surface. An MCRT method is used to identify the heat flux distribution on the outer surface of the absorber tube, and this is coupled

with the Finite Volume Method (FVM). The overall scope of the pin arrays inserted was to reduce the temperature gradient of the absorber tube. The results show that the Nusselt number (Nu) increased by up to 9%, with an overall heat transfer performance increase up to 12%. Although the heat transfer characteristics have significantly improved, the pressure drop was also increased significantly, which must be considered in this kind of analysis.

Chen et al. (2015) also examined the thermal performance of a new absorber tube with fins inserted. As was expected, the wall temperature for the same HTF temperature is decreased. The wall temperature has a significant influence on the reduction of heat losses because of the better heat transfer performance (the viscosity of the fluid was rising, and so the Re). They concluded that cavity absorber tubes have a good potential and can replace the evacuated tubes for middle-temperature range applications.

Xiao et al. (2014) tried to modify the inner shape of the absorber tube to improve the optical efficiency. They proposed a novel V cavity absorber tube that maximizes the optical efficiency due to the repeated reflections inside the cavity of the absorber. The fins inserted improved the heat transfer characteristics because of the better heat exchange between the absorber and the HTF. The non-uniform heat flux distribution is predicted by an MCRT method, and it is coupled with ANSYS FLUENT. It revealed that the wall average temperature decreased to 14.7 °C, and it obtained a higher HTF outlet temperature of 1.1 °C. Finally, the authors concluded that, if the mass flow rate is increased, the outlet temperature of HTF is decreased, and as the DNI is increased, the outlet temperature of HTF is also increased.

Zhai et al., 2009 examined the optical and thermal efficiency of four different designs of absorber designs. The circular, semicircular, square, and triangular tube configurations were tested at a temperature range of 90 to 150 °C. The best optical performance (99%) occurred in the triangular receiver due to the fact that the incident rays can be reflected in the cavity several times. Regarding the thermal losses, when the inlet temperature was 90 - 150 °C, they were 20 – 41 W, respectively.

Additionally, Song et al. (2014a) managed to eliminate the temperature gradient of the absorber by inserting a helical screw-tape and thus improving the thermal efficiency. A heat transfer model is developed to estimate the heat losses, the circumferential temperature difference, and

the maximum temperature. The MCRT method is applied to predict the non-uniform heat flux distribution which is later used as a boundary condition. By comparing a smooth and the new absorber tube, the maximum temperature occurred at the bottom of the absorber tube. Additionally, the HTF temperature is more uniform in the case of the new absorber tube. The authors also concluded that the heat losses were six times lower than the smooth absorber. Finally, the case of inserting helical screw-tape increases 23 times the pressure drop compared with a smooth absorber.

Muñoz et al. (2011) investigated with CFD analysis in ANSYS FLUENT the design of four fins configurations in the same outer absorber diameter. These improvements could increase the overall plant efficiency by 2%. Although the absorber was durable, the manufacturing cost is raised by 5%, with a total plant cost increased by 0.5%.

Furthermore, Huang et al. (2015) numerically investigated the effect of the heat transfer characteristics and flow resistance for three different inner surface configuration of absorber tube (i: dimples; ii: protrusions; iii: helical fins) at a Re number ranging from $1x10^4$ to $2x10^4$ (fully turbulent flow). All the tubes had an outer diameter equal to 70 mm and an inner diameter equal to 54 mm constructed with stainless steel. Comparatively, the friction factor (FF) and Nu number were higher for the dimple absorber. The performance is calculated for each case in two different Re numbers, and it revealed that for low Re numbers, the dimpled tube has better performance. Although the Re number increased, the better performance occurred for the dimpled absorber. Finally, the authors concluded that the case (i) with deeper depth and narrower pitch obtained better heat transfer characteristics.

Furthermore, the generation of turbulent flow inside the absorber tube improves the convection heat transfer coefficient. Ghadirijafarbeigloo et al. (2014) investigated three different twist ratios of perforated louvered twisted - tape (LTT), at an inlet temperature of 353 K. The non-uniform flux distribution is calculated by using SOLTRACE software, and the heat transfer rate and pressure drop are estimated for different Re numbers according to the diameter and mass flow rate. By comparing the LTT with a typical twisted tape, although the pressure drop increased, the Nu and FF were 150% and 210% higher, respectively. Consequently, the authors proposed the optimum twist ratio to be 2.67 and the Re=5000.

Mwesigye et al. (2014) considered the circumferential temperature gradient caused by non-uniform heat flux. This heat flux distribution is calculated with the SOLTRACE software for a rim angle of 80^o and 120^o with an aperture of 6 m and a CR of 86. High-temperature abnormalities cause several issues, such as the bending of the receiver and breakage of the glass. A failure of the glass cover affects the maintenance of vacuum in the annulus which creates high thermal losses. The authors proposed the case of inserting perforated plates in the absorber tube. Different configurations (angle, spacing, orientation) and geometry of the plates are examined. Besides, different Re numbers were tested to define the optimum values of the heat transfer characteristics. The configuration of the plate (spacing and size) influences the FF, Nu, and Re number and the thermal efficiency is raised from 1.2% to 8%. Equally important is the fact that the temperature distribution is reduced by 67%, which is valuable for low mass flow rates. From the thermodynamic point of view analysis, the entropy generation rate decreased to the maximum value of 52.7%.

The case of porous plates inside the absorber tube investigated by Kumar et al. (2008). A three-dimensional numerical model is developed by using FVM in ANSYS FLUENT software. The overall scope was to increase the heat transfer area, thermal conductivity and heat transfer rate. Various geometries of angle, orientation, and size, the configuration of porous on the plate (top, bottom), and space are examined for different heat flux cases. The authors concluded that the shape of a porous top plate increases the value of Nu number by 64.2%, and although the heat transfer coefficient improved, the pressure drop has also increased.

Eiamsa-Ard et al. (2009) examined the case of a twisted - tape inserted inside the absorber tube. The FF, Nu number, and thermal performance are examined by numerical simulation. They observed that for a twist ratio of 2.5 (length/width) and clearance ratio between the edge of tape and tube wall to tube diameter of zero, the heat transfer rate was 73.6% higher than a plain absorber tube.

Furthermore, Kumar et al. (2012) found that in laminar flow, the twisted tape and modified twisted tape inserts have better heat transfer characteristics with respect to turbulent flow when the pressure drop is significant. Moreover, by comparing the twisted tape with revised geometry with a dull and modified twisted tape, the heat transfer performance is improved due to the

turbulent flow generated inside the tube. For laminar and turbulent flow, the revised twisted tape geometry obtained best heat transfer performance.

Vicente et al. (2001) experimentally investigated the case of inserting helically dimpled tubes inside the absorber tubes. The different geometric configurations of the absorber tube are tested to define the advantages of using dimpled tubes. Firstly, the case of inserting dimpled tubes improves the FF from 150 – 350% and the Nu number up to 250%. Moreover, if the Re number is in the range of 2,000 to 40,000, the dimpled tubes significantly affect the heat transfer performance by 20 - 110% compared to a smooth absorber.

Using a three-dimensional numerical model, the heat transfer characteristics of a new dimpled absorber tube is investigated by Huang et al. (2017). The two cases of shallow and dimpled absorber were tested under non-uniform heat flux distribution on the outer surface. In the first case, the average FF and Nu number were raised from 1% to 34% and from 1% to 21% and in the second case from 1% to 28% and 1% to 18%, respectively.

Concluding, although all these solutions present an increase of the collector performance no one is adopted by the relevant industry yet, mainly due to manufacturing difficulties and associated cost and the marginal increase of the actual performance.

2.1.2 Thermal Energy Storage (TES) Systems

A TES system is essential for any solar thermal system as it can collect energy and use it at a later time (3 to 15 hours). The main scope of a TES is to cover the thermal requirements of the industry during hours of cloudy weather or insufficient solar radiation. It can also be used in the early morning hours for preheating purposes when the sun is not shining. For a steam production to begin at 7 am, most of the industries are starting 2 to 3 hours before, when there is no solar radiation, to preheat their equipment, SGs, and pipelines. So, a highly efficient TES can supply heat during these hours and cover their needs. A TES can also be used as a buffer to maintain a more stable system condition (temperature, pressure). It also minimizes the abnormalities of the system behavior in case of significant fluctuation of solar radiation. By implementing a TES in a solar system, the solar fraction is increased, leading to significant advantages due to lower fuel consumption, environmental impact, and less payback time. According to González-Roubaud et

al. (2017), as can be seen in Figure 15, 83% of the solar thermal system installed or are under construction are using thermal energy storage (excluding the PTC system in Oman). Several TES systems that were installed in solar thermal plants, mostly for electricity applications, also incorporate a TES as presented in Table 2.

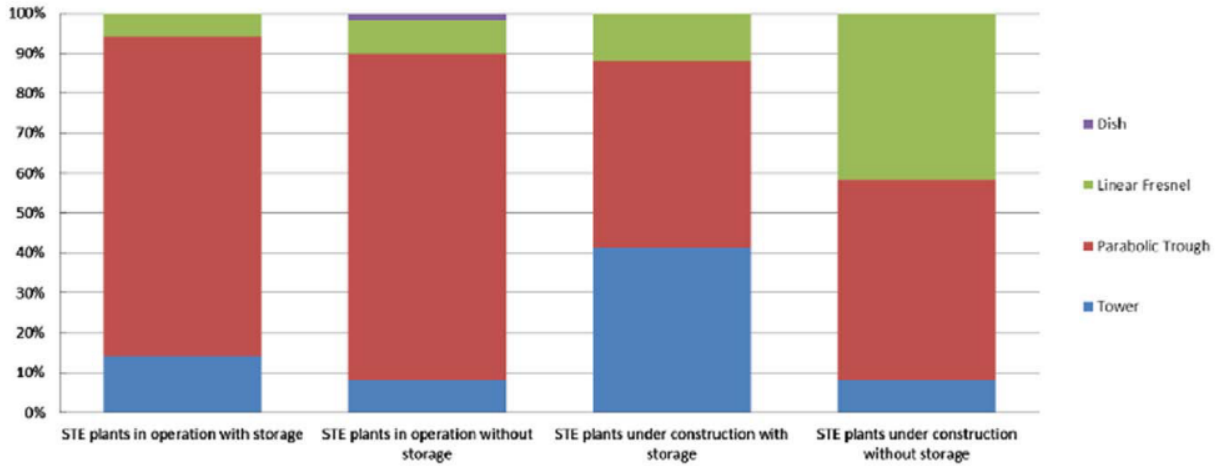

Figure 15: Solar thermal system worldwide capacity categorized by technology with and without storage (González-Roubaud et al. 2017).

Table 2: TES systems (Solar International GmbH, 1999).

Project	Collector Type	Storage medium	Cooling Loop	Nominal Temperature Cold (°C)	Nominal Temperature Hot (°C)	Storage Concept	Tank Volume (m^3)	Thermal Capacity (MWh_{th})
Irrigation pump Coolidge, AZ, USA	PTC	Oil	Oil	200	228	One tank thermocline	114	3
IEA-SSPS Almeria, Spain	PTC	Oil	Oil	225	295	One tank thermocline	200	5
SEGS I Daggett, CA, USA	PTC	Oil	Oil	240	307	Cold-Tank Hot-Tank	4160 4540	120
IEA-SSPS Almeria, Spain	PTC	Oil	Oil	225	295	1 Dual Medium Tank	100	4

A sufficient TES, according to Solar International GmbH (1999), must satisfy several design criteria. The cost of storing and providing the energy is related to the storage material, insulation,

and the heat exchanger used. The storage material must satisfy essential requirements in order to achieve an extended period of delivering power, such as (Solar International GmbH, 1999):

- the energy density per unit mass or volume must be at a high level
- thermal conductivity between itself and the HTF must be high
- must have mechanical and chemical stability
- the HTF and heat exchanger must be compatible
- it must be able to achieve complete reversibility for charging and discharging cycles
- must have low thermal losses
- must be easy to control the system

Wyman et al. (1980) explained the most important methods and media used for thermal storage. The thermal energy can be stored as a change in the internal energy of the material. For TES using chemical storage, the chemical energy can be stored as the bond energy of a chemical compound. A survey of the types of thermal and chemical TES is presented graphically in Figure 16.

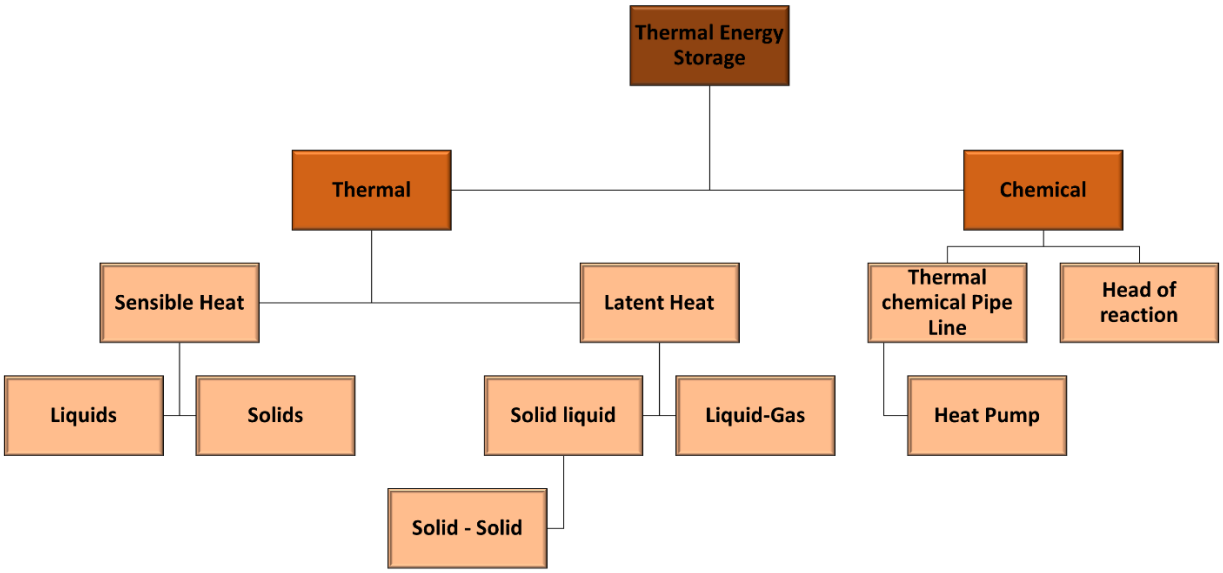

Figure 16: Types of TES.

The typical types of TES systems are shown in Table 3. The most common TES is the sensible heat storage using hot water, and according to Sarbu et al. (2018) the most efficient storage can be achieved with chemical reactions.

Table 3: Typical parameters of TES systems (Sarbu et al., 2018).

TES System	Capacity (kWh/t)	Power (MW)	Efficiency (%)	Storage Period	Cost (€/kWh)
Sensible (hot water)	10-50	0.001-10.0	50-90	Days/months	0.1-10
Phase-change material (PCM)	50-150	0.001-1.0	75-90	Hours/months	10-50
Chemical reactions	120-250	0.01-1.0	75-100	Hours/days	8-100

In sensible heat, the temperature of a solid or liquid is increased to store thermal energy. Some of the liquids used are water, organic oils, molten salts, and liquid metals. Table 4 presents the characteristics of solid and liquid materials such as the low and high-temperature limit, average mass density, heat capacity, and the volume-specific heat capacity per cubic meter.

Table 4: Solid and liquids materials for sensible heat (Zhang et al., 2016).

Storage	Temperature		Average density (kg/m^3)	Average heat conductivity (W/mK)	Average heat capacity (kJ/kg K)	Volume specific heat capacity (kWh_{th}/m^3)
	Cold (°C)	Hot (°C)				
Solid media						
Sand-rock mineral oil	200	300	1700	1.0	1.30	60
Reinforced concrete	200	400	2200	1.5	0.85	100
NaCl (solid)	200	500	2160	7.0	0.85	150
Cast Iron	200	400	7200	37.0	0.56	160
Cast steel	200	700	7800	40.0	0.60	450
Silica fire bricks	200	700	1820	1.5	1.00	150
Magnesia fire bricks	200	1200	3000	5.0	1.15	600
Liquid media						
Mineral oil	200	300	770	0.12	2.6	55
Synthetic oil	250	350	900	0.11	2.3	57
Silicone oil	300	400	900	0.10	2.1	52
Nitrite salts	250	450	1825	0.57	1.5	152
Nitrate salts	265	565	1870	0.52	1.6	250
Carbonate salts	450	850	2100	2.0	1.8	430
Liquid sodium	270	530	850	71.0	1.3	80
Phase change media						
$NaNO_3$	308	2257	0.5	200	125	0.20
KNO_3	333	2110	0.5	267	156	0.30
Salt-ceramics ($NaCo_3$-$BaCO_3$/MgO)	500-850	2600	5.0	420	300	2.00
NaCl	802	2160	5.0	520	280	0.15
Na_2CO_3	854	2533	2.0	276	194	0.20
K_2CO_3	897	2290	2.0	236	150	0.60

In latent heat/phase change, the material's internal energy is changed. This phase change can be achieved both on solid-liquid or solid-solid transformation materials. The heat capacity of various storage materials is shown in Table 5.

Table 5: Latent heat storage (Geyer, 1991).

Storage	Heat capacity kW_{th}/m^3
$NaNO_3$	125
KNO_3	156
KOH	85

Regarding the heat of chemical reaction, the thermal energy is stored as the bond energy of a chemical compound. The energy is repeatedly stored and released in the same materials by reversible chemical reactions.

Powell et al. (2012) have produced a simulation model for solar system employing a two-tank-direct storage method. In the cold tank, the storage materials are circulated and heated through the solar field (SF) and stored at a higher temperature in the hot tank. The heated HTF from the TES is fed to the SG for the production of saturated steam and return to the cold tank. The scope of this work was to investigate the behavior of the TES when it interacts with the other parts of the system, the increase of the solar share, and the fuel reduction due to the use of TES. Comparing the solar power delivered from a system with no storage (Figure 17a) and from a system with 8 of hours TES (Figure 17b) it is observed that with TES, more production hours are covered. The solar share on a clear day without TES was 47.6% compared to the case of storage, which was 70.1%. On a cloudy day, both systems have the same solar share of ≈34%. However, the TES maintained a constant power output, which was essential in the industrial process.

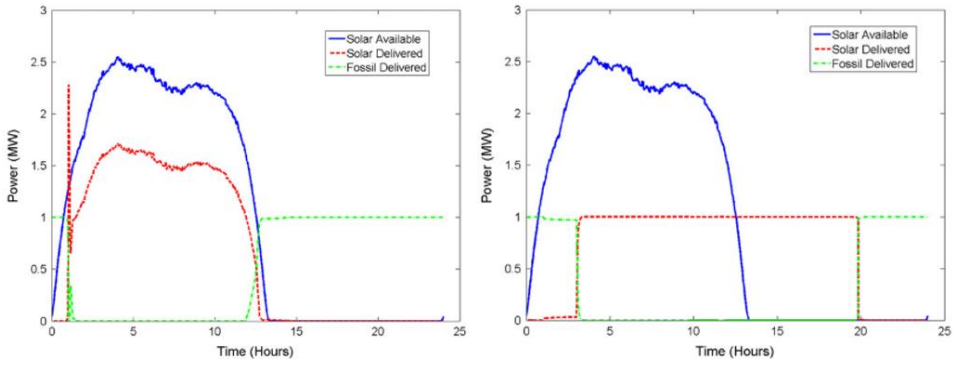

Figure 17: Solar share for (a) case of a clear day without TES (b) case of a clear day with TES (Powell et al., 2012).

Kumaresan et al. (2012) showed an experimental setup of the PTC system, including TES, pump, and a tracking unit. The PTC array has a total aperture area of 7.5 m^2. The TES system used consists of a vertical cylindrical storage tank (550 mm in diameter and 1100 mm in length) with a volume of 230 L. The TES is made from a vertical plate with a 5 mm thickness and insulated with glass wool (0.15 mm). The HTF used is Therminol 55, which is stored in the well-insulated tank and circulated through the system. The authors examined the instantaneous efficiency, which varied from 50 - 62.5%, with the peak efficiency occurring at noon. As the TES is charged at 120 °C and left undistributed for 45 h, they concluded that the average heat loss per hour is 1120 kJ. The ratio of the energy collected to the energy stored from 8 am to 2 pm varied from 60% to 41%. The maximum overall system efficiency was close to 40%.

Boukelia et al. (2015) investigated eight PTC system configurations with and without molten salt TES. The authors concluded that the highest overall energy efficiency occurred with the arrangement of using TES, although from an environmental point of view, the case of adding TES and auxiliary system is not favorable, this however is more economical.

Furthermore, the most severe challenge regarding TES is the high investment cost. Many researches are focused their work on how to achieve a better TES performance at a lower price. In PSA in Spain, the German Aerospace Center (DLR) tested the first TES using concrete, which is a cheaper storage technology. Concerning storage capacity, thermal conductivity and sufficient permeability of the vapor (so it will not be damaged), they demonstrated and tested a concrete storage module. It consists of 132 tubes (9 m length 18 mm diameter), special concrete and pressure-resistant thermal insulation. The tests were performed for four months for a temperature range between 300 °C to 400 °C. For six hours of charging and discharging the module estimated to have a total capacity of 25.6 kWh/m^3 (Laing et al., 2008).

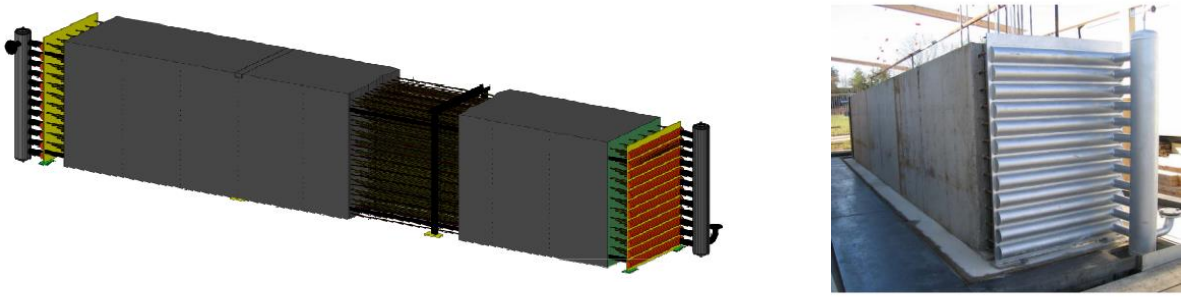

Figure 18: Concrete storage modules (Laing et al., 2008).

John et al. (2013) investigated the curing, thermal conductivity, specific heat, and thermal cycling procedure of different concrete mixtures. The results of this investigation are shown in Table 6 and Table 7 for 26 concrete mixtures. These concrete mixtures were charged and discharged in a thermocline with molten salt as the HTF. The concrete storage has a high heat capacity and low cost proving the potential of involving it as the thermal energy storage. A concrete mixture must have high porosity, and it comprises:

- Cementitious materials (Portland cement, calcium aluminate cement, calcium silicate hydrate)
- Coarse aggregates
- Fine aggregates
- Water
- Chemical admixtures
- Other cementitious materials (fly ash, slag cement silica fume)

Table 6: Concrete mixtures 1-14 (John et al., 2013).

Materials (kg/m$^{3)}$	**1**	**2**	**3**	**4**	**5**	**6**	**7**	**8**	**9**	**10**	**11**	**12**	**13**	**14**
Cement[a]	400	236	480	400	265	237	160	142	320	285	214	190	214	190
Fly ash (FA)	400	550	320	320	265	237	374	332	214	190	320	285	267	237
Silica fume (SF)	-	-	-	80	-	-	-	-	-	-	-	-	54	48
Fine aggregates	1005	1100	1160	1130	771	741	741	756	771	750	762	732	762	732
Coarse aggregates	-	-	-	-	771[b]	741[b]	790[b]	756[b]	791[b]	750[b]	762	734[b]	762[b]	734[b]
Water	288	236	240	240	192	237	181	214	197	237	193	237	192	237
PP fiber	2.0	2.0	2.0	2.0	2.0	2.0	2.0	2.0	2.0	2.0	2.0	2.0	2.0	2.0
w/cm	0.36	0.30	0.30	0.30	0.36	0.50	0.34	0.45	0.37	0.50	0.36	0.50	0.36	0.50

[a] Calcium aluminate cement (CAC), w/cm – water to cementitious material ratio.
[b] Sandstone (max. agg. Size 12.7 mm).

Table 7: Concrete mixtures 15-26 (John et al., 2013).

Materials (kg/m^3)	15	16	17	18	19	20	21	22	23	24	25	26
Cement[c]	400	400	107	107	193	200	178	386	193	193	193	-
Fly ash (FA)	400	320	249	249	174	180	160	-	193	193	193	-
Silica fume (SF)	-	80	-	-	19	20	18	-	-	-	-	-
Fine aggregates	1173	1131	633	633	688	652	640	874	688	688	688	-
Coarse aggregates	-	-	1127[d]	1127[e]	1008[d]	1008f	1127[e]	890[e]	1008[e]	1008[f]	1008[d]	-
Water	224	240	171	171	193	200	178	193	193	193	193	140
PP fiber	2.0	2.0	2.0	2.0	2.0	2.0	2.0	2.0	2.0	2.0	2.0	2.0
Steel fiber								-	-	-	-	156
HRWR	1.2	2.4	-	-	-	-	-	-	-	-	-	30
Premix								-	-	-	-	2217
w/cm	0.28	0.30	0.48	0.48	0.50	0.50	0.50	0.50	0.50	0.50	0.50	-

[c] Ordinary Portland cement (OPC), w/cm – water to cementitious material ratio
[d] Limestone (max. agg. size 9.5 mm).
[e] Sandstone (max. agg. size 12.7 mm).
[f] Syenite (single size of 4.70 mm), HRWR – high range water reducer.

The high thermal conductivity and specific heat, the excellent mechanical properties, the similar thermal expansion rate of cement with steel pipes, and the low cost of the material make the concrete TES very promising for future implementation. Martins et al. (2015) examined concrete TES for PTC systems at 393 °C with a capacity of 280 kW_{th} under real solar conditions. A comparison of its concrete mixture (Heatcrete®) with two existing concrete mixtures, DLR and UA, the characteristics of which are shown in Table 8, revealed that the most promising properties identified are for the Heatcrete® combination. As can be seen, the presence of cracks in DLR and UA concrete at higher temperatures are due to the different thermal expansion factor between a concrete mixture and the steel pipes. After several thermal cycles of the UA concrete, the compressive strength was reduced significantly due to the local overpressure in the porous system. Thermal cycles occurring on Heatcrete® concrete show good performance regarding the degradation, change of color, and crack formation. However, there was a weight loss at the beginning of the tests because of the vapor leakages which were trapped at samples due to the thermal decomposition accompanied by the release of Carbon dioxide. This weight loss is not significant and the Heatcrete® behavior is stable up to 400 °C. As shown in Table 8 the specific heat of Heatcrete® is also high at 0.75 kWh/m^3·K.

Table 8: Concrete mixtures (Martins et al., 2015).

Materials (kg/m$^{3)}$	DLR concrete[1]	UA concrete[2]	Heatcrete®[3]
Density (kg/m^3)	2250	2278	2364
Specific heat capacity (kWh/m^3·K)	0.66	0.61	0.75
Thermal conductivity (W/m·K)	1.2	2.16	2.2
Crack initiation	Several cracks	Micro-cracks	No visible cracks

[1]Data obtained at 400 °C
[2]Data obtained at room temperature °C, average values obtained from 26 samples
[3]Data obtained at 340 °C

It is observed that many researchers are trying to conclude to the parameters of the optimum TES. This should have high heat capacity, low thermal losses, and low cost. The CTES could be a profitable solution as it could be combined with solar thermal systems and fulfill the thermal energy needs of the industry through the day, even in the early morning hours or periods with insufficient solar radiation. In this study, a new concrete mixture is used for TES at the PTC system installed in the Cyprus industry and it is evaluated in section 3.3

2.1.3 Industrial Process Heat Systems experimental studies

Many solar thermal systems for IPH are reported worldwide. According to IEA (IEA, 2016), 120 solar thermal plants are in operation, covering an area of 125,000 m^2 (88 MW_{th}).

Table 9 presents the current total thermal power, the gross area covered and the number of PTC plants installed per sector. As can be seen, up to now, there are 61 PTC systems installed and operating worldwide for IPH applications, with a total thermal power of 17.23 MW_{th}, and most of them are in Mexico. Details of these plants are tabulated in Appendix 1. The dominant sector in terms of PTC plants number is the dairy and beverage with 19 PTC plants installed, while in terms of installed power capacity, the dominant sector is the food products with 7 MW_{th} (Solar Thermal Plants Database, 2021). The biggest PTC plant, shown in Figure 19, is under construction in a mining and quarrying factory in South Oman which is expected to be able to produce 6000 tons of steam per day (Miraah Solar, 2019).

Figure 19: PTC plant in South Oman (Solar Energy in Oman - Miraah | GlassPoint Solar, 2019).

Table 9: Thermal energy installed per industrial sector.

Sector	Thermal power installed kW_{th}	Installed Collector Area (m^2)	Number of PTC plants
Manufacture of dairy products	2201.60	6744.71	19
Manufacture of food products	7087.13	14434.83	8
Manufacture of beverages	571.59	2326.01	5
Manufacture of prepared animal feeds	723.89	3613.38	5
Manufacture of basic pharmaceutical products and pharmaceutical preparations	1361.67	2010.00	2
Manufacture of processing and preserving of meat and meat products	130.41	735.48	3
Manufacture of Processing and preserving of fruit and vegetables	134.00	175.00	1
Manufacture of computer, electronic and optical products	40.00	100.00	1
Agriculture, forestry, and fishing	256.00	552.00	2
Manufacture of textiles products	234.10	363.00	2
Manufacture of chemicals and chemical products	1050.00	4600.00	1
Manufacture of Mining and quarrying	1021.00	3000.00	1
Manufacture of fabricated metal products, except machinery and equipment	333.60	1408.00	4
Manufacture of paper and paper products	800.00	1490.00	1
Other manufacturing	110.88	158.40	1
Professional scientific and technical activities	562.70	1034.10	2
Water supply; sewerage; waste management and remediation activities	578.00	841.00	2
Human health and social work activities	35.00	50.00	1

Note: Compiled from data obtained from Solar Thermal Plants Database | Solar Heat for Industrial Processes (SHIP) Plants Database, (2021)

A performance investigation of a PTC system installed in 1989 at a silk factory of Mysore is presented by Thomas (1992). The system consists of 30 collectors arranged in five rows of six collectors, covering 192 m^2. The plant is producing steam for the factory processes by pressurizing heating water at 150 °C in a flash SG. The mass flow rate of the HTF is 4000 kg/h, and the peak HTF outlet temperature is 179 °C. The HTF is water and the system performance is evaluated on a clear day of April with average daily efficiency equal to 33.5% (energy collected to steam produced). The main problems observed during the operation were the corrosion of the absorber tubes and the non-uniform flow distribution. This is caused because the flash steam enters the absorber tube which prevents the flow of the HTF resulting in a further temperature increase and the generation of steam in some collector rows.

Pietruschka et al. (2012) noted that a severe problem of innovative technologies is the reliable performance of the production process. The two main issues that industrials consider are the long production process performance and the payback period which should not exceed 3 to 5 years. A big dairy factory in Spain has a high thermal need for hot air at 185 °C, which is approximately equal to 1.5 MW_{th} per day. The most significant energy consumption process is the milk drying process with a gas consumption of 35,000 kWh_{th} per day. To cover these needs, a water to air heat exchanger is used consuming a high amount of gas. A PTC system is installed to supplement energy production and reduce the fuel consumption, covering an area of 2040 m^2. The HTF is thermo oil and the maximum HTF temperature is 200 °C. The HTF is fed to an indirect SG to produce and supply steam to the industry's steam network. The steam could also support the milk pasteurization, washing processes and washing machines if the milk drying process is not in operation. Because of the PTC system, the estimated CO_2 reduction per year is around 290 tons. A dynamic simulation model is also developed to control the various processes, detect faults, and improve large-scale solar process heat application reliability and performance.

In Texas, Johnson & Johnson manufacturing plant installed a PTC plant that produces steam at 174 °C, covering an area of 1,068 m^2. The HTF is pressurized water that flashes to an SG and then the steam is supplied to the industrial processes. The system began its operation in January 1980. Brink et al. (2010) investigated and presented the evaluation of the system on a clear day of September. The average daily efficiency was 30-40%, and the average hourly efficiency varies from 38% to 42% in clear days.

Vannoni et al. (2008) highlighted the potential of installing a solar thermal collector to produce steam or hot water for an industry. The study carried out consider applications in Austria, Spain, Portugal, Italy, Netherlands, Belgium, Australia, Greece, and Germany. It should also be noted that various types of industries, such as food and beverage, textile, transport equipment, metal, and plastic treatment, were examined. The chemical has the most remarkable share of heat demand that should not be ignored.

Moreover, NEP solar company has installed three PTC plants for IPH in different industries located in Switzerland (Minder, 2012). The first is a dairy industry in Bever in which a PTC system is installed on the roof of the factory. It covers an area of 115 m^2 and produces steam at 190°C for milk processing. A bigger plant has been installed at a cheese manufacturing at Saignelegier. This system has an area of 627 m^2 and produces steam at 125°C. The system is combined with two oil-fired boilers of 1 MW_{th} for preheating when the solar radiation is low. The third solar plant is installed in Fribourg and covers 587 m^2. The HTF is water heated at 165°C for milk processing. In this case, it should be noted that heat is wasted for freeze protection. Rittmann-Frank et al. (2018) have also carried out a technical evaluation of these three factories. At Bever, the annual efficiency of the system was 23% in 2014. Improvement tasks have been carried out to increase the performance of the plant. At Saignelegier, the highest performance in a three-year period examined (2014, 2015, 2016) was 37% (year: 2015), which corresponded to 263 MWh and met the expected production. The PTC production covers 12% of the load and has an annual CO_2 saving of 69 tons. At Fribourg the annual performance was 40% (year: 2016) which corresponded to more than 220 MWh_{th} and exceeded the design expectations.

Another PTC system is installed in a textile industry in Germany, with a nominal capacity of 50 kW_{th}. The heat demand is pressurized water at 4 bar, 140 °C feeding a SG. The plant is constructed by SMirro Gmbh and is in operation since 2012. Abengoa Solar also installed a PTC plant at Frito Lay potato chips factory, which is in operation since 2008. The system covers an area of 5068 m^2 and is used for producing steam at 250 °C (Kumar et al., 2014).

Finally, a PTC system is installed in Egypt and produces 1.3 tons/h steam at 8 bar and 175 °C, and it covers an area of 1958.4 m^2. Abdel-Dayem (2011) evaluated the system's performance by developing a mathematical model simulating the process. The authors concluded that the number

of collectors connected in series should be three and not 36 as installed. Based on the economic analysis (life cycle savings method), the optimized area of the collector should be 538 m^2. This proposed system can cover 10% of the heat demand of the factory.

Concluding that, many of the PTC plants are pilot and they have been installed as part of research funding projects. Thus, there is plenty of research work done to evaluate the performance and operation of these systems. The experience earned from these plants is significant in optimizing the existing and new plants and developing systems with higher efficiency in the future.

2.1.4 Industrial Process Heat Systems simulation model studies

In general, many simulation models have been developed to predict, evaluate and optimize PTC system´s operation. Using the simulation models is also useful for examining the effect of several parameters on the system operation and performance. Kalogirou (2003) investigated the viability of using a PTC system for industrial heat generation in Cyprus. The system is investigated thermally and economically in TRNSYS simulation tool for a typical meteorological year (TMY) data for Nicosia, Cyprus. Another study has also done by Kalogirou (2002) considering the same location, but in this study, more focus is given on real factories as case studies for the feasibility analysis. It is worth mentioning that the opportunities for the application of PTC solar energy systems for IPH are enormous in Cyprus. However, many years later, there is still no implementation of these systems in Cyprus, although there is excellent potential for their utilization. The problem is not mainly economic but the motivation to the industrialists to invest on such a system. Ghazouani et al., (2020) have validated an algorithm with experimental data from the literature and proved that the average unit cost per 10 m^2 does not exceed 0.022 USD/kWh with a CO_2 replacement of more than 4.1 tons/y.

Cotrado et al. (2014) presented a dynamic simulation model and monitoring data of a large-scale solar plant for IPH for a meat factory in Austria. The dynamic model is developed in TRNSYS simulation tool, and the simulation results agree with the measured monitored data of the field. However, complete validation of the model was not possible because there were not enough experimental data for one year by that time. From the economic analysis, it is concluded that 50.7 m^3 of oil is saved every year when the energy required is covered by the solar system. This

corresponds to 26.9% of the total oil required by the factory and the cost savings were approximately €507,000. The heat from the solar system is employed for air conditioning systems (21%) and for feed water preheating of the SG.

Biencinto et al. (2016) presented a simulation model for DSG in the PTC system validated with real experimental data obtained from the DIrect Solar Steam (DISS) solar test loop in Spain. The simulation model is developed in TRNSYS simulation tool and the simulation results are compared with experimental data measured over more than 20 days from 2000 to 2003. To allow a reliable evaluation of the model performance, the authors selected three days when the system was operated at different working pressures of 3, 6, and 10 MPa.

Moreover, Cundapí et al. (2017) carried out a thermo-hydraulic study of the water-steam flow for a small size PTC for IPH applications and performed an analysis to investigate the effects of inlet temperature and pressure. The model of the study was not validated with experimental data since the system was not in operation during the study. Thus, it was decided to validate the code by comparing the results with experimental data from the DISS PTC system (Eck et al., 2003).

Ghazzani et al. (2017) carried out a dynamic simulation of a small PTC plant by using the TRNSYS simulation tool. The PTC plant generates heated air for an industrial food factory, which requires heated air at 150 °C from 8.30 am to midnight daily throughout the year. The simulation model results were analyzed in terms of the energetic and exegetic performance, and the environmental impact analysis determined that up to 57% of CO_2 emissions can be avoided annually with the use of the solar plant.

He et al. (2012) simulated in TRNSYS a typical PTC system with Organic Rankine Cycle (ORC). The performance of the system is investigated by changing several parameters, including the pressure between the absorber tube and the glass and the mass flow. The authors concluded that at the beginning, the heat losses are increased rapidly as the pressure between the absorber tube and the glass increased and then remained stable. The same behavior is also presented for the heat collecting efficiency, which rises sharply as the mass flow rate increases. The effect of the solar intensity compared with the optimum storage volume is also examined and it is concluded that for spring equinox, the optimum quantity is 100 m^3, for summer solstice 150 m^3, for autumn equinox 50 m^3 and winter solstice 0 m^3 (no storage).

Powell et al. (2012) developed a dynamic model to simulate the two-tank-direct method of TES in a CSP plant (3000 m^2). The HTF is stored in the cold tank at a lower temperature, circulated and heated through the SF, and stored in a hot tank. The TES could achieve feeding constant power and adapting the production according to the consumer's demand curves. With a TES, power output fluctuation is avoided because of clouds or hours with lower radiation as shown in Figure 20. The authors concluded that adding a TES system in a CSP plant could increase the production to 47% and reduce the fuel requirements by 43%, at a constant load of 1 MW.

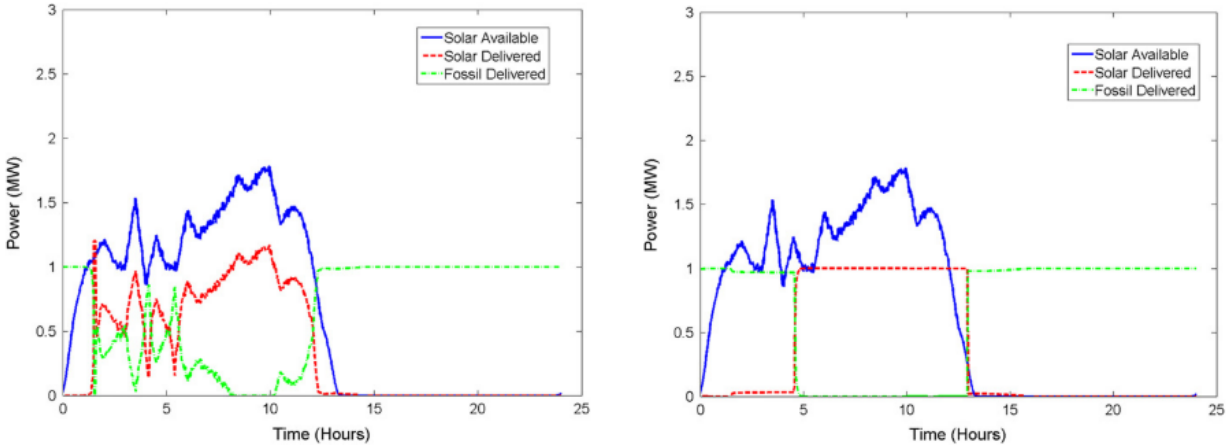

Figure 20: (A) Solar power delivered without storage (B) Solar power delivered with a storage (Powell et al., 2012).

Silva et al. (2013) presented a simulation model of a PTC system developed in Modelica coupled with TRNSYS simulation tool. The model is based at the PSA PTC system in Spain and the comparison of the experimental with real data shows an error of 1.2%. Based on the model developed, the optimum mass flow rate was calculated to be 0.22 $kg/s \cdot m^2$. The effect of the absorber emittance to the thermal performance is also investigated and showed a reduction of 60% from the reference scenario which increases the thermal efficiency by 2% (at 200 °C HTF temperature). For a reference scenario under the South European climate (Spain), the case of installing a PTC system of 1000 m^2 to cover an industrial thermal load of 100 kW_{th}, showed that the thermal efficiency could be 44% and an annual solar fraction of 67% could be achieved.

Pressure loss is one of the most significant problems faced by the SF designers. Lobón et al. (2013) examined the impact of pressure losses in small size PTCs during DSG. Based on a software tool developed, a thermo-hydraulic behavior of a PTC system designed for IPH, with a

collector aperture area of 2 m^2 and water/steam as HTF. The overall scope is to generate saturated steam in SF. The conclusion drawn from this work was that the inlet water pressure is the most important parameter. For an inlet pressure of 1 MPa, the pressure loss was significant. For an inlet pressure of 2 MPa it was concluded that a considerable reduction of pressure losses occurs, and the steam generated temperature and pressure were stable. According to their numerical results, a small size PTCs could be feasible for DSG in a wide range of temperatures for IPH applications.

During the design of a solar plant, the economic model has a significant role in the sustainability of the plant. Several parameters must be considered to maintain a cost-efficient system. The critical design parameters are the number of collectors and rows, the spacing between them, and the storage volume. Moreover, economic parameters such as the influence of fuel price increase, the plant location, the demand profile, operation conditions, plant orientation, and radiation availability uncertainty are also significant. Silva et al. (2014) have used a memetic algorithm to make a thermo-economic design optimization of a PTC plant for IPH. The authors estimated a Levelized cost of energy of 5 c€/kWh under the Mediterranean weather conditions. For a basic scenario, the payback period according to Life Cycle Cost Analysis (LCCA) is eight years. However, they strongly believe that the expected future increase of the fuel cost will substantially change the economic status of these plants.

In Southern Spain, a PTC system for IPH is installed in a vegetable preservation industry. The heat demand of this industry is steam at 7 bar, and the annual load is 148 MWh. The thermal process is mainly cooking/evaporation, and sterilization. It is important to note that the thermal load is different in each operation day, so the system must adapt to the demand. A stratified energy storage, a pre-heating heat exchanger and a SG are also simulated. Ricardo Silva et al. (2014) studied the case of installing a PTC system to cover a fraction of the factory load. They concluded that during summer, there is a considerable period where the production is much more than the demand; however, more storage would not be a feasible solution from the economic point of view. During this period the efficiency is less than 20% due to the waste of energy. The average annual solar fraction was 34.9%, and the overall annual efficiency was 30.4%. The case of installing the PTC in N-S and E-W orientations is also examined, and revealed that N-S orientation has a higher solar energy contribution due to the increased annual energy collected.

They also suggested that if the return temperature of the SG is lower, then the efficiency will increase, and the heat losses will also be reduced. To achieve that, a preheating heat exchanger should be inserted, which allows a small reduction in the return temperature. Finally, considering to cover more periods with no sufficient solar radiation, the best option is to increase the temperature difference between the return and the outlet temperature of the tank. In this way, the energy density per unit area will increase without a need for more storage tanks.

Additionally, technical and economic analyses have been carried out in TRNSYS simulation tool for a PTC system installed in a factory by Castro et al. (2018). The system preheats the feed water supplied to SG which converts it to steam for an expanded cork agglomerate production process. The design without a buffer tank consists of 6 rows of 6 collectors on each series. According to the analysis carried out using a TMY, the preheating cost could be 8.92 c€/kWh to cover a fraction of 36.9% of the total energy consumed for this process (757 MWh).

In addition, Guerrero-Quijano et al. (2011) presented a TRNSYS simulation model of a small size PTC system with pressurized water as a HTF, supplying heat to a cork factory in Spain. The heat demand of the factory is hot water at 98 °C and it was the first time to use this type of system in a cork industry. They have concluded that the annual system efficiency was 50%, and the system could satisfy a fraction of 65% of the industry load. The PTC modeled was a CAPSOL-02 prototype, and all its performance parameters are considered.

Moreover, Walker et al., (2007) developed a simulation model to examine the annual performance of the PTC system installed in the Frito Lay factory. The model simulates 16 rows of 24 PTC modules, the piping, the SG, and the hot water heat exchanger. The simulation results have shown an average steam production of 4044 MWh/ year.

Odeh et al. (2006) investigated the problems that occurred because of unsteady-state radiation conditions, which causes various thermal and operation issues. A simulation model is developed, and the results showed that the TES required size should be bigger than 14.51/m^2 of collector area. The orientation of the PTCs is also investigated and concluded that for N-S the annual contribution is higher (53% efficiency) comparing the E-W orientation (48% efficiency).

A simplified method has been developed by Ahlgren et al. (2018), to identify the annual thermal performance of PTCs using the annual DNI. The authors developed a simulation model in

TRNSYS simulation tool for 316 locations concerning three operating temperature scenarios worldwide, and they suggested a linear relation between the annual yield of the system and the annual DNI. The simulation model has been validated with a PTC array at the Technical University of Denmark. Additionally, in Morocco, a PTC system with a nominal thermal power of 186 kW_{th}, has been investigated for medium temperature heat production. The PTC system is validated with experimental data of a real system in the research facility of Green Energy Park, showing a good agreement, with the deviation not exceeding 4.8%. The authors proposed this system to be installed in an industry, and they predicted an annual steam production of 388 tons of saturated steam at 5 Bars and a payback period of 6 years (Mouaky et al., 2019).

Performance analysis of a solar cooling system has been done using the TRNSYS simulation tool for an industrial application by Cascetta et al., (2018). The analysis has been done comparing evacuated solar collectors and PTC with a storage tank volume of 5 m^3. The scope is to keep a room which is 11 m long 9.5 m wide and 3.2 m high at 10 °C. It was concluded that during the summer period, the PTC is a more efficient system limiting the operation of the conventional boiler (Cascetta et al., 2018).

Finally, a PTC system with a two-tank molten salt TES system is developed by Akba et al., (2020) to investigate the design parameters of collector field, location, load type, and storage size. They observed that the need for TES is increasing as the solar fraction is increasing. For a significant system cost range, the solar fraction is proportional to the initial investment cost, and as the solar fraction approaches one, the relation becomes asymptotic. Finally, they noted that 15% less DNI leads to a 10% lower solar fraction (Akba et al., 2020).

In conclusion, although a number of PTC systems have been designed and simulated, no one is combining CTES with a PTC system for industrial process heat applications. So this model which will be also validated with a real system could give valuable results about the system performance of this kind of system under various design parameters.

2.2 Overview of the Cyprus Energy Situation

The island has a small and isolated energy system which is not connected with any other energy networks, and there are no fossil fuel resources (European Council, 2017). Thus, Cyprus depends

on imported fuels, and 94% of the country's energy needs are covered by oil (Cyprus Energy efficiency report, 2011). However, during the last years, there is a shift to Renewable Energy Systems (RES), but there is still an ample space of improvement to have a significant production of energy from RES. As a EU member, Cyprus has a target of energy efficiency for 2030 and needs to upgrade its energy consumption strategies. The Cyprus government adopts several measures, but there is a lot to do to achieve a more energy-efficient country status.

2.2.1 Energy production and consumption analysis

In Cyprus, the energy demand is mainly categorized as electricity and thermal energy. The Electricity Authority of Cyprus (EAC), with a total installed power of 1,478 MW_e covers the main electricity demand of the island. At the same time, a minimal contribution comes from the RES adopted since the year 2004 with plants <5 MW and from the year 2010 with plants ≥ 5 MW (Statistical Services - Energy, 2021).

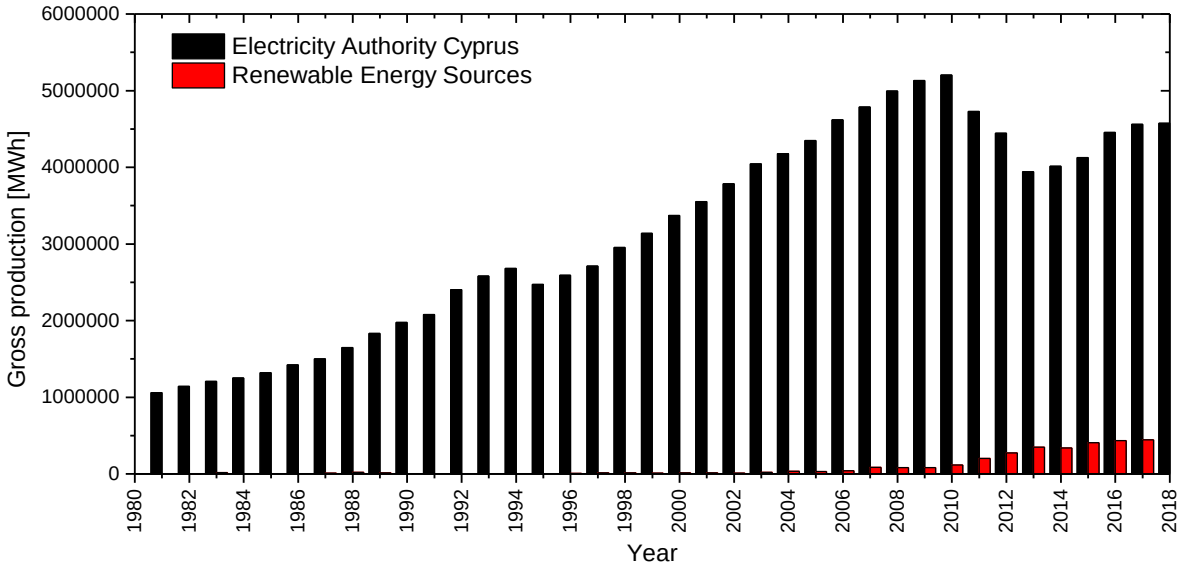

*Gross Production refers to the amount of electric energy produced, as metered at output terminals in the power stations.
**Renewable Energy Sources. Includes production from systems which are not connected to EAC's grid.

Figure 21: Gross production of Electricity, by Electricity Authority of Cyprus and RES (compiled from records given by Cyprus Statistical Services - Energy, 2021).

For electricity production, three power stations are operating in seaside areas. Photo of the three stations are shown in Figure 22. The higher electricity production comes from the Vasilikos station with an installed power of 868 MW_e. Electricity is produced by three steam-electric units

(390 MW), a gas turbine (38 MW), and two combined-cycle units (440 MW). The second electricity production station is in Dekelia with an installed power of 460 MW_e (six steam-electric units of 60 MW and two internal combustion engines of 50 MW). The lowest installed capacity (150 MW_e) is in Moni station, where four gas turbines produce 37.5MW each (EAC, 2014). It is important to note that production of 41.9 MW is from other installations by off-grid production (renewable or conventional).

Figure 22: Power stations of Dekelia, Moni, and Vasilikos (EAC, 2014).

As can be seen in Figure 23a, from 2010 to 2014, a significant reduction in consumption is evident due to the economic crisis. The main electricity consumers are the domestic, commercial, and industrial sectors, and from 2000-2018, they have paid an annual average cost of 216.3 MEUR, 252.46 MEUR, and 92.94 MEUR, respectively (Cyprus Statistical Services - Energy, 2021). From 2000 to 2018 the total electricity consumption has increased by 52%. The consumption corresponds to public lighting (1.9%), agriculture (3.4%), domestic (19.3%), commercial (39.7%) and industrial sectors (35.5%).

Cypriots are paying the fourth-highest electricity price for non-household energy consumers (Eurostat Statistics Explained, 2021). By comparing the consumption of different sectors (Figure 23a) with the cost of electricity (Figure 23b) during the last 18 years, it can be seen that when the consumption is decreased, the cost of electricity is increased rapidly, with a peak value in 2012. Additionally, after 2012, because of the national reduction of imports, and some improvements of electric power stations, the cost of electricity had been decreased.

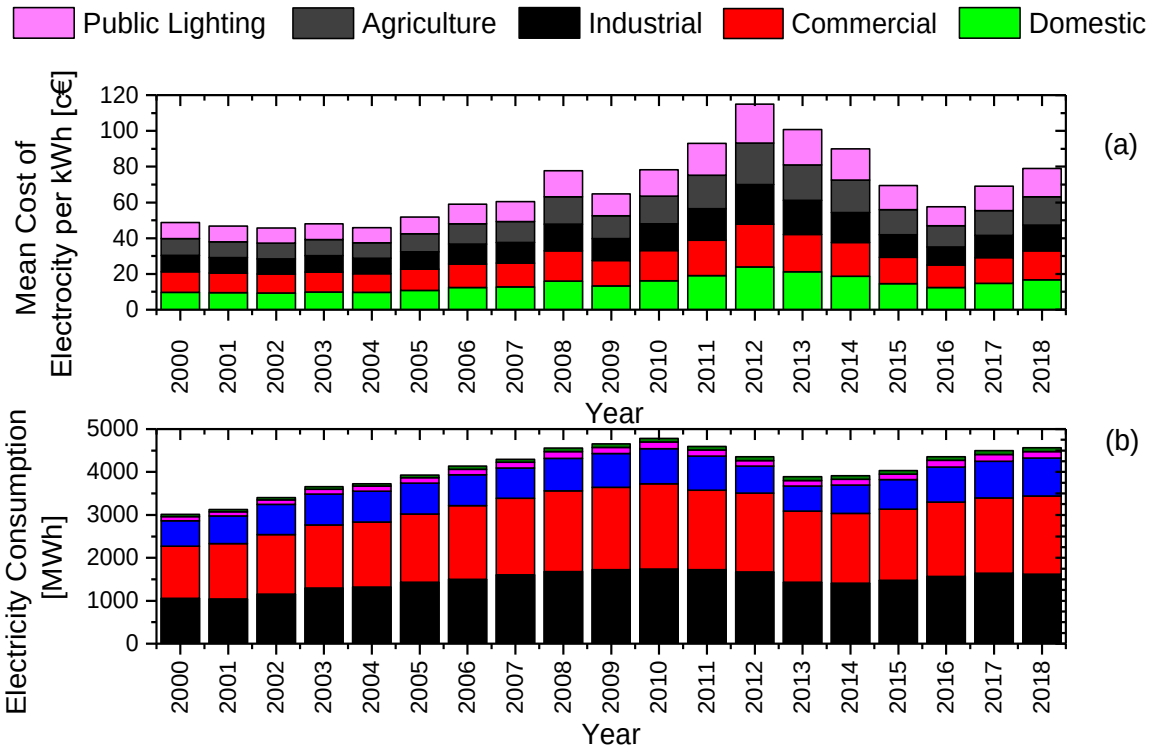

Figure 23: (a) Electricity consumption by sector (electricity production only by EAC), (b) mean cost of electricity per sector (excluding the value-added tax and the levy for the promotion of renewable energy sources) (compiled from records given by Cyprus Statistical Services - Energy, 2021).

Regarding thermal energy production, the processes employed by industry mainly use coal and oil products such as kerosene, gas oil, light fuel oil, heavy fuel oil, and liquid petroleum gasses to cover their thermal energy needs. In Figure 24, the fluctuation of the oil products are presented over the years (Cyprus Statistical Services - Energy, 2021) As shown, in 2009, 2010, 2014, 2015 and 2016 the prices have been decreased.

As the industrial sector is the main consumer of various oil products, the fuel cost fluctuation over the years is directly affected by the final price of the industrial products. As a result, there is a necessity to keep the cost of fuel production stable and low.

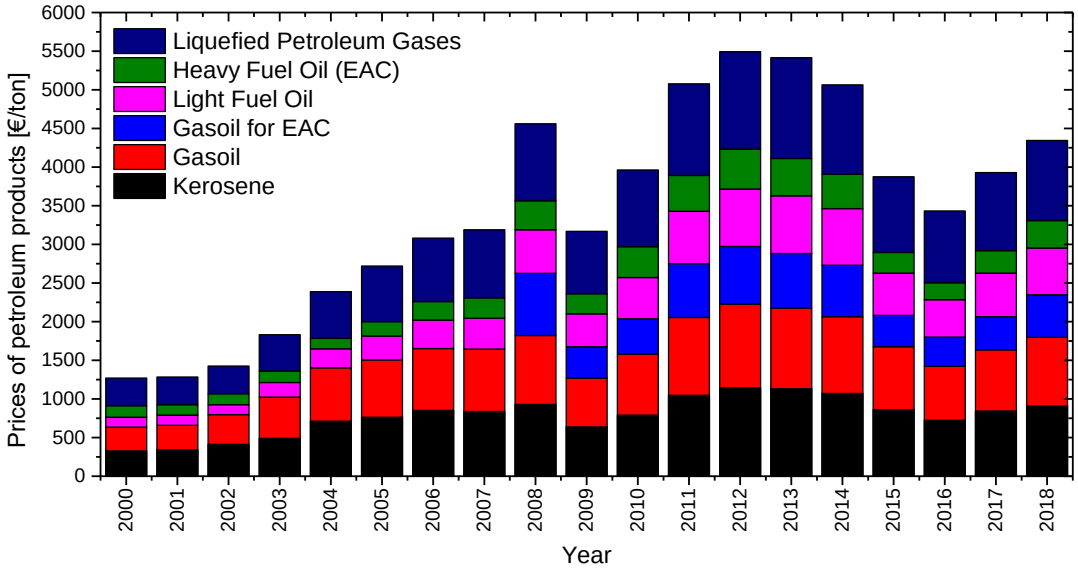

Figure 24: Fluctuation of the fuel prices (excluding VAT) (compiled from records given by Statistical Services, 2021).

2.2.2 Renewable energy systems

Cyprus is the third biggest island in the Mediterranean, with an area of 9,254 km^2, having a population of 1.17 million people. The island is located at 35^o latitude and 33^o longitude (Figure 25). The climate is typical Mediterranean with warm and dry summer conditions from May until October and mild winter from November to April (Ministry of Agriculture, 2021).

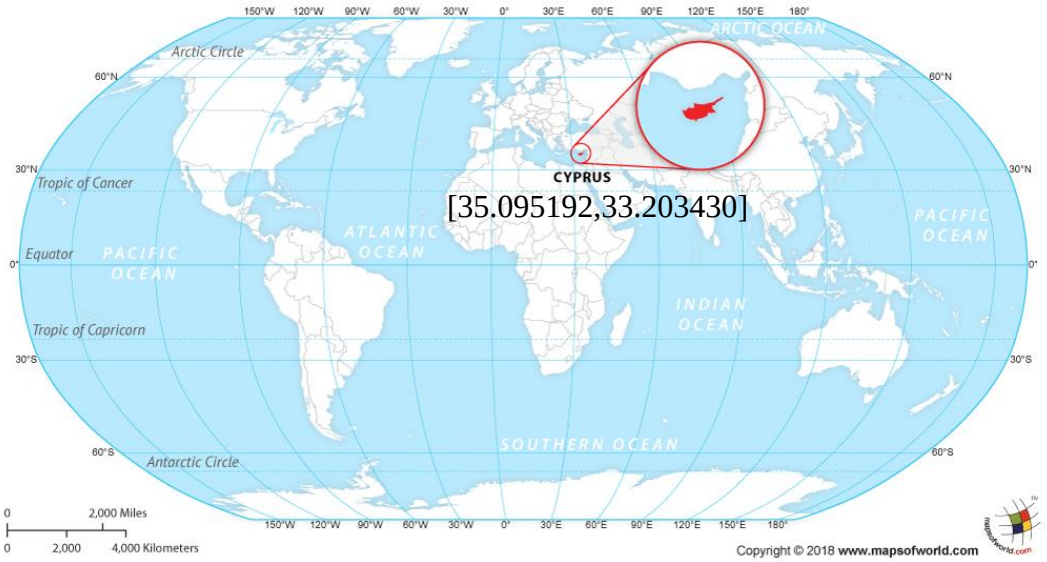

Figure 25: Cyprus country location.

Comparing the temperature distribution in the last 30 years in various Cyprus cities shown in Figure 26, the lowest monthly average temperature is above 10 °C except for the winter months December, January, and February for Prodromos.

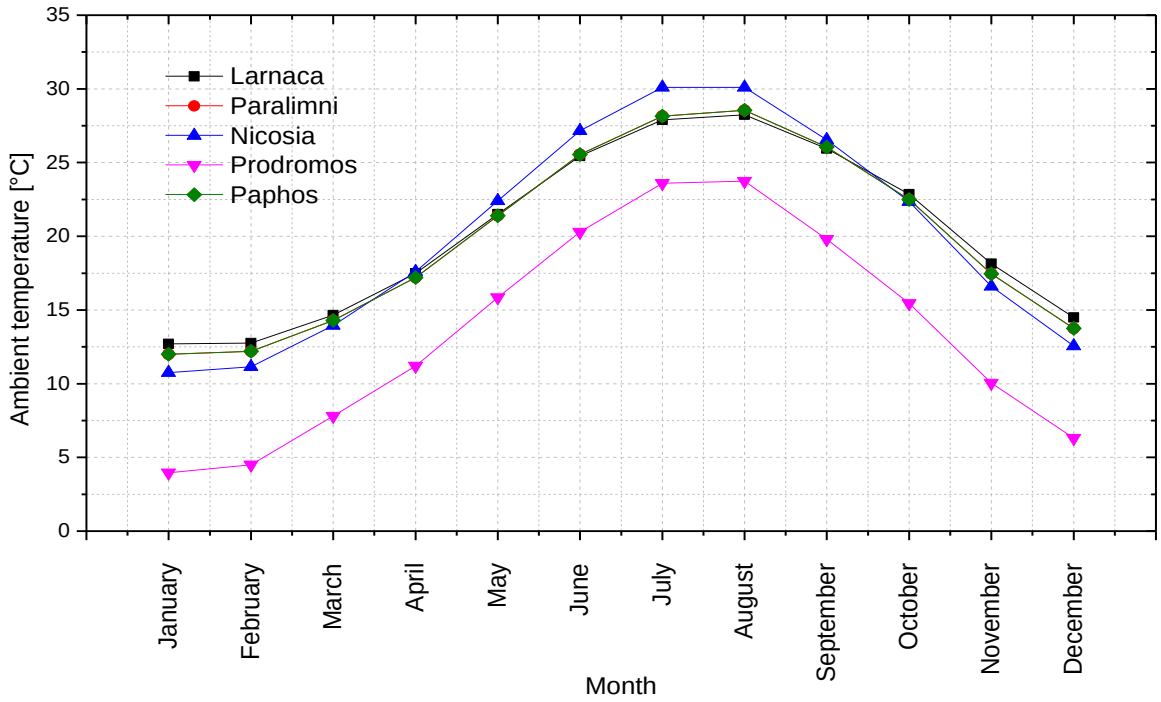

Figure 26: Monthly average temperature distribution in different Cyprus regions (compiled from records given by Ministry of Agriculture, 2021).

Besides, Cyprus is well known as an island with abundant solar radiation throughout the year. It is significant to note that the cloud period does not exceed three consecutive days in total. In the summer period, the temperature is high, the sky is clear, and the rainfall is less than 5% of the total annual amount. The maximum sunshine duration in the summer period is 14.5 h per day and in the winter period is 9.8 h (Ministry of Agriculture, 2021).

The daily average solar radiation is about 5.4 kWh/m^2 on a horizontal surface. As shown in Figure 27, the amount of global radiation falling on a horizontal surface with average weather conditions is 1727 kWh/m^2 per year. The direct to diffuse solar radiation ratio is 70:30, proving the high potential to use solar energy systems and specifically concentrated solar collectors which mainly use direct solar radiation.

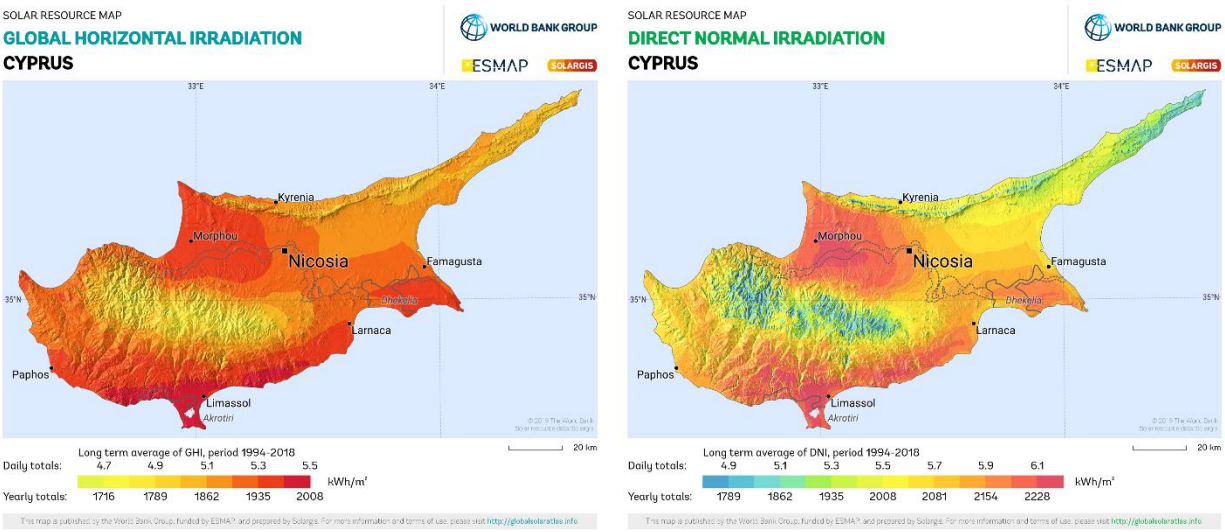

Figure 27: Global Horizontal Irradiation and Direct Normal Irradiation in Cyprus country (Solargis, 2019).

From the amount of RES installed, wind systems are the leader. Six-wind parks are operating since 2010 and contribute to electricity production with an installed power capacity of 157.5 MW. However, the PV systems are the most spread RES used in the country with an installed power of 74.647 MW until 2017 (Figure 28). The biomass systems are used for ethanol, biodiesel, and electricity production.

Compared to other renewable systems, the interest in PV systems has been increased by 96% from 2010-2018, which is quite significant, proving the potential of the exploitation of solar energy in Cyprus. As can be seen from Figure 28, during the last years there is a positive trend in the use of PVs for electricity production. Due to the solar abundance in Cyprus and the recommendations of the EU 2020 and 2030 about energy-efficient systems, the government promoted this technology as a cost-effective investment (French et al., 2016). Moreover, as the nearly zero energy buildings regulation is in full operation from 2020, the domestic and non-domestic installation of the PV system has increased rapidly, with a peak increment noted after 2011. Additionally, many enterprises are already promoting PV systems (Cyprus Statistical Services - Energy, 2021).

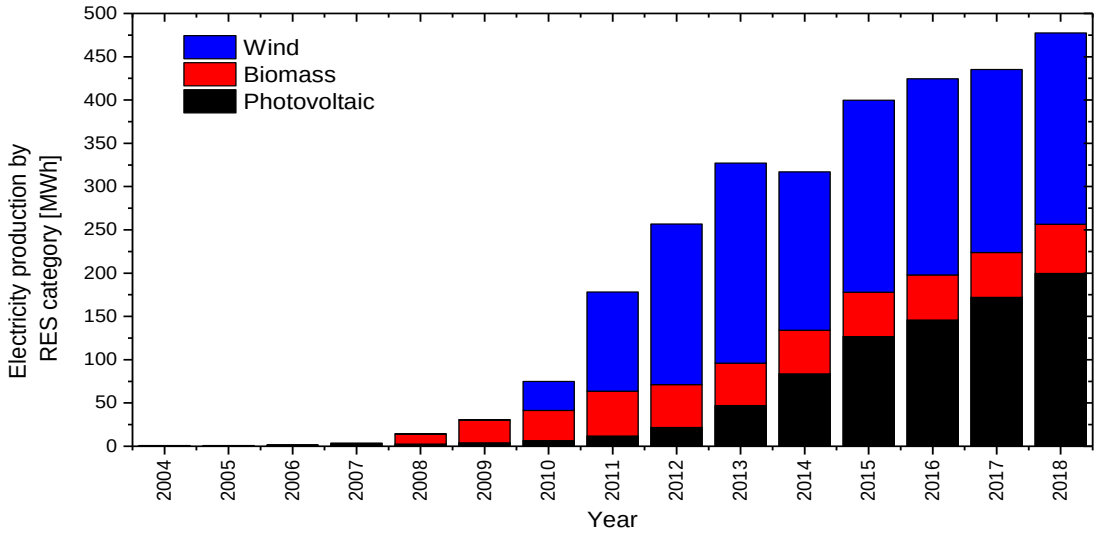

Figure 28: Electricity production in Cyprus using solar energy (compiled from records given by Cyprus Statistical Services - Energy, 2021).

Solar energy is the most widespread form of renewable energy sources due to the good solar resource, and the easier applicability of the solar systems than other RES. Every year there is an increase in the total installed capacity of the solar energy systems worldwide. The solar energy potential of Cyprus is high, due to the average global radiation exceeding the value of 2000 kWh/m^2 (Ministry of Agriculture, 2021). The fact that Cyprus is one of the worldwide leader countries in the use of the thermosiphon solar water heating systems proves that it has a great potential to use more solar thermal energy systems to cover a large amount of energy that is now covered by the use of fossil fuels (Franz et al., 2013).

The significant growth of energy production by the PV systems is evident after four big solar parks are installed and are operating in Cyprus. The biggest PV park is in Frenaros with an installed capacity of 5 MW, with the solar parks in Tseri following with an installed capacity of 3 MW (Tseri Photovoltaic Park, n.d.).

Except for the electricity production by RES, part of the thermal demand is also covered. For thermal energy, solar panels, geothermal and biomass systems are also used. According to the Cyprus Statistical Services - Energy, (2021), until 2018, the thermal production for renewables was 3.289 TJ with the production of 3.015 TJ related to solar panels (92%), 65 TJ to geothermal (2%), and 209 TJ to biomass (6%).

As mentioned before, Cyprus is a worldwide leader country using solar water heating systems per capita. The total capacity of glazed water collectors in 2013 was 423.3 kW_{th} per 1000 inhabitants, making Cyprus the leading country. Currently, 92% of the annual thermal production for domestic water heating is covered from the thermosyphon solar collectors as practically on the roof of every house there is a solar water heating system installed (Figure 29). The total thermal production by solar water heating systems doubled in 18 years period (Figure 30) as this is a proven sustainable solar thermal energy system (Cyprus Statistical Services - Energy, 2021).

Figure 29: Thermosiphon solar water heating type installed on the roof of the domestic sector and tourist apartments.

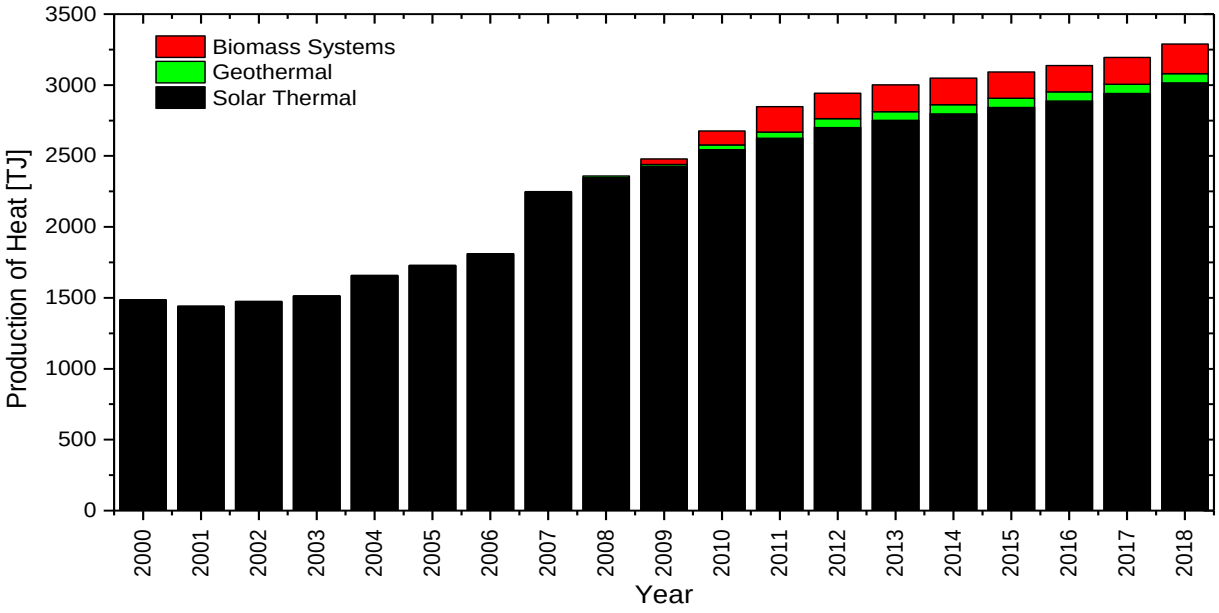

Figure 30: Total thermal production by solar panels for Cyprus compared with other systems (compiled from records given by Cyprus Statistical Services - Energy, 2021).

Considering all the above, it is concluded that the abundance of solar radiation on the island throughout the year and the fact that Cyprus needs to upgrade the energy consumption strategies and energy-efficient system using RES, revealed the great potential to use more solar thermal energy systems.

2.2.3 Cyprus Energy Targets

The high energy consumption of the European countries has forced the EU to promote a series of measures and Directives to eliminate energy consumption. The Directives are based on the capabilities of each country. For most of the EU countries, this was a kick-start to energy efficiency. The primary Directive for 2020 had set a target of 20% reduction of energy consumption in the EU, 20% of CO_2 emissions reduction, and 20% increase in the use of renewable energy sources (European Union, 2017).

The replacement of the old energy intensive systems with energy-efficient systems was crucial to achieve energy savings. However, the worldwide economic crisis from 2009-2014, and the warmer winter seasons (which leads to lower thermal demands), due to climate change, were the main reasons for lower energy demands in all sectors. Then in 2015 and 2016, when the worldwide financial situation rebounded, the energy consumption raised again.

Energy data showed that the 2020 energy efficiency target was feasible. In 2016, the EU revised the goal for 32.5% energy efficiency to be achieved until 2030, so as the fossil fuels imports to be reduced by 12%. That means a 13% reduction in the final energy consumption and a 17% reduction in the primary energy consumption comparing with the predictions of the year 2007. Additionally, 32% of the energy consumption should come from renewable energy sources (European Commission, 2019). Subsequently, for the year 2030 Cyprus must increase the use of RES for:

i. the energy consumption to 23-26%,
ii. the heating and cooling up to 39%,
iii. for transportation up to 14%,

It is important to note that the 2020 target was achieved by 2018 when Cyprus covered by RES the 13.8% of the final energy consumption (Eurostat, 2020). Figure 31 shows the share of RES in

final energy consumption per sector. It is important to mention that while the target for the heating and cooling sector was 23.5%, higher percentage is achieved (36.76%) due to the use of heat pumps, forest biomass and solar thermal system for hot water. The contribution of RES in transportation had started in 2011 when all the fuel suppliers were forced to use 2.4% biofuels in gasoline and diesel (ΚΔΠ 431/2011).

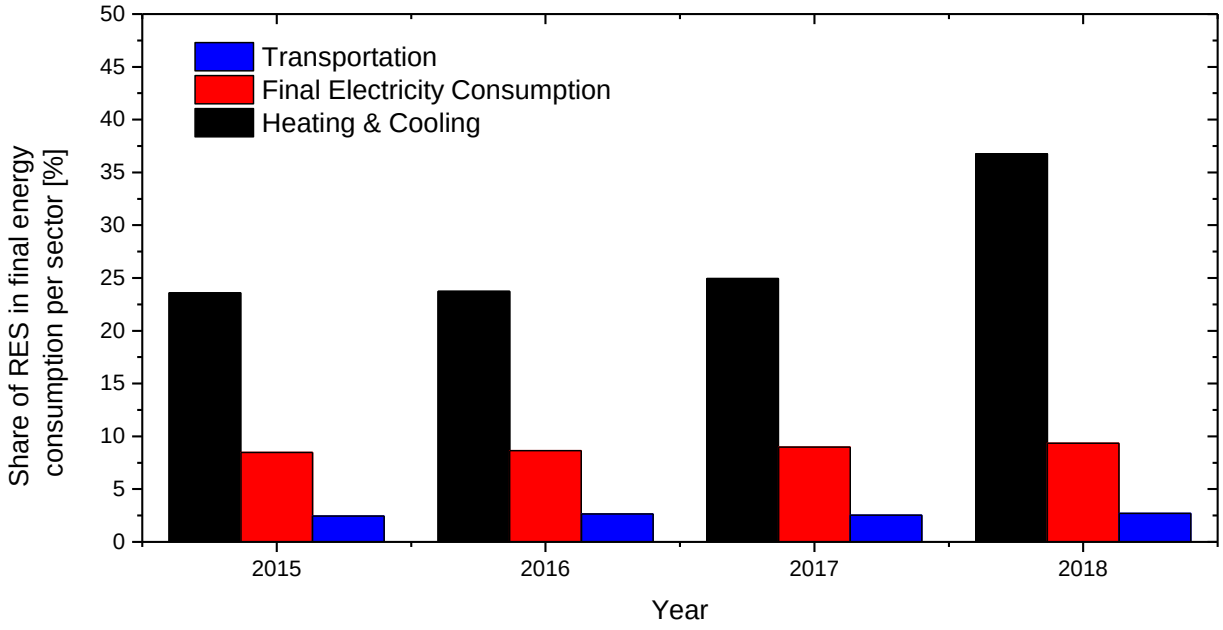

Figure 31: Share of RES in final energy consumption per sector [%] (compiled from records given from Cyprus National Plan for Energy and Climate, 2018)

Furthermore, several measures have been adopted by Cyprus, as an EU member country after 2004. The energy savings target on the final consumption is achieved, and in 2016, the energy-saving goal was 242.317 ktoe (European Council, 2017). Regarding the primary energy consumption, the objective was 2.2 Mtoe per year and had already been achieved in 2013, 2014, and 2015.

Despite the above, Cyprus was one of the eight EU countries that were far away from the primary energy savings target 2010-2020. It is important to note that the economic crisis from 2010-2014 in Cyprus had an essential role in the energy savings target. The objective criterion is energy consumption reduction when the economy is rising. It is revealed that as the economy is recovering, energy consumption is also increasing proportionally to the energy demands to control energy consumption. In 2015, when the Cyprus economy was slightly improved (by

0.4%), and the energy demand remained stable, and the final energy and electricity consumption raised by 3.9% and 2.5%, respectively (European Council, 2017).

Consequently, the measures on which Cyprus must focus are how to achieve maximum energy savings and minimize energy consumption and how to change the consumer's behavior. To accomplish this, highly energy-intensive consumers must be defined and examined to find solutions for a more energy-efficient country. Consumers have an essential role in energy efficiency since there is too much energy wasted because people are not well informed on how to use their systems effectively.

2.2.4 Cyprus potential industrial sectors for PTC applications

Under the 2030 energy-efficient target, the EU countries must reduce their energy consumption by using more energy-efficient systems. It is important to note that these systems will offset the increase in energy consumption due to economic improvements. In Cyprus, as is presented in Figure 32, the main energy-intensive sectors are transport (52%), residential (19%), services (13%), industry (13%), agriculture and fishing (2%), and others (1%) (International Energy Agency, 2017).

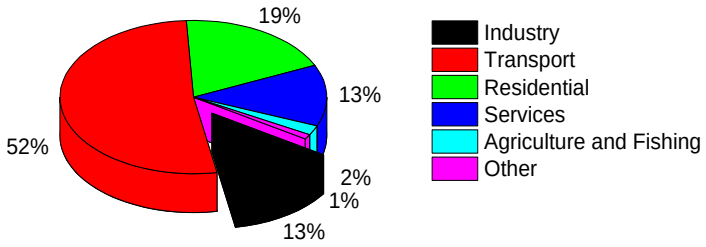

Figure 32: Final energy consumption by sector in 2015 (compiled from records given by International Energy Agency, 2017).

From 2005 to 2015, the highest reduction in final energy consumption in Europe has been achieved by the industrial sector by 16%. Thus, the residential and transportation sectors have also reduced their consumption by 11% and 3%, respectively. However, the consumption of the service sector has been increased during these years by 2%.

In 2015 the industrial sector in Cyprus had the fourth higher (13%) average energy consumption with an energy consumption of 0.2 Mtoe. Despite the overall reduction in energy intensity of EU

countries (19%), Cyprus is one of four countries that increased its final energy consumption by 11% (per gross added value). As a result, Cyprus industries did not take the required measures to decrease their energy consumption. The Cyprus industry must find a direct and effective way to improve the energy efficiency of the industrial sector. Any improvement in this field will affect the total energy efficiency of the county (European Commision, 2017).

The energy demand of industries is covered by oil products (71%), electricity (29%), with very little use of coal, and renewable energy. The use of coal has been decreased rapidly after 2006 and abandoned completely after 2012. The utilization of renewable systems is increased in the last years, especially after 2011 by the use of biofuel and municipal and industrial waste. For the electricity demand and by investigating a 15 years period (2000 – 2018) it is observed that 18% of electricity consumption is related to industries as shown in Figure 33, which is the third higher consumer after the commercial (41%) and domestic (36%) sectors.

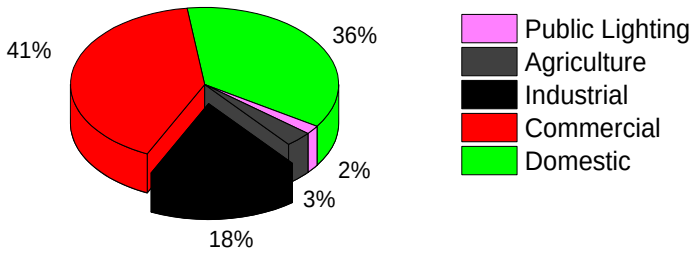

Figure 33: Electricity consumption by consumers (compiled from records given by Cyprus Statistical Services - Energy, 2021).

As can be seen in Figure 34 from 2000 to 2010 the electricity consumption was increased (except for 2007). After 2010 the consumption decreased rapidly with a peak reduction that occurred in 2013 when Cyprus had the worst economic situation. After 2013 the electricity consumption increased again (Cyprus Statistical Services - Energy, 2021).

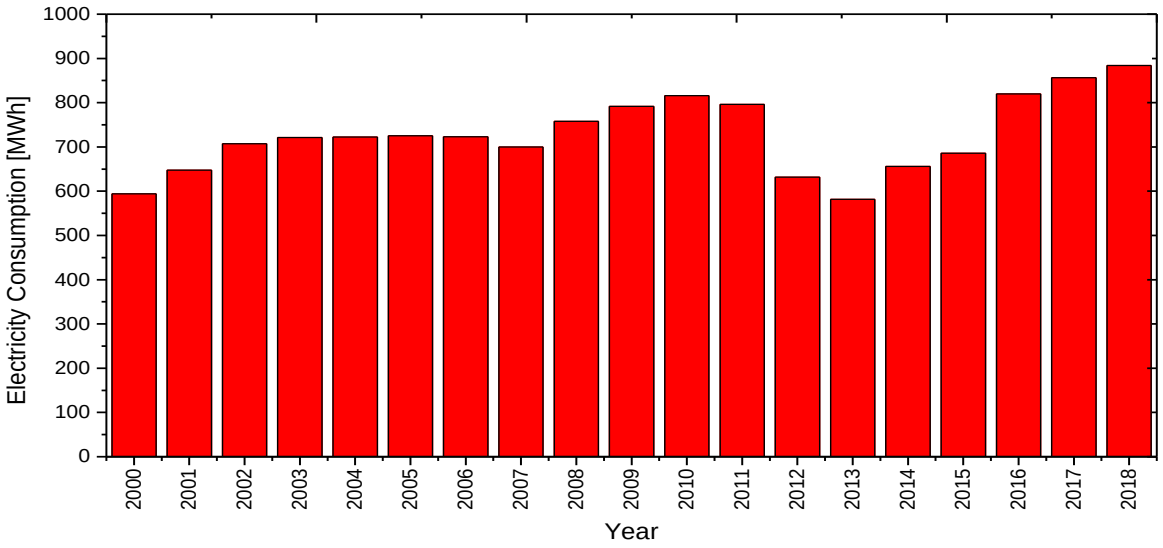

Figure 34: Electricity consumption by industries (compiled from records given by Cyprus Statistical Services - Energy, 2021).

It is important to define the highly intensive industrial sectors related to electricity consumption. By investigating the last year's final consumption, it can be concluded that the manufacturing sector is the main consumer with 493 GWh electricity consumption (Statistical Services - Energy, 2021).

Figure 35 shows the share of electricity consumption in different manufacturing categories. From 2010-2017, the higher consumer is the food and beverages, with an average consumption of 37.01%. The non-metallic mineral products also observe significant consumption with an average consumption of 34.73%. The annual average consumption in these sectors is 170,136 MWh and 159,667 MWh, respectively. Additionally, in these industries, the cost of electricity is also high. The manufacturing sectors of food products, beverages have paid an average cost of 32.33 MEUR for the years 2010-2017, and the nonmetallic mineral products have paid an average cost of 21.61 MEUR for the same years (Statistical Services - Energy, 2021).

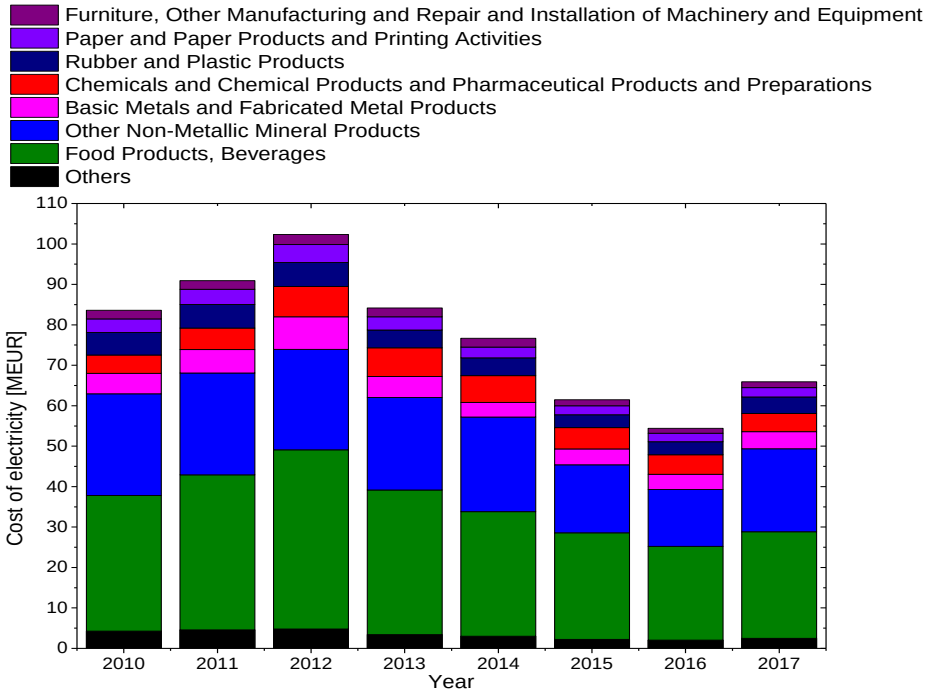

Figure 35: Cost of final electricity consumption by manufacturer used in production (compiled from records given by (Cyprus Statistical Service - Industry, 2021).

However, the dominant energy source of industries to cover their thermal demands is oil (71%). Comparing the final consumption of oil products imports shown in Figure 36, the industrial sector is the second higher consumer (20%) after the transport sector (57%). As a result, the possibility of reducing the consumption of oil products for thermal energy production in the industrial sector by using energy-efficient systems is very attractive in terms of fuel cost (International Energy Agency, 2017).

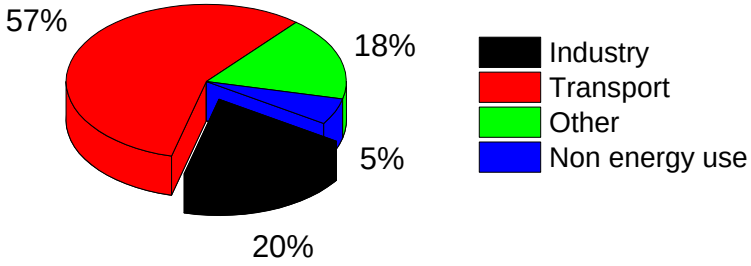

Figure 36: Oil consumption by sector (compiled from records given by International Energy Agency, 2017).

The oil product consumption by industries is presented in Figure 37. As can be seen after 2004 the consumption was reduced rapidly until 2006 where it remained stable for three years. After

2009 during the global economic crisis, the consumption reduced further, and during the year 2012, the lowest consumption occurred. In 2014 the consumption was increased and in 2015 was reduced again by the same level as 2012 (International Energy Agency, 2017).

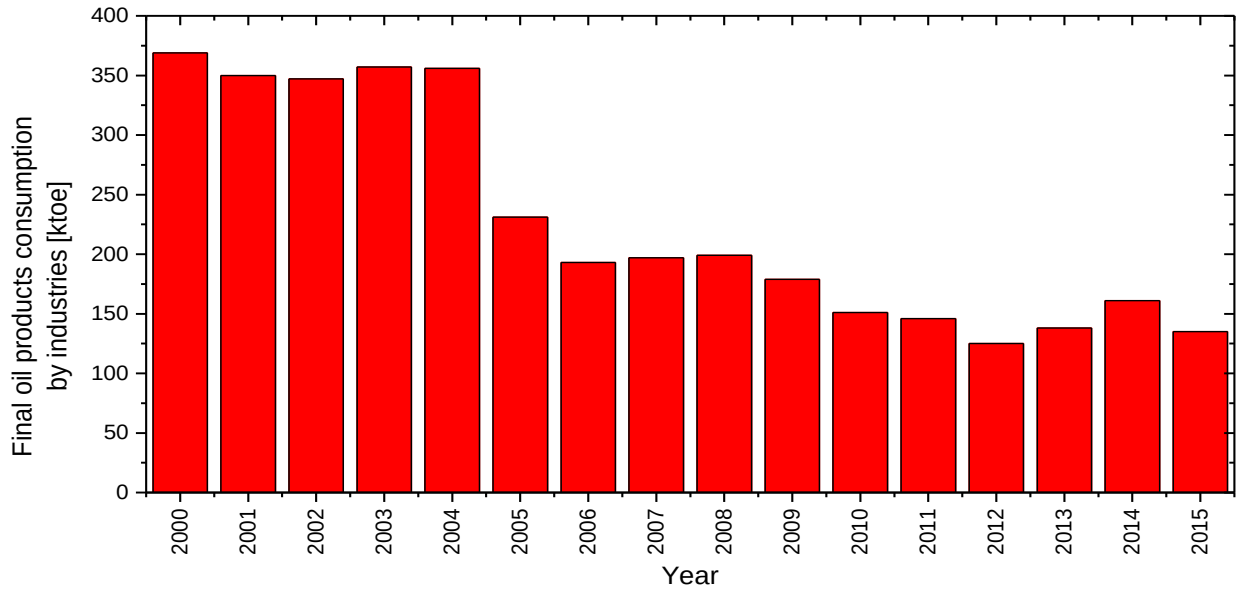

Figure 37: Final oil products consumption (compiled from records given by International Energy Agency, 2017).

The leading industrial sector in the use of oil products for thermal demand purposes is manufacturing. From 2010-2017, and by comparing the different categories of the manufacturing sector it is observed that the manufacture of food and beverage products and the manufacture of other non-metallic mineral products are the more intensive sectors by paying the higher cost in oil products to cover their thermal demands as shown in Figure 38 (Republic of Cyprus, Ministry of Finance, 2020).

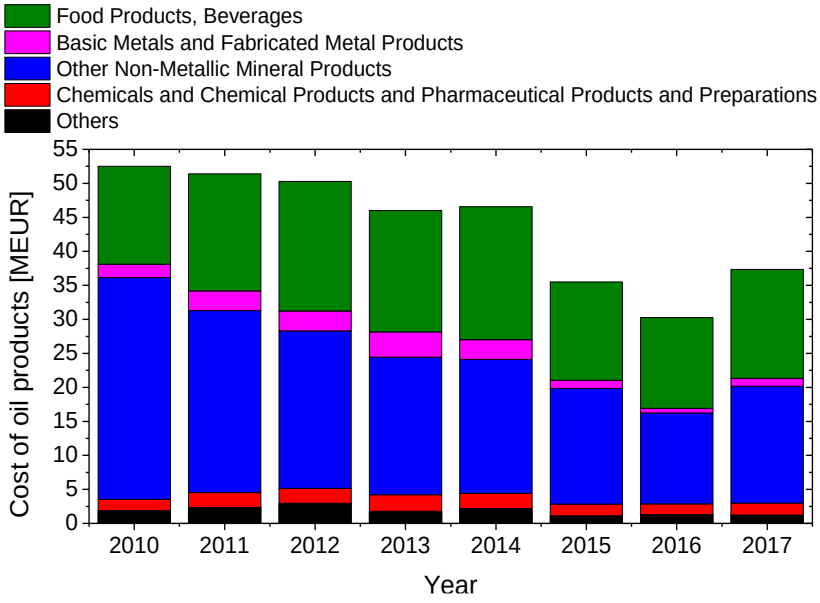

Figure 38: Cost of oil products by manufacturer used in production (compiled from records given by Statistical Service - Industry, 2021)

However, to identify the industries that are responsible for oil consumption, the average cost of oil for thermal production from 2010-2015 is estimated. According to Cyprus Statistical Service - Industry, (2021), for the manufacturing of food and beverages products, the dominated industries are the manufacture of bread, fresh pastry goods and cakes that have an average cost of 6.2 MEUR per year. A high cost is also observed for the operation of dairies and cheese making, with an average cost of 3.5 MEUR per year (Figure 39).

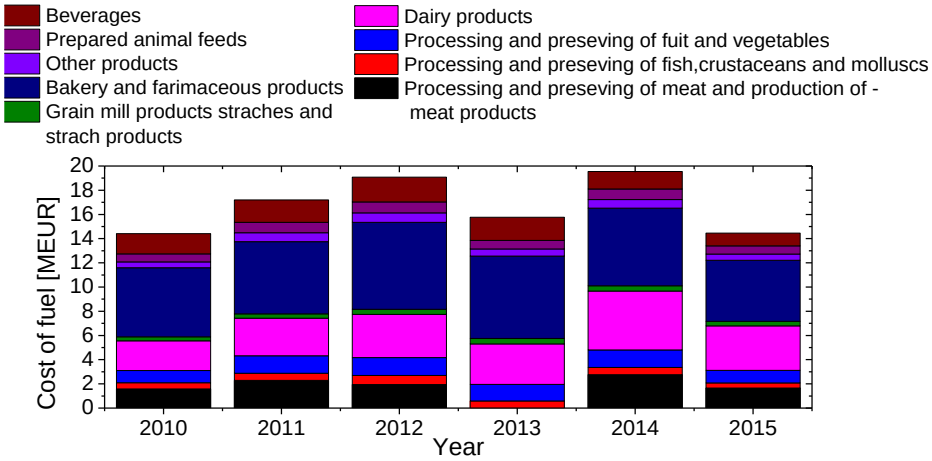

Figure 39: Average cost for the manufacture of food and beverages (compiled from records given by Cyprus Statistical Service - Industry, 2021).

For the manufacturers of other non-metallic mineral products, the dominated industries excluding the year 2010 is the manufacturing of refractory products, cement, lime and plaster with an average annual cost of 10.65 MEUR. Significant intensive industries are also the Manufacture of articles of concrete, cement and plaster and the manufacture of lay building materials with an average annual fuel cost of 2.74 and 2.51 MEUR, respectively. As can be seen in Figure 40 after 2010 the cement industry stopped using coal as fuel thus, the fuel consumption was decreased drastically.

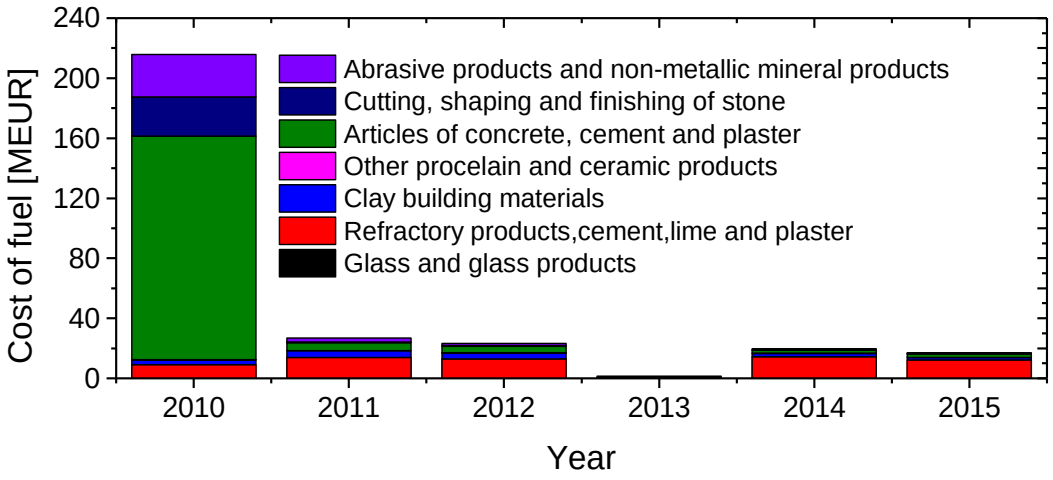

Figure 40: Average cost for manufacture of other non-metallic mineral products (compiled from records given by Cyprus Statistical Service - Industry, 2021).

Considering the above, the industrial sector is a significant energy consumer, with the most significant thermal energy consumption occurring in industries of non-metallic minerals and food and beverage products. The food and beverage industries have a fuel consumption of 37.01% of the total use, which corresponds to a consumption of 171.6 MW_{th}/yr and an annual average cost of 16.5 MEUR (Cyprus Statistical Service - Industry, 2021).

For the food and beverage sector which has a thermal need that a PTC system can cover, a survey has been done to identify the thermal energy demand of various Cyprus factories presented in Figure 41.

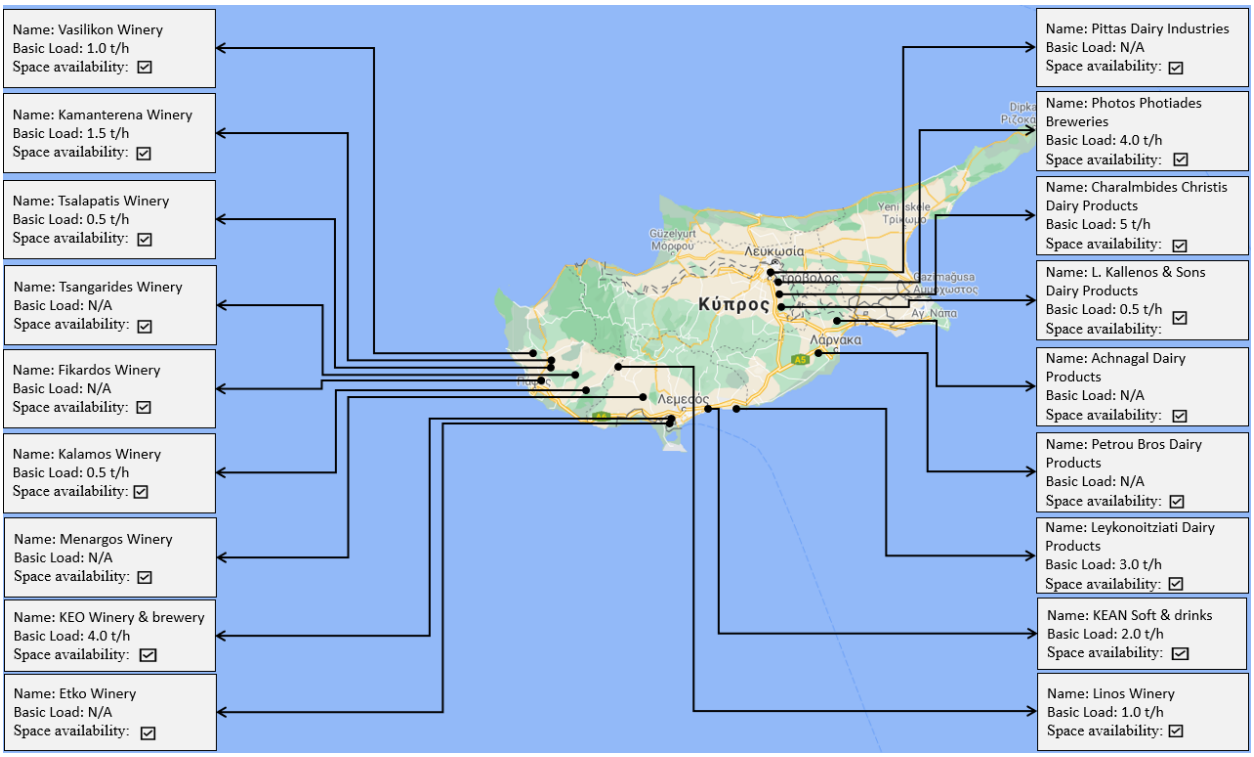

Figure 41: Mapping of food and beverage Cyprus industries (compiled from records given by the industries).

All these industries are entirely dependent on fossil fuels, and except of KEAN, none of them have installed any RES to cover their thermal energy demand. All these companies with high thermal energy needs could have used solar energy systems for their thermal energy.

Considering the markets that should implement solar energy systems for electricity or heat energy generation, there is an excellent potential for PTC systems. Looking at the required amount of oil to cover the heat energy needs of the industrial sector, a considerable market potential exists for medium to high-temperature applications. For the industrial sector, the flat plate solar collectors already in use in the building sector are not the best option since higher temperatures are required. The most appropriate system to cover these needs would be a PTC system, which can work at elevated temperatures with excellent efficiency.

Thus, PTC systems could be a sustainable and profitable technology, especially for the Cypriot industries. With the proper investigation of a TES system, the energy can also become dispatchable.

2.3 Subject and Aim of this Study

An overview of the PTC field and the current energy and solar energy situation in Cyprus has been given in the above literature review. The two main parts of a PTC system are the collector and the TES. These have an important role in the thermo-economic efficiency for covering the thermal needs in an industrial process. The combination of these could give a high efficient PTC system that can produce steam or hot water for IPH. For this reason, many researchers have focused on the development and optimization of PTC prototypes. They have mainly focused on the absorber tube improvements by inserting fins, changing the design, and the inner configuration. By modifying the absorber, a better efficiency has occurred; however, other system parameters are affected and may harm the system operation. TES is a challenging system, as this can give dispatchability of the energy produced by the system. The ideal TES is the one that can store a significant amount of energy effectively in a cost-efficient way and can support thermal production when there is a need.

Additionally, as described before, different storage technologies exist that can be applied to a PTC system. Up to now, there is a list of 61 PTC systems worldwide that have been installed for IPH applications. These systems are installed using different types of PTC collectors and thermal storage to achieve the optimum balance between cost and efficiency. To evaluate these systems, real data analysis and simulation models have been developed. Using these models, the real thermal production is simulated and this is a much easier and cost-effective way to investigate means of improving and optimizing the PTC systems. Furthermore, more research on possible modifications of the absorber tube or new TES improvements would not lead to significantly higher system performance. The absorber and TES designs are at a high level, and it is not believed that a novel technology in these could drastically increase the system performance. However, by focusing on specific operation parameters and optimizing them, the performance of the system could be increased considerably. These parameters could be the operation modes, strategies, and maintenance, mainly mirror cleaning procedures.

From the extensive overview analysis carried out on the Cyprus Energy situation, it has been stated that Cyprus has high solar energy potential. Since it was revealed that the industrial sector is one of the main fuel and energy consumer, the PTC technology for IPH applications is

suitable. This work is involved in installing and operating the first PTC system in the Cyprus industry. The main scope is to focus on operation modes and strategies which can make the system dispatchable following the production shifts of the industry. Performance analysis of the PTC system will be done, and later on, a dynamic simulation model will be built in TRNSYS simulation tool and be validated with experimental data. This study aims to use the validated dynamic simulation model to develop a tool for PTC parameters selection based on IPH application under Cyprus climate.

The PTC system is installed in KEAN factory. By using this system, the performance of the operating parameters will be investigated. Initially, operation modes will be developed and optimized, ensuring the highest possible performance, which makes the system produce steam at the required temperature and pressure, according to the thermal needs and shifts of KEAN factory. By analyzing these operation modes, the performance characteristics of the system will be determined. It is important to note that the TES system is a concrete mixture and the response of the novel Concrete Thermal Energy Storage (CTES) will also be examined with an overall target to make the PTC system dispatchable.

Furthermore, as the PTC system is fully operational, a model will be developed to simulate its operation. The literature review concludes that the best way to model the PTC system is with the TRNSYS simulation tool, giving highly accurate results. All the parameters, components, and parts of the system will be modeled to simulate the operation process. The model will be validated by comparing real experimental data with the simulation results. Thus, the validated model can be used to investigate the system under different operation strategies and modes. The dynamic simulation model must be able to adapt to the actual operation strategy and mode that the real system operates. Additionally, the model will have the capability to record several parameters of each component to evaluate the performance and compare it with the real PTC system output.

Moreover, as the literature concludes, the PTC system technology has a high potential for IPH in Cyprus, although excluding the KEAN's system, none of the Cyprus factories has adopted this technology. Thus, the validated simulation model will be used to define the most appropriate system for industries with larger thermal energy needs in Cyprus. The novelty of this work is the

new design tool that can take as inputs the thermal energy demand and steam demand temperature of the industry and provide as output several information on the sizing and finance characteristics of the optimum PTC plant that can be installed. To achieve this, a Life Cycle Cost Analysis (LCCA) has also been carried out, which calculates the solar saving and CO_2 emissions of the selected system.

According to the literature review, there are currently no similar available tools for industries. Another approach is thermo-economic evaluation of the PTC system, concluding to optimize a specific demand, and with LCCA, the cost of thermal energy produced is stated.

2.3.1 Outline of this study

In this project, a novel design tool for modeling and evaluating the PTC system for IPH applications in Cyprus is developed. The structure of this study is shown schematically in Figure 42.

In the first chapter a discussion on the general information regarding important PTC system progress steps and IPH applications was presented. In the second chapter, an extensive survey has been done on the PTC fields and the current energy situation is examined. Additionally, the novel features of this study are described. In the third chapter, the first PTC system installed in a soft drinks industry in Cyprus is described. The data obtained from the initial operating period, the operation Strategies and Modes developed are explained, and an experimental analysis has been done to quantify the behavior of the system, on particular days and in a longer period of two continuous months of operation. The novel CTES system is also experimentally investigated and its heat loss behavior was tested. In the fourth chapter, the validated Dynamic Simulation Model analysis carried out in TRNSYS simulation tool is presented in combination with the mathematical model of the PTC system. It should be noted that there is no such models available in the literature. So it is the first time TRNSYS is used to model a PTC system with CTES for process heat. Chapter 5 presents the ultimate goal of this study which is a novel design tool for PTC parameters selection based on IPH applications, also developed for the fist time.

Finally, the conclusions obtained from this study are presented as well as recommendations for future work.

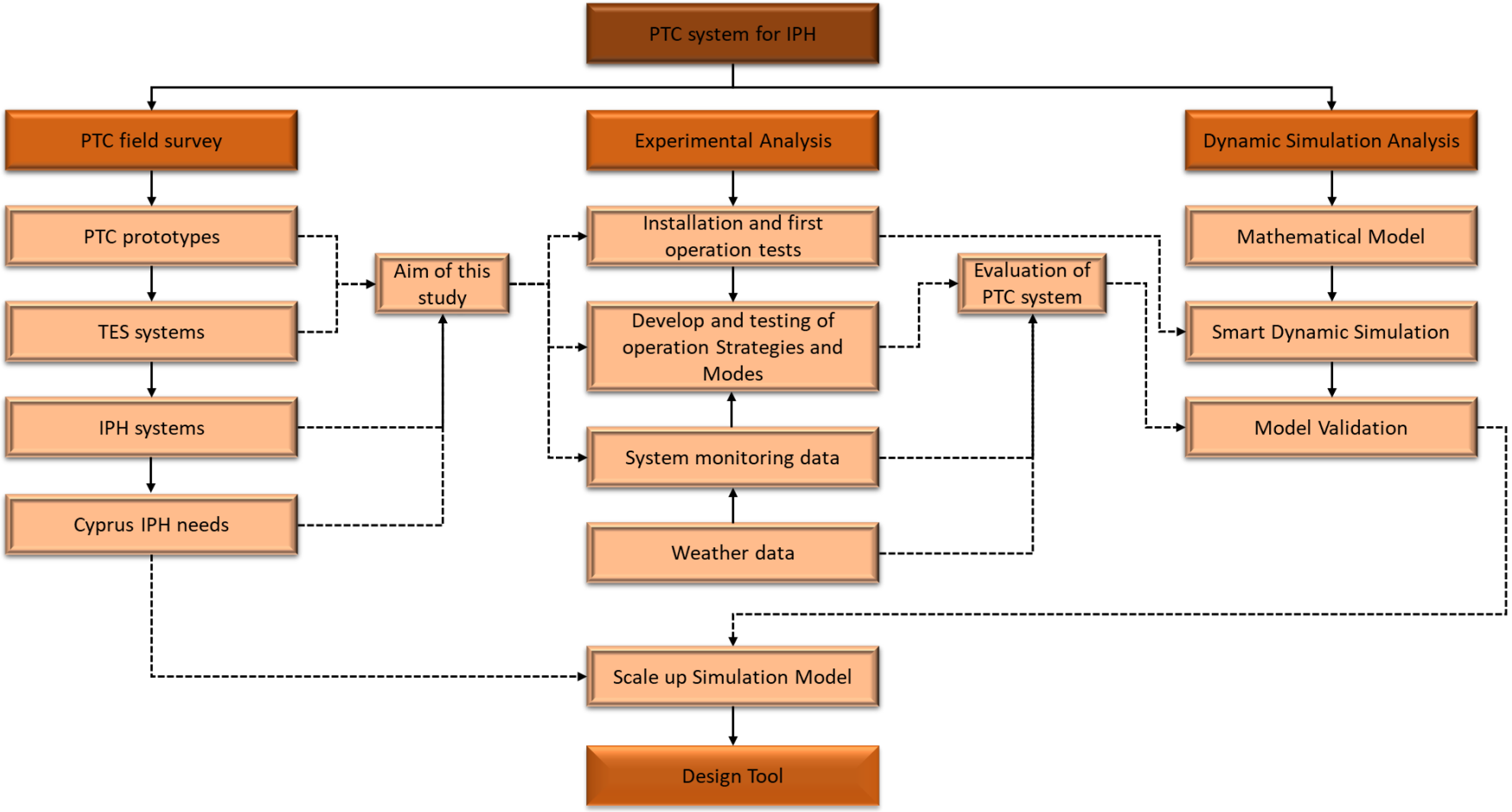

Figure 42: Approach of PTC system investigation in this study.

CHAPTER 3

3 Experimental Analysis

Based on the literature review and the current energy situation in Cyprus, it is revealed that the most significant energy consumer from the industrial sector, with a medium temperature steam demand, is the food and beverage industry. Thus, the Cyprus University of Technology (CUT) and KEAN soft drinks industry with the partners Protarget AG, CADE Engineered Solutions, Solar-Institute Julich and DLR, as part of the EDITOR European project, have design and install the first novel PTC system for IPH, located in Limassol, Cyprus (EDITOR, 2019). A sky-view photo of the factory is shown in Figure 43.

Figure 43: Sky-view showing the KEAN factory and the location of the PTC system and its components.

3.1 Installation and first operation tests

The first task was to define the most suitable factory for installing the PTC system. The final selection has been done between wineries and beverage industries (some of them shown in Figure 41). The primary criterion was that the system's thermal production should satisfy the factory's thermal needs. KEAN is one of the largest soft drinks industries in Cyprus, and the installation of a PTC can support part of its thermal load.

The processes that require heat are cleaning/disinfecting the glass bottles, pasteurization, and sterilization (Figure 44). It should be noted that the size of the solar system is a fraction of the actual heat demand required by the industry, but this is installed mainly for demonstration purposes.

Figure 44: Process in Kean factory which requires thermal energy.

Following the industry selection, the consortium designed the system and prepared the area for the installation of the system. In November 2017 the installations started, and in June 2018, the system was able to produce steam for the first time in a manual operation. Initially, the CTES was shipped and connected on-site and the PTCs were assembled. Two hydraulic tracking mechanisms were installed in the two series of collectors to track the sun with high accuracy, ensuring the highest performance. The next step was the welding of the absorber tubes on the

focal line of the PTCs. Additionally, flexible pipes and relief valves were installed at the edge of each row and the absorber tubes were connected with these and the inlet and outlet valves of the control room, creating a loop. Then the parabolic mirrors were installed and adjusted on the right angle of the PTC structure to avoid misalignment between the mirrors. A feedwater tank was also placed on the roof of the plantroom and then the SG was installed. The last step was to fill up the expansion tank with nitrogen and the whole system with the HTF. As nitrogen is a compressible fluid, it acts as a damper to absorb sudden changes and maintain the pressure of the closed loop system constant. A bridge was also constructed to support the steam pipe going from the control room to the industry steam circuit.

Subsequently, a pressure test is done to the loop to ensure that there are no leakages through the piping. All containers were painted, and the ground area was asphalt-covered. Additionally, the whole system was protected by a fence that was placed around the site.

Several technical changes, modifications, and optimization have been done for a year by Protarget AG, CUT, and an external partner from Italy (who done the coding) to make the system operate autonomous, producing steam and support KEAN's thermal energy load. It is important to mention that two-stage alarms and safety sensors have been installed and connected with the main system processor. Additionally, to minimize heat losses, insulation was placed on pipes and parts of the system.

It is significant to note that during the installation and first test operation, the presence of Protarget AG and CUT member in KEAN for running the system ensured that the PTC system produces steam to support the KEAN load. Several photos of the installation and first test operation procedure are shown in Figure 45 and APPENDIX II.

Figure 45: Photos of installation procedure and first operation tests.

The installed PTC system is a pilot system, with the primary objective to prove that this technology is feasible. It comprises three components: (i) the SF, (ii) the CTES, and (iii) the SG. The PTC system installed and operating as it is now, is shown in Figure 46.

Figure 46: PTC system installed and operating.

The SF consists of 8 PTC (CF100) connected in 2 parallel rows of 4, with an aperture of 3 m and a length of 12 m with high reflectance up to 94% and high absorbance by the receiver tube up to 95% (Figure 47). The nominal thermal power of the system is 125 kW_{th}. The CF100 PTCs used have been built by Protarget AG in cooperation with the DLR and other industrial partners (Protarget AG, 2020). These PTCs employ a high efficient receiver tube for operation at temperatures up to 425 °C. A vacuum is maintained between the receiver tube and the glass envelope to avoid thermal losses and make the collector operating at high efficiency. The PTCs track the sun from East to West with the implementation of two hydraulic systems one for each

series. The HTF is a new environmental-friendly silicone-based thermal oil named HELISOL®XA. The fluid is non-reactive polydimethylsiloxane, which is clear, odorless, and colorless. It has a long life, no hazard classification and it is also non-corrosive (DLR, 2020). Details about the absorber tube and HTF are presented in Table 10.

Table 10: Properties of absorber tube and HTF properties (Protarget AG, 2020); (DLR, 2020).

Receiver tube parameters	Value
Mirror reflectivity	0.94
The outer radius of the absorber pipe	19 mm
Outer radius of glass envelope	50 mm
Absorption coefficient for absorber tube	0.95
Transmissivity of the glass envelope	0.91
HELIOSOL®XA parameters	**Value**
Recommended use temperature	-40 °C - 425 °C
Boiling point	375 °C
Density @ 25 °C	0.93 g/cm^3
Specific heat @ 400 °C	2.3 kJ/kgK

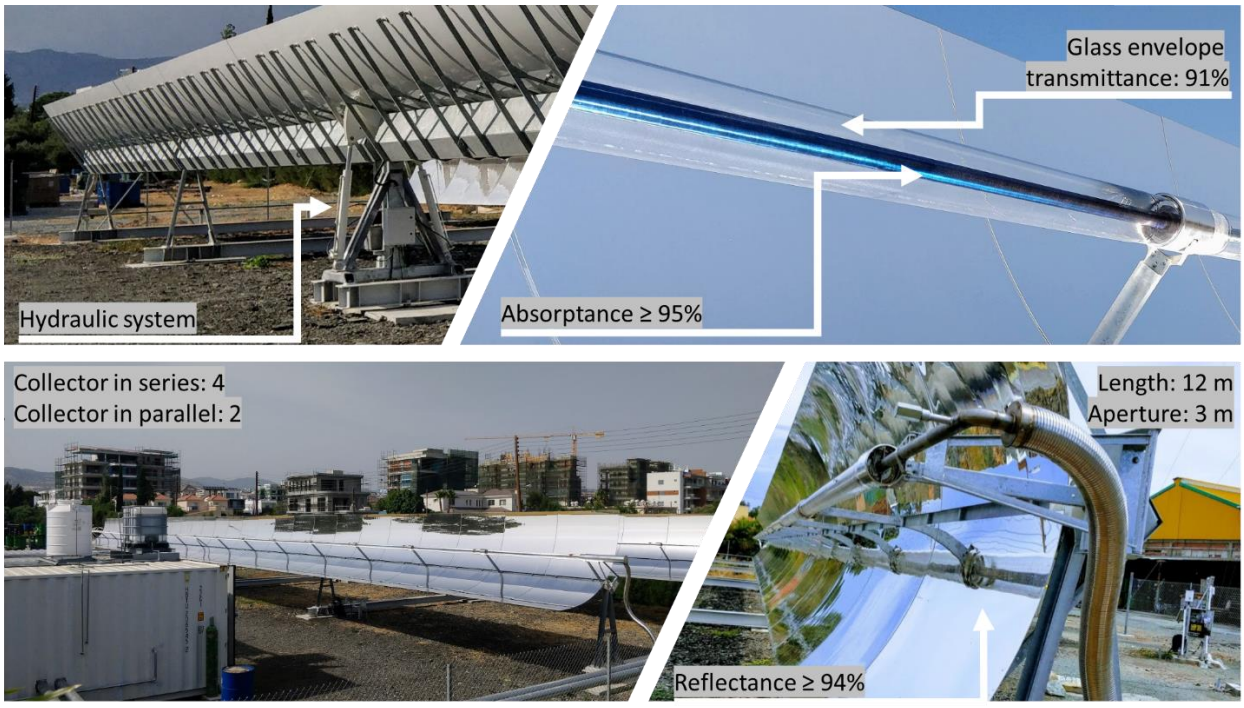

Figure 47: The SF installed in KEAN soft and drinks industry.

The new TES is designed and constructed by CADE Engineered Solutions (CADE Engineered Technologies, 2020) and it has high performance at temperatures up to 400 °C. It stores heat in a new-based concrete mixture and supplies heat to the industry when it is needed. It is important to note that with the new concrete composition, higher storage capacity and thermal conductivity are achieved. The performance of concrete volume, density, conductivity, and specific heat is also improved. The pipes where the HTF circulates into the CTES are running through four concrete modules. The four modules are enclosed in two containers, two blocks in each container as shown in Figure 48 and they have a thermal capacity of 640 kWh_{th}. The total mass of 28,157 kg (5x0.548x0.670 m) and the storage modules are surrounded by thermal insulation. To avoid thermal losses, pipes on the outside were insulated. Measurements had shown that when the HTF temperature inside the pipe was 320 °C, the outer surface temperature of that pipe was 38.5 °C.

Figure 48: CTES system.

The third part is the SG shown in Figure 49a. This is constructed by Protarget AG to produce steam at 10 Bar_g, 188 °C. In the SG, freshwater enters at ambient conditions from a water tank installed at the container's roof (Figure 49b). The SG is filling with fresh water up to a predefined level, leaving space for the steam. The HTF is circulated through the spiral pipes inside the SG, and thus transferring heat from the HTF to the freshwater and thus saturated steam

at 188 °C is produced. The HTF employed is circulated by the variable speed pump (Figure 49c). A number of motorised control valves are also placed to control the system's operation modes and strategies (Figure 49d).

Figure 49: (a) SG (b) Feed water tank (c)Variable speed pump (d) Control valves.

For the evaluation of the system, various sensors were used to measure a large number of parameters such as:

- the temperature of the HTF at the outlet of the collector and at various points throughout the system's workflow
- the temperature of the CTES modules at various locations
- the pressure at the SG
- the pressure at the variable speed pump
- the mass flow rate at the variable speed pump and from the feed water tank to the SG
- the power of the PTC, CTES, SG (see section 3.2.1)
- the pressure at the outlet of the collector

The main variable measured and analyzed for evaluating the system is the temperature at different parts of the system. For the temperature measurements, isolated thermocouples Type K, were used with the specifications shown in Table 11.

Table 11: Specifications of the thermocouples.

Type	K
Range	-250 °C to 1200 °C
Accuracy	± 0.5 °C
Resolution	0.1 °C (1 μV)
Accuracy	-250 το 1200 °C: ±0.5%

Regarding the temperature of the CTES, 24 measurement points were set to record the temperature of both the fluid in the storage and the concrete itself, shown in Figure 50. All measurements were performed with a time interval of 1 minute and the data were stored at the main processor in the control unit, which was accessible for analysis at any time.

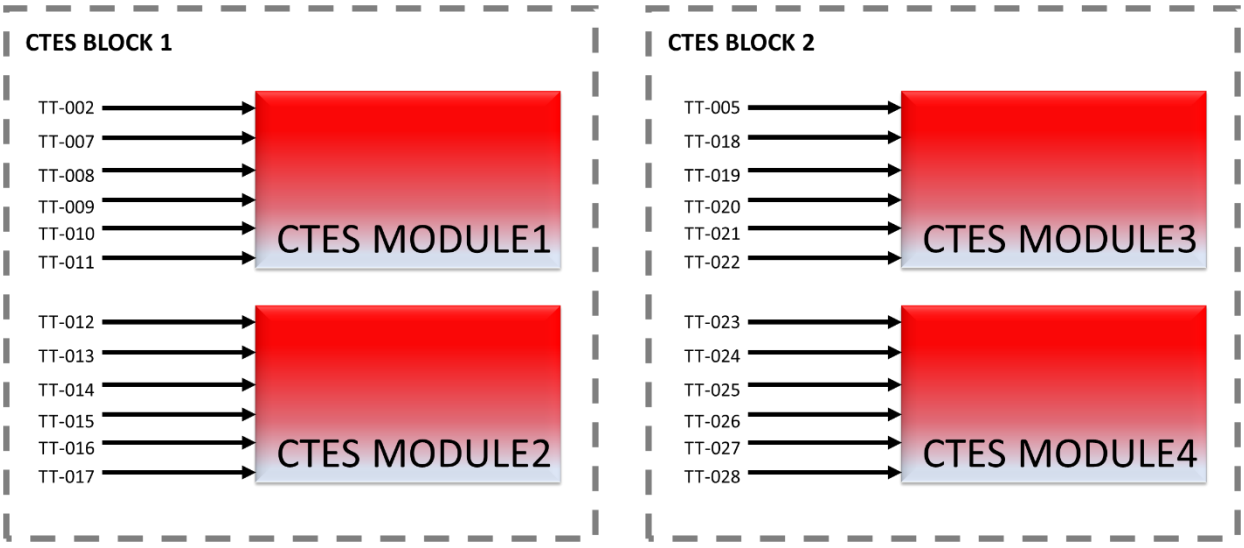

Figure 50: Measurement points to record the temperature through CTES.

To investigate the system's performance, in addition to the various sensors installed on the various parts of the system, a weather station, as shown in Figure 51a provided by Solar-Institut Julich (University of Applied Sciences, 2020) is used. The station consists of a wind mast where an anemometer and a wind direction vane are installed to measure the wind velocity and direction (Figure 51b). A rotating shadow band radiometer is installed on the control box (constructed by

CSP Technology) to measure the direct, ground, and diffuse solar irradiation (Figure 51e). A temperature, RH probes (Figure 51c) and a rain gauge (Figure 51d) are also installed to measure the ambient temperature and relative humidity and rainfall. All measured data are sent to the PC400 software and then transferred directly to the computer system in the control room. Finally, the control box is fed by a battery, which a 50W PV-panel charge.

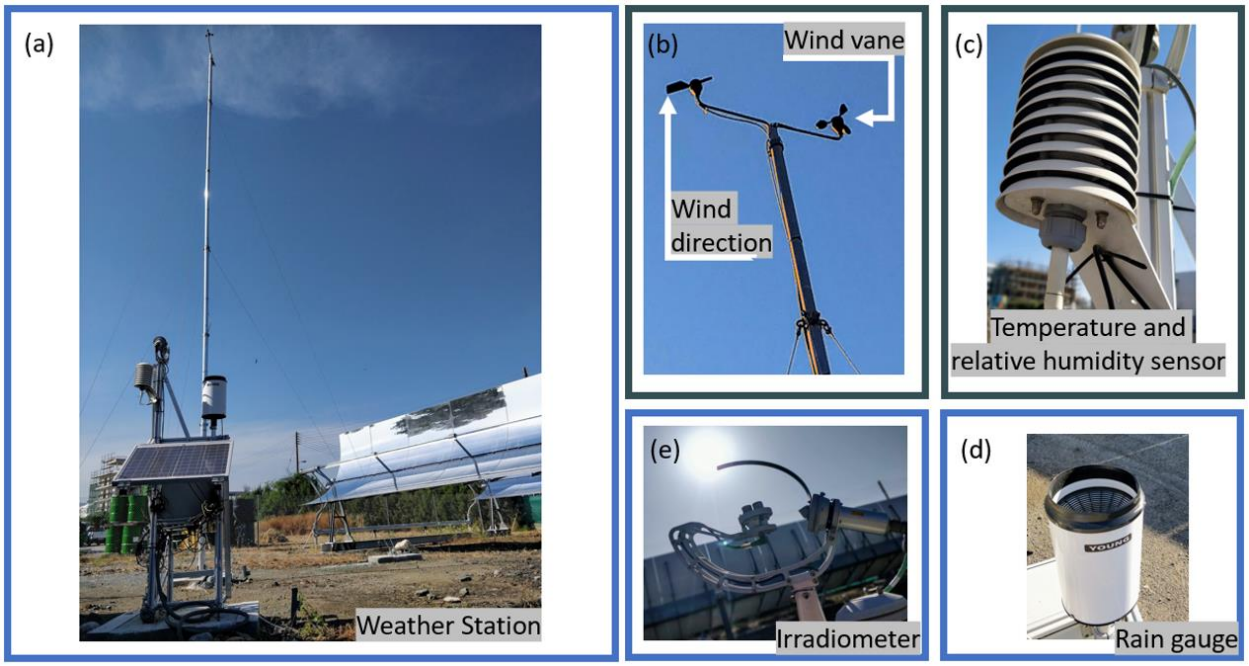

Figure 51: (a) Anemometer and wind direction vane, (b) Temperature & RH probes, (c) Rain gauge. (d) Irradiometer (e) Weather station.

When the system installation was completed, several operation tests have been done to define the optimum operation modes and strategies, which will be analyzed in section 3.2. The purpose of those tests was to investigate the behavior of the system under the steam production process, charging the CTES and providing steam to the SG from the CTES. Therefore, some significant conclusions drawn from the first operational tests are:

i. The SG needs around 1 hour to increase its pressure (Pr_{steam}) at 10 Bar_g when the CTES supplies the steam (Figure 52a).
ii. The PTC thermal power (P_{PTC}) varies from 100 kW_{th} to 140 kW_{th} during peak hours (Figure 52b).

iii. The maximum HTF outlet temperature ($T_{PTC,o}$) is around 350 °C with a mass flow rate of 0.7 kg/s during peak hours (Figure 52c).

iv. The PTC outlet temperature ($T_{PTC,o}$) increases by 200 °C up to 7:30 during the early morning hours with a DNI around 250 W/m^2 (Figure 52d).

v. The CTES temperature ($T_{CTES,av}$) increases by about 10 °C – 15 °C per hour during charging (Figure 52e).

vi. The maximum $T_{PTC,o}$ measured from the experiments carried out was 415 °C (Figure 52f).

vii. The water consumption for the mirror cleaning is 7-8 m^3 per year.

viii. The maximum steam production measured from the experiments carried out was 1 ton.

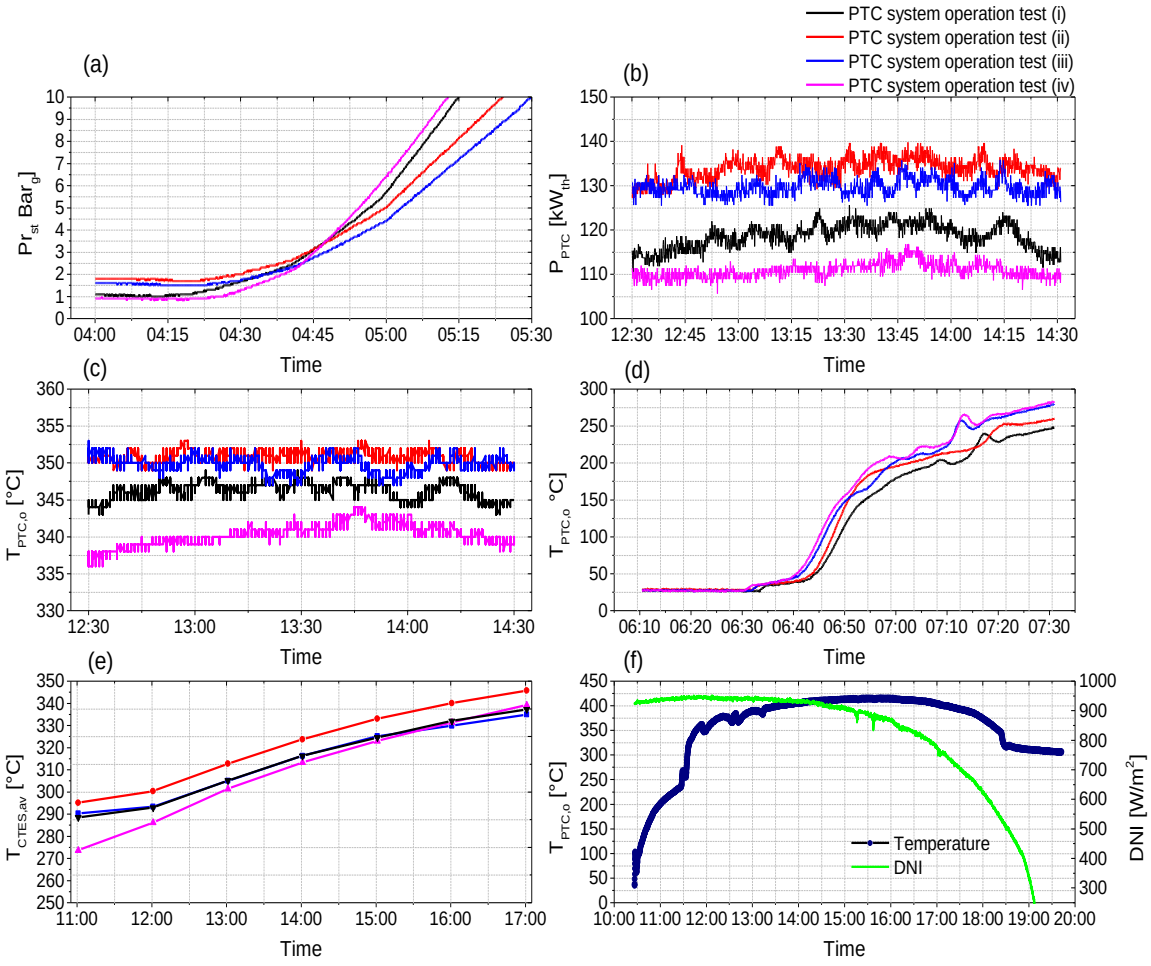

Figure 52: First operation test (random selection from one-year tests); (a) Pr_{st} at the early morning hours, (b) P_{PTC} during peak hours, (c) $T_{PTC,o}$ during peak hours, (d) $T_{PTC,o}$ at the early morning hours, (e) $T_{CTES,av}$ during charging days, (f) Maximum $T_{PTC,o}$ measured from the experiments carried out.

The final system was the key start of this study, to be used as a demonstration plant. The purpose is to use the knowledge earned from the installation and first operation tests procedure in order to investigate the system's performance experimentally and then develop a dynamic simulation model that will be later on validated with real monitored data.

3.2 PTC system operation strategies and operation modes

The way that the components described above interact is determined by the operation modes covering all the possible strategies of an operating day. The overall scope is to exploit the input solar energy at maximum to produce steam when needed and collect the available solar energy and store it in the CTES when there is no steam demand.

A schematic diagram of the system is shown in Figure 53. In general, the incident rays of the sun fall on the parabolic reflector, which has a reflectivity close to 95%, and the DNI is concentrated on the absorber tube where the HTF is circulating. The HTF is then directed to the SG or to the CTES, depending on the operation modes. As shown in Figure 53, the CTES is connected in parallel and it is enabled according to the operation modes with the help of various electric valves. It should be noted that in Figure 53, V denotes valve and T the temperature measurement point. As already mentioned, there are 24 temperature measurement points in the CTES module, 6 in each one, as shown in Figure 53 for module 1, only for clarity.

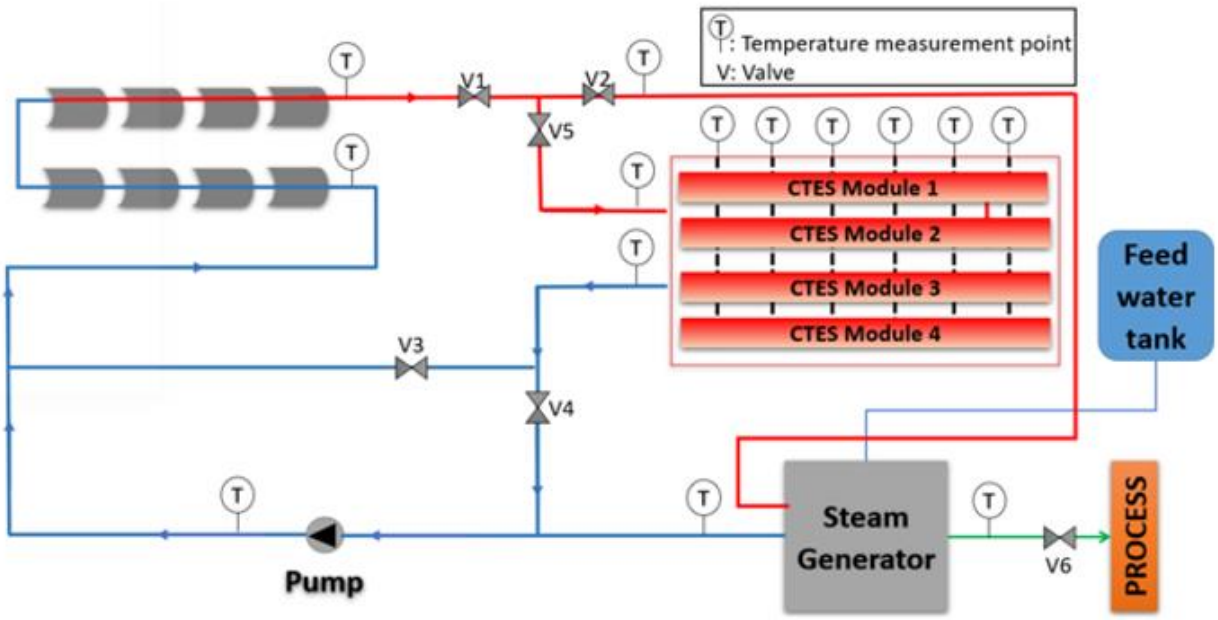

Mode	Pump	V1	V2	V3	V4	V5	V6
TES Cold Start	ON	C	O	O	C	R	C
TES Discharge	ON	C	O	O	C	R	O
TES Discharge and SF recirculation	ON	R	O	O	C	R	O
TES Discharge and Generation	ON	R	O	O	C	R	O
Generation	ON	O	O	C	O	C	O
TES Charge	ON	O	C	C	O	O	C
SF Preheating	ON	R	O	C	C	C	C
Plant Off	OFF	O	C	C	O	C	C

Note:
O: open
C: close
R: regulated

Figure 53: System workflow configuration and table showing the valve's condition for the various modes of operation.

To achieve the different operation strategies, individual operation modes have been developed and optimized for the whole system. Depending on the operation mode and strategy, the corresponding valves are opened or closed. The scope of these modes and strategies is to make the system dispatchable and autonomous. The only constraint is that the system must always follow the steam demand according to the production shifts of the industry.

Thus, the KEAN industry operation is divided into two strategies, one from Monday to Friday with a need of steam demand at 188 °C and 10 Bar_g from 5 am to 3 pm and one during the weekend with no steam demand. Consequently, Strategies 1 and 2 have been developed to satisfy the thermal needs of the industry from Monday to Friday and to charge the CTES on Saturday and Sunday. The two operation strategies are shown in Figure 54.

During the two strategies, various modes are enabled and disabled based on the temperature of the HTF, the average temperature of the CTES, the energy needs of the factory processes and the solar radiation availability.

It is significant to note that the final operation modes and strategies were decided after several tests and optimizations to achieve the best PTC system performance. The two strategies are as follows:

- Strategy 1 enables the following modes: TES Cold-Start Mode, TES Discharge Mode, TES Discharge and SF Recirculation Mode, TES discharge and Generation Mode, Generation Mode and TES Charging Mode (blue colored process in Figure 54).
- Strategy 2 enables the following modes: SF Preheating Mode and TES Charging Mode (brown colored process in Figure 54).

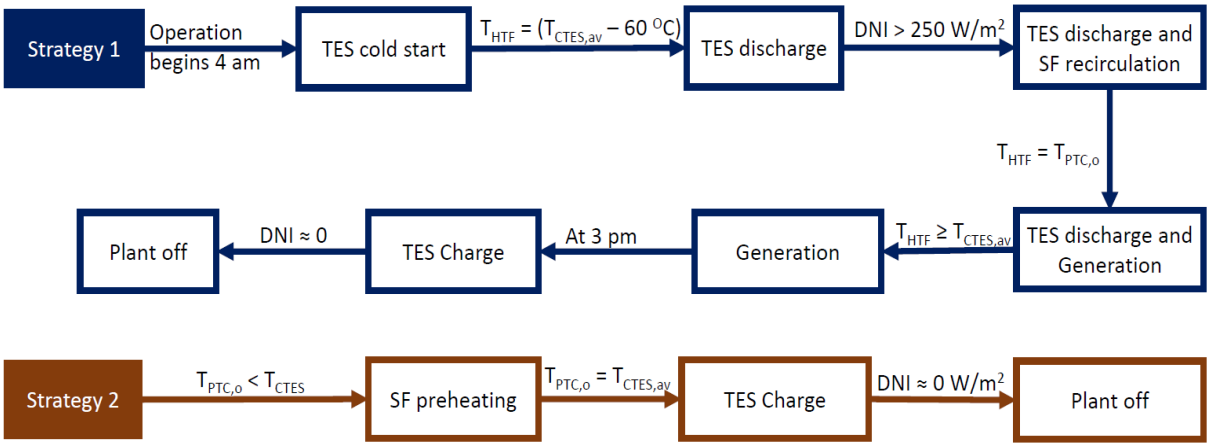

Figure 54: System operation strategies and operation modes.

Strategy 1 is enabled at 4 am and the system is set on the 'TES Cold-Start Mode'. During this mode, the thermal energy stored in the CTES is transferred to the SG with the circulation of the HTF between the CTES and the SG. This mode is used to increase the HTF temperature from 35

°C until it has a temperature difference of 60 °C from the CTES. To achieve this increment, without damaging the concrete structure (cracking), the process is ramped up slowly, with a low mass flow rate and by controlling Valve 5 opening (valve numbers are shown in Figure 53). At the same time, the SG pressure is also increased. As the HTF temperature rises to a difference of 60 °C from the CTES and the time is 5 am the 'TES Discharge Mode' is enabled. If by 5 am this temperature is not achieved, some more time is allowed until this temperature is reached. This mode is enabled while the solar radiation is close to zero and the HTF flows from the CTES directly to the SG at 50% pump speed to provide the required power at the desired steam temperature and pressure. This mode ensures steam provision from the solar system (actually from CTES) to the industry when the solar radiation is zero. Valves 1 and 4 remain closed during this process and Valves 2, 3 and 6 are fully opened. As the solar radiation is increasing both troughs are set on tracking mode, and the 'TES Discharge & SF Recirculation Mode' and 'TES Discharge & Generation Mode' are enabled. In the first hybrid mode the energy is transferred from the CTES to the SG for steam production and the HTF is circulated through the SF to increase its temperature. As the HTF temperature homogenize while circulating through the system, the 'TES Discharge & Generation Mode' is enabled. To achieve this mode Valves 2, 3 and 6 open and Valve 4 closes. Additionally, Valves 1 and 5 are regulating.

When the temperature of the HTF coming from the SF ($T_{PTC,o}$) is greater than the CTES average temperature ($T_{CTES,av}$) 'Generation Mode' is enabled. This is done automatically based on the HTF temperature and the pressure difference which is controlled by the valve openings. In this mode the HTF circulates through the SG and the SF, transferring the energy collected to the SG. The feed water tank supplies make-up water at ambient conditions to the SG, and steam is produced from the SG and delivered to the industrial processes. During this mode, the system operates with a HTF collector outlet temperature around 350 °C that corresponds to 125 kW_{th} of power to produce steam at 10 Bar_g (±0.2 Bar_g). This mode is enabled until 3 pm where the industry production shift ends. During 'Generation Mode' Valves 1, 2, 4 and 6 are open and Valves 3 and 5 remain closed.

After 3 pm the solar radiation is still high and the system turns automatically to the 'TES Charge Mode'. During this mode the SG is isolated and the HTF is circulating through the SF and CTES transferring the energy collected to the CTES. In charging mode Valves 2 and 3 remain closed

and Valve 1, 4 and 5 remain open. Subsequently, when the solar radiation is insufficient, around 6:30 pm, the plant is set to off until the next day at 4 am, where the cycle is repeated. The analytical description of the various steps of the operational strategy is shown in Table 12.

On Saturday and Sunday, as there is no steam demand from the industry, the system works with Strategy 2. When the solar radiation increases, both troughs are on tracking mode and the SF is preheating. When the HTF temperature gets equal to the average CTES temperature, Valve 5 opens and the 'TES Charge Mode' is enabled until the solar radiation is sufficient. The analytical description of the various steps of the operational strategy 2 is shown in Table 13.

Table 12: Analytical description of the various steps of the operational strategy 1.

Mode	Thermal Energy Transfer	Mode Change Conditional Statement	V1	V2	V3	V4	V5	V6
TES COLD START MODE	From CTES to SG	$T_{HTF} = (T_{CTES,av} - 60\ °C)$	C	O	O	C	R	C
TES Discharge	From CTES to SG	DNI > 250 W/m^2	C	O	O	C	R	O
TES Discharge and SF recirculation	From CTES to SG and SF	$T_{HTF} = T_{PTC,o}$	R	O	O	C	R	O
TES Discharge and Generation	From CTES to SG and SF	$T_{HTF \geq} T_{CTES,av}$	R	O	O	C	R	O
Generation	From SF to SG	Up to 3 pm	O	O	C	O	C	O
TES Charge	From SF to CTES	DNI ≈ 0 W/m^2	O	C	C	O	O	C
Plant Off	OFF		O	C	C	O	C	C

Table 13: Analytical description of the various steps of the operational strategy 2.

Mode	Thermal Energy Transfer	Mode Change Conditional Statement	V1	V2	V3	V4	V5	V6
SF Preheating	From SF to SG	$T_{HTF} = T_{CTES,av}$	ON	R	O	C	C	C
TES Charge	From SF to CTES	DNI ≈ 0 W/m^2	O	C	C	O	O	C
Plant Off	OFF		O	C	C	O	C	C

The motorized control valves are also placed in such a way to control the system's operation modes and strategies as presented in Figure 53. It is important to mention that the developed operation modes and strategies do not cover the case of a long period of insufficient solar radiation. For instance, if there is insufficient solar radiation during the early morning hours, the system will produce steam from the TES discharge mode but if there is lower radiation later, the production will continue from the TES discharging mode until pressure of the SG is less than 10 Bar_g which means that thermal energy from the CTES is exhausted. Then, the system will be turned off manually by the plant operator. This case is considered in the dynamic simulation model that will be presented in the next chapter and it is also planned to be considered in the second phase of the operation strategies planning which has started on September 2021 as part of the second phase of the EU project. On the contrary, when there is excess heat from the collector, the system cannot charge the CTES and produce steam at the same time. This case is again considered in the dynamic simulation model and results are presented in Chapter 5.2.

On-site data measurements from the system are analyzed in order to evaluate the various operation modes involved in the two operation strategies. Two clear days during the summer period were selected for evaluation for the two strategies as described in the next two sections.

3.2.1 Performance Evaluation: Strategy 1

For the evaluation of Strategy 1, one typical day during summer is examined. Figure 55 shows the steam pressure (Pr_{st}) in the steam line, the DNI, the temperature of the HTF at the outlet of the collector ($T_{PTC,o}$), the temperature of the HTF circulating in the CTES ($T_{charging,discharging}$) and the average temperature of the CTES ($T_{CTES,av}$) concerning this day, for Strategy 1.

At 4 am, the system is in the 'TES Cold-Start Mode'. As the solar radiation is zero, the CTES heats the HTF slowly to 236 °C and the steam pressure rises to 5.1 Bar_g. The $T_{CTES,av}$ at that time is 279 °C in that particular day. As the HTF had a temperature difference of less than 60 °C compared to that of CTES, the system is turned to the 'TES Discharge Mode' at 5 am. From 5 am to 6:30 am, steam is produced solely from the CTES. The steam pressure has raised to 10 Bar_g and the HTF temperature was 242 °C by 6:30 am. Then as the solar radiation is increased, the HTF temperature in the SF, which is at ambient temperature, must homogenize with HTF

circulating from the CTES. Both troughs are set on tracking mode and the hybrid mode 'CTES Discharge and SF Recirculation Mode' is enabled until 7:42 am, when the temperature of the HTF of the whole system is homogenized at 233 °C. Then, the 'TES Discharging and Generation Mode' is enabled, producing steam up to 8 am. At that time, the $T_{PTC,o}$ was 259 °C and exceeded the $T_{CTES,av}$ which was 253 °C. Consequently, the system turns to the 'Generation Mode' with steam production only from the SF until 3 pm. During this time, the $T_{PTC,o}$ was maintained at 350 °C to satisfy the SG parameters. The 'Generation Mode' was operating in an average DNI of 783 W/m^2. Later on, at 3 pm, the 'TES Charge Mode' is initiated until sunset and the $T_{CTES,av}$ increased from 245 to 282 °C for an average DNI of 756 W/m^2. Finally, the $T_{CTES,av}$ was 284 °C at 4 am, and droped to 245 °C at 3 pm and through the charging mode which started at 3 pm and ended at 6:30 pm, it was raised again to 284 °C. The temperatures and hours referred to the day analyzed here regarding the various actions of the system, are very similar for every day of the week, except weekends.

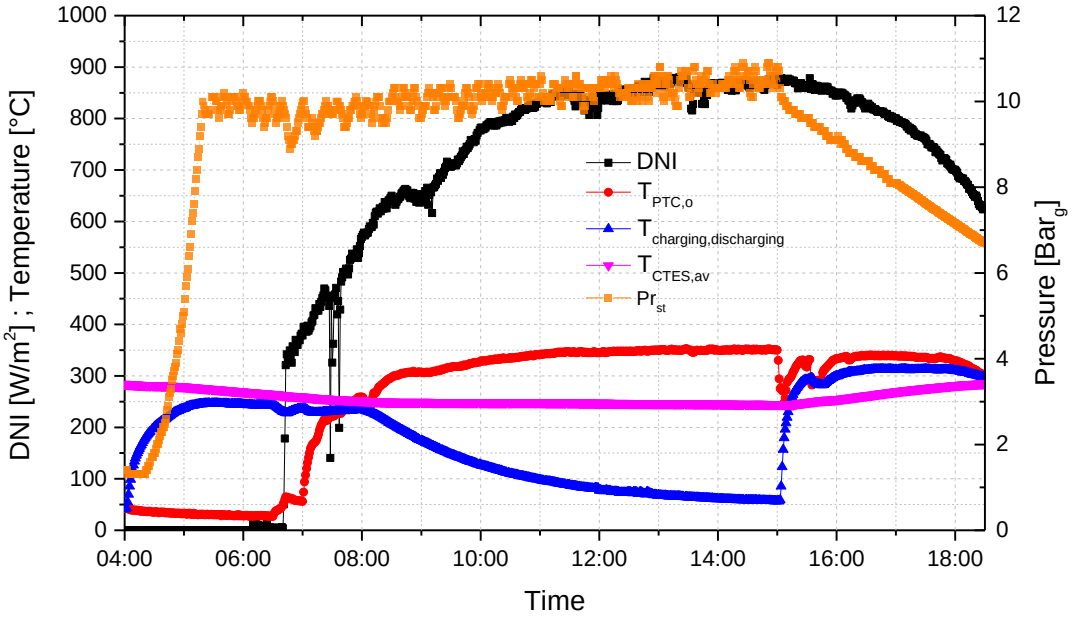

Figure 55: Variation of the HTF temperature, DNI and steam pressure with respect to time during the operation Strategy 1.

Figure 56 shows the power produced from the collector (P_{PTC}), the power of steam production from the SG (P_{SG}) and the power transfer from and to the CTES (P_{CTES}). As can be observed,

there is an uninterrupted steam supply from 5 am to 3 pm, proving that the PTC system can satisfy the thermal needs of the industry according to the production shifts.

The CTES makes the system dispatchable as in the early morning hours, although there is no solar radiation, the system can produce steam. For that reason the P_{CTES} appears to have negative values on the graph at the early morning hours, due to the energy which is transferred from the CTES to the SG (and later to the SF) and after 3 pm has positive values due to the energy transferred from the PTC to the CTES for charging purposes. Additionally, the P_{PTC} in the early morning hours is also negative, since the energy is transferred from the CTES to the SF in order to homogenize the HTF temperature.

The P_{CTES}, P_{PTC} and the P_{SG} (all in kW) are calculated using the following equations:

$$P_{CTES} = \dot{m}_{HTF} \cdot c_{p,HTF} \cdot (T_{CTES,o} - T_{CTES,i}) \quad \textbf{Eq. (1)}$$

$$P_{PTC} = \dot{m}_{HTF} \cdot c_{p,HTF} \cdot (T_{PTC,o} - T_{PTC,i}) \quad \textbf{Eq. (2)}$$

$$P_{SG} = \dot{m}_{w} \cdot c_{p,w} \cdot (T_{st,o} - T_{w,i}) \quad \textbf{Eq. (3)}$$

Where $\dot{m}$ is the mass flow (kg/s), c_p is the specific heat (kJ/kg·K), $T_{CTES,i}$ is the temperature of the HTF at the inlet of the CTES (°C), $T_{CTES,o}$ is the temperature of the HTF at the outlet of the CTES (°C), $T_{st,o}$ is the steam temperature at the outlet of the SG (°C) and the $T_{w,i}$ the temperature of the water entering the SG (°C).

The steam produced for the examined day is 940 L which is calculated by measuring the quantity of the make-up water. For this particular day, the total thermal energy produced by the SG (Q_{st}) was estimated to be around 601 MJ. The total thermal energy stored (Q_{CTES}) from 3 pm to 6:30 pm was calculated using Eq. (4) and is equal to 77.5 kWh_{th}.

$$Q_{CTES} = \sum \dot{m}_{HTF} \cdot c_{p,HTF} \cdot (T_{CTES,av,j+1} - T_{CTES,av,j}) \quad \textbf{Eq. (4)}$$

The $T_{CTES,av,j}$ is the average temperature from the 24 thermocouples installed at various heights of CTES at any time j, and $T_{CTES.av,j+1}$ is the average temperature from the 24 thermocouples at various heights of CTES after an interval of one minute.

Furthermore, it is significant to examine the performance of the system during the steam production process. Firstly, the incident power absorbed by the collectors (P_{inc}) is estimated by:

$$P_{inc} = \text{DNI} \cdot \text{N} \cdot \text{L} \cdot \text{w} \qquad \text{(kW)} \qquad \textbf{Eq. (5)}$$

Where N is the number of collectors. L is the length, and w is the width of each collector.

The energy efficiency of the collector ($\eta_{ene,PTC}$), is estimated using Eq. (6). As shown in Figure 56 the energy efficiency of the PTC in an average DNI of 781 W/m^2 is 47%.

$$\eta_{ene,PTC} = \frac{P_{PTC}}{P_{inc}} \qquad \textbf{Eq. (6)}$$

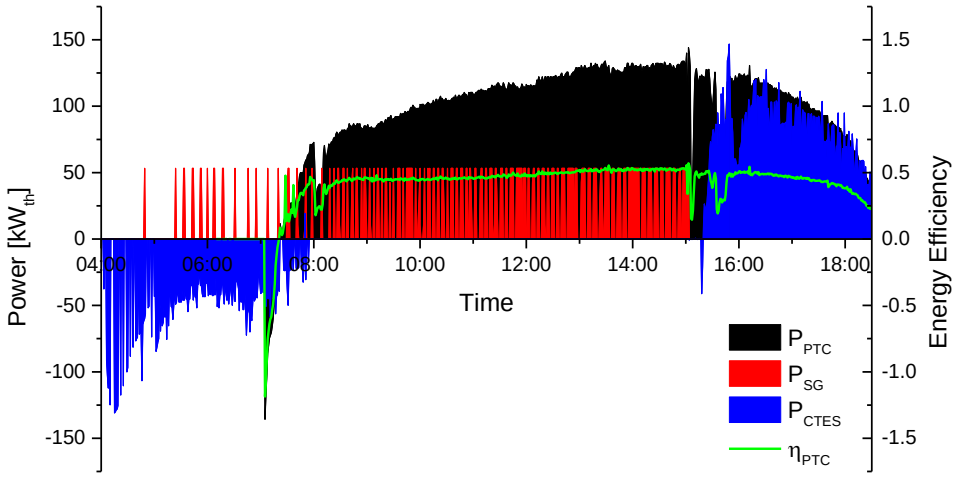

Figure 56: Variation of the PTC, CTES, steam power and the PTC efficiency with respect to time during Strategy 1.

Although energy analysis is a widespread method to evaluate the performance of the system, it is significant to estimate the exergy of the system as well (Kumar et al., 2012). Exergy analysis is a methodology for the evaluation of the performance of devices and processes and involves the examination of the exergy at different points of the various energy conversion steps of any system and procedure. Most of the times exergy analysis is done to estimate the magnitute of exergy destruction which identifies the location and magnitute of thermodynamic inefficiencies in a thermal system. Normally energy and exergy analyses involve balance equations for each control volume of the system at steady state conditions including or not the potential and kinetic energy changes of the various systems or sub-systems. Herein, an exergy analysis is carried out estimating the exergy change at the various systems of the thermal plant.

The exergy change of the HTF in the receiver ($\dot{E}x_{PTC}$), the exergy change of the HTF in the SG ($\dot{E}x_{SG}$), and the exergy change of the HTF in the CTES ($\dot{E}x_{CTES}$), are calculated using the following equations (kW):

$$\dot{E}x_{PTC} = \dot{m}_{HTF}\left(\dot{E}x_{HTF,PTC,o} - \dot{E}x_{HTF,PTC,i}\right) = \dot{m}_{HTF}\left[\left(h_{HTF,PTC,o} - h_{HTF,PTC,i}\right) - T_a\left(s_{HTF,PTC,o} - s_{HTF,PTC,i}\right)\right] \quad \textbf{Eq. (7)}$$

$$\dot{E}x_{SG} = \dot{m}_w\left(\dot{E}x_{st,o} - \dot{E}x_{w,i}\right) = \dot{m}_w\left[\left(h_{st,o} - h_{w,i}\right) - T_a\left(s_{st,o} - s_{w,i}\right)\right] \quad \textbf{Eq. (8)}$$

$$\dot{E}x_{CTES} = \dot{m}_{HTF}\left(\dot{E}x_{HTF,CTES,\iota} - \dot{E}x_{HTF,CTES,o}\right) = \dot{m}_{HTF}\left[\left(h_{HTF,CTES,\iota} - h_{HTF,CTES,o}\right) - T_a\left(s_{HTF,CTES,\iota} - s_{HTF,CTES,o}\right)\right] \quad \textbf{Eq. (9)}$$

Where h and s are the enthalpy (kJ/kg) and the entropy (kJ/kg·K) of the HTF outlet and inlet at the various systems of the thermal plant.

Furthermore, the rate of exergy received by the concentrator, ($\dot{E}x_{inc}$) can be estimated by (Kalogirou et al., 2016):

$$\dot{E}x_{inc} = P_{inc}\left[1 - \frac{4T_a}{3T_{sun}}(1 - 0.28\ln f)\right] \quad \text{(kW)} \quad \textbf{Eq. (10)}$$

Where the T_α, T_{sun} is the ambient temperature and sun temperature in Kelvin, and *f* is the dilution factor equals to 1.3 x10^{-5}, which measures the mixing ratio of solar radiation from the sun (T_{sun}) and radiation from the surroundings.

Subsequently, the exergy efficiency of the PTC $\eta_{exe,PTC}$ is given by Eq. (11) and it is estimated to be around 23% during the steam production process.

$$\eta_{exe,PTC} = \frac{\dot{E}x_{PTC}}{\dot{E}x_{inc}} \quad \textbf{Eq. (11)}$$

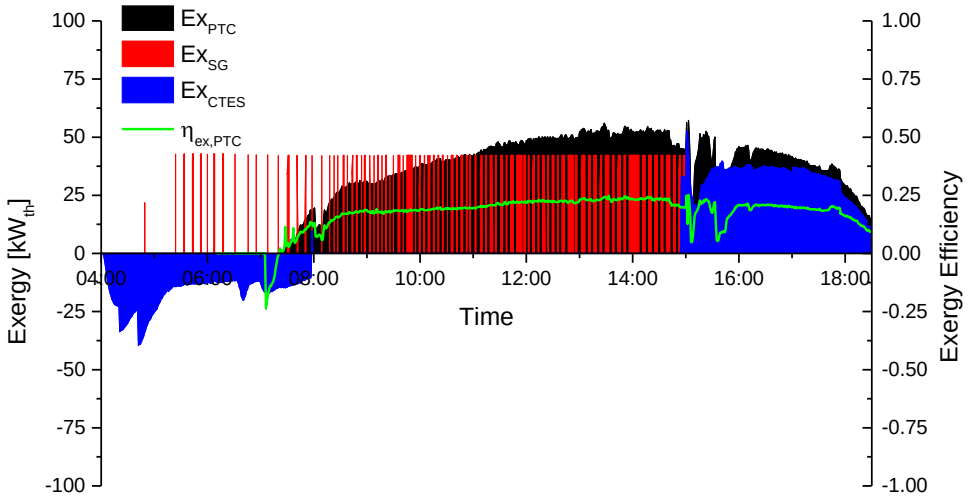

Figure 57: Variation of the Exergy of PTC, CTES, SG and the PTC exergy efficiency with respect to time during Strategy 1.

In conclusion, the main part of the system responsible for this is the PTC since only 23% of the received exergy by the concentrator could be converted to useful exergy. The main reasons could be the optical efficiency of the receiver, the heat transfer coefficient of the HTF, the circulated HTF mass flow rate, and the cleanliness of the concentrator. The most common reason for this kind of collector is the heat losses from the HTF to the surroundings and the thermal differential in the flow direction (Kalogirou et al., 2016; Kumar et al., 2020; Mansour et al., 2018).

3.2.2 Performance Evaluation: Strategy 2

Regarding the operation Strategy 2, Figure 58 shows the DNI, the $T_{PTC,o}$, the $T_{charging,discharging}$ and the $T_{CTES,av}$ concerning one day of Strategy 2.

As can be seen, the preheating of the HTF occurs from 10 am to 11 am with an average DNI of 755 W/m^2 and the $T_{PTC,o}$ increased from 41 °C to 296 °C. As the $T_{PTC,o}$ was equal to the $T_{CTES,av}$ (296 °C) the 'TES charge mode' is enabled until sunset. The $T_{CTES,av}$ was thus increased from 296 °C to 348 °C during this particular day which has an average DNI of 753 W/m^2.

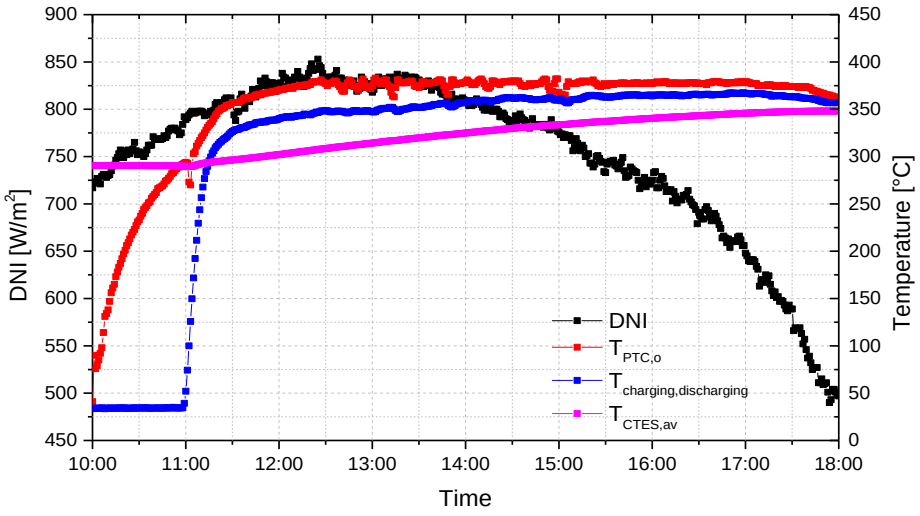

Figure 58: Variation of the HTF temperature, DNI and steam pressure with respect to time during the operation Strategy 2.

Figure 59 shows the P_{PTC}, the P_{CTES} and the η_{PTC} estimated using the equations (2), (1), and (6) respectively. As can be observed, at 11 am for 10 minutes the P_{CTES} is negative because of the HTF which was in the pipe just outside the CTES, passing from Valve 5 to the CTES, where although there is thermal insulation, it is exposed to ambient conditions. Thus, it took 10 minutes to the HTF temperature to homogenize with the overall HTF temperature. The Q_{CTES} for 7 hours of operation during Strategy 2 was 107.3 kWh_{th}, estimated with Eq. (4). The η_{PTC} varied from 35% to 48% (Figure 59) and the average η_{PTC} during the day is equal to 39%.

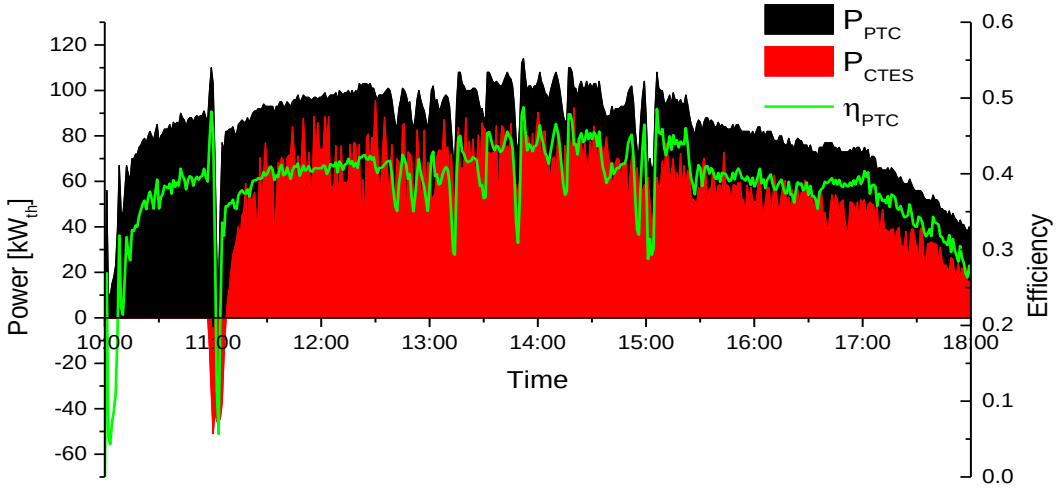

Figure 59: Variation of the PTC, CTES power and the PTC efficiency with respect to time during Strategy 2.

3.2.3 Performance Evaluation: Strategies 1 & 2

The system is also examined for a longer period for two continuous months, from August to September. The various parameters for this period is shown in Figure 60. As can be seen from Figure 60, the system is operating at about 350 °C ($T_{PTC,o}$) and the average temperature of the fluid in the storage ($T_{CTES,av}$) is about 350 °C during the weekends and 200 °C on Fridays. As the CTES is charging after 3 pm every day, the system becomes dispatchable as it can follow the steam demand in the morning hours where there is no solar radiation. During August (Month 1) there is a gap during the production because of the summer holidays of the industry. During this period, the solar system was shut down and the two troughs remained parked not able to receive any sunshine. The total of steam produced during this period was 36 tons which corresponds to 23 GJ.

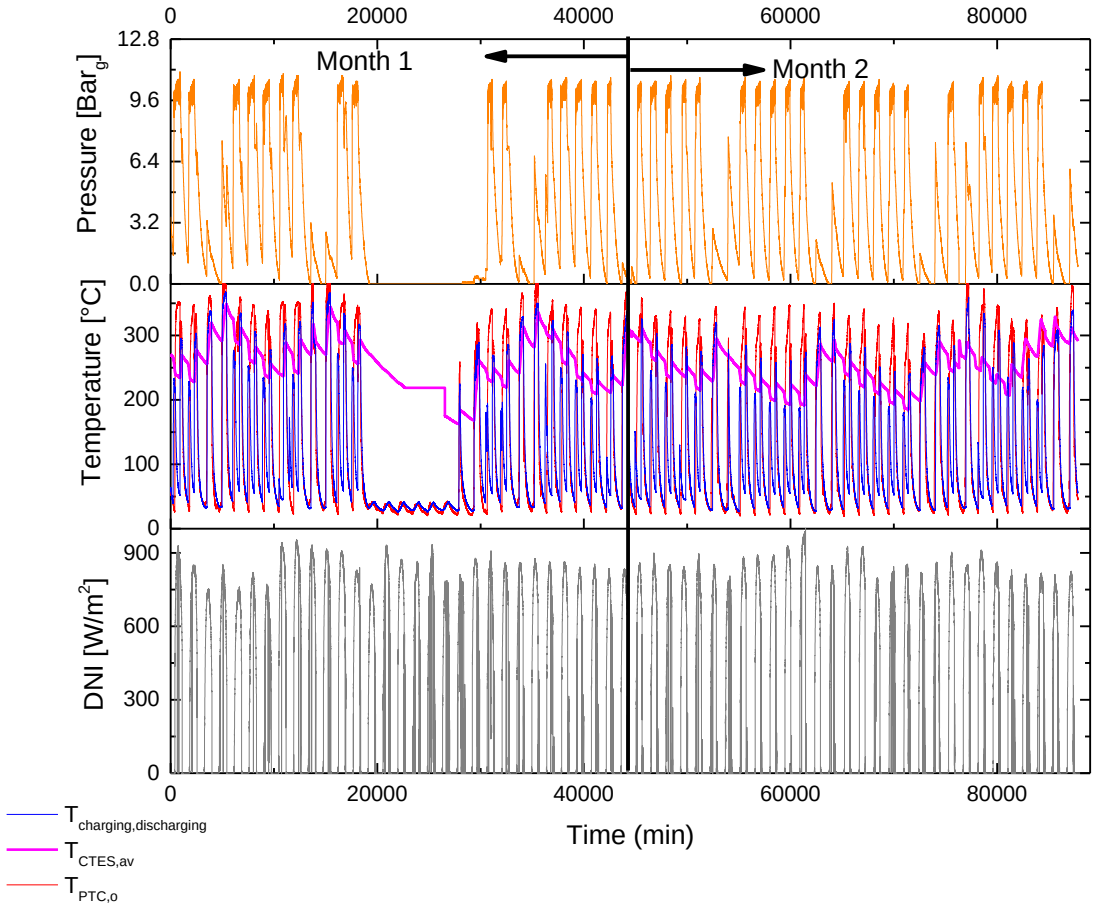

Figure 60: Variation of the HTF temperature, DNI and steam pressure with respect to time during two continuous months of operation (August, September).

3.3 Evaluation of the Concrete Thermal Energy Storage

Since CTES is one of the most important parts of the system, another test which have been carried out during the first operating period of the system is the CTES heat loss behavior when remained with no HTF distribution (i.e., without charging) for 209 hours. The ambient temperature during this period of 9 days is shown in Figure 61.

The temperature measured at the four blocks of CTES during this period of 209 hours that it was left uncharged is shown in Figure 62. The measured values are shown with uncertainty boxes since numerous thermocouples were measuring, as mentioned before. However, as can be seen, the CTES average temperature dropped from 268 °C to 132 °C during this period. From Figure 63 which shows the CTES temperature drop for 9 days, it can be observed that during the 1st and 2nd day the temperature drop was around 23 °C and later it was less than 17 °C per day.

The overall heat losses (U_{loss}) for a temperature drop of 10 °C for the four CTES modules are calculated using Eq. (12) and it is shown in Figure 64. As can be seen, the U_{loss} varies from 12 to 21 W/m^2·K for all four CTES modules. In Figure 62 - Figure 64, the asterix denotes extreme values, the square the mean value and the uncertainty boxes the most frequently appearing values.

$$U_{loss} = \frac{Q_{loss}}{A_{st} x LMTD} \quad \textbf{Eq. (12)}$$

Where A_{st} is the surface area of the storage blocks (m^2). The energy loss (Q_{loss}) and Log Mean Temperature Difference (LMTD) values are estimated with the Eq. (13) and (8) respectively:

$$Q_{loss} = \frac{m_{CTES} \cdot Cp_{CTES} \cdot \left(T_{CTES,j} - T_{CTES,j+1}\right)_{st}}{t} \quad \textbf{Eq. (13)}$$

$$LMTD = \frac{\left(T_{CTES,j} - T_a\right) - \left(T_{CTES,j+1} - T_a\right)}{\ln\left(\frac{T_{CTES,j} - T_a}{T_{CTES,j+1} - T_a}\right)} \quad \textbf{Eq. (14)}$$

Where, m_{CTES} is the mass of the concrete mixture in the CTES (kg), Cp_{CTES} is the specific heat of the concrete mixture (kJ/kg·K), t is the duration of the time step between the time intervals j

and j+1 which corresponds to 3600 s, T_{CTES} is the temperature measured from the thermocouples in the CTES at time steps j and j+1, and T_a is the ambient temperature (°C).

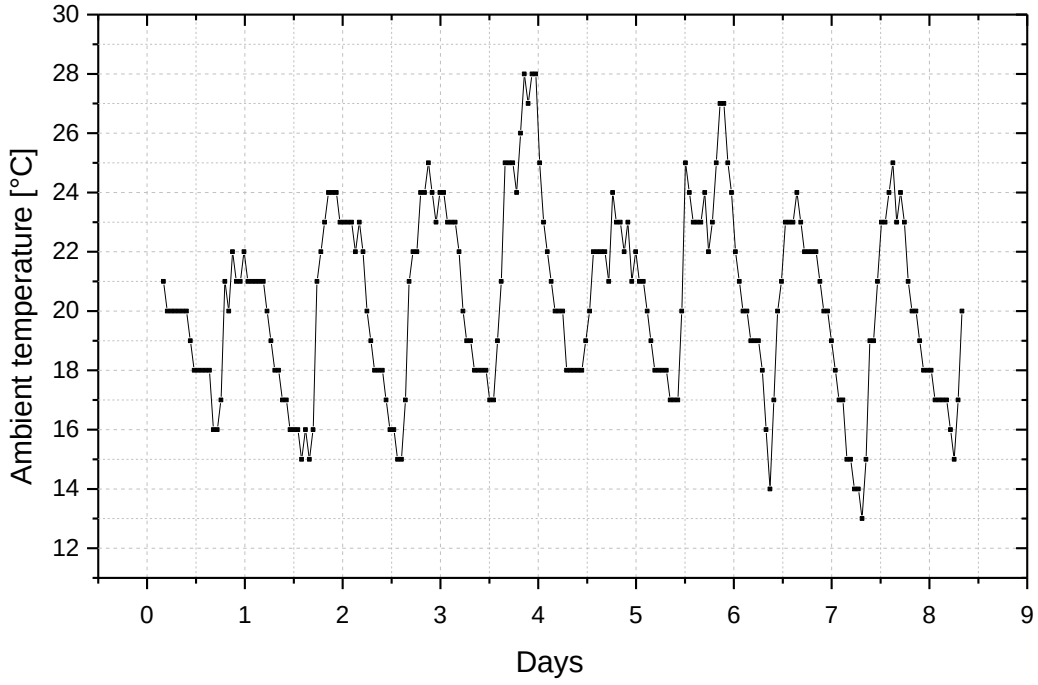

Figure 61. The ambient temperature during the CTES loss behavior test.

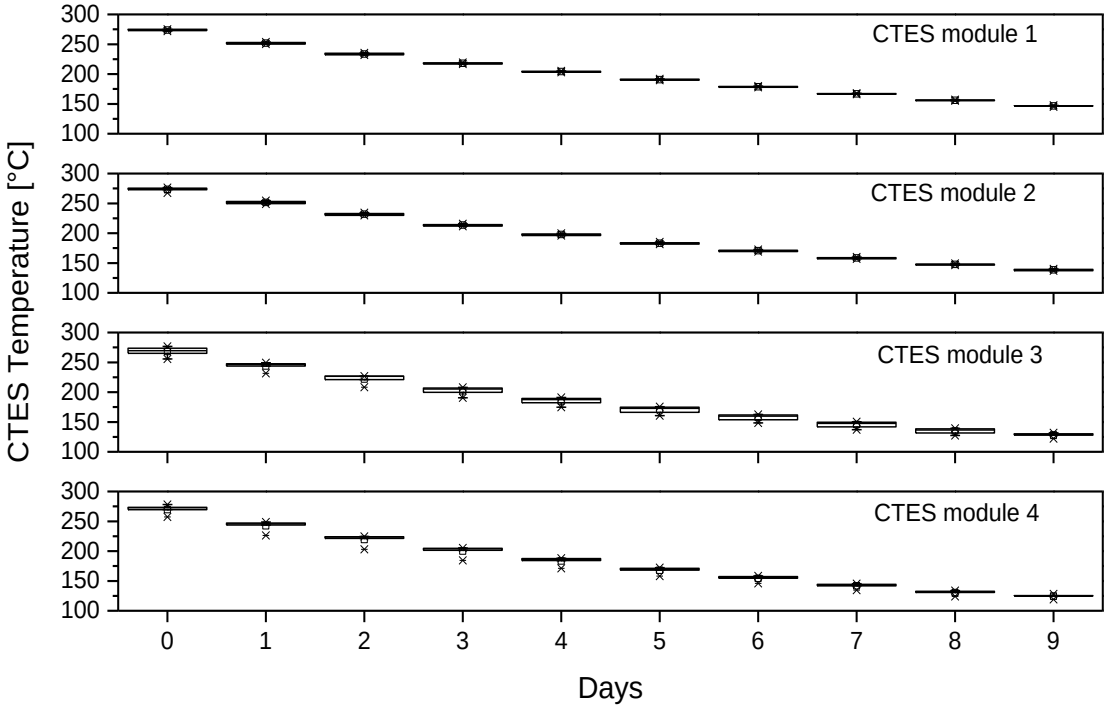

Figure 62. CTES blocks temperature over a period of 209 hours measured on-site.

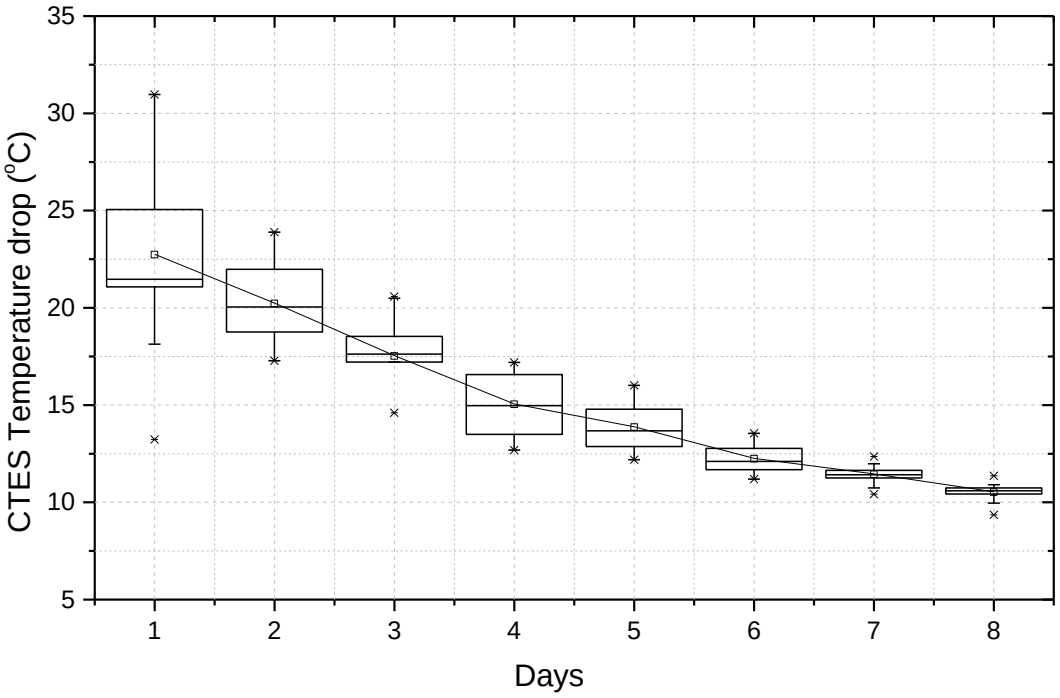

Figure 63. CTES temperature drop for 9 days.

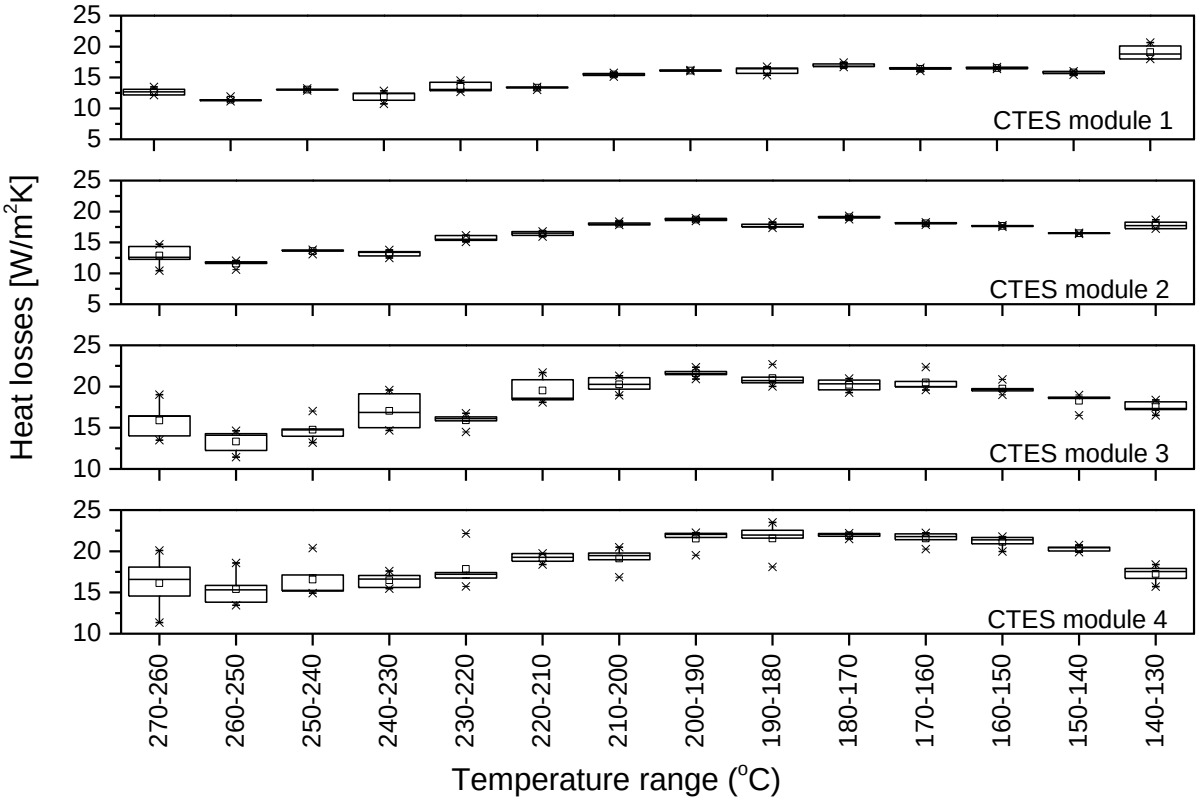

Figure 64. Heat losses estimation for each CTES module.

3.4 Mirror Reflectivity Measurements

Since all the above data were measured during the initial operating period of the system, the effect of the dust accumulation on the mirrors of the PTC had to be investigated as well. Mirror reflectivity measurements were performed using a Condor reflectometer from Abengoa Solar (Condor reflectometer, 2019). There are ten measurement points for each collector row along their length, where three sets of reflectivity measurements were taken. The measurement points are at the middle and at two edges of the mirrors at four different locations as shown in Figure 65.

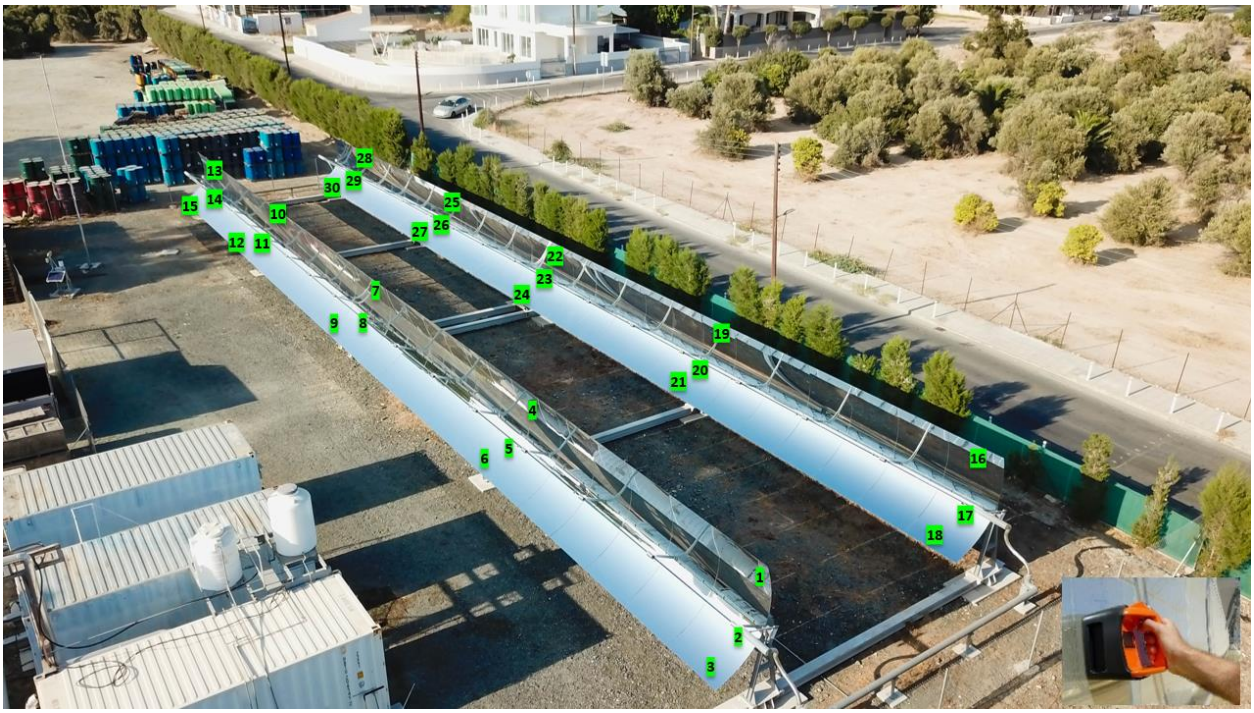

Figure 65: Reflectivity measurement points along the collector length.

In Figure 66a, the average reflectivity measurements during a year operation is presented. As can be seen, the weekly mirror cleaning make sure that the reflectivity drop is not exceeding 0.9. This ensures that the maximum percentage of incidence sun rays are reflected by the mirror and absorbed by the receiver tube. The mirror cleaning task is decided based on Figure 66b. The dirt coefficient is estimated to be 0.96, i.e., a drop of 4% from the clean value, thus the mirrors cleaning once a week keeps reflectivity at high levels. For the existing system, it was decided to use pressurized water for half an hour.

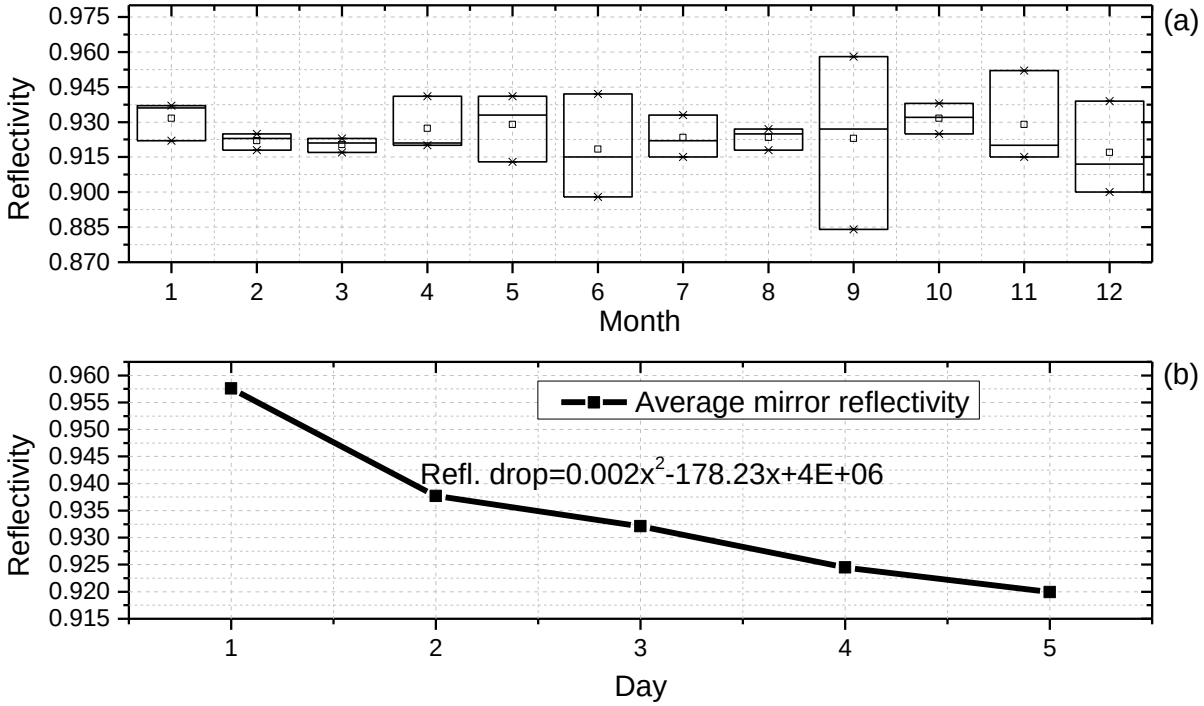

Figure 66: (a) Reflectivity measurements for a year (b) Reflectivity reduction in one typical summer week.

3.5 Discussion

This chapter presented the data obtained from the initial operating period of the first PTC system installed in Cyprus for IPH. The operation Strategies and Modes are explained, and real measured data were used to quantify the behavior of the system, not only on particular days but also in a longer period of two continuous months of operation. Furthermore, the CTES heat loss behavior was tested as well as the dirt mirror reflectivity coefficient.

More specifically, under the Strategy 1 with average DNI of 757 W/m^2, the CTES stored 77.5 kWh$_{th}$ in 3.5 hours and the PTC system produced 940 L of steam which is supplied to the factory for the various industrial process which corresponds to 601 MJ of energy. Additionally, from 5 am to 8 am the steam was produced from the energy stored in the CTES and from 8 am to 3 pm the steam was produced only from the PTC system. The CTES is charging after 3 pm every day and thus it can follow the steam demand in the morning hours where there is no solar radiation. Finally in the early morning hours when solar radiation is zero, the system is in the 'TES Cold-Start Mode' and the HTF is being heated from the CTES to 236 °C.

Under Strategy 2, on a day with average DNI of 753 W/m^2, the CTES temperature increased from 290 to 348 °C, the HTF temperature homogenized in 10 minutes, and the total energy stored in the CTES for 7 hours of operation was 107.3 kWh$_{th}$. The instantaneous PTC efficiency varied from 35%-48% and the average efficiency during the day was equal to 39%. For two months of operation, the total steam produced was 36 tons (23 GJ).

In the experimental procedure where the CTES left undisturbed and uncharged for 209 hours, its temperature dropped by 136 °C during this period. Although this is not a real problem, considering the solar radiation that prevails in Cyprus, there is no possibility for the system to be without solar radiation for such a long period, but the factory has its conventional boilers as a backup in the worst-case scenario. In addition, the overall thermal losses coefficient of the CTES vary from 12-21 W/m^2·K for a temperature drop of 10 °C.

Furthermore, reflectivity measurements taken on a daily basis when the mirrors were left uncleaned showed that the reflectivity dropped 4% during 5 days and thus it was concluded that they need to be cleaned once a week for half an hour with pressurized water.

Concerning the results presented, it can be concluded that the system responds perfectly to the Strategies and Modes developed to satisfy the particular needs of the factory. This is happening even in the early morning hours when there is no solar radiation, with the support of the CTES, which makes the system dispatchable. It is believed that such a system has great potential for countries with good solar resources since it is able to provide heat at the required pressure and temperature continuously.

CHAPTER 4

4 Dynamic Simulation Model Analysis

A dynamic simulation model was built in the TRNSYS simulation tool implementing all the operation modes and strategies of the system, in order to simulate the real operation conditions system. The simulation analysis can provide valuable information on the long-term performance of solar energy systems and system dynamics.

TRNSYS is a quasi-steady simulation model developed at the University of Wisconsin and is written in the FORTRAN computer language by the members of the Solar Energy Laboratory (TRNSYS, 2020). It includes a large range of system components called ‘Types’, such as solar collectors, differential controllers, pumps, hot water cylinders, etc. (Kalogirou, 2014b). These components are written by the TRNSYS developers and by independent engineering consulting companies specializing in the modeling and analyzing of innovative energy systems and buildings. Each component has a unique number and in the environment of TRNSYS studio it is represented as an image (which corresponds to the appropriate program). Types require several constant parameters and time-dependent inputs to produce time-dependent outputs. TRNSYS can interconnect its system components in any desired manner, solve differential equations, and facilitate information output. The components are interconnected with connecting lines that move the information between them (Kalogirou, 2014b). TRNSYS serves as a valid simulation

program for a real system and it is widely used for solar thermal system applications in the literature (see section 2.1.4).

The idea behind modelling with TRNSYS is to combine ready-made component models in such a way to construct a model that takes into account all parameters and variables affecting the operation of the system so as to behave the same way with the real system.

The developed model in this study is validated with real measurement data under different operation strategies, and it can be used for an extended operation period of one year (Ktistis et al., 2021). For the development of the dynamic model, various types have been used for several components such as the Type 536 for the PTC, Type 430 for CTES and Type 636 for the SG and several parameters and inputs were set and used to solve the various predefined equations in TRNSYS.

4.1 TRNSYS Simulation Model

Several parameters and inputs were set for the dynamic model development and used to solve the various predefined equations in TRNSYS. The simulation studio project of TRNSYS model is shown in Figure 68.

The developed model can simulate the real operation strategies and operation modes described in section 3.2 (Ktistis et al., 2021). The model can run continuously and alternate from Strategy 1 to 2 automatically, depending on the operation day. This is achieved with equations and load profiles that control the variable speed pump and corresponding valves of the system.

The load profiles introduced to the model are shown in Figure 67 :

i. System Profile: The variable speed pump is on from 4 am up to 7 pm from Monday to Friday and during the weekend from 10 am to 7 pm (Figure 67a).
ii. Charging Profile: The HTF charging the CTES from Monday to Friday from 3 pm to 7 pm and during the weekend from 11 am to 7 pm (Figure 67b).
iii. SG Profile: The SG profile is on from 4 am up to 3 pm and during the weekend from 10 am to 12 am (Figure 67c). This is done to preheat the HTF to the CTES temperature by circulation the HTF between the PTC and the SG. Once the CTES temperature is reached the fluid is directed to the CTES.

The SF is simulated using TYPE 536 from TRNSYS Library (TESS Models). With reference to Figure 68, the mass flow rate and the PTC inlet temperature ($T_{PTC,i}$) are taken as input data from the outlet port of the controlling Valve 4. The $T_{PTC,o}$ and flow rate are set as an input to the control Valve 1. Control Valves 1 and 4 can isolate the SF when the DNI is less than 250 W/m^2. The HTF is fed to the divert Valve-1, which has two outlet ports. Outlet port 1 directs the HTF to the SG and outlet port 2 directs it to the CTES for charging. All inputs and parameters of main components of TRNSYS can be found in Appendix III.

For the weather data to be considered in the dynamic simulation model, a weather data file is used as input file with values of the DNI and the T_a which are taken from the weather station installed next to the SF.

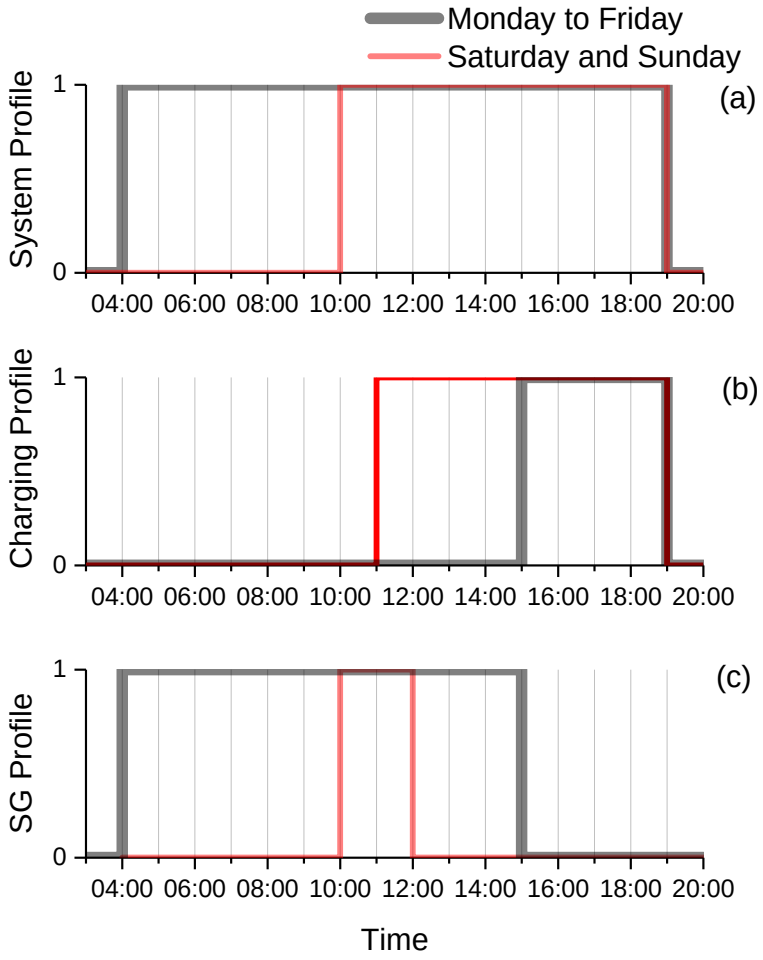

Figure 67: (a) System Profile, (b) Charging Profile, (c) SG profile.

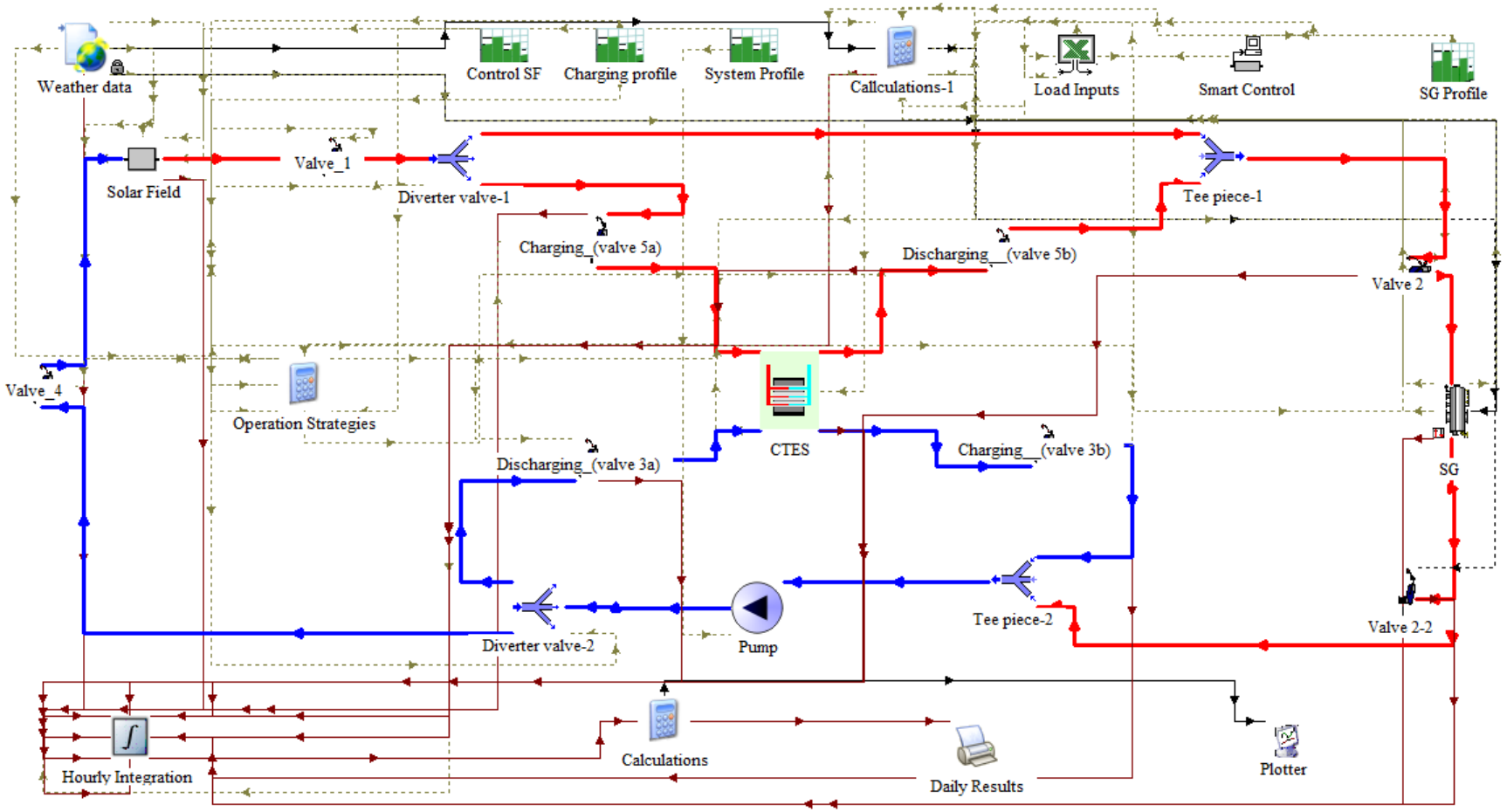

Figure 68: Simulation model in simulation studio project of TRNSYS.

The procedure followed in the model for charging, discharging and steam production are described below:

Charging: The model checks if the charging profile is enabled and if the $T_{PTC,o}$ is higher than the CTES average temperature ($T_{CTES,av}$). If both statements are TRUE, then the HTF is fed for charging purposes, so the outlet port 2 (TYPE 647) and the charging valve-5a (TYPE 978) is open. Otherwise, the HTF continues to circulate through the SG (TYPE 636) until the $T_{PTC,o}$ exceeds the $T_{CTES,av}$. Then, the heated HTF enters the CTES (TYPE 10), and the heat is transferred to the concrete storage. The CTES models a multi-zone TES which can charge and discharge by circulating the HTF through the concrete storage, respectively. As the HTF transfers heat to the CTES, its temperature drops and then it is directed to the charging valve-3b (TYPE 978), then to the tee-piece-2 (TYPE 649), and finally to the variable speed pump (TYPE 3) for recirculation.

Steam production: The HTF is directed for charging from valve-1 and it is fed to the control valve-2 (TYPE 978). Valve-2 is controlled by the SG load profile, so it is open only when there is a need for steam production or preheating purposes. The SG (TYPE 636) is fed with fresh water at ambient conditions from a feedwater tank. The heated HTF heats the water in the SG, and steam is produced at 188 °C, 10 Bar_g. The heated HTF temperature and flowrate are taken as an input from the control valve-2 (TYPE 978). As the HTF temperature decreases, the HTF is fed to the control valve-2-2 (TYPE 978), then to the tee-piece-2 (TYPE 649), and finally to the variable speed pump (TYPE 3).

Discharging: From the variable speed pump, the HTF is fed to the diverter valve-2 (TYPE 647), which decides if the HTF will go for discharging (outlet port-1) or return to the SF (outlet port-2). In the early morning hours when the solar radiation is low, the HTF temperature must follow this path: (task 1) preheating, (task 2) produce steam solely from CTES, (task 3) produce steam from CTES and recirculate through the SF, (task 4) produce steam partially from CTES and SF (task 5), and produce steam only from the SF. Thus, the first task is to check if the $T_{PTC,o}$ is lower than the $T_{CTES,av}$, the DNI is higher than 250 $W/m^{2,}$ and the charging profile is off. If these three statements are TRUE, then the HTF is fed to the CTES (TYPE 10) to satisfy tasks 1 and 2. As the DNI increases more than 250 W/m^2 then the diverter valve-2 (TYPE 647) will partially

open both ports, the control valve 4 and 1 (TYPE 978) will also open, and the HTF will also circulate through the SF serving the task 4. As the HTF temperature becomes equal with the $T_{CTES,av}$, the SF will also contribute to the steam production. As the $T_{PTC,o}$ becomes higher than the $T_{CTES,av}$, the diverter valve-2 (TYPE 647) drives the HTF only from outlet port-1, and steam will be produced solely from the SF (task 5).

4.2 Mathematical Model

The mathematical model of the three main components of the model which are the PTC, the CTES, and the SG, is obtained by the TRNSYS mathematical reference (TRNSYS, 2020). The output of these components will be used to determine the accuracy of the model. Firstly, the useful energy gain ($\dot{Q}_u$) and the collector outlet temperature ($T_{PTC,o}$) should be estimated. The $\dot{Q}_u$ (kJ/h) can be estimated from the Eq. (15), which is based on the standard collector performance Eq. (16):

$$\dot{Q}_u = R_1.R_2 \cdot A_{aperture} \cdot N_{parallel} \cdot \left[F_R(\tau\alpha)_n \cdot IAM \cdot I_{beam} - \frac{F_R U_L}{CR}\left(T_{PTC,i} - T_a\right)\right] \quad \textbf{Eq. (15)}$$

$$\dot{Q}_u = A_{aperture}\left[F_R(\tau\alpha)_n I_{beam} - F_R U_L\left(T_{PTC,i} - T_a\right)\right] \quad \textbf{Eq. (16)}$$

Where:

- R_{test}, R_1,R_2 are modifiers and correct the standard collector performance equation for other flow rates than the one used under test conditions and account for more than one collector in a series string (see bellow).
- $A_{aperture}$ is the aperture area of the collector (m^2).
- $N_{parallel}$ is the number of collectors placed in parallel.
- $F_R(\tau\alpha)_n$ is the efficiency with which solar radiation is absorbed by the tube and removed by fluid flowing through the PTC.
- The Incidence Angle Modifier (IAM), which is a property of the CF100 collector which accounts for the incident angle effects.
- I_{beam} is the beam radiation ($kJ/hr \cdot m^2$).
- $F_R U_L$ is the collector loss rate.
- CR is the concentration ratio.

- $T_{PTC,i}$ is the temperature of the fluid entering the collector array (°C).
- T_a is the ambient temperature (°C).

In order to calculate the $\dot{Q}_u$ for each time step, all these parameters need to be estimated. The concentration ratio (CR) can be defined by:

$$CR = \frac{A_{aperture}}{\text{Receive area of the absorber}} \quad \textbf{Eq. (17)}$$

The modified loss coefficient ($F'U_L$) must be calculated based on the standard F_RU_L, which corrects the manufacturer specified loss coefficient for flow rates other than the rated flow rate. This, it is calculated using the equation below based on the CF100 collector's properties.

$$F'U_L = \begin{Bmatrix} F_RU_L \quad \text{if} \quad \frac{F_RU_L}{\dot{m}_{HTF,test}Cp_{HTF}CR} \geq 1 \\ \dot{m}_{HTF,test}cp_{HTF}\left(1 - e^{(F_RU_L/\,(\dot{m}_{HTF,test}Cp_{HTF}CR)}\right) \text{if} \ \frac{F_RU_L}{\dot{m}_{HTF,test}Cp_{HTF}CR} < 1 \end{Bmatrix} \quad \textbf{Eq. (18)}$$

Where the Cp_{HTF} is the specific heat of the collector fluid HELIOSOL$^{(R)}$XA (kJ/Kg·K) , and the $\dot{m}_{HTF,test}$ is the mass flow rate of the fluid flowing through the collector under test conditions (kg/hr).

The modifiers R_{test}, R_1, R_2 are estimated using Eq. (19), Eq. (20) and Eq. (21), respectively. These factors correct the standard collector performance equation for other flow rates than the one used under test conditions and account for more than one collector in a series string. The N_{series} and $N_{parallel}$ represent the number of collectors in series and parallel, and the mass flow rate ($\dot{m}_{HTF}$) is introduced as an input by a variable speed pump circulating the HTF through the system.

$$R_{test} = \dot{m}_{HTF,test}Cp_{HTF}\left(1 - e^{\frac{-F'U_L}{(\dot{m}_{HTF,test}Cp_{HTF})}}\right) \quad \textbf{Eq. (19)}$$

$$R_1 = \frac{N_{series}\dot{m}_{HTF}Cp_{HTF}}{A_{aperture}}\left(\frac{1 - e^{\frac{-F'U_L\,A_{aperture}}{(N_{series}\dot{m}_{HTF}Cp_{HTF})}}}{R_{test}}\right) \quad \textbf{Eq. (20)}$$

$$R_2 = \frac{1 - \left(1 - \frac{R_1 A_{aperture} F_R U_L}{\dot{m}_{HTF} Cp_{HTF} N_{series} CR}\right)^{N_{series}}}{N_{series}\left(\frac{R_1 A_{aperture} F_R U_L}{\dot{m}_{HTF} Cp_{HTF} N_{series} CR}\right)} \quad \textbf{Eq. (21)}$$

The $T_{PTC,o}$ is calculated using the equation below.

$$T_{PTC,o} = T_{PTC,i} + \frac{\dot{Q}_u}{\dot{m}_{HTF} Cp_{HTF}} \quad \textbf{Eq. (22)}$$

The IAM is calculated according to the incidence angle (θ) by using the following equation, given by the PTC manufacturer (obtained experimentally):

$$K_{IAM}^{t} = 1 - 2 \cdot 10^{-6} \cdot (\theta^t)^3 + 6 \cdot 10^{-5} \cdot (\theta^t)^2 - 0.0007 \cdot \theta^t \quad \textbf{Eq. (23)}$$

The CTES model considers equally spaced tubes in the concrete. It is divided into five segments as shown in Figure 69. An ordinary differential equation is written for each segment depending on the charging and discharging procedure, using finite difference methods. This model takes into account the thermal capacity of the concrete mass, the HTF and the thermal losses of the concrete mixture to environment. It is important to note that it does not takes into account the thermal capacity of the steel pipes in the concrete mixture. The equations for the 5 segments for the charging and discharging procedures are as follows:

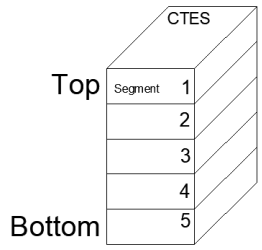

Figure 69: CTES segments separation for modelling.

Charging procedure: the HTF flows Downwards from Segment 1 to 5:

For i=1:
$$\frac{V_c}{5}\rho_c Cp_c \frac{dT_1}{dt} = \dot{m}_{HTF} Cp_{HTF}(T_i - T_1) - \frac{U_c p_c L_c}{5}(T_1 - T_a) - \frac{k_c A_{cs}}{L/5}(T_1 - T_2) \quad \textbf{Eq. (24)}$$

For i=2-4:
$$\frac{V_c}{5}\rho_c Cp_c \frac{dT_1}{dt} = \dot{m}_{HTF} Cp_{HTF}(T_{i-1} - T_i) - \frac{U_c p_c L_c}{5}(T_i - T_a) - \frac{k_c A_{cs}}{L/5}(T_{i-1} - T_i) - \frac{k_c A_{cs}}{L/5}(T_i - T_{i+1}) \quad \textbf{Eq. (25)}$$

For i=5: $$\frac{V_c}{5}\rho_c Cp_c \frac{dT_5}{dt} = \dot{m}_{HTF} Cp_{HTF}(T_4 - T_5) - \frac{U_c p_c L_c}{5}(T_5 - T_a) - \frac{k_c A_{cs}}{L/5}(T_4 - T_5)$$ **Eq. (26)**

Discharging procedure: the HTF flows Upwards from Segment 5 to 1:

For i=5: $$\frac{V_c}{5}\rho_c Cp_c \frac{dT_5}{dt} = \dot{m}_{HTF} Cp_{HTF}(T_i - T_5) - \frac{U_c p_c L_c}{5}(T_5 - T_{env}) - \frac{k_c A_{cs}}{L/5}(T_5 - T_4)$$ **Eq. (27)**

For i=2-4: $$\frac{V_c}{5}\rho_c Cp_c \frac{dT_i}{dt} = \dot{m}_{HTF} Cp_{HTF}(T_{i+1} - T_i) - \frac{U_c p_c L_c}{5}(T_i - T_{env}) - \frac{k_c A_{cs}}{L/5}(T_{i-1} - T_i) - \frac{k_c A_{cs}}{L/5}(T_i - T_{i+1})$$ **Eq. (28)**

For i=1: $$\frac{V_c}{5}\rho_c Cp_c \frac{dT_1}{dt} = \dot{m}_{HTF} Cp_{HTF}(T_2 - T_1) - \frac{U_c p_c L_c}{5}(T_1 - T_{env}) - \frac{k_c A_{cs}}{L/5}(T_2 - T_1)$$ **Eq. (29)**

Where V_c is the volume of the concrete (m^3), ρ_c is the density of the concrete mixture (kg/m^3), Cp_c is the specific heat of the concrete (kJ/Kg·K), U_c is the loss coefficient (kJ/h·K), p_c is the perimeter of the concrete (m), L_p is the length of the concrete (m) in the flow direction, k_c is the effective thermal conductivity of the concrete in the axial direction (kJ/m·h·K) and A_{cs} is the cross-sectional area of the pipes (m^2). All these were introduced as parameters to the model based on the data provided by CADE (shown in Appenix III. The $\dot{m}_{HTF}$ and the temperatures are also taken as inputs.

Regarding the SG, the heat is transferred from the HTF to feed water, and steam is produced at the target enthalpy ($H_{desired,st}$) (kJ/kg·K). The energy required to heat the feed water to the saturated vapor point ($\dot{Q}_{w,st}$) is calculated using Eq. (30) and the desired steam temperature ($T_{st,o}$) using Eq. (31). The HTF outlet temperature ($T_{HTF,o}$) is calculated in each timestep using Eq. (33), based on the energy calculated ($\dot{Q}_{HTF,o}$) from Eq. (32).

$$\dot{Q}_{w,st} = \dot{m}_w \cdot Cp_w \cdot (T_{st} - T_w)$$ **Eq. (30)**

$$T_{st,o} = T_{w,in} - \frac{\dot{Q}_{w,st}}{\dot{m}_{water} \cdot Cp_w}$$ **Eq. (31)**

$$\dot{Q}_{HTF,o} = \dot{m}_{HTF} \cdot Cp_{HTF} \cdot (T_{HTF,o} - T_{HTF,in})$$ **Eq. (32)**

$$T_{HTF,o} = T_{HTF,i} - \frac{\dot{Q}_{HTF,o}}{\dot{m}_{HTF} \cdot Cp_{HTF}}$$ **Eq. (33)**

4.3 Validation of the Dynamic Simulation Model

The data acquisition system used has the capability to record the temperatures of the SF (inlet and outlet), CTES and SG, the mass flow of the variable speed pump and the make-up water to the SG. Temperatures are measured with a time interval of 5 seconds, and the CTES has 24 thermocouples in different elevations. All these parameters are used to validate the simulation model.

Subsequently, a considerable amount of data were collected and stored which are available for analysis. To be able to compare the real to the simulated data so as to check the validation of the model during Strategies 1 and 2, the real measured values of the most important parameters were analyzed and plotted to ease comparison. These are the temperature of the HTF coming from the SF ($T_{PTC,o}$), the CTES average temperature (T_{CTES}), the power produced from the collector (P_{PTC}), and the power transfer from and to the CTES (P_{CTES}). These parameters are plotted in Figure 70 in graphs a, b, c and d, respectively, for two typical summer days. The graphs show the real measured data recorded every 5 seconds and the average values of these data for one hour. Later these averaged data will be compared to the simulation data. Similarly, the average from the real monitored data was taken for a week and will be also compared.

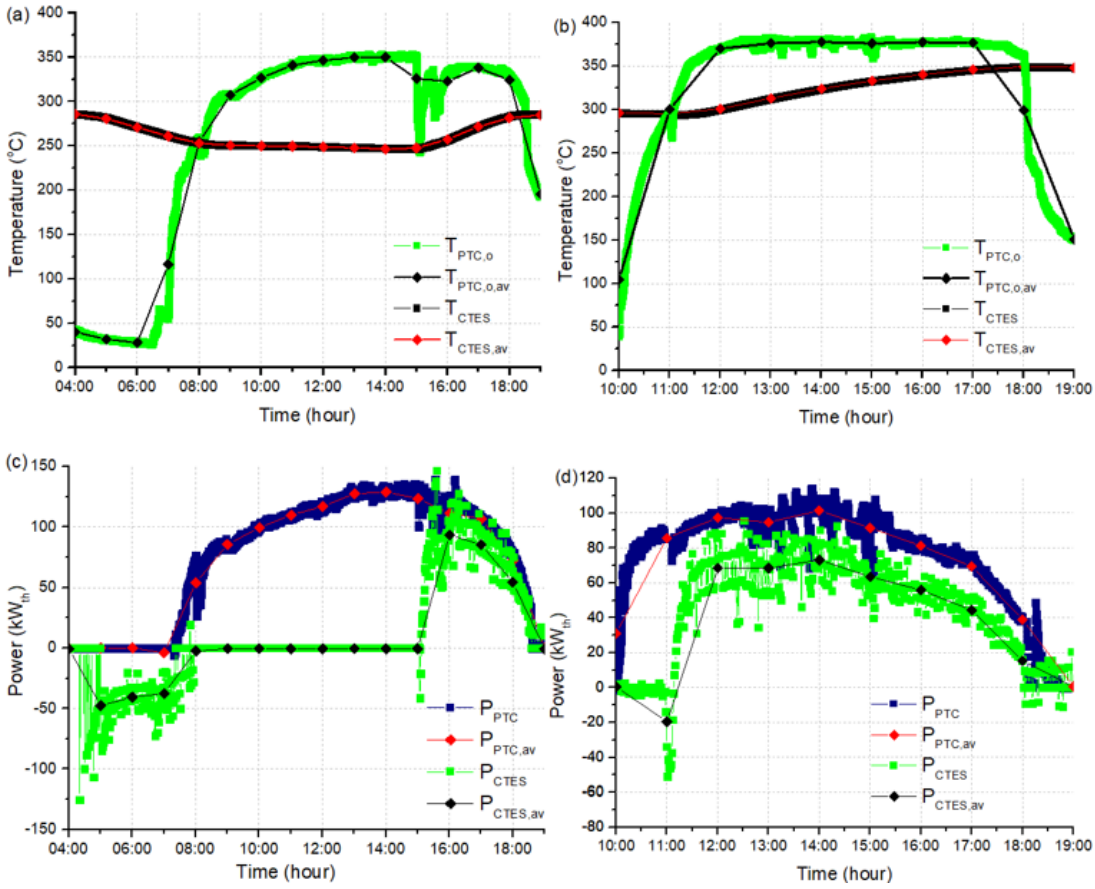

Figure 70: (a) Measured temperatures on Strategy 1 (b) Measured temperatures on Strategy 2 test (c) Measured power fluctuation on Strategy 1 (d) Measured power fluctuation on Strategy 2.

The dynamic simulation model is tested under operation Strategies 1 and 2 separately and during a complete week when both strategies are applied. The scope is to validate under continuous operation the simulation model. The Percentage Relative Error (PRE) estimated by Eq. (34) between the real and simulated data for the steam produced at the end of the day should be low in order to have a reliable simulation model.

$$\mathrm{PRE} = \frac{|\mathrm{measured} - \mathrm{real}|}{\mathrm{real}} \cdot 100 \qquad \textbf{Eq. (34)}$$

Each real parameter is the average value of the monitored data collected for one hour. The $T_{CTES,o}$ corresponds to the HTF outlet temperature from the CTES and the $T_{CTES,i}$ the temperature of the HTF entering the CTES. The $T_{PTC,o}$ corresponds to the HTF outlet temperature from the PTC array and the $T_{PTC,i}$ the temperature of the HTF entering the PTC array.

The first comparison concerns Strategy 1 during a clear day. The real and simulation data are shown in Figure 71. At 4 am the initial $T_{CTES,av}$ of the system was 285 °C, which is decreasing due to the TES Cold Start mode and TES discharge mode (Figure 71a). As can be observed, from 4 am to 8 am, the P_{CTES} is negative. This is because the stored thermal energy is used to preheat the system and produce steam for the industry (Figure 71b). At 5 am, steam is produced solely from CTES with TES discharge mode with the $P_{CTES,real}$ being -47 kWh_{th} and the $P_{CTES,sim}$ -49.6 kWh_{th} (PRE=5.2%). At around 7 am, the DNI exceeded the 250 W/m^2 (Figure 71c), so the PTCs are set on tracking mode, and thus the $T_{PTC,o}$ started to increase (Figure 71a) and the TES discharge and SF recirculation mode is enabled. The average discharging thermal energy monitored is -37 kWh_{th} and the simulated is -38.85 kWh_{th} (PRE=4.76%). At around 8 am the $T_{PTC,o}$ gets equal with the $T_{CTES,av}$ (253 °C real and 250 °C simulated values), so steam is produced from the CTES and the SF as shown in Figure 71b while the system runs with the TES Discharge and Generation modes. Finally, after 8 am the charging valves are shut off, and the energy collected from the SF is transferred directly to the SG to produce steam ($P_{CTES,real}$=0 kWh_{th}). At 3 pm, when the charging profile is enabled and the $T_{PTC,o}$ is higher than the $T_{CTES,av}$ the model turns its strategy from Generation mode to Charging mode and the $T_{CTES,av}$ starts to increase its temperature (Figure 71a). At the end of the charging mode, the $T_{CTES,av,real}$ was 284 °C, and the $T_{CTES,av,sim}$ was 281 °C. The average PRE of the $T_{CTES,av}$ during the charging mode is 0.71%.

The PTC efficiency (η_{PTC}) for the real measured data is estimated using Eq. (6) and the results are shown in Figure 71d. As can be seen from Figure 71d, the $\eta_{PTC,real}$ varied from 36% to 52%, and in the $\eta_{PTC,sim}$ from 33% to 52%. A significant difference between the values is observed at 9 am (real: 46% and simulated: 33%). This occurs due to the fact that the real data are averaged from 8:30 to 9:30 whereas the simulated data are for 9 am exactly and during this time period the DNI is increasing rapidly. The average PRE for the η_{PTC} through the day is 9.84%. Excluding the early morning and late afternoon hours and considering only the period where the system is stable (when DNI was stable), the PRE is lower (2% from 11 am to 3 pm).

The energy of steam produced (Q_{st}) based on the measured data is 601 MJ as shown in section 3.2 whereas the make-up water (m_w) from the feed water tank to the SG was 940 L (at the end of

the day). According to the simulation results, the calculated Q_{st} in a saturated temperature of 188 °C was 563 MJ and thus the PRE between the values is 6.32%.

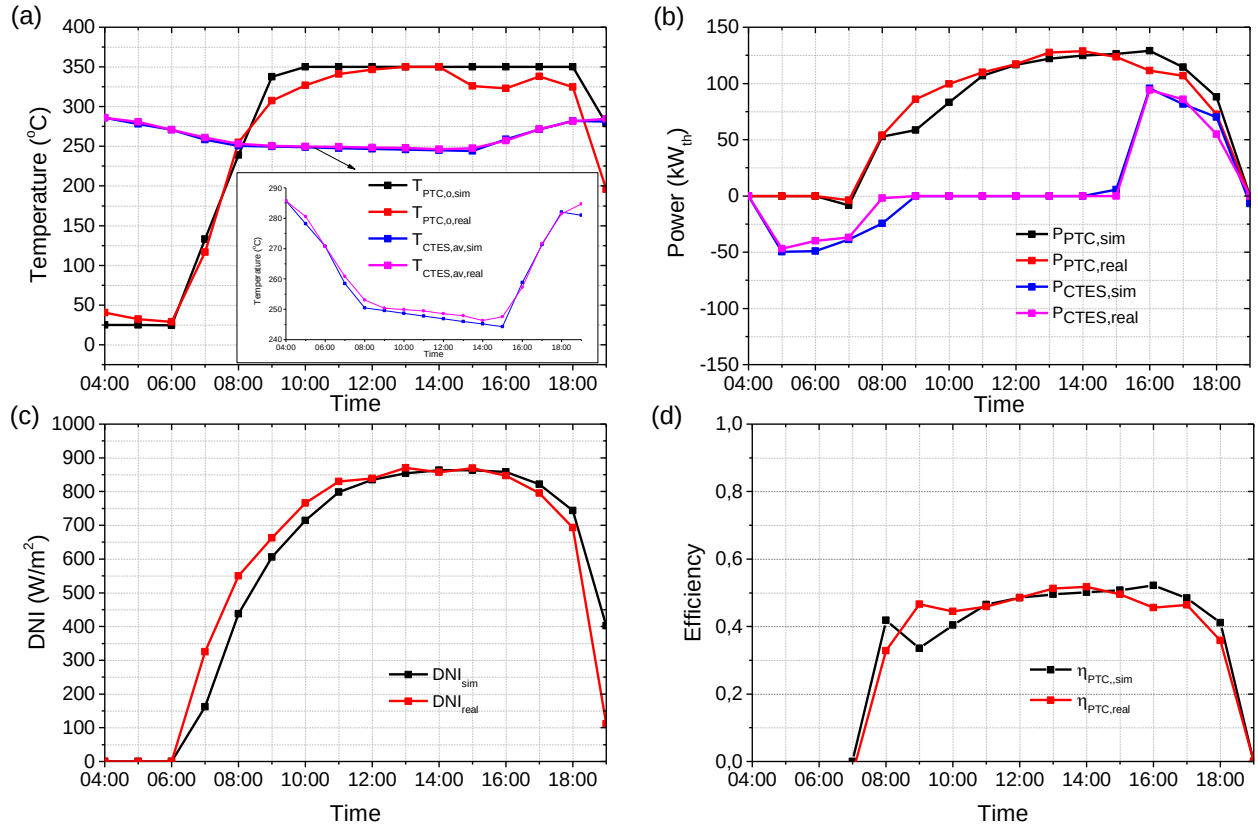

Figure 71: (a) The $T_{PTC,o,real}$ and $T_{CTES,av,real}$ compared with the $T_{PTC,o,sim}$ and $T_{CTES,av,sim}$, (b) the $P_{PTC,real}$, and $P_{CTES,real}$ compared with $P_{PTC,sim}$, and $P_{CTES,sim}$ (c) the DNI measured on site and the DNI used in the simulation model.

The second comparison has been done during a clear day when there was no steam demand from the industry and the P_{PTC} was supporting the CTES for Charging under Strategy 2. From 10 am to 11 am, the SF preheating mode was enabled and the HTF was circulating to increase its temperature. At 11 am the $T_{PTC,o}$ was already higher than the $T_{CTES,av}$, so the Charging mode was enabled. As shown in Figure 72, the increment of the $T_{CTES,av}$ is very close (PRE:1.03%). The initial $T_{CTES,av,sim}$ is 299 °C and at the end of the day is increased to 345 °C while the initial $T_{CTES,av,real}$ is 296 °C and is increased to 348 °C.

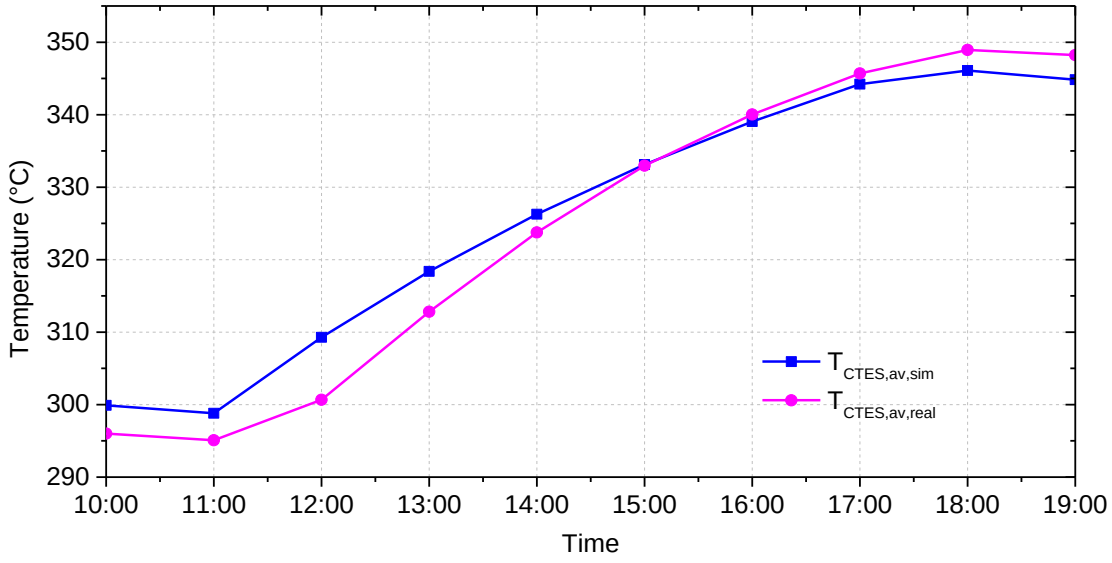

Figure 72: The $T_{CTES,av,real}$ compared with the $T_{CTES,av,sim}$.

The last comparison is made between the real and measured data while the system was autonomous and switching from Strategy 1 to Strategy 2 for one complete week of operation, from Thursday to Wednesday. This period was selected to check how effectively the two strategies adapt. The comparison between the real and simulated data is shown in Figure 73. As can be observed, there is a good agreement between the measured and simulation data. All strategies and operation modes introduced in the model are functional, and this makes the PTC system dispatchable as it can supply heat from the early morning hours when the P_{PTC} is zero for all days of the whole week. This is achieved due to the CTES, which supplies heat to the SG in the early morning hours, and it is charging during the afternoon when there is solar radiation availability (Figure 73a)

The P_{PTC} results showed a PRE of 10.14%. The η_{PTC} varied from 40% to 57% (Figure 73b). The η_{PTC} through the week obtained from the measured data is 42%, and from the simulation data 39% which corresponds to a PRE of 7.6% (absolute difference of 3%), which is well within acceptable limits.

The simulated and measured $T_{CTES,av}$ is shown in Figure 73c with a PRE of 3.53%. The $Q_{st,sim}$ during this week, was 2.61 GJ and the corresponding value based on the real data was 2.79 GJ, equivalent to 4.37 tons of steam (PRE: 6.45%).

A drawback of the simulation is that the model does not consider the heat capacity of the materials used to construct the system. These explain the small differences shown in Figure 73c.

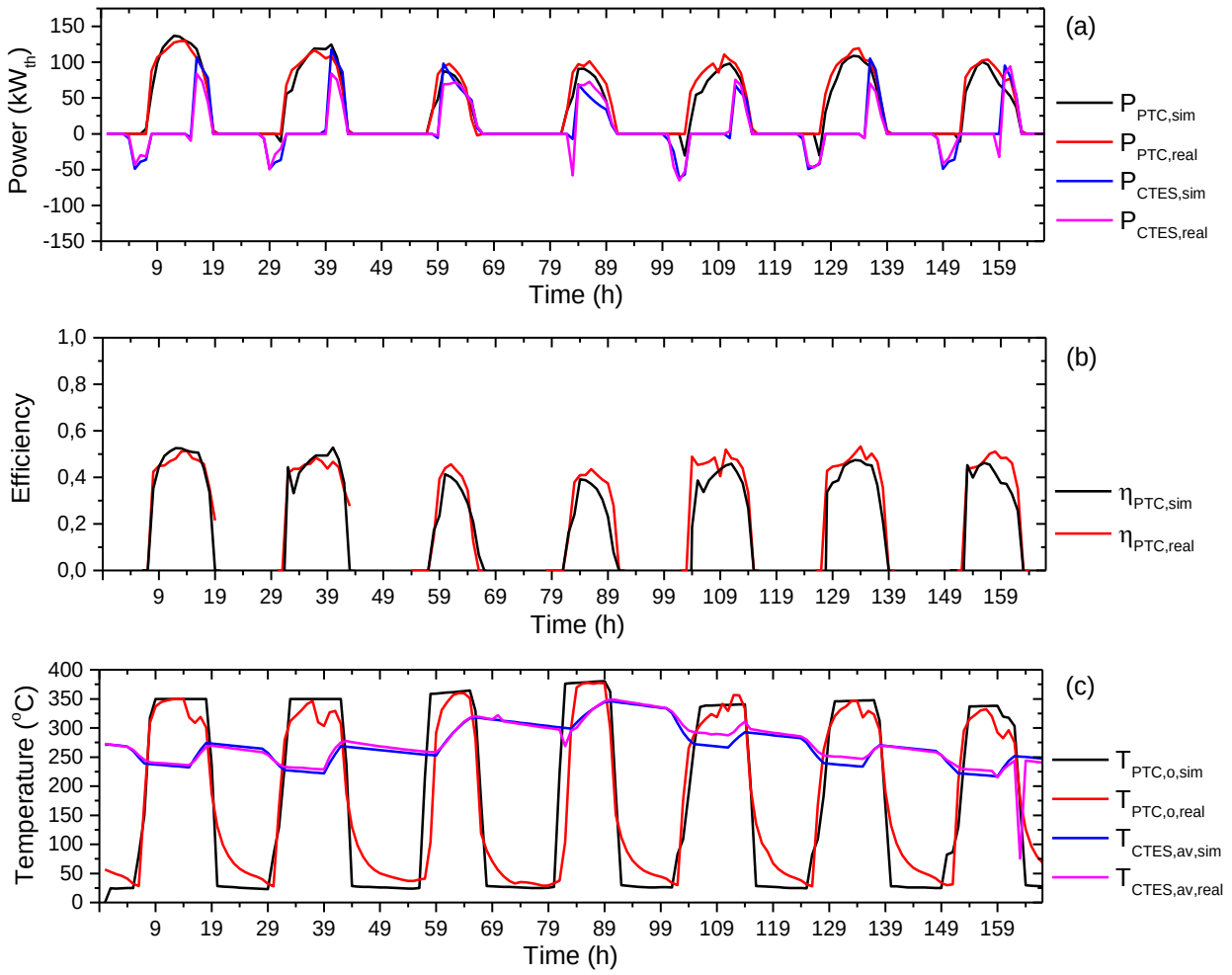

Figure 73: (a)The $P_{PTC,real}$, and $P_{CTES,real}$ compared with $P_{PTC,sim}$, and $P_{CTES,sim}$, (b) The $\eta_{PTC,real}$ with the $\eta_{PTC,sim}$, (c) The $T_{PTC,o,real}$ and $T_{CTES,av,real}$ compared with the $T_{PTC,o,sim}$ and $T_{CTES,av,sim}$.

4.4 Discussion

This study presents a dynamic simulation model developed for the investigation of the performance of the first PTC system installed in a Cyprus industry. The model has been built in TRNSYS simulation tool and has been validated using on-site experimental data. The system operates with different strategies and modes depending on the steam demand and industry shifts. The dynamic simulation model takes all operation strategies and modes into consideration and shows a good agreement between the measured data and simulation results.

It is proved that the model corresponds to the actual behavior of the operation modes of the system during a steam production day and has a very good fitting with the real data from the early morning hours until late in the afternoon. The average PRE between $P_{CTES,sim}$ and $P_{CTES,real}$ at 5 am, 6 am, and 7 am when steam is produced from the heat stored in the CTES is 11% with the $T_{CTES,av}$ decreased from 285 °C to 258 °C from the simulation and to 260 °C from the measured data. Additionally, the steam produced throughout the day was 563 MJ from simulation and 601 MJ from real data with a PRE of 6.32%. The CTES temperature during a charging day (Strategy 2) increased from 46 °C based on the measured values to 52 °C based on the model estimations. It is observed, that for a long-term operation, the PRE for the steam production was 6.45% with the PRE of the overall efficiency was equal to 7.6%.

CHAPTER 5

5 Design Tool for PTC systems parameters selection based on IPH applications

In this section, the previously validated simulation model has been used to create a design tool that can be used to design systems with higher thermal loads and higher steam demand temperatures than KEAN needs. This analysis examines the feasibility of installing a PTC system with CTES in different size industries in Cyprus.

5.1 Methodology

For the design tool, various simulation runs have been done for thermal loads from 1 ton/h to 4 tons/h (with step of 0.5 ton/h) and a range of steam demand temperatures from 110 °C to 250 °C. The steam demand temperature is the saturated temperature of steam that the industry needs for its processes, and the thermal load represents the tons of steam that the industry needs per hour.

It is important to mention that the design tool considers that the operation profile (production hours, charging period) of the potentially interested industries is the same as those of KEAN, the operation strategies are also the same as the ones developed for KEAN, and all simulations were

carried out for the TMY data of Cyprus. It is believed that the operation profile and strategy of KEAN is typical for other industries on the island which operate on a single daily shift basis.

In order to modify the model to correspond to higher loads for other industries, the parameters that need to vary for each simulation run are the number of collectors, the size of the SG, the steam demand temperature, and the size and heat capacity of the CTES.

The design tool can provide to the potential industries several information parameters regarding the system that fits their needs. The information that can be given is:

- The steam production for a storage duration of 3h, 6h, 9h, 12h and 15h and steam demand temperature of 110 °C to 250 °C with step of 10 °C, for thermal loads demand from 1 ton/h to 4 tons/h.
- The solar contribution for storage duration of 3h, 6h, 9h, 12h and 15h and steam demand temperature of 110 °C to 250 °C with step of 10 °C, for thermal loads demand from 1 ton/h to 4 tons/h.
- The sizing of the system regarding the area of the collectors, capacity of the SG and land requirements for thermal loads from 1 ton/h to 4 tons/h.
- The CTES capacity required for the required storage duration of 3h, 6h, 9h, 12h and 15h, for thermal loads from 1 ton/h to 4 tons/h.
- The solar savings (thousands of EUR) of the system at the end of its life cycle, for steam demand temperature of 110 °C to 250 °C for thermal loads demand from 1 ton/h to 4 tons/h for the optimum storage capacity based on LCCA. Solar savings is the money saved in the whole life of the system against the cost of fuel and maintenance cost of a non-solar system.
- The payback period (years) for steam demand temperature of 110 °C to 250 °C for thermal loads demand from 1 ton/h to 4 tons/h for the optimum storage capacity based on LCCA.
- The CO_2 savings (tons of CO_2) of the system at the end of its life cycle, for steam demand temperature of 110 °C to 250 °C for thermal loads demand from 1 ton/h to 4 tons/h for the optimum storage capacity based on LCCA.

For the LCCA, the following parameters were considered:

- Market discount rate and a mortgage interest rate of 7% (constant).
- A down pay of 20% and a life cycle and loan of the system equal to 20 years.
- Maintenance cost of 3.5 Euro per ton of steam with 1% increase every year which includes mirror cleaning, spare parts, staff for running and maintaining the system, insurance, and electricity for running the plant.
- The value of land required to install the system is not included as the PTC system could be installed on the roof of the buildings as well.
- Auxiliary fuel cost of 13.4 Euro/GJ with an increase of 1% every year.
- The turnkey cost of the PTC system, including engineering, assembly, and commissioning, is shown in Figure 74.

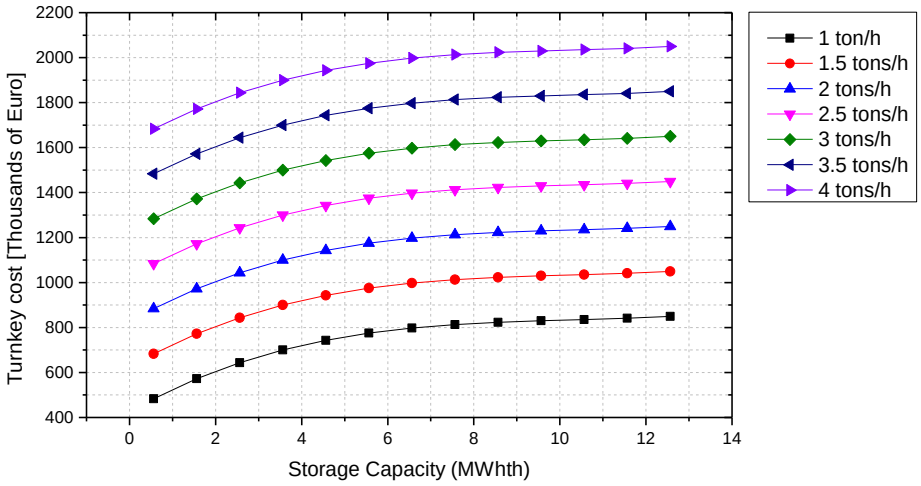

Figure 74: The turnkey cost used for the LCCA.

For each thermal load demand, for different storage periods of each system examined, the Life Cycle Savings are estimated, and the optimized selection is the one that gives the maximum savings.

As shown by Eq. (35) the amount of CO_2 savings is estimated by the amount of conventional fuel savings divided by the rate of fuel cost in €/GJ plus any annual increase of fuel cost rate.

$$CO_{2,savings} = \sum_{1}^{20} \left[\frac{\text{Annual Fuel Savings}}{\text{Fuel Cost Rate} + \text{Increase of Fuel Cost Rate}} \cdot \text{Fuel Emissions} \right] \qquad \textbf{Eq. (35)}$$

Where the Annual Fuel Savings is the cost of the fuel savings for each year of operation (€), Fuel Cost Rate is in €/GJ, and the Fuel Emissions which are 77.4 tons CO_2/TJ (Jurich, 2016).

5.2 Results

Based on the methodology presented above, the results of the design tool are given in this section. All data are provided in the form of graphs[1] and allow anyone using as input data the thermal energy demand and steam demand temperature of the industry, to easily retrieve information about the suitable system depending on each case. Tables presented in Appendix III also give more details of the data plotted. Figure 75a to Figure 75g show the steam production (tons/year) and solar contribution for storage duration of 3h, 6h, 9h, 12h and 15h and steam demand temperature of 110 °C to 250 °C with step of 10 °C, for thermal load demand from 1 ton/h to 4 tons/h. It should be noted that the solar contribution is a fraction with respect to the actual demand. As expected, the annual steam production increases as the duration of storage increases and decreases as the steam demand temperature increases. For example, from Figure 75c, at a steam demand temperature of 170 °C, 3 hours of storage give 4,095 tons of steam per year and solar contribution is 0.71, whereas 15 hours of storage give 4,436 tons of steam per year and solar contribution is 0.77. Therefore, according to the thermal load demand (tons/h) the appropriate graph (Figure 75a to Figure 75g) can be used, which according to the steam demand temperature required by an industry (x-scale of graphs), a designer can obtain for various hours of storage duration (different curves) the steam production and the solar contribution per year.

Figure 75h shows according to the hourly thermal load demand, the sizing of the system regarding the number of collectors, land area requirements and the capacity of the SG. Figure 75i shows again for the hourly load demand the CTES capacity required according to the required storage duration of 3h, 6h, 9h, 12h and 15h, decided before. Concerning the design process, from Figure 75h according to the thermal load demand the number of collectors, the size of the SG and the land area needed are obtained. Finally, from Figure 75i, the CTES capacity for the various hours of storage can be obtained. The final optimum storage size will be decided from the economic analysis as follows.

[1] Large size graphs are given in Appendix III.

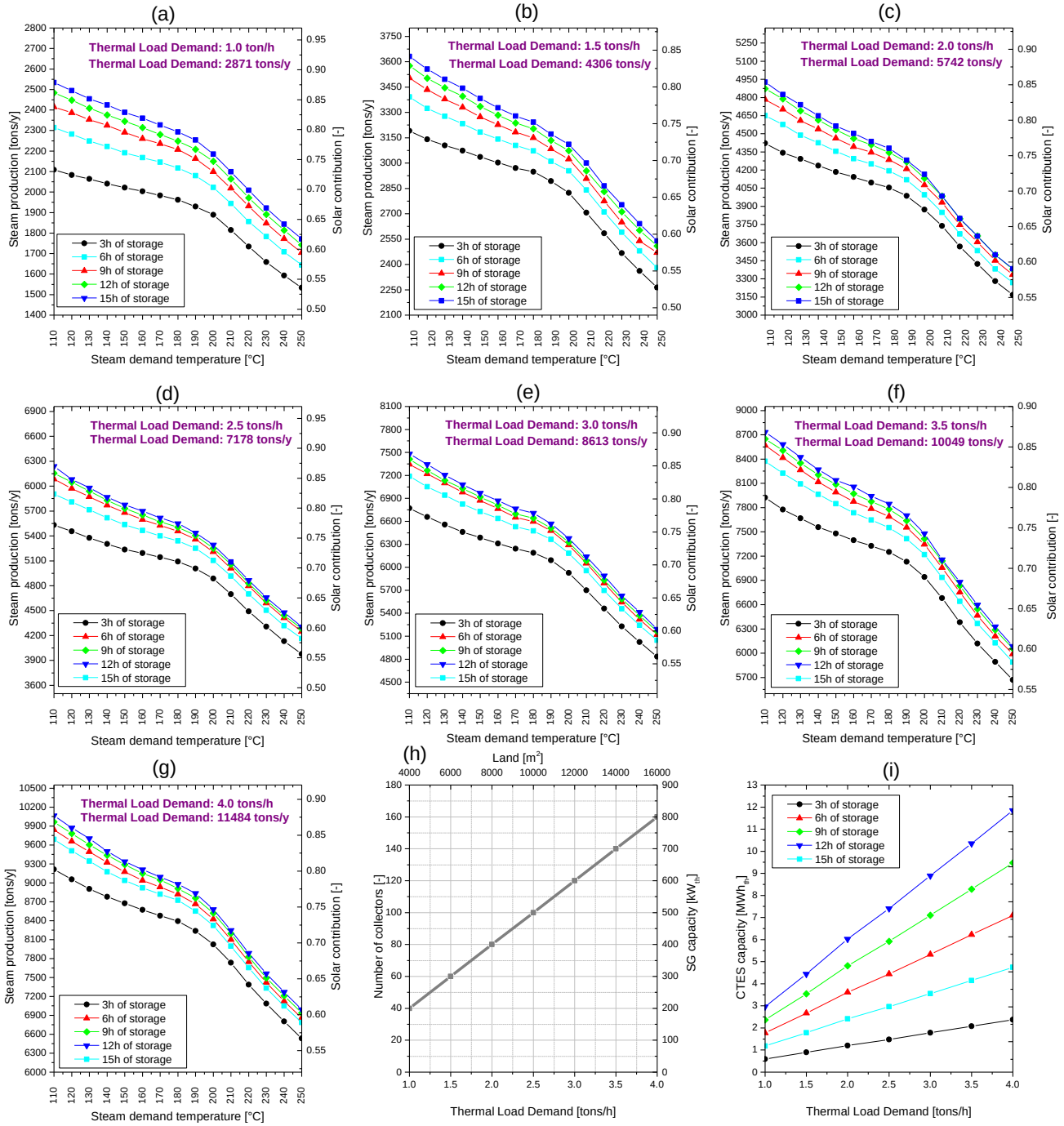

Figure 75: (a) – (g) The steam production, solar contribution for storage duration of 3h, 6h, 9h, 12h and 15h and steam demand temperature of 110 °C to 250 °C with step of 10 °C, for thermal loads demand from 1 ton/h to 4 tons/h, (h) the sizing of the system regarding area of the collectors, capacity of the SG and land requirements for thermal loads from 1 ton/h to 4 tons/h, (i) the CTES capacity required for required storage duration of 3h, 6h, 9h, 12h and 15h, for thermal loads from 1 ton/h to 4 tons/h.

For all the possible systems presented in Figure 75a to Figure 75g, an LCCA was carried out in order to identify the optimum systems for all cases, based on the maximum solar savings observed for different storage durations. Solar saving represents the difference between the costs of conventional system and the cost of solar energy system. Thus, the optimization criteria is the solar saving of the system through its life cycle. It is obvious that smaller systems have lower payback period but the smaller systems do not necessarily contribute the best way to the production from the economical point of view through their life cycle. On the other hand, a big system with high solar contribution does not necessarily have high solar savings. For these reasons, herein, the optimum combination between solar savings and contribution was selected and the payback period of the selected case is then estimated.

Figure 76a to Figure 76g shows the solar savings (thousands of EUR) of the system at the end of its life cycle (curves with square), payback period (years) and CO_2 savings (tons of CO_2) for steam demand temperature of 110 °C to 250 °C (curves with circle) for thermal load demand from 1 ton/h to 4 tons/h. As mentioned above, these graphs show only the optimum storage capacity based on LCCA.

For example, for a thermal load demand of 3 tons/h and a steam demand temperature of 140 °C, the optimum storage duration is 3h which has a payback period of 3 years which give solar savings of 1,201 thousand of EUR and CO_2 savings of 1,634 tons. For the same thermal load demand and a steam demand temperature of 220 °C, the optimum storage duration is 3h which has a payback period of 4 years, solar savings of 819 thousand of EUR and CO_2 savings of 1,341 tons.

Therefore, according to the thermal load demand and steam demand temperature required for an industry the final solution is obtained based on economic parameters from the appropriate Figure 76.

Accordingly, after the technical parameters of the system required are decided from Figure 75, the financial information and CO_2 savings can be obtained from Figure 76. As can be seen, in all cases examined, the payback period varies from 2 to 6 years depending on the size of the system.

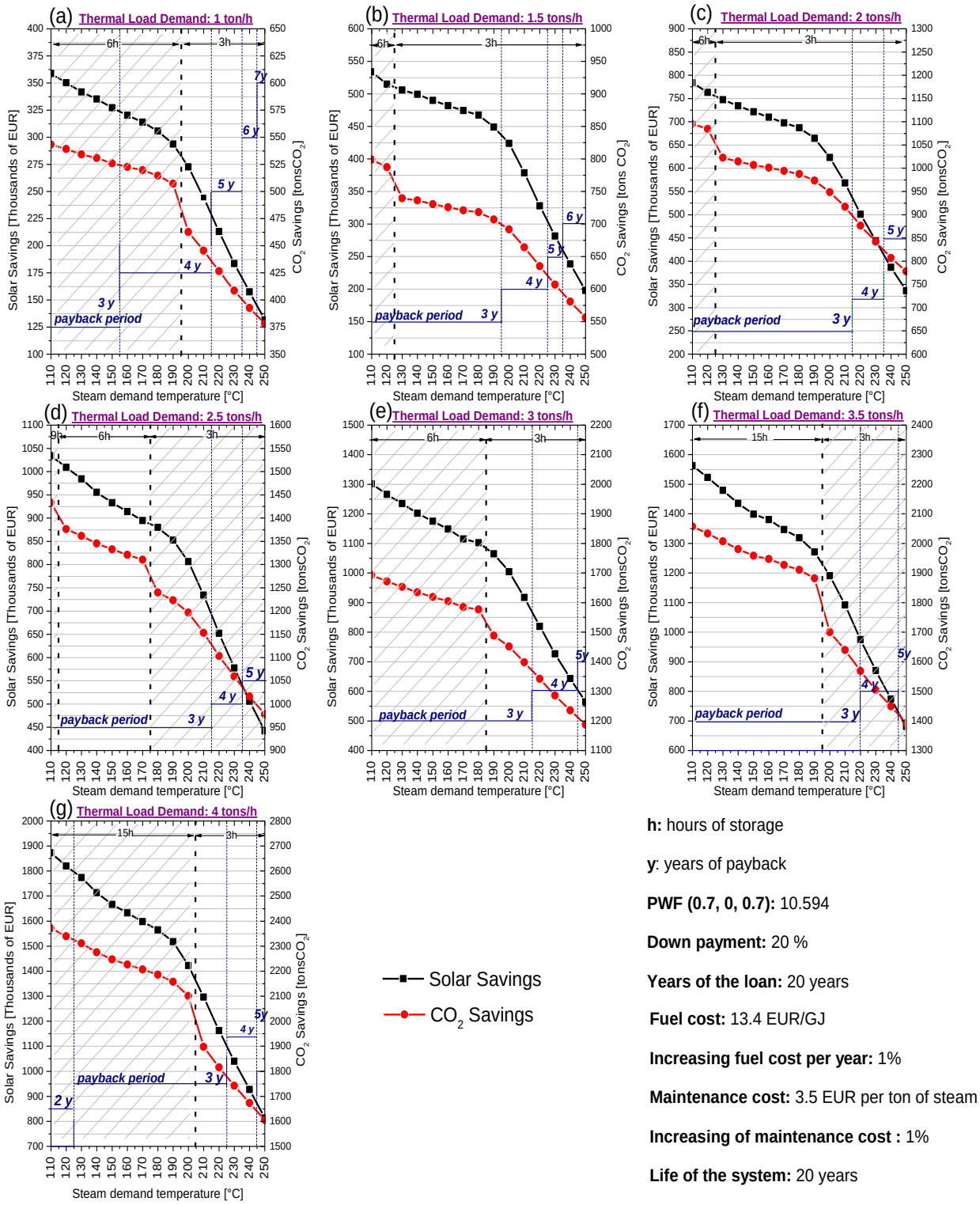

Figure 76: The solar savings (Thousand of EUR), payback period and CO2 savings, of the system at the end of its life cycle, for steam demand temperature of 110 °C to 250 °C for thermal loads demand from 1 ton/h to 4 tons/h for the optimum storage capacity based on LCCA.

From Figure 75 presented earlier, it was observed that the steam production is decreasing rapidly after 200°C. The reason for this drop, is the fact that the charging period is limited since it occurs only in the afternoons and weekends, and the CTES cannot be fully charged to that high temperatures during the weekdays. As a result, the heat stored during these days (especially if there was not good solar irradiation) is insufficient to supply heat to the industry when it is needed. It is important to mention that as the storage capacity increases, the CTES losses reduce and stabilize and thus, increasing the storage capacity does not necessarily lead to higher steam production. To overcome these issues, a model with hybrid mode is developed to be implemented when the steam load of the industry is already covered, feeding the excess heat directly to the CTES. However, it should be stated that this mode is not validated with real operation data since significant changes have to be made to the actual system.

Figure 77 shows a comparison of the annual steam production for 3h of storage and thermal loads of 1-4 tons/h from 200 °C to 250 °C for the design tool (dashed line) and the scale-up model with the hybrid mode (continuous line). The results show that the hybrid mode can successfully increase the solar contribution of the system from 3.5 to 8%.

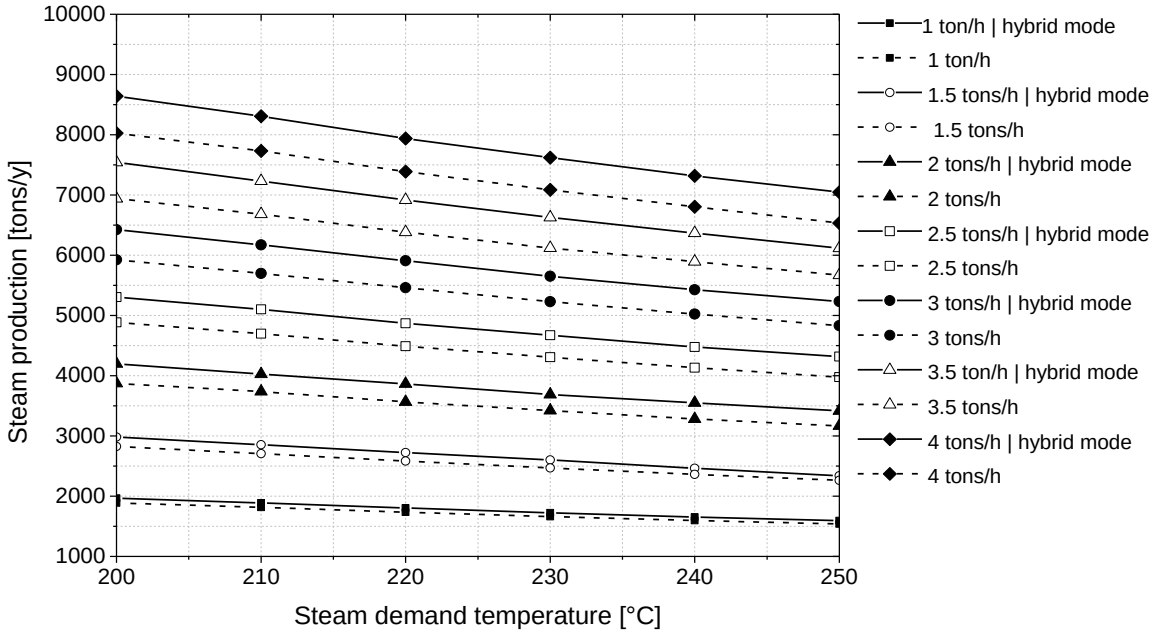

Figure 77: Comparison of the steam production for storage duration of 3h and steam demand temperature of 200 °C to 250 °C, for thermal loads demand from 1 ton/h to 4 tons/h, between the design tool and the model with the hybrid mode.

5.3 Discussion

The main objective of this study is to use the validated model to develop a design tool able to examine larger thermal loads and steam demand temperatures that other industries may have, and use it as a design tool. Such a tool can be used by other interested industries to examine the feasibility of installing such a system. From this analysis, an interested industry can obtain useful information about the sizing, the solar contribution and financial information of the suggested system depending on their own needs. For the financial data, an LCCA has been carried out to provide details of the investment of each system suggested, including the system payback period.

The design tool provides information of the steam production, solar contribution, sizing of the system and CTES capacity for storage duration of 3h, 6h, 9h, 12h and 15h and steam demand temperature of 110 °C to 250 °C with step of 10 °C, for thermal loads demand from 1 ton/h to 4 tons/h. All data are provided in the form of graphs and allow anyone using as input data the thermal energy demand and steam temperature of the industry, to easily retrieve information about the suitable system depending on each case.

Additionally, a scale-up simulation model is developed with a hybrid mode enabled. The hybrid mode considers that when the steam load of the industry is already covered, the excess heat is fed directly to the CTES. The system with the hybrid mode proved that the steam production can be increased up to 8% when considering high steam demand temperature (above 200 °C). From the LCCA carried out, one can read from the graphs developed the solar savings (thousands of EUR) and CO_2 savings (tons of CO_2) of the system at the end of its life cycle, and the payback period (years). The payback period for all cases examined, varies from 2 to 6 years, depending on the size of the system, which is very feasible. The design tool developed can be used for further evaluation of the most significant parameters that affect the performance of the PTC system.

It is believed that the tool developed and presented in this work will be a valuable tool for various industries to examine the space required, investment and economic viability of installing such a system and this could enable more use of solar IPH by the Cypriot industries. This model can be used in countries with similar solar potential and similar latitude (e.g. Crete, Naples, Athens, Israel, Syria), or the model can run again using other meteorological data to provide the data for different countries.

CHAPTER 6

6 Conclusions and Future work

As it was found from the literature review, more research on possible modifications of the absorber tube or new TES improvements would not lead to significantly higher system performance. The absorber and TES designs are at a high level, and it is not believed that a novel technology in these could drastically increase the system performance. Additionally, it was observed from the various experimental and simulation studies that the PTC system for IPH application could be a profitable solution to contribute to the thermal energy load of the industries. Moreover, the simulation models studies revealed that the TRNSYS simulation tool is the most appropriate software for modeling and used to predict, evaluate and optimize PTC system´s operation. It is also useful for examining the effect of several parameters on the system operation and performance.

From the extensive overview of the current Cyprus energy situation it is evident that the island has a small and isolated energy system which is not connected with any other energy networks, and there are no fossil fuel resources. It depends on imported fuels, and 94% of the country's energy needs are covered by oil. As this work aims to focus on PTC systems for IPH application,

it was observed that the industrial sector is using oil products such as kerosene, gas oil, light fuel oil, heavy fuel oil, and liquid petroleum gasses to cover their thermal energy needs. Additionally, there is very little use of coal and renewable energy; coal has been decreased rapidly after 2006 and abandoned completely in 2012. It was revealed that the leading industrial sector in the use of oil products to satisfy the thermal demand is the manufacturing sector. Particularly, the manufacture of food and beverage products and other non-metallic mineral products are paying the highest cost in oil products to cover their thermal demands.

Furthermore, Cyprus has abundant solar radiation throughout the year. The cloud period does not exceed three consecutive days, with average global radiation exceeding the value of 1727 kWh/m^2. Additionally, the direct to diffuse solar radiation ratio is 70:30, proving the high potential to use solar energy systems and specifically concentrated solar collectors which mainly use direct solar radiation. Although there is an abundance of solar radiation and the PTC system is a matured technology to use for IPH in Cyprus, excluding the KEAN's system, none of the Cyprus factories has adopted this technology yet.

This work has focused on a PTC system installed in Cyprus's biggest soft drinks industry, consisting of 2 parallel rows of 4 PTCs and a novel concrete-based TES system. The nominal thermal power of the system is 125 kW_{th}. Its novel CTES has high performance at temperatures up to 400 °C. It stores heat in a new-based concrete mixture and supplies heat to the industry when it is needed. The new composition of the concrete lead to higher storage capacity, thermal conductivity. Additionally, concrete volume, density, conductivity, and specific heat are improved. The TES employed in the system has a thermal capacity of 640 kWh_{th} and a total mass of 28,157 kg (5x0.548x0.670 m).

After the installation and first operation tests, the first goal of this work was to focus on the operation strategies and modes that can make the PTC system dispatchable. After several tests and optimizations, two operation strategies and internal operation modes are developed to make the PTC system dispatchable. Under Strategy 1 with an average DNI of 757 W/m^2, the CTES stored 77.5 kWh_{th} in 3.5 hours. The PTC system produced 940 liters of steam per day supplied to the factory in various process, which corresponds to 601 MJ of energy. In addition, when the system was operating under Strategy 1, from 5 am to 8 am the steam was produced from the

energy stored in the CTES and from 8 am to 3 pm the steam was produced only from the PTC system.

Moreover, in the experimental procedure where the CTES left undisturbed and uncharged for 209 hours, its temperature dropped by 136 °C. Although this is not a bad outcome, considering the solar radiation that prevails in Cyprus, there is no possibility for the system to be without solar radiation for such a long period. Still, the factory has as a backup in the worst-case scenario its conventional boilers. Additionally, the overall thermal loss coefficient of the CTES vary from 12-21 $W/m^2 \cdot K$ for a temperature drop of 10 °C. The system is also tested for two months of operation, and the total steam produced was 36 tons (23 GJ).

The second goal was to develop a validated dynamic simulation model that could be used to investigate the system further. This model is validated with real measurement data under different operation strategies, and it can also be used for an extended period of the system operation analysis. The simulation model takes all operation strategies and modes into consideration and shows a good agreement between the measured data and simulation results.

The third and ultimate goal of this work was to design a novel tool that allow anyone using as input data the thermal energy demand and steam temperature demand by the industry to easily retrieve information about the suitable system depending on each case. Subsequently, the design tool can be used to design systems with higher thermal loads and higher steam demand temperatures than KEAN needs. The tool provides information of the steam production, solar contribution, sizing of the system and CTES capacity for storage duration of 3h, 6h, 9h, 12h and 15h and steam demand temperature of 110 °C to 250 °C with step of 10 °C, for thermal loads demand from 1 ton/h to 4 tons/h. All data are provided in the form of graphs and allow anyone using as input data the thermal energy demand and steam temperature required by the industry to easily retrieve information about the suitable system depending on each case. From the LCCA carried out, one can read from the graphs developed the solar savings (thousands of EUR) and CO_2 savings (tons of CO_2) of the system at the end of its life cycle, and the payback period (years). The payback period for all cases examined, varies from 2 to 6 years, depending on the size of the system, which is very feasible.

Finally, based on the validated dynamic simulation model, a scale-up simulation model is developed with a hybrid mode enabled. The hybrid mode considers that when the steam load of the industry is already covered, the excess heat is fed directly to the CTES. The system with the hybrid mode proved that the steam production can be increased up to 8% when considering a high steam demand temperature (above 200 °C). The scale-up model developed can be used for further evaluation of the most significant parameters that affect the performance of the PTC system.

Consequently, the outcome of this work was first to identify the potential and feasibility of using PTC systems for IPH and then focus on the industries that need an alternate green solution to cover their thermal energy load. In implementing this work under the EDITOR project to install and operate the first PTC system, a dispatchable PTC system is delivered. A validated simulation model is developed based on the existing system. Finally the outcome of this work is the novel design tool developed based on a real system and the validated simulation model. This tool is designed for Cyprus industries to retrieve the system dimensions, its thermal energy contribution, and economic viability information for their demands.

Some general conclusions drawn from this work are:

- Currently, 120 solar thermal plants are in operation worldwide, covering an area of 125,000 m^2 (88 MW_{th}). From them, 61 PTC systems are installed and operating worldwide for IPH applications, with a total thermal power of 17.23 MW_{th}, for IPH applications installed and operating worldwide, and most of them are in Mexico.
- The dominant sector in terms of PTC plants number is the dairy and beverage with 19 PTC plants installed, while in terms of installed power capacity, the dominant sector is the food products with 7 MW_{th}.
- The biggest PTC plant is under construction in a mining and quarrying factory in South Oman which is expected to be able to produce 6000 tons of steam per day.
- The main energy-intensive sectors in Cyprus are transport (52.4%), residential (19.3%), services (12.7%), industry (12%), agriculture and fishing (2.4%), and others (1.2%). Comparing the final consumption of oil products imports, the industrial sector is the second higher consumer (20%) after the transport sector (57%).

- Regarding RES use in Cyprus, wind systems are the leader with an installed power capacity of 157.5 MW but PV systems are the most spread with an installed power of 74.647 MW until 2017.
- Currently, 92% of the annual thermal load for water heating is covered from the thermosyphon solar collectors. The total thermal production by solar water heating systems doubled in 18 years period and it is proven to be a sustainable solar energy system.
- KEAN soft drinks industry is the first industry incorporating a PTC system in Cyprus. The system is installed under the project 'EDITOR' and this study evaluates its performance, operation modes and potential future use, both experimentally and through simulation analyses.
- Based on the analyses carried out, the average efficiency of the system was 44%, and it can produce up to about l ton of steam per day.
- The reflectivity measurements taken on a daily basis when the mirrors were left uncleaned showed that the reflectivity dropped by 4% during 5 days and thus was concluded that they need to be cleaned once a week with water.
- Dynamic simulation model results showed a good agreement with the experimental on-site measurements of the system, with low PRE.

Future Work

The subject can be further investigated from the following points of view:

- Use the Dynamic Simulation Model to develop a design tool for other countries using as an additional input meteorological data such as annual solar radiation and mean ambient temperature, or latitude, etc.
- By using the design tool to investigate the case of installing PTC systems to all food and beverage industries in Cyprus, and estimate the financial and environmental benefits.
- Validate and optimise the hybrid mode with experimental and simulation operation test and then introduce it to the existing operation strategies of KEAN industry.
- Developed and validate new optimized strategies to use in case of cloudy weather.

Publications from this Study

During the PhD studies two journal papers and eleven conference papers are published and presented as are listed below:

Journal publications:

1. **Ktistis, P.K**, Agathokleous, R.A., Kalogirou, S.A., 2021. A design tool for a parabolic trough collector system for industrial process heat based on dynamic simulation. Renew. Energy 183, 502–514.
2. **Ktistis, P.K**., Agathokleous, R.A., Kalogirou, S.A., 2021. Experimental performance of a parabolic trough collector system for an industrial process heat application. Energy 215, 119288.

Conference papers:

1. **Ktistis P.K**., Agathokleous R.A., Kalogirou S.A., (2018). Simulation based performance investigation of an industrial PTC system in Cyprus. CPOTE 2018, International Conference Contemporary Problemso of Thermal Energy Systems in the Near Future: Energy, Ecology and Economics Gliwice, Poland.
2. **Ktistis P.K**., Agathokleous R.A., Kalogirou S.A., (2018). A Pilot PTC System Installed in an Industrial factory of Cyprus: Feasibility for the Wider Use in the Cyprus Industry. PRES 2018, CHISA 2018, Chemical Engineering Transactions (presented as poster), 70, pp. 1039-1044, Prague, Czech Republic.
3. **Ktistis P.K**., Agathokleous R.A., Kalogirou S.A., (2018). Potential of the parabolic trough collectors use in a food and beverage industrial factory in Cyprus: Simulation analysis for performance prediction. International conference on Energy, Sustainability and Climate Change, ESCC 2018, Mykonos, Greece.
4. **Ktistis P.K**., Agathokleous R.A., Kalogirou S.A., (2018). Potential of the parabolic trough collectors use in the industry of Cyprus: Current status and proposed scenarios. International conference Sustainable Energy and Environmental Protection, SEEP 2018, Glasgow, Scotland.

5. Sattler, J. C., Alexopoulos, S., Caminos, R. A. C., Mitchell, J., Ruiz, V., Kalogirou, S., **Panayiotis Ktistis**, Rafaela Agathokleous... Herrmann, U. (2019). Dynamic simulation model of a parabolic trough collector system with concrete thermal energy storage for process steam generation. Paper presented at the AIP Conference Proceedings, 2126 doi:10.1063/1.5117663

6. **Ktistis P.K**., Agathokleous R.A., Kalogirou S.A., (2019). Testing of the 1st PTC system in Cyprus' Biggest Soft Drinks Factory. International conference on 'Energy, Sustainability and Climate Change', ESCC 2019, Chania, Greece.

7. **Ktistis P.K.**, Agathokleous R.A., Kalogirou S.A., (2018). Testing of the first PTC system in Cyprus' biggest soft drinks factory. International conference Sustainable Energy and Environmental Protection, SEEP 2019, Sharjah

8. Sattler, J. C., Caminos, R. A. C., Atti, V., Ürlings, N., Dutta, S., Ruiz, V., Kalogirou S., **Ktistis P.**, ..., Herrmann, U. (2020). Dynamic simulation tool for a performance evaluation and sensitivity study of a parabolic trough collector system with concrete thermal energy storage. Paper presented at the AIP Conference Proceedings, , 2303 doi:10.1063/5.0029277

9. Sattler, J. C., Caminos, R. A. C., Ürlings, N., Dutta, S., Ruiz, V., Kalogirou, S., **Ktistis P.**, ... Herrmann, U. (2020). Operational experience and behaviour of a parabolic trough collector system with concrete thermal energy storage for process steam generation in cyprus. Paper presented at the AIP Conference Proceedings, 2303 doi:10.1063/5.0029278

10. **Ktistis P.K.**, Agathokleous R.A., Kalogirou S.A., (2020). Performance analysis of the first parabolic trough collector system for industrial process heating in Cyprus' biggest soft drinks factory. CPOTE 2020, International Conference Contemporary Problems of Thermal Engineering, Krakow, Poland.

11. **Κτίστης Π.Κ**., Αγαθοκλέους Ρ.Α, Καλογήρου Σ.Α., (2021) Μελέτη απόδοσης συστήματος παραβολικού συλλέκτη με αποθήκευση θερμικής ενέργειας σε μπετόν, για παραγωγή ατμού σε βιομηχανία. 12ο Εθνικο Συνέδριο για τις Ήπιες Μορφές Ενέργειας Θεσσαλονίκη 2021

References

Abdel-Dayem, A.M., 2011. Numerical-simulation and experimental- validation of the largest Egyptian solar process-heat system.

Ahlgren, B., Tian, Z., Perers, B., Dragsted, J., Johansson, E., Lundberg, K., Mossegård, J., Byström, J., Olsson, O., 2018. A simplified model for linear correlation between annual yield and DNI for parabolic trough collectors. Energy Convers. Manag. 174, 295–308.

Akba, T., Baker, D., Yazıcıoğlu, A.G., 2020. Modeling, transient simulations and parametric studies of parabolic trough collectors with thermal energy storage. Sol. Energy 199, 497–509.

Anzazu, A., Andez-García, F., Rojas, E., Erez, M.P., Silva, R., Hern Andez-Escobedo, Q., Manzano-Agugliaro, F., Fernández-García, A., Rojas, E., Pérez, M., Silva, R., Hernández-Escobedo, Q., Manzano-Agugliaro, F., 2015. A parabolic-trough collector for cleaner industrial process heat. J. Clean. Prod. 89, 272–285.

Arasu, A.V., Sornakumar, T., 2007. Design, manufacture and testing of fiberglass reinforced parabola trough for parabolic trough solar collectors.

Bakos, G.C., 2006. Design and construction of a two-axis Sun tracking system for parabolic trough collector (PTC) efficiency improvement. Renew. Energy 31, 2411–2421.

Biencinto, M., González, L., Valenzuela, L., 2016. A quasi-dynamic simulation model for direct steam generation in parabolic troughs using TRNSYS. Appl. Energy 161, 133–142.

Boukelia, T.E., Mecibah, M.S., Kumar, B.N., Reddy, K.S., 2015. Investigation of solar parabolic trough power plants with and without integrated TES (thermal energy storage) and FBS (fuel backup system) using thermic oil and solar salt. Energy 88, 292–303.

Brink, D.F., Youngblood, S.B., 2010. Operation and Performance of the Solar Steam System at the Johnson & Johnson Plant in Sherman, Texas. J. Sol. Energy Eng. 104, 139.

CADE Engineered Technologies - CADE Soluciones de Ingeniería , 2020. URL https://cadeengineering.com/ (accessed 3.3.20).

Cascetta, F., Cirillo, L., Nardini, S., Vigna, S., 2018. Transient Simulation of a Solar Cooling

System for an Agro-Industrial Application. In: Energy Procedia. Elsevier Ltd, pp. 328–335.

Castro, A., Cardoso, J.P., Mendes, L.F., Azevedo, P., Mendes, J.F., 2018. Pre-heating boiler feedwater for expanded cork agglomerate production using a parabolic trough system. AIP Conf. Proc. 2033.

Chen, F., Li, M., Zhang, P., Luo, X., 2015. Thermal performance of a novel linear cavity absorber for parabolic trough solar concentrator. Energy Convers. Manag. 90, 292–299.

Cheng, Z.D., He, Y.L., Cui, F.Q., 2012. Numerical study of heat transfer enhancement by unilateral longitudinal vortex generators inside parabolic trough solar receivers.

Coccia, G., Nicola, G. Di, Sotte, M., Di Nicola, G., Sotte, M., 2015. Design, manufacture, and test of a prototype for a parabolic trough collector for industrial process heat. Renew. Energy 74, 727–736.

Condor reflectometer 2019. . Abengoa. URL https://www.energy-xprt.com/products/condor-portable-reflectometer-530335 (accessed 3.26.20).

Cotrado, M., Dalibard, A., Söll, R., Pietruschka, D., 2014. Design, control and first monitoring data of a large scale solar plant at the meat factory Berger, Austria. Energy Procedia 48, 1144–1151.

Cundapí, R., Moya, S.L., Valenzuela, L., 2017. Approaches to modelling a solar field for direct generation of industrial steam. Renew. Energy 103, 666–681.

Cyprus Energy efficiency report, 2013. . Ctry. Rep.

Cyprus National Plan for Energy and Climate, 2018.

Cyprus Statistical Service - Industry, 2021. URL https://www.mof.gov.cy/Mof/cystaT/STATisTiCS.nsF/industry_construction_61main_en/industry_construction_61main_en?OpenForm&sub=1&sel=1 (accessed 5.25.21).

Cyprus Statistical Services - Energy, 2021. URL https://www.mof.gov.cy/mof/cystat/statistics.nsf/agriculture_51main_en/agriculture_51main_en?OpenForm&sub=1&sel=2 (accessed 5.12.21).

EAC, 2014. The history of electricity in Cyprus and the Electricity Authority of Cyprus. URL

https://www.eac.com.cy/EN/eac/abouteac/Pages/History.aspx (accessed 2.22.18).

EAC, 2019. Tseri Photovoltaic Park. URL https://www.eac.com.cy/EN/nonregulatedactivities/photovoltaicparktseri/Pages/default.aspx (accessed 1.3.20).

Eck, M., Zarza, E., Eickhoff, M., Rheinlander, J., Valenzuela, L., 2003. A pplied research concerning the direct steam generation in parabolic troughs. Sol. Energy 74, 341–351.

Eiamsa-Ard, S., Wongcharee, K., Sripattanapipat, S., 2009. 3-D Numerical simulation of swirling flow and convective heat transfer in a circular tube induced by means of loose-fit twisted tapes ☆. Int. Commun. Heat Mass Transf. 36, 947–955.

Emergo Wealth Ltd, 2016. Energy Sector Dynamics.

European Commision, 2017. Report from the commission to the European Parliament and the Council.

European Commission, 2019. 2030 Climate &Amp; Energy Framework . Eur. Comm. URL https://ec.europa.eu/clima/policies/strategies/2030_en (accessed 1.16.20).

European Council, 2017. 4th National Energy Efficiency Action Plan. Nicosia.

European Union, 2017. Statistical Pocketbook 2017: Energy, Publications Office of the European Union.

Eurostat, 2020. Short Assessment of Renewable Energy Sources . Eurostat. URL https://ec.europa.eu/eurostat/web/energy/data/shares (accessed 5.14.21).

Eurostat Statistics Explained , 2021. URL https://ec.europa.eu/eurostat/statistics-explained/index.php?title=Electricity_price_statistics#Electricity_prices_for_non-household_consumers (accessed 5.12.21).

Fachhochschule Aachen, University of Applied Sciences , 2020. URL https://www.fh-aachen.de/ (accessed 5.28.20).

Farjana, S.H., Huda, N., Mahmud, M.A.A.P., Saidur, R., 2017. Solar process heat in industrial systems – A global review. Renew. Sustain. Energy Rev. 82, 2270–2286.

Ferná Ndez-García, A., Zarza, E., Valenzuela, L., Pé Rez, M., 2010. Parabolic-trough solar collectors and their applications. Renew. Sustain. Energy Rev. 14, 1695–1721.

Franz Mauthner, W.W., 2013. Solar Heat Worldwide: Market and Contribution to the Energy Supply. Int. Energy Agency.

Fuqiang, W., Qingzhi, L., Huaizhi, H., Jianyu, T., 2016. Parabolic trough receiver with corrugated tube for improving heat transfer and thermal deformation characteristics. Appl. Energy 164, 411–424.

German Aerospae Center, 2020. URL https://www.dlr.de/EN/Home/home_node.html (accessed 3.3.20).

Ghadirijafarbeigloo, S., Zamzamian, A.H., Yaghoubi, M., 2014. 3-D numerical simulation of heat transfer and turbulent flow in a receiver tube of solar parabolic trough concentrator with louvered twisted-tape inserts. Energy Procedia 49, 373–380.

Ghazouani, M., Bouya, M., Benaissa, M., 2020a. Thermo-economic and exergy analysis and optimization of small PTC collectors for solar heat integration in industrial processes. Renew. Energy 152, 984–998.

Ghazouani, M., Bouya, M., Benaissa, M., 2020b. Thermo-economic and exergy analysis and optimization of small PTC collectors for solar heat integration in industrial processes. Renew. Energy 152, 984–998.

Ghazzani, B. El, Plaza, D.M., Ait, R., Cadi, E., Ihlal, A., Abnay, B., Bouabid, K., 2017. Thermal plant based on parabolic trough collectors for industrial process heat generation in Morocco. Renew. Energy 113, 1261–1275.

González-Roubaud, E., Pérez-Osorio, D., Prieto, C., 2017. Review of commercial thermal energy storage in concentrated solar power plants: Steam vs. molten salts. Renew. Sustain. Energy Rev.

Guerrero-Quijano, Á., Fernández-García, A., Pérez, M., Zarza, E., Valenzuela, L., 2011. Modelling of a small-sized parabolic - trough solar collector field for process heat in the cork industry. In: ISES Solar World Congress 2011.

Halimi, M., Outana, I., Diouri, J., Amrani, A. El, Messaoudi, C., El Amrani, A., Messaoudi, C., 2018. Experimental investigation of absorbed flux circumferential distribution of an absorber with U-pipe tube exchanger for Parabolic Trough Collectors. Appl. Therm. Eng. 129, 1230–1239.

He, Y.-L., Mei, D.-H., Tao, W.-Q., Yang, W.-W., Liu, H.-L., 2012. Simulation of the parabolic trough solar energy generation system with Organic Rankine Cycle. Appl. Energy 97, 630–641.

He, Y.L., Wang, K., Qiu, Y., Du, B.C., Liang, Q., Du, S., 2019. Review of the solar flux distribution in concentrated solar power: Non-uniform features, challenges, and solutions. Appl. Therm. Eng.

Huang, Z., Li, Z.-Y., Yu, G.-L., Tao, W.-Q., 2017. Numerical investigations on fully-developed mixed turbulent convection in dimpled parabolic trough receiver tubes.

Huang, Z., Yu, G.L., Li, Z.Y., Tao, W.Q., 2015. ScienceDirect Numerical study on heat transfer enhancement in a receiver tube of parabolic trough solar collector with dimples, protrusions and helical fins. Energy Procedia 69, 1306–1316.

IEA, 2016. SHC Task 49 . Iea Shc. URL http://task49.iea-shc.org/ (accessed 12.18.19).

International Energy Agency, 2017. Cyprus: Balances for 2015 . URL https://www.iea.org/statistics/statisticssearch/report/?country=CYPRUS&product=balances&year=2015 (accessed 2.22.18).

Jebasingh, V.K., Herbert, G.M.J., 2016. A review of solar parabolic trough collector. Renew. Sustain. Energy Rev. 54, 1085–1091.

John, E., Hale, M., Selvam, P., 2013. Concrete as a thermal energy storage medium for thermocline solar energy storage systems. Sol. Energy 96, 194–204.

Jurich, K., 2016. CO2 Emission Factors for Fossil Fuels.

Kalogirou, S., 2003. The potential of solar industrial process heat applications. Appl. Energy 76, 337–361.

Kalogirou, S.A., 2002. Parabolic trough collectors for industrial process heat in Cyprus. Energy

27, 813–830.

Kalogirou, S.A., 2004. Solar thermal collectors and applications. Prog. Energy Combust. Sci. 30, 231–295.

Kalogirou, S.A., 2014a. Chapter 7 - Industrial Process Heat, Chemistry Applications, and Solar Dryers. In: Kalogirou, S.A.B.T.-S.E.E. (Second E. (Ed.), . Academic Press, Boston, pp. 397–429.

Kalogirou, S.A., 2014b. Solar Energy Engineering Processes and Systems. Book 1–527.

Kalogirou, S.A., Karellas, S., Braimakis, K., Stanciu, C., Badescu, V., 2016. Exergy analysis of solar thermal collectors and processes. Prog. Energy Combust. Sci. 56, 106–137.

Ktistis, P., Agathokleous, R.A., Kalogirou, S.A., 2021. A design tool for a parabolic trough collector system for industrial process heat based on dynamic simulation. Renew. Energy 183, 502–514.

Ktistis, P.K., Agathokleous, R.A., Kalogirou, S.A., 2021. Experimental performance of a parabolic trough collector system for an industrial process heat application. Energy 215, 119288.

Kumar, A., Sharma, M., Thakur, P., Thakur, V.K., Rahatekar, S.S., Kumar, R., 2020. A review on exergy analysis of solar parabolic collectors. Sol. Energy 197, 411–432.

Kumar, C.N., Murugesan, P., 2012. Review on Twisted Tapes Heat Transfer Enhancement. Int. J. Sci. Eng. Res. 3.

Kumar, K.R., Reddy, K.S., 2008. Thermal analysis of solar parabolic trough with porous disc receiver. Appl. Energy 86, 1804–1812.

Kumar, P., Ms, M., Mathur, N., Ms, T., Paul, S., Design, T., Production, T., Mr, V., Kumar, T., Mr, R.K., Joshi, T., Mr, A., Sachdeva, T., 2014. India’s quest for solar steam and process.

Kumaresan, G., Sridhar, R., Velraj, R., 2012. Performance studies of a solar parabolic trough collector with a thermal energy storage system. Energy 47, 395–402.

Laing, D., Lehmann, D., Bahl, C., Ag, E.Z., 2008. Concrete Storage for Solar Thermal Power Plants and Industrial Process Heat. Conf. Proc. 1–6.

Li, M., Shimizu, M., Hatano, R., 2015. Evaluation of N2O and CO2 hot moments in managed grassland and cornfield, southern Hokkaido, Japan. Catena 133, 1–13.

Lobón, D.H., Valenzuela, L., 2013. Impact of pressure losses in small-sized parabolic-trough collectors for direct steam generation. Energy 61, 502–512.

Manikandan, G.K., Iniyan, S., Goic, R., 2019. Enhancing the optical and thermal efficiency of a parabolic trough collector – A review. Appl. Energy.

Mansour, K., Boudries, R., Dizene, R., 2018. Optical, 2D thermal modeling and exergy analysis applied for performance prediction of a solar PTC. Sol. Energy 174, 1169–1184.

Martins, M., Villalobos, U., Delclos, T., Armstrong, P., Bergan, P.G., Calvet, N., 2015. New Concentrating Solar Power Facility for Testing High Temperature Concrete Thermal Energy Storage. Energy Procedia 75, 2144–2149.

Matthias Günther, A., Joemann, M., Csambor, S., Amenallah Guizani, R., Krüger, D., Hirsch, T., 2015. Advanced CSP Teaching Materials Parabolic Trough Technology.

Minder, S., 2012. Example of concentrated solar systems (PTC) in the dairy industry in Switzerland.

Ministry of Agriculture, R.D. and E., 2021. Department of meteorology . URL http://www.moa.gov.cy/moa/dm/dm.nsf/home/home?OpenForm (accessed 5.12.21).

Miraah Solar , n.d. URL https://www.pdo.co.om/en/technical-expertise/solar-project-miraah/Pages/default.aspx (accessed 9.3.19).

Mouaky, A., Alami Merrouni, A., Laadel, N.E., Bennouna, E.G., 2019. Simulation and experimental validation of a parabolic trough plant for solar thermal applications under the semi-arid climate conditions. Sol. Energy 194, 969–985.

Muñoz, J., Abánades, A., 2011. Analysis of internal helically finned tubes for parabolic trough design by CFD tools. Appl. Energy 88, 4139–4149.

Mwesigye, A., Bello-Ochende, T., Meyer, J.P., 2014. Heat transfer and thermodynamic performance of a parabolic trough receiver with centrally placed perforated plate inserts. Appl. Energy 136, 989–1003.

Odeh, S.D., Morrison, G.L., 2006. Optimization of parabolic trough solar collector system. Int. J. Energy Res.

Página Não Encontrada, 2010. URL https://www.brewersassociation.org/programs/craftbeer-com/undefined%0Ahttps://www.mendeley.com/download-desktop/Windows/undefined/ (accessed 12.18.19).

Pietruschka, D., Fedrizzi, R., Orioli, F., Söll, R., Stauss, R., 2012. Demonstration of three large scale solar process heat applications with different solar thermal collector technologies. Energy Procedia 30, 755–764.

Powell, K.M., Edgar, T.F., 2012. Modeling and control of a solar thermal power plant with thermal energy storage. Chem. Eng. Sci. 71, 138–145.

Pytilinski, J.T., 1978. Solar energy installations for pumping irrigation water, Solar Energy.

Qu, W., Wang, R., Hong, H., Sun, J., Jin, H., 2017. ScienceDirect Prototype testing of a 300kW th solar parabolic-trough collector using rotatable axis tracking. Energy Procedia 105, 780–786.

Ravi Kumar, K., Reddy, K.S., 2012. 4-E (energy-exergy-environmental-economic) analyses of line-focusing stand-alone concentrating solar power plants. Int. J. Low-Carbon Technol. 7, 82–96.

Rittmann-Frank, M.H., Möllenkamp, J., Caflisch, M., Häberle, A., 2018. Evaluation of solar process heat systems in Switzerland. AIP Conf. Proc. 2033.

Sandia National Laboratories: Exceptional Service in the National Interest , 2020. URL https://www.sandia.gov/ (accessed 9.2.19).

Sarbu, I., Sebarchievici, C., 2018. A comprehensive review of thermal energy storage. Sustain.

SIJ, 2019. Project EDITOR. url https://www.fh-aachen.de/forschung/solar-institut-juelich/schwerpunkte/editor/ (accessed 3.3.20).

Silva, R, Berenguel, M., Pérez, M., Fernández-Garcia, A., 2014. Thermo-economic design optimization of parabolic trough solar plants for industrial process heat applications with memetic algorithms. Appl. Energy 113, 603–614.

Silva, Ricardo, Cabrera, F.J., Pérez-García, M., 2014. Process heat generation with parabolic trough collectors for a vegetables preservation industry in Southern Spain. Energy Procedia 48, 1210–1216.

Silva, R., Pérez, M., Fernández-Garcia, A., 2013. Modeling and co-simulation of a parabolic trough solar plant for industrial process heat. Appl. Energy 106, 287–300.

Solar Energy in Oman - Miraah | GlassPoint Solar , 2020. URL https://www.glasspoint.com/miraah/ (accessed 1.7.20).

Solar International GmbH, P., 1999. Survey of Thermal Storage for Parabolic Trough Power Plants.

Solar Thermal Energy – Protarget AG , 2020. URL https://protarget-ag.com/en/solar-thermal-energy/ (accessed 3.3.20).

Solar Thermal Plants Database | Solar Heat for Industrial Processes (SHIP) Plants Database , 2021. URL http://ship-plants.info/solar-thermal-plants?collector_type=5 (accessed 7.19.19).

Solargis, 2019. Global Solar Atlas 2.0 . URL https://solargis.com/maps-and-gis-data/download/cyprus (accessed 5.12.21).

Song, X., Dong, G., Gao, F., Diao, X., Zheng, L., Zhou, F., 2014. A numerical study of parabolic trough receiver with nonuniform heat flux and helical screw-tape inserts. Energy 77, 771–782.

Spencer, L.C., 1989. A comprehensive review of small solar-powered heat engines: Part I. A history of solar-powered devices up to 1950. Sol. Energy 43, 191–196.

Thomas, A., 1992. Operation and performance of the solar steam generation system installed at the government silk factory. Energy Convers. Mgmt 33, 191–196.

TRNSYS - Official Website, 2020. URL https://sel.me.wisc.edu/trnsys/ (accessed 5.28.20).

Vannoni, C., Battisti, R., Drigo, S., 2008. Task 33/IV – Potential for Solar Heat in Industrial Processes Solar Potential for Solar Heat in Industrial Processes. Dep. Mech. Aeronaut. - Univ. Rome “La Sapienza” This.

Vicente, P.G., Garc Õa, A., Viedma, A., n.d. Heat transfer and pressure drop for low Reynolds

turbulent ¯ow in helically dimpled tubes.

Walker, A., Kutscher, C., Halvorsen, A., McKenna, C., Chambers, D., May, K., 2007. Design and Analysis of a Large Solar Industrial Heat Plant for Frito Lay in Modesto California. In: ASME 2007 Energy Sustainability Conference. ASME, pp. 657–662.

Wang, P., Liu, D.Y., Xu, C., 2013. Numerical study of heat transfer enhancement in the receiver tube of direct steam generation with parabolic trough by inserting metal foams. Appl. Energy 102, 449–460.

Wyman, C., Castle, J., Kreith, F., 1980. A review of collector and energy storage technology for intermediate temperature applications. Sol. Energy 24, 517–540.

Xiangtao, G., Fuqiang, W., Haiyan, W., Jianyu, T., Qingzhi, L., Huaizhi, H., 2017. Heat transfer enhancement analysis of tube receiver for parabolic trough solar collector with pin fin arrays inserting.

Xiao, X., Zhang, P., Shao, D.D., Li, M., 2014. Experimental and numerical heat transfer analysis of a V-cavity absorber for linear parabolic trough solar collector. Energy Convers. Manag. 86, 49–59.

Xu, C., Chen, Z., Li, M., Zhang, P., Ji, X., Luo, X., Liu, J., 2014. Research on the compensation of the end loss effect for parabolic trough solar collectors. Appl. Energy 115, 128–139.

Zhai, H., Dai, Y., Wu, J., Wang, R., 2009. Study on Trough Receiver for Linear Concentrating Solar Collector. In: Goswami, D.Y., Zhao, Y. (Eds.), Proceedings of ISES World Congress 2007 (Vol. I -- Vol. V). Springer Berlin Heidelberg, Berlin, Heidelberg, pp. 711–715.

Zhang, H., Baeyens, J., Cáceres, G., Degrève, J., Lv, Y., 2016. Thermal energy storage: Recent developments and practical aspects. Prog. Energy Combust. Sci. 53, 1–40.

Appendix I Details of available PTC plants for IPH applications, worldwide.

Manufacture of Mining and quarrying								
Year of operation start	**Installed**	**Country**	**Installed Collector Area (grossed) m^2**	**Installed thermal power [Kw_{th}]**	**Process**	**Total investment costs [turnkey]**	**Specific investment cost [€/m^2]**	**Company**
2017	Ground	Oman	630000	300000.0	Other process heating	-	-	Glasspoint
Manufacture of Processing and preserving of fruit and vegetables								
Year of operation start	**Installed**	**Country**	**Installed Collector Area (grossed) m^2**	**Installed thermal power [Kw_{th}]**	**Process**	**Total investment costs [turnkey]**	**Specific investment cost [€/m^2]**	**Company**
2013	Rooftop	Spain	175	134	Cooking	156,216.00	892.66	Rackam
Manufacture of Processing and preserving of meat and production of meat products								
Year of operation start	**Installed**	**Country**	**Installed Collector Area (grossed) m^2**	**Installed thermal power [Kw_{th}]**	**Process**	**Total investment costs [turnkey]**	**Specific investment cost [€/m^2]**	**Company**
2015	Rooftop	Mexico	89.48	22.2	Cleaning	13,281.00	148.42	INVENTIVE POWER SA PI DE CV
2015	Ground	Mexico	250	43.38	Other process heating	44,145.00	176.58	INVENTIVE POWER SA PI DE CV
2017	Ground	Mexico	396	64.83	Cooking	59,449.00	150.12	INVENTIVE POWER SA PI DE CV
Manufacture of prepared animal feeds								
Year of operation start	**Installed**	**Country**	**Installed Collector Area (grossed) m^2**	**Installed thermal power [Kw_{th}]**	**Process**	**Total investment costs [turnkey]**	**Specific investment cost [€/m^2]**	**Company**
2014	Ground	Mexico	310	97.2	Cooking	58,000.00	187.1	INVENTIVE POWER SA PI DE CV
2015	Ground	Mexico	540	126.3	Other process heating	68,889.00	127.57	INVENTIVE POWER SA PI DE CV
2016	Rooftop	Mexico	577.13	118	cooling processes	84,307.00	146.08	INVENTIVE POWER SA PI DE CV
2017	Rooftop	Mexico	1031.25	179.85	General process heating	125,686.00	121.88	INVENTIVE POWER SA PI DE CV
2017	Ground	Mexico	1155	202.54	Other process heating	118,414.00	102.52	INVENTIVE POWER SA PI DE CV
Manufacture of textiles products								
Year of operation start	**Installed**	**Country**	**Installed Collector Area (grossed) m^2**	**Installed thermal power [Kw_{th}]**	**Process**	**Total investment costs [turnkey]**	**Specific investment cost [€/m^2]**	**Company**
-	-	Germany	100	50	Other process heating	-	-	Smirro GmbH
2014	Rooftop	India	263	184.1	Cleaning	34,544.00	131.35	Leveragenet Solutions Pvt. Ltd.

Manufacture of dairy products								
Year of operation start	**Installed**	**Country**	**Installed Collector Area (grossed) m^2**	**Installed thermal power [Kw_{th}]**	**Process**	**Total investment costs [turnkey]**	**Specific investment cost [€/m^2]**	**Company**
2011	Ground	canada	82	46	Cleaning	96,000.00	1170.73	Rackam
2011	Rooftop	Switzerland	115	67	General process heating	252,000.00	2191.3	NEP Solar AG
2012	Rooftop	Switzerland	627.0	360	General process heating	300,000.00	478.47	NEP Solar AG
2012	Rooftop	Mexico	401.1	74	Other process heating	44,200.00	110.2	INVENTIVE POWER SAPI DE CV
2013	Rooftop	Switzerland	581	330	Sterilization	700,000.00	1204.82	NEP Solar AG
2013	Ground	Mexico	265.68	46.2	Pasteurization	40,000.00	150.56	INVENTIVE POWER SAPI DE CV
2013	Rooftop	Mexico	66	46.2	General process heating	23,039.00	349.08	INVENTIVE POWER SAPI DE CV
2014	Ground	Mexico	460	126	Pasteurization	100,000.00	217.39	INVENTIVE POWER SAPI DE CV
2014	Rooftop	Mexico	462	137	Pasteurization	130,000.00	97.92	INVENTIVE POWER SAPI DE CV
2014	Rooftop	Mexico	66	22.2	Pasteurization	18,000.00	272.73	INVENTIVE POWER SAPI DE CV
2014	Ground	Mexico	250.0	62.72	Other process heating	32,677.00	130.71	INVENTIVE POWER SAPI DE CV
2015	Rooftop	Marocco	110	61	Pasteurization	45556	414.15	Rackam
2015	Ground	Mexico	422	94.5	Cleaning	46,144.00	109.35	INVENTIVE POWER SAPI DE CV
2015	Rooftop	Mexico	250	42	Pasteurization	28,046.00	112.18	INVENTIVE POWER SAPI DE CV
2015	Rooftop	Mexico	1641.25	240	Pasteurization	160,000.00	97.49	INVENTIVE POWER SAPI DE CV
2016	Rooftop	Mexico	132	59.88	Pasteurization	36,894.00	279.5	INVENTIVE POWER SAPI DE CV
2017	Ground	Mexico	226.78	59.9	Other process heating	48,050.00	211.88	INVENTIVE POWER SAPI DE CV
2018	Ground	India	576.0	320	Drying	150,000.00	260.42	Protarget AG
-	-	Greece	10	7	General process heating	-	-	Absolicion
Manufacture of food products								
Year of operation start	**Installed**	**Country**	**Installed Collector Area (grossed) m^2**	**Installed thermal power [Kw_{th}]**	**Process**	**Total investment costs [turnkey]**	**Specific investment cost [€/m^2]**	**Company**
2008	-	United States	5068	3547.6	General process heating	-	-	-
2015	Ground	Mexico	577.13	116.02	Cooking	115,000.00	199.26	INVENTIVE POWER SAPI DE CV
2017	Ground	Mexico	165	35.34	Other process heating	22,706.00	137.61	INVENTIVE POWER SAPI DE CV
2017	Ground	Mexico	529.2	77.9	Cooking	81,349.00	153.72	INVENTIVE POWER SAPI DE CV
2017	Rooftop	Mexico	660	104.81	Cooking	117,365.00	177.83	INVENTIVE POWER SAPI DE CV
2017	Rooftop	Mexico	742.5	112.85	Other process heating	110,435.00	148.73	INVENTIVE POWER SAPI DE CV
2017	Ground	Mexico	693	92.61	Cooking	103,491.00	149.34	INVENTIVE POWER SAPI DE CV
2020	-	Turkey	6000	3000	General process heating			Soliterm

Manufacture of bevarage products								
Year of operation start	**Installed**	**Country**	**Installed Collector Area (grossed) m^2**	**Installed thermal power [Kw_{th}]**	**Process**	**Total investment costs [turnkey]**	**Specific investment cost [€/m^2]**	**Company**
2015		Mexico	610	94.6	Evaporation and Distillation	59,403.00	97.38	INVENTIVE POWER SAPI DE CV
2017	Rooftop	Mexico	34.13	15.05	Pasteurization	24,131.00	707.03	INVENTIVE POWER SAPI DE CV
2017	Rooftop	Mexico	577.13	123.55	Pasteurization	94,736.00	164.15	INVENTIVE POWER SAPI DE CV
2018	Rooftop	Mexico	816.75	136.79	Evaporation and Distillation	109,007.00	133.46	INVENTIVE POWER SAPI DE CV
2018	Ground	Cyprus	288	201.6	Pasteurization	150,000.00	520.83	protarget AG
Agriculture, forestry and fishing								
Year of operation start	**Installed**	**Country**	**Installed Collector Area (grossed) m^2**	**Installed thermal power [Kw_{th}]**	**Process**	**Total investment costs [turnkey]**	**Specific investment cost [€/m^2]**	**Company**
2008	Ground	Germany	440	220	Other process heating	200,000.00	454.55	Solarlite CSP Technology GmbH
2013	Ground	Mexico	112	36	heating of production halls	20,000.00	178.57	INVENTIVE POWER SAPI DE CV
Manufacture of paper and paper products								
Year of operation start	**Installed**	**Country**	**Installed Collector Area (grossed) m^2**	**Installed thermal power [Kw_{th}]**	**Process**	**Total investment costs [turnkey]**	**Specific investment cost [€/m^2]**	**Company**
2014	Ground	Canada	1490	800	Drying	650,000.00	436.24	Rackam
Manufacture of chemicals and chemical products								
Year of operation start	**Installed**	**Country**	**Installed Collector Area (grossed) m^2**	**Installed thermal power [Kw_{th}]**	**Process**	**Total investment costs [turnkey]**	**Specific investment cost [€/m^2]**	**Company**
2016	Rooftop	China	4600	1050	Evaporation and Distillation	574,520.00	124.9	Vicot Solar Technology Co., Ltd
Manufacture of basic pharmaceutical products and pharmaceutical preparations								
Year of operation start	**Installed**	**Country**	**Installed Collector Area (grossed) m^2**	**Installed thermal power [Kw_{th}]**	**Process**	**Total investment costs [turnkey]**	**Specific investment cost [€/m^2]**	**Company**
2003	-	Egypt	1900	1330	General process heating	-	-	Lotus Solar Technologies, Fichtner Solar GmbH
2014	-	Mexico	110	31.67	General process heating	28,038.00	254.89	INVENTIVE POWER SAPI DE CV

Manufacture of fabricated metal products, except machinery and equipment								
Year of operation start	**Installed**	**Country**	**Installed Collector Area (grossed) m^2**	**Installed thermal power [Kw_{th}]**	**Process**	**Total investment costs [turnkey]**	**Specific investment cost [€/m^2]**	**Company**
-	-	Germany	108	75.6	General process heating	-	-	Solitem
2012	-	India	400	72	surface treatment	74,096.21	185.24	Thermax Limited
2014	-	Portugal	450	119	Drying	-	-	-
2014	Ground	Portugal	450	67	Drying	100,000.00	222.22	Rackam
Manufacture of computer, electronic and optical products								
Year of operation start	**Installed**	**Country**	**Installed Collector Area (grossed) m^2**	**Installed thermal power [Kw_{th}]**	**Process**	**Total investment costs [turnkey]**	**Specific investment cost [€/m^2]**	**Company**
-	-	Sweden	100	40	surface treatment	-	-	Absolicion
Other manufacturing								
Year of operation start	**Installed**	**Country**	**Installed Collector Area (grossed) m^2**	**Installed thermal power [Kw_{th}]**	**Process**	**Total investment costs [turnkey]**	**Specific investment cost [€/m^2]**	**Company**
2018	Ground	Mexico	158.4	110.88	Other process heating	80,000.00	505.05	CITRUS JMK S.A. DE C.V.
Water supply; sewerage; waste managment and remediation activities								
Year of operation start	**Installed**	**Country**	**Installed Collector Area (grossed) m^2**	**Installed thermal power [Kw_{th}]**	**Process**	**Total investment costs [turnkey]**	**Specific investment cost [€/m^2]**	**Company**
2013	Ground	United States	690	480	Evaporation and Distillation	-	-	SkyFuel, Inc.
2017	Ground	United States	151	98	Drying	58,608.00	388.13	Rackam
Professional, scientific and technical activities								
Year of operation start	**Installed**	**Country**	**Installed Collector Area (grossed) m^2**	**Installed thermal power [Kw_{th}]**	**Process**	**Total investment costs [turnkey]**	**Specific investment cost [€/m^2]**	**Company**
2011	Ground	Thailand	928	500	Other process heating	600,000.00	450000	Solarlite CSP Technology GmbH
2016	Rooftop	Mexico	106.1	62.7	Other process heating	22,928.00	216.1	INVENTIVE POWER SAPI DE CV
Human health and social work activities								
Year of operation start	**Installed**	**Country**	**Installed Collector Area (grossed) m^2**	**Installed thermal power [Kw_{th}]**	**Process**	**Total investment costs [turnkey]**	**Specific investment cost [€/m^2]**	**Company**
2015	Rooftop	India	50	35	Drying	20,592.00	411.84	Greenera Energy

Appendix II System installation process.

Regarding the installation process, most of the system parts and components were shipped in boxes in Cyprus and assembled on site. These are the PTCs, pipes, the two containers with the CTES modules, the control room, the valves and pipes (Figure 78).

Figure 78: Components of the PTC.

As shown in Figure 79, the installation procedure started by the CTES installation and the control room containers on the concrete base constructed previously.

Figure 79: CTES facilities.

The next step was to place the I-beams on the concrete infrastructure (Figure 80). On these beams the PTCs was mounted. This was done to simulate that these collectors could also be mounted on the roof of the building.

Figure 80: I-beams connected to the concrete infrastructure.

Then, the 8 PTCs were placed in northsouth orientation tracking the sun from east to west (Figure 81). For the collector series, two hydraulic tracking mechanismswere installed to track the sun with a high accuracy, ensuring the highest performance (Figure 82 - Figure 83).

Figure 81: Collectors assembled

Figure 82: Main support of the PTC system.

Figure 83: Mirror, absorber tube basis, and setting the PTC on the structure.

Subsequently, the absorber tubes were alighned on the focal line of the collector. Initially, the PTCs were mounted at 90° to be accessible. For each welding, a camera was inserted inside the

absorber tube for the welding evaluation. If it was insufficient, the welding process was repeated and the absorber tube was then placed on the supporting structure (Figure 84-Figure 86).

Figure 84: Preparation of the collectors for a ticking welding.

Figure 85: The welding procedure.

Figure 86: Testing the welding by a camera.

Flexible and relief valves were placed at the edge of each row, and the supporting structure of the inlet and outlet tubes were also constructed (Figure 87). The absorber tubes were connected with the flexibles and the inlet and outlet valves of the control room, creating a loop. A bridge was also constructed to support the steam pipe going from the control room to the steam – end (Figure 88).

Figure 87: Connection of the PTC receiver tube with distribution pipe via a flexible connector.

Figure 88: Supply of the produced steam with the industry's steam distribution system.

Furthermore, a pressure test was done to the loop to ensure that there are no leakages through the piping as can be seen in Figure 89. All beams and containers were painted and the ground area was asphalt-covered. Also, the whole system is surrounded with protecting fences and a

feedwater tank was placed on the roof between the control room and the CTES container (Figure 90).

Figure 89: Pressure test.

Figure 90: Painting the containers and other equipment, and the installation of the feed water tank.

A weather station was shipped and assembled as shown in Figure 91 to Figure 93 Finally, the steam generator was shipped to Cyprus and installed in the control room.

Figure 91: Installation of the weather station.

Figure 92: Steam Generator shipped and ready to be installed.

Figure 93: Steam Generator and parts installed.

After, the installation of the SG, the next step was the filling of the expansion tank with nitrogen and the whole system with the heat transfer fluid (HTF) (Figure 94).

Figure 94: System filled up with HTF and the expansion tank with nitrogen.

Finally, the parabolic mirrors were installed and adjusted to the right angle on the PTC structure (Figure 95).

Figure 95: Adjustment of mirrors on the right angle.

After the mirrors were installed on the structure, a long period was spent on operation tests, maintenance of components and improvements before the operation of the PTC system at an autonomous level. The valves, sensors, and alarms were connected with the central control processor (Figure 96) and leakages of fittings were fixed (Figure 97).

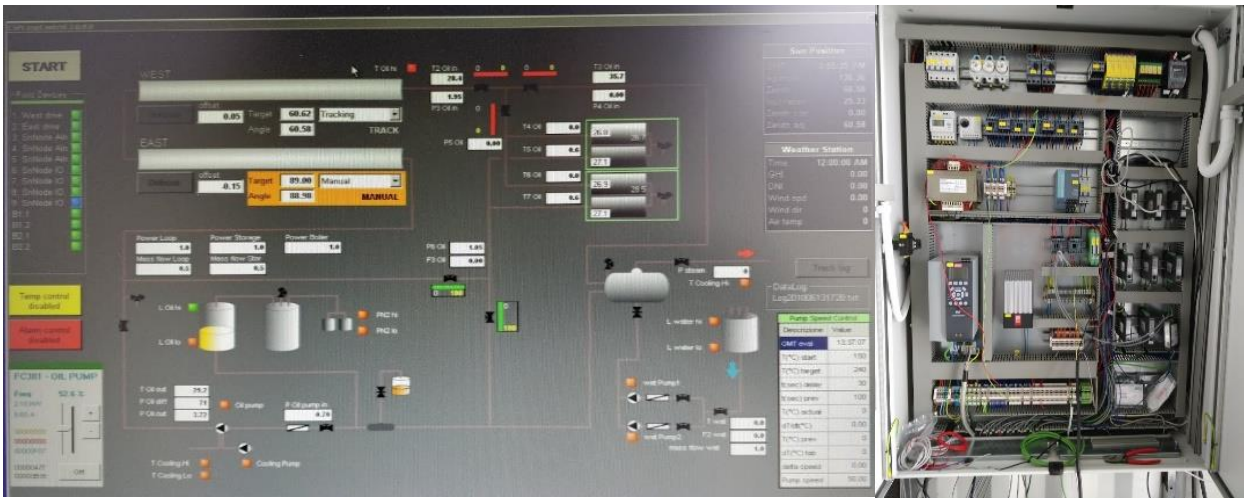

Figure 96: Set up the control system.

Figure 97: Elimination of leakages and installation of instruments and alarms.

To minimize the heat losses, insulation was placed on pipes and other parts of the system as can be seen in Figure 98. The operation modes have been developed during the first few months to make the decisions required to make the system autonomous.

Figure 98: Thermal insulation on various parts of the system.

The operation modes designed and optimized are, the half production, half charge, half preheating, production, charge, preheating, and plant off. Finally, the system was successfully operating in autonomous mode, and able to supply approximately a ton of steam per day to KEAN industry (Figure 99, Figure 100).

Figure 99: First operation tests and steam production @10 bar pressure.

Figure 100: PTC system hand – over to KEAN industry.

Appendix III Inputs and parameters of main TYPES of TRNSYS.

SOLAR FIELD [TYPE 536]	Parameters
Number of collectors in series	4
Number of collectors in parallel	2
Aperture area	36 m^2
Concentration ratio	27
Intercept efficiency (FrTan)	0.8
Efficiency slope (FrUl)	B0= 0 /K
	B1=0.03 $W/m^2 \cdot K$
	B2=-6E^{-5} $W/m^2 \cdot K^2$
	B3=1.1E^{-6} $W/m^2 \cdot K^3$
Fluid specific heat	2.3 kJ/kg·K
Logical unit	52
Number of IAM points	10
Tested flow rate	50 kg/h.m^2
IAM points	0° - 1 10° - 0.997 20° - 0.994 30° - 0.979 40° - 0.940 50° - 0.865 60° - 0.742 70° - 0.559 80° - 0.304 90° - 0

SOLAR FIELD [TYPE 536]	Inputs
Inlet temperature	From Valve 4
Inlet flow rate	From Valve 4
Ambient temperature	From file (KEAN weather data)
Incident beam radiation	From file (KEAN weather data)
Incident angle	Weahter data file
Maximum outlet temperature	350 °C

CTES [TYPE 430]	Parameters
HTF specific heat	2.3 kJ/kg·K
HTF density	580 kg/m^3
Total cross sec area of pipes	0.003921 m^2
Length of storage	20 m
Concrete specific heat	2.2 kJ/kg·K
Concrete total mass	28157 kg
Overall heat transfer coefficient at reference flow rate	19969.78 kJ/hr·K
Overall loss coefficient	250 kJ/hr·K
Number of nodes	5
Reference flow rate	0.000277 kg/s
ak0 parameter for scaling of heat transfer coeff.	1
ak1	0
ak2	0
ak3	0
ak4	0
ak5	0

SOLAR FIELD [TYPE 536]	Inputs
HTF temp entering on top	From charging valve 3
HTF flow rate entering on top	From charging valve 3
HTF temp entering at bottom	From charging valve 5
HTF flow rate entering at bottom	From charging valve 5
Ambient temperature	From file (KEAN weather data)

STEAM GENERATOR [TYPE 636]	Parameters
Pinchpoint Temperature Difference	50 deltaC
Source Fluid Specific Heat	2.3 kJ/kg·K
Heat Exchanger Configuration	1

STEAM GENERATOR [TYPE 636]	Inputs
Source HTF inlet temperature	From Valve 2
Source HTF inlet flowrate	From Valve 2
Water Inlet Temperature	From file (KEAN weather data)
Water Inlet Flowrate	195 Kg/h
Water Inlet Pressure	101.325 kPa
Water inlet enthalpy	104.86 kJ/Kg
Desired Steam enthalpy	2783 Kj/kgK

Pump [TYPE 3]	Parameters
Fluid flow rate	1.2 kg/s
Fluid specific heat	2.3 kJ/kg·K

Pump [TYPE 3]	Inputs
Inlet fluid temperature	From tee piece -2
Inlet mass flow rate	From tee piece -2
Control signal	From Strategies Control

Appendix IV Selection of the suitable system depending on each design case in form of tables.

Steam demanding temperature 250 °C															
Load [tons/h]	Number of PTCs	CTES capacity [kW_{th}]	CTES mass [kg]	CTES length [m]	Hours of storage [h]	SG capacity [kWh_{th}]	Solar production [tons/y]	Load [tons/y]	Solar Contribution [%]	PTC system cost [€]	Land [m^2]	Load [GJ/y]	Total Solar Savings [€]	Total CO_2 savings [$kgCO_2$]	Payback period [y]
1	40	627	27594	19.6	3	207	1538.2	2871.00	53.58%	489783	4000	7620	131456.7	378017.2	6.6
1	40	1248	54906	39.0	6	207	1646.72	2871.00	57.36%	546128	4000	7620	119332.9	404685.9	7.5
1	40	1875	82500	58.6	9	207	1705.94	2871.00	59.42%	596125	4000	7620	93534.95	419219.6	9.0
1	40	2483	109249	77.6	12	207	1743.74	2871.00	60.74%	638400	4000	7620	66819.46	428532.4	10.9
1	40	3104	136561	97.0	15	207	1772.16	2871.00	61.73%	675738	4000	7620	41179.89	435517.1	13.1
1.5	60	928	40828	29.0	3	311	2263.06	4306.49	52.55%	717966	6000	11431	197839.2	556124.2	6.5
1.5	60	1875	82500	58.6	6	311	2380.15	4306.40	55.27%	796125	6000	11430	167481.7	584897.8	7.7
1.5	60	2803	123328	87.6	9	311	2469.54	4306.84	57.34%	858352	6000	11432	141760.9	606864.5	8.8
1.5	60	3731	164155	116.6	12	311	2509	4306.56	58.26%	907957	6000	11431	108385.6	616561.4	10.3
1.5	60	4659	204983	145.6	15	311	2538.77	4306.65	58.95%	946507	6000	11431	82084.91	623877.1	11.7
2	80	1248	54906	39.0	3	415	3166.81	5742.18	55.15%	946128	8000	15241	336689.4	778211.6	5.4
2	80	2496	109812	78.0	6	415	3267.27	5742.13	56.90%	1039227	8000	15241	284737	802898.6	6.5
2	80	3744	164718	117.0	9	415	3334.65	5742.47	58.07%	1108560	8000	15242	243037.5	819456.6	7.5
2	80	4960	218217	155.0	12	415	3380.45	5742.23	58.87%	1156892	8000	15242	213495.4	830711.5	8.3
2	80	6208	273123	194.0	15	415	3383.58	5741.69	58.93%	1190498	8000	15240	181329.9	831480.6	9.2
2.5	100	1536	67577	48.0	3	518	3977.7	7177.37	55.42%	1169921	10000	19051	442296.2	977479.6	5.1
2.5	100	3104	136561	97.0	6	518	4164.01	7178.09	58.01%	1275738	10000	19053	412444.3	1023263	5.8
2.5	100	4672	205546	146.0	9	518	4245.83	7178.07	59.15%	1346969	10000	19053	374701	1043370	6.4
2.5	100	6208	273123	194.0	12	518	4282.17	7177.62	59.66%	1390498	10000	19052	346107.7	1052300	6.9
2.5	100	7776	342108	243.0	15	518	4307.02	7177.17	60.01%	1415572	10000	19050	331222.5	1058407	7.2
3	120	1856	81655	58.0	3	622	4831.6	8612.48	56.10%	1394693	12000	22860	564340	1187317	4.9
3	120	3712	163311	116.0	6	622	5045.04	8613.69	58.57%	1507048	12000	22863	538965.4	1239768	5.4
3	120	5600	246374	175.0	9	622	5120.29	8612.77	59.45%	1575914	12000	22861	500916	1258260	5.8
3	120	7456	328029	233.0	12	622	5162.62	8612.98	59.94%	1611680	12000	22861	482470	1268662	6.1
3	120	9344	411092	292.0	15	622	5193.26	8612.37	60.30%	1628596	12000	22860	478044	1276191	6.2
3.5	140	2176	95734	68.0	3	726	5669.75	10049.18	56.42%	1617774	14000	26674	681691	1393284	4.7
3.5	140	4352	191468	136.0	6	726	5890.88	10049.27	58.62%	1734873	14000	26674	654709	1447624	5.2
3.5	140	6528	287201	204.0	9	726	5989.65	10048.06	59.61%	1796961	14000	26671	632923.2	1471896	5.4
3.5	140	8704	382935	272.0	12	726	6056.97	10048.06	60.28%	1824251	14000	26671	633026	1488439	5.5
3.5	140	10880	478669	340.0	15	726	6085.05	10047.97	60.56%	1836955	14000	26670	631754	1495340	5.5
4	160	2464	108404	77.0	3	830	6533.85	11483.04	56.90%	1837153	16000	30479	813228	1605628	4.6
4	160	4960	218217	155.0	6	830	6785.76	11483.77	59.09%	1956892	16000	30481	796080	1667532	4.9
4	160	7456	328029	233.0	9	830	6858.25	11484.01	59.72%	2011680	16000	30482	770919	1685346	5.1
4	160	9920	436434	310.0	12	830	6939.03	11484.66	60.42%	2031853	16000	30484	783549	1705197	5.1
4	160	12416	546246	388.0	15	830	6994.45	11483.25	60.91%	2048118	16000	30480	789801.8	1718816	5.1

Steam demanding temperature 240 °C															
Load [tons/h]	Number of PTCs	CTES capacity [kW_{th}]	CTES mass [kg]	CTES length [m]	Hours of storage [h]	SG capacity [kWh_{th}]	Solar production [tons/y]	Load [tons/y]	Solar Contribution [%]	PTC system cost [€]	Land [m^2]	Load [GJ/y]	Total Solar Savings [€]	Total CO_2 savings [$kgCO_2$]	Payback period [y]
1	40	608	26749	19.0	3	206	1596.2	2871.00	55.60%	487927	4000	7627	157290.5	392579.1	5.8
1	40	1229	54061	38.4	6	206	1710.58	2871.00	59.58%	544490	4000	7627	147310.3	420681	6.5
1	40	1856	81655	58.0	9	206	1773.17	2871.00	61.76%	594693	4000	7627	122721.9	436073.4	7.7
1	40	2464	108404	77.0	12	206	1814.16	2871.00	63.19%	637153	4000	7627	97113.33	446170.4	9.2
1	40	3091	135998	96.6	15	206	1843.05	2871.00	64.20%	675024	4000	7627	71185.48	453301.7	10.9
1.5	60	928	40828	29.0	3	309	2361.42	4306.80	54.83%	717966	6000	11441	238411	580754.3	5.7
1.5	60	1850	81374	57.8	6	309	2479.91	4306.15	57.59%	794214	6000	11439	210558.8	609895	6.6
1.5	60	2784	122483	87.0	9	309	2538.63	4306.41	58.95%	857198	6000	11440	171689.4	624336.3	7.9
1.5	60	3712	163311	116.0	12	309	2601.93	4306.41	60.42%	907048	6000	11440	147740.7	639903.9	8.8
1.5	60	4621	203294	144.4	15	309	2640.39	4306.62	61.31%	945111	6000	11440	125454.8	649362.6	9.8
2	80	1216	53498	38.0	3	412	3281.47	5741.85	57.15%	943394	8000	15253	386873.5	807026.1	4.8
2	80	2464	108404	77.0	6	412	3380.82	5741.88	58.88%	1037153	8000	15253	333847.4	831459.7	5.8
2	80	3712	163311	116.0	9	412	3451.47	5741.92	60.11%	1107048	8000	15253	292935.4	848835	6.6
2	80	4928	216809	154.0	12	412	3498.11	5742.14	60.92%	1155833	8000	15253	263297.2	860305.3	7.3
2	80	6176	271715	193.0	15	412	3498.99	5741.70	60.94%	1189808	8000	15252	229854.5	860521.8	8.1
2.5	100	1536	67577	48.0	3	515	4132.12	7177.56	57.57%	1169921	10000	19066	506127.9	1016230	4.6
2.5	100	3072	135154	96.0	6	515	4317.43	7177.77	60.15%	1273949	10000	19067	477709.5	1061804	5.2
2.5	100	4608	202730	144.0	9	515	4412.75	7177.54	61.48%	1344642	10000	19066	445997.6	1085247	5.7
2.5	100	6176	271715	193.0	12	515	4444.74	7177.04	61.93%	1389808	10000	19065	414025.2	1093114	6.1
2.5	100	7744	340700	242.0	15	515	4477.07	7177.09	62.38%	1415206	10000	19065	401855.3	1101065	6.3
3	120	1856	81655	58.0	3	618	5022.36	8613.21	58.31%	1394693	12000	22880	643167	1235171	4.4
3	120	3680	161903	115.0	6	618	5242.82	8613.14	60.87%	1505522	12000	22880	622222.2	1289389	4.8
3	120	5536	243558	173.0	9	618	5319.86	8612.37	61.77%	1574189	12000	22878	585121	1308336	5.2
3	120	7392	325213	231.0	12	618	5369.06	8612.54	62.34%	1610835	12000	22878	568595	1320436	5.4
3	120	9280	408277	290.0	15	618	5416	8613.23	62.88%	1628204	12000	22880	570333	1331980	5.5
3.5	140	2176	95734	68.0	3	721	5892.02	10047.78	58.64%	1617774	14000	26691	773552	1449050	4.3
3.5	140	4352	191468	136.0	6	721	6125.6	10048.56	60.96%	1734873	14000	26693	751684	1506495	4.6
3.5	140	6464	284386	202.0	9	721	6209.95	10048.46	61.80%	1795731	14000	26693	725312.3	1527240	4.9
3.5	140	8640	380120	270.0	12	721	6286.68	10049.04	62.56%	1823755	14000	26694	728517	1546110	4.9
3.5	140	10816	475853	338.0	15	721	6327.07	10047.75	62.97%	1836600	14000	26691	732101	1556044	4.9
4	160	2432	106997	76.0	3	824	6803.53	11484.69	59.24%	1835064	16000	30508	926651	1673222	4.1
4	160	4909	215964	153.4	6	824	7048.49	11483.37	61.38%	1955192	16000	30504	906380	1733466	4.4
4	160	7392	325213	231.0	9	824	7124.95	11484.45	62.04%	2010835	16000	30507	881999	1752270	4.6
4	160	9856	433618	308.0	12	824	7208.56	11484.08	62.77%	2031510	16000	30506	895303	1772832	4.6
4	160	12352	543430	386.0	15	824	7268.79	11484.89	63.29%	2047504	16000	30508	903791.6	1787645	4.6

Steam demanding temperature 230 °C															
Load [tons/h]	Number of PTCs	CTES capacity [kW_{th}]	CTES mass [kg]	CTES length [m]	Hours of storage [h]	SG capacity [kWh_{th}]	Solar production [tons/y]	Load [tons/y]	Solar Contribution [%]	PTC system cost [€]	Land [m^2]	Load [GJ/y]	Total Solar Savings [€]	Total CO_2 savings [$kgCO_2$]	Payback period [y]
1	40	608	26749	19.0	3	205	1661.05	2871.00	57.86%	487927	4000	7626	183550.9	408521	5.2
1	40	1229	54061	38.4	6	205	1783.4	2871.00	62.12%	544490	4000	7626	176825.4	438598.8	5.8
1	40	1837	80811	57.4	9	205	1847.73	2871.00	64.36%	593255	4000	7626	154364.5	454414.4	6.7
1	40	2445	107560	76.4	12	205	1890.62	2871.00	65.85%	635901	4000	7626	129268	464934.5	7.8
1	40	3059	134590	95.6	15	205	1920.07	2871.00	66.88%	673230	4000	7626	104111.4	472206.8	9.1
1.5	60	928	40828	29.0	3	307	2467.61	4306.47	57.30%	717966	6000	11439	281392.5	606847.2	5.0
1.5	60	1850	81374	57.8	6	307	2591.04	4306.20	60.17%	794214	6000	11439	255539.7	637201.7	5.8
1.5	60	2752	121075	86.0	9	307	2650.34	4306.69	61.54%	855262	6000	11440	218830	651785.1	6.8
1.5	60	3680	161903	115.0	12	307	2711.47	4306.66	62.96%	905522	6000	11440	193593.1	666818.5	7.6
1.5	60	4595	202167	143.6	15	307	2752.62	4306.35	63.92%	944171	6000	11439	171813.9	676938.3	8.3
2	80	1216	53498	38.0	3	409	3423.03	5742.38	59.61%	943394	8000	15253	444169.3	841808.9	4.3
2	80	2464	108404	77.0	6	409	3532.15	5742.40	61.51%	1037153	8000	15254	395099.5	868644.3	5.1
2	80	3680	161903	115.0	9	409	3603.99	5741.58	62.77%	1105522	8000	15251	356186	886311.5	5.8
2	80	4896	215401	153.0	12	409	3654.2	5741.99	63.64%	1154763	8000	15252	327540	898659.4	6.3
2	80	6144	270307	192.0	15	409	3653.91	5742.43	63.63%	1189109	8000	15254	293253.9	898588.1	6.9
2.5	100	1536	67577	48.0	3	511	4308.05	7177.69	60.02%	1169921	10000	19066	577334	1059458	4.2
2.5	100	3072	135154	96.0	6	511	4503.89	7177.51	62.75%	1273949	10000	19066	553178.4	1107619	4.6
2.5	100	4576	201323	143.0	9	511	4590.43	7177.03	63.96%	1343462	10000	19064	519082.8	1128902	5.1
2.5	100	6112	268899	191.0	12	511	4621.38	7177.17	64.39%	1388402	10000	19065	486912.1	1136513	5.4
2.5	100	7648	336476	239.0	15	511	4658.96	7177.57	64.91%	1414079	10000	19066	476592.1	1145755	5.6
3	120	1856	81655	58.0	3	613	5228.56	8612.35	60.71%	1394693	12000	22877	726622	1285834	4.0
3	120	3680	161903	115.0	6	613	5456.98	8612.66	63.36%	1505522	12000	22878	708898.3	1342008	4.3
3	120	5504	242150	172.0	9	613	5543.08	8612.62	64.36%	1573312	12000	22878	676338	1363182	4.7
3	120	7360	323806	230.0	12	613	5585.55	8607.72	64.89%	1610405	12000	22865	656642	1373627	4.9
3	120	9216	405461	288.0	15	613	5627.8	8613.10	65.34%	1627803	12000	22879	656449	1384017	4.9
3.5	140	2112	92918	66.0	3	716	6119.69	10048.75	60.90%	1613290	14000	26693	870151	1504985	3.9
3.5	140	4288	188652	134.0	6	716	6366.81	10048.63	63.36%	1732313	14000	26692	851851	1565758	4.2
3.5	140	6464	284386	202.0	9	716	6465.18	10048.46	64.34%	1795731	14000	26692	828611.1	1589950	4.4
3.5	140	8576	377304	268.0	12	716	6547.16	10047.82	65.16%	1823247	14000	26690	834447	1610111	4.4
3.5	140	10752	473038	336.0	15	716	6597.94	10048.64	65.66%	1836249	14000	26692	842083	1622599	4.4
4	160	2432	106997	76.0	3	818	7084.64	11484.26	61.69%	1835064	16000	30506	1040424	1742291	3.7
4	160	4909	215964	153.4	6	818	7330.71	11484.74	63.83%	1955192	16000	30507	1020599	1802805	4.0
4	160	7328	322398	229.0	9	818	7419.11	11484.69	64.60%	2009968	16000	30507	1001918	1824545	4.1
4	160	9792	430802	306.0	12	818	7491.63	11483.19	65.24%	2031163	16000	30503	1010210	1842380	4.1
4	160	12288	540614	384.0	15	818	7561.03	11483.95	65.84%	2046907	16000	30505	1022661	1859447	4.1

Steam demanding temperature 220 °C															
Load [tons/h]	Number of PTCs	CTES capacity [kW_{th}]	CTES mass [kg]	CTES length [m]	Hours of storage [h]	SG capacity [kWh_{th}]	Solar production [tons/y]	Load [tons/y]	Solar Contribution [%]	PTC system cost [€]	Land [m^2]	Load [GJ/y]	Total Solar Savings [€]	Total CO_2 savings [$kgCO_2$]	Payback period [y]
1	40	608	26749	19.0	3	203	1735.46	2871.00	60.45%	487927	4000	7620	213144.3	426486.4	4.6
1	40	1216	53498	38.0	6	203	1855.85	2871.00	64.64%	543394	4000	7620	206657.9	456047.7	5.1
1	40	1824	80247	57.0	9	203	1929.74	2871.00	67.21%	592293	4000	7620	187879.6	474179.5	5.9
1	40	2432	106997	76.0	12	203	1969.43	2871.00	68.60%	635064	4000	7620	161484.3	483986.2	6.8
1	40	3040	133746	95.0	15	203	2006.44	2871.00	69.89%	672147	4000	7620	139584.6	493087.4	7.7
1.5	60	928	40828	29.0	3	305	2583.98	4306.63	60.00%	717966	6000	11431	327745.8	634987	4.4
1.5	60	1824	80247	57.0	6	305	2710.56	4306.58	62.94%	792293	6000	11431	305041.8	666092.8	5.1
1.5	60	2752	121075	86.0	9	305	2775.13	4306.53	64.44%	855262	6000	11431	268535.9	681960.2	5.9
1.5	60	3648	160495	114.0	12	305	2831.75	4306.19	65.76%	903984	6000	11430	242985.4	695874	6.6
1.5	60	4576	201323	143.0	15	305	2864.49	4306.21	66.52%	943462	6000	11430	216964.7	703919.5	7.3
2	80	1216	53498	38.0	3	406	3565.87	5742.14	62.10%	943394	8000	15241	500946	876276.6	3.9
2	80	2432	106997	76.0	6	406	3670.57	5742.44	63.92%	1035064	8000	15242	452132.7	902005.5	4.6
2	80	3648	160495	114.0	9	406	3746.73	5742.11	65.25%	1103984	8000	15241	414397.8	920721.1	5.2
2	80	4864	213993	152.0	12	406	3796.82	5742.32	66.12%	1153683	8000	15242	385232.1	933030.2	5.6
2	80	6080	267492	190.0	15	406	3798.89	5741.97	66.16%	1187687	8000	15241	352241	933538.9	6.1
2.5	100	1504	66169	47.0	3	508	4489.76	7177.87	62.55%	1167349	10000	19052	652134.6	1103313	3.8
2.5	100	3040	133746	95.0	6	508	4701.4	7177.71	65.50%	1272147	10000	19052	633548.9	1155322	4.1
2.5	100	4544	199915	142.0	9	508	4796.95	7177.84	66.83%	1342270	10000	19052	602466.7	1178802	4.5
2.5	100	6080	267492	190.0	12	508	4828.871	7177.28	67.28%	1387687	10000	19051	570205.1	1186646	4.8
2.5	100	7616	335068	238.0	15	508	4864.46	7177.90	67.77%	1413692	10000	19052	558740.6	1195392	5.0
3	120	1856	81655	58.0	3	609	5460.79	8613.23	63.40%	1394693	12000	22862	819033	1341934	3.6
3	120	3648	160495	114.0	6	609	5697.23	8612.59	66.15%	1503984	12000	22860	806016.4	1400037	3.9
3	120	5504	242150	172.0	9	609	5791.9	8612.49	67.25%	1573312	12000	22860	775368	1423301	4.2
3	120	7296	320990	228.0	12	609	5833.47	8612.83	67.73%	1609525	12000	22861	756169	1433516	4.3
3	120	9152	402645	286.0	15	609	5889.36	8611.43	68.39%	1627394	12000	22857	761017	1447251	4.4
3.5	140	2112	92918	66.0	3	711	6381.96	10048.75	63.51%	1613290	14000	26672	974450	1568302	3.5
3.5	140	4256	187244	133.0	6	711	6640.11	10048.59	66.08%	1731015	14000	26672	961831	1631740	3.8
3.5	140	6400	281570	200.0	9	711	6752.79	10048.79	67.20%	1794470	14000	26673	944316.5	1659430	4.0
3.5	140	8512	374488	266.0	12	711	6833.09	10048.66	68.00%	1822724	14000	26672	948713	1679163	4.0
3.5	140	10688	470222	334.0	15	711	6879.76	10047.85	68.47%	1835903	14000	26670	954495	1690632	4.0
4	160	2400	105589	75.0	3	812	7387.32	11483.48	64.33%	1832958	16000	30481	1162881	1815359	3.4
4	160	4909	215964	153.4	6	812	7653.2	11484.39	66.64%	1955192	16000	30483	1148906	1880697	3.6
4	160	7296	320990	228.0	9	812	7748.58	11484.48	67.47%	2009525	16000	30483	1133462	1904135	3.7
4	160	9728	427986	304.0	12	812	7826.63	11484.42	68.15%	2030812	16000	30483	1143880	1923315	3.7
4	160	12160	534983	380.0	15	812	7884.44	11483.31	68.66%	2045761	16000	30480	1152409	1937522	3.7

Steam demanding temperature 210 °C															
Load [tons/h]	Number of PTCs	CTES capacity [kW_{th}]	CTES mass [kg]	CTES length [m]	Hours of storage [h]	SG capacity [kWh_{th}]	Solar production [tons/y]	Load [tons/y]	Solar Contribution [%]	PTC system cost [€]	Land [m^2]	Load [GJ/y]	Total Solar Savings [€]	Total CO_2 savings [$kgCO_2$]	Payback period [y]
1	40	608	26749	19.0	3	202	1815.4	2871.00	63.23%	487927	4000	7610	244455.8	445494.8	4.1
1	40	1216	53498	38.0	6	202	1942.79	2871.00	67.67%	543394	4000	7610	240804.9	476777.4	4.6
1	40	1824	80247	57.0	9	202	2015.5	2871.00	70.20%	592293	4000	7610	221521.8	494602.8	5.2
1	40	2419	106433	75.6	12	202	2059.91	2871.00	71.75%	634223	4000	7610	197797.5	505523.5	5.9
1	40	3027	133183	94.6	15	202	2093.57	2871.00	72.97%	671422	4000	7610	174950.5	514119.2	6.7
1.5	60	896	39420	28.0	3	302	2706.38	4306.78	62.84%	715048	6000	11416	378710.1	664163.6	3.9
1.5	60	1824	80247	57.0	6	302	2841.01	4306.52	65.97%	792293	6000	11415	356287.5	697202.7	4.5
1.5	60	2720	119667	85.0	9	302	2907.07	4306.77	67.50%	853311	6000	11416	322289.1	713414.2	5.2
1.5	60	3616	159087	113.0	12	302	2953.75	4306.39	68.59%	902432	6000	11415	292292.6	724869.8	5.8
1.5	60	4544	199915	142.0	15	302	3000.45	4306.66	69.67%	942270	6000	11416	271539.1	736330.3	6.3
2	80	1216	53498	38.0	3	403	3737.06	5742.26	65.08%	943394	8000	15221	568191.1	917099.2	3.5
2	80	2400	105589	75.0	6	403	3849.57	5742.20	67.04%	1032958	8000	15221	524571.9	944709.9	4.1
2	80	3616	159087	113.0	9	403	3931.13	5742.23	68.46%	1102432	8000	15221	488427.6	964725.3	4.6
2	80	4832	212585	151.0	12	403	3984.15	5741.68	69.39%	1152591	8000	15219	459960.5	977736.8	4.9
2	80	6048	266084	189.0	15	403	3984.39	5742.02	69.39%	1186964	8000	15220	425862.6	977795.7	5.4
2.5	100	1504	66169	47.0	3	504	4698.51	7177.68	65.46%	1167349	10000	19026	734055.8	1153045	3.4
2.5	100	3040	133746	95.0	6	504	4915.66	7177.19	68.49%	1272147	10000	19025	717581.3	1206335	3.7
2.5	100	4544	199915	142.0	9	504	5009.35	7177.75	69.79%	1342270	10000	19026	685694.8	1229328	4.1
2.5	100	6048	266084	189.0	12	504	5056.3	7177.15	70.45%	1386964	10000	19024	660210.9	1240849	4.3
2.5	100	7584	333660	237.0	15	504	5085.59	7177.97	70.85%	1413301	10000	19027	645850.3	1248037	4.4
3	120	1792	78840	56.0	3	605	5698.63	8613.41	66.16%	1389876	12000	22832	916972	1398482	3.2
3	120	3616	159087	113.0	6	605	5954.97	8612.92	69.14%	1502432	12000	22830	908622.7	1461389	3.5
3	120	5408	237927	169.0	9	605	6052.53	8613.25	70.27%	1570625	12000	22831	880220	1485331	3.7
3	120	7232	318174	226.0	12	605	6086.28	8613.47	70.66%	1608622	12000	22832	856063	1493613	3.9
3	120	9088	399829	284.0	15	605	6139.92	8612.60	71.29%	1626976	12000	22829	859487	1506777	3.9
3.5	140	2112	92918	66.0	3	706	6681.66	10049.12	66.49%	1613290	14000	26637	1092099	1639724	3.2
3.5	140	4224	185836	132.0	6	706	6934.89	10049.11	69.01%	1729705	14000	26637	1078652	1701868	3.4
3.5	140	6336	278754	198.0	9	706	7057.39	10048.97	70.23%	1793178	14000	26637	1065028	1731930	3.6
3.5	140	8448	371672	264.0	12	706	7141.62	10048.71	71.07%	1822188	14000	26636	1070217	1752601	3.6
3.5	140	10560	464591	330.0	15	706	7156.07	10047.84	71.22%	1835218	14000	26634	1063095	1756147	3.6
4	160	2432	106997	76.0	3	806	7732.7	11484.78	67.33%	1835064	16000	30443	1296349	1897656	3.1
4	160	4800	211178	150.0	6	806	7996.68	11484.53	69.63%	1951489	16000	30442	1287238	1962438	3.2
4	160	7232	318174	226.0	9	806	8099.51	11483.78	70.53%	2008622	16000	30440	1271969	1987673	3.4
4	160	9664	425171	302.0	12	806	8194.61	11483.48	71.36%	2030456	16000	30439	1288691	2011012	3.4
4	160	12096	532167	378.0	15	806	8247.93	11484.17	71.82%	2045211	16000	30441	1295567	2024097	3.4

Steam demanding temperature 200 °C															
Load [tons/h]	Number of PTCs	CTES capacity [kW_{th}]	CTES mass [kg]	CTES length [m]	Hours of storage [h]	SG capacity [kWh_{th}]	Solar production [tons/y]	Load [tons/y]	Solar Contribution [%]	PTC system cost [€]	Land [m^2]	Load [GJ/y]	Total Solar Savings [€]	Total CO_2 savings [$kgCO_2$]	Payback period [y]
1	40	608	26749	19.0	3	200	1888.54	2871.00	65.78%	487927	4000	7595	272524.3	462534.5	3.8
1	40	1197	52654	37.4	6	200	2020.06	2871.00	70.36%	541746	4000	7595	272032.3	494738.9	4.1
1	40	1792	78840	56.0	9	200	2095.22	2871.00	72.98%	589876	4000	7595	254497.1	513161.5	4.6
1	40	2400	105589	75.0	12	200	2144.96	2871.00	74.71%	632958	4000	7595	231675.8	525326.1	5.3
1	40	3008	132338	94.0	15	200	2179.52	2871.00	75.92%	670330	4000	7595	208512.4	533834.2	5.9
1.5	60	896	39420	28.0	3	300	2824.26	4306.59	65.58%	715048	6000	11393	424079.7	691706.3	3.6
1.5	60	1792	78840	56.0	6	300	2953.54	4306.71	68.58%	789876	6000	11393	401794.4	723369	4.1
1.5	60	2688	118259	84.0	9	300	3023.81	4306.19	70.22%	851345	6000	11392	368992.4	740579.2	4.6
1.5	60	3584	157679	112.0	12	300	3074.09	4306.65	71.38%	900866	6000	11393	340012	752893.6	5.2
1.5	60	4480	197099	140.0	15	300	3110.41	4306.26	72.23%	939851	6000	11392	315882	761789	5.6
2	80	1184	52090	37.0	3	400	3873.49	5741.91	67.46%	940643	8000	15190	622948.9	948679.4	3.2
2	80	2400	105589	75.0	6	400	3995	5741.59	69.58%	1032958	8000	15189	580132.2	978439.1	3.7
2	80	3584	157679	112.0	9	400	4076.79	5741.96	71.00%	1100866	8000	15190	545572	998470.8	4.2
2	80	4800	211178	150.0	12	400	4132.58	5742.09	71.97%	1151489	8000	15190	517718.9	1012135	4.5
2	80	6016	264676	188.0	15	400	4163.93	5741.77	72.52%	1186232	8000	15189	495803.5	1019813	4.8
2.5	100	1504	66169	47.0	3	500	4886.64	7177.79	68.08%	1167349	10000	18988	806156.7	1196816	3.1
2.5	100	3008	132338	94.0	6	500	5104.95	7177.94	71.12%	1270330	10000	18989	791782.4	1250284	3.4
2.5	100	4480	197099	140.0	9	500	5209.27	7177.28	72.58%	1339851	10000	18987	764707.2	1275833	3.7
2.5	100	5984	263268	187.0	12	500	5250.04	7177.09	73.15%	1385491	10000	18986	735750.8	1285818	3.9
2.5	100	7488	329437	234.0	15	500	5293.42	7177.52	73.75%	1412093	10000	18987	726787.3	1296443	4.0
3	120	1792	78840	56.0	3	601	5925.49	8612.63	68.80%	1389876	12000	22784	1003890	1451247	3.0
3	120	3584	157679	112.0	6	601	6183.38	8613.15	71.79%	1500866	12000	22785	997515.7	1514408	3.2
3	120	5376	236519	168.0	9	601	6290.14	8613.09	73.03%	1569710	12000	22785	972099	1540556	3.4
3	120	7232	318174	226.0	12	601	6326.71	8612.46	73.46%	1608622	12000	22783	948141	1549512	3.6
3	120	8960	394198	280.0	15	601	6377.21	8613.20	74.04%	1626111	12000	22785	951116	1561880	3.6
3.5	140	2112	92918	66.0	3	701	6940.18	10048.04	69.07%	1613290	14000	26581	1190995	1699761	2.9
3.5	140	4173	183584	130.4	6	701	7217.92	10045.82	71.85%	1727584	14000	26575	1189342	1767784	3.1
3.5	140	6272	275939	196.0	9	701	7345.34	10048.34	73.10%	1791854	14000	26582	1176810	1798991	3.3
3.5	140	8384	368857	262.0	12	701	7416.1	10048.92	73.80%	1821637	14000	26583	1175728	1816321	3.3
3.5	140	10496	461775	328.0	15	701	7480.31	10048.78	74.44%	1834880	14000	26583	1188458	1832047	3.3
4	160	2368	104181	74.0	3	801	8024.99	11483.96	69.88%	1830837	16000	30380	1412224	1965448	2.8
4	160	4800	211178	150.0	6	801	8322.29	11483.77	72.47%	1951489	16000	30379	1412138	2038261	3.0
4	160	7168	315358	224.0	9	801	8422.78	11484.57	73.34%	2007695	16000	30381	1396764	2062873	3.1
4	160	9600	422355	300.0	12	801	8521.03	11483.87	74.20%	2030096	16000	30379	1414116	2086936	3.1
4	160	12032	529352	376.0	15	801	8577.77	11484.50	74.69%	2044676	16000	30381	1422503	2100833	3.1

Steam demanding temperature 190 °C															
Load [tons/h]	Number of PTCs	CTES capacity [kW_{th}]	CTES mass [kg]	CTES length [m]	Hours of storage [h]	SG capacity [kWh_{th}]	Solar production [tons/y]	Load [tons/y]	Solar Contribution [%]	PTC system cost [€]	Land [m^2]	Load [GJ/y]	Total Solar Savings [€]	Total CO_2 savings [$kgCO_2$]	Payback period [y]
1	40	589	25904	18.4	3	199	1927.74	2871.00	67.15%	486063	4000	7576	288276.6	470971.8	3.6
1	40	1184	52090	37.0	6	199	2076.29	2871.00	72.32%	540643	4000	7576	293710	507232.8	3.8
1	40	1792	78840	56.0	9	199	2151.75	2871.00	75.13%	589876	4000	7576	277195.9	526941.4	4.3
1	40	2381	104744	74.4	12	199	2202.43	2871.00	76.71%	631687	4000	7576	253855.1	538023	4.9
1	40	2989	131493	93.4	15	199	2246.97	2871.00	78.26%	669232	4000	7576	234411.7	548894.3	5.5
1.5	60	896	39420	28.0	3	298	2892.93	4306.24	67.18%	715048	6000	11363	448827.8	706730.2	3.4
1.5	60	1792	78840	56.0	6	298	3011.16	4306.58	69.92%	789876	6000	11364	421963.7	735613.2	3.9
1.5	60	2688	118259	84.0	9	298	3084.11	4306.21	71.62%	851345	6000	11363	390168.4	753434.6	4.4
1.5	60	3584	157679	112.0	12	298	3134.47	4306.77	72.78%	900866	6000	11364	361168.8	765737.3	4.9
1.5	60	4480	197099	140.0	15	298	3171.61	4306.33	73.65%	939851	6000	11363	337331.7	774810.5	5.4
2	80	1184	52090	37.0	3	397	3985.16	5742.31	69.40%	940643	8000	15152	663928.7	973557.2	3.1
2	80	2368	104181	74.0	6	397	4119.68	5741.71	71.75%	1030837	8000	15151	628333.6	1006420	3.5
2	80	3584	157679	112.0	9	397	4209.23	5741.69	73.31%	1100866	8000	15151	594702.3	1028297	3.9
2	80	4768	209770	149.0	12	397	4266.28	5741.97	74.30%	1150376	8000	15151	568406.8	1042234	4.2
2	80	5952	261860	186.0	15	397	4280.4	5741.65	74.55%	1184742	8000	15150	539900.2	1045683	4.5
2.5	100	1472	64761	46.0	3	497	5007.62	7177.33	69.77%	1164759	10000	18939	852424.7	1223340	3.0
2.5	100	2976	130930	93.0	6	497	5250.54	7177.77	73.15%	1268498	10000	18940	846976.1	1282684	3.2
2.5	100	4480	197099	140.0	9	497	5357.29	7177.51	74.64%	1339851	10000	18939	818949.9	1308763	3.5
2.5	100	5952	261860	186.0	12	497	5406.6	7177.22	75.33%	1384742	10000	18939	794133.9	1320809	3.7
2.5	100	7456	328029	233.0	15	497	5437.89	7177.79	75.76%	1411680	10000	18940	779927	1328453	3.8
3	120	1792	78840	56.0	3	596	6091.58	8612.44	70.73%	1389876	12000	22726	1064673	1488146	2.8
3	120	3584	157679	112.0	6	596	6363.65	8613.49	73.88%	1500866	12000	22728	1063741	1554612	3.0
3	120	5376	236519	168.0	9	596	6477.54	8612.60	75.21%	1569710	12000	22726	1041085	1582435	3.2
3	120	7168	315358	224.0	12	596	6512.44	8613.20	75.61%	1607695	12000	22728	1017340	1590961	3.4
3	120	8960	394198	280.0	15	596	6568.31	8613.05	76.26%	1626111	12000	22727	1021502	1604609	3.4
3.5	140	2112	92918	66.0	3	696	7130.64	10048.82	70.96%	1613290	14000	26516	1260547	1741984	2.8
3.5	140	4160	183021	130.0	6	696	7415.09	10048.91	73.79%	1727049	14000	26516	1261843	1811474	3.0
3.5	140	6272	275939	196.0	9	696	7555	10047.88	75.19%	1791854	14000	26513	1253675	1845654	3.1
3.5	140	8320	366041	260.0	12	696	7637.49	10048.01	76.01%	1821071	14000	26514	1257804	1865805	3.1
3.5	140	10432	458959	326.0	15	696	7703.67	10049.14	76.66%	1834543	14000	26517	1271033	1881973	3.1
4	160	2368	104181	74.0	3	795	8236.88	11484.77	71.72%	1830837	16000	30305	1489292	2012234	2.7
4	160	4800	211178	150.0	6	795	8550.52	11483.37	74.46%	1951489	16000	30301	1495477	2088855	2.8
4	160	7168	315358	224.0	9	795	8665.65	11483.77	75.46%	2007695	16000	30302	1485892	2116980	2.9
4	160	9536	419539	298.0	12	795	8756.53	11483.97	76.25%	2029731	16000	30303	1500542	2139182	2.9
4	160	11904	523720	372.0	15	795	8833.05	11483.42	76.92%	2043647	16000	30301	1517490	2157876	2.9

Steam demanding temperature 180 °C															
Load [tons/h]	Number of PTCs	CTES capacity [kW_{th}]	CTES mass [kg]	CTES length [m]	Hours of storage [h]	SG capacity [kWh_{th}]	Solar production [tons/y]	Load [tons/y]	Solar Contribution [%]	PTC system cost [€]	Land [m^2]	Load [GJ/y]	Total Solar Savings [€]	Total CO_2 savings [$kgCO_2$]	Payback period [y]
1	40	589	25904	18.4	3	197	1959.82	2871.00	68.26%	486063	4000	7552	298679.9	477287.4	3.5
1	40	1184	52090	37.0	6	197	2112.48	2871.00	73.58%	540643	4000	7552	305657.6	514485.9	3.7
1	40	1773	77995	55.4	9	197	2199.99	2871.00	76.63%	588418	4000	7552	293259	535812.1	4.1
1	40	2368	104181	74.0	12	197	2241.8	2871.00	78.08%	630837	4000	7552	267760.1	545950.8	4.7
1	40	2963	130367	92.6	15	197	2285.57	2871.00	79.61%	667761	4000	7552	248648.9	556648.9	5.2
1.5	60	896	39420	28.0	3	296	2948.56	4306.35	68.47%	715048	6000	11328	467571.8	718109.2	3.3
1.5	60	1773	77995	55.4	6	296	3072.79	4306.64	71.35%	788418	6000	11329	444419.6	748364.9	3.7
1.5	60	2656	116852	83.0	9	296	3149.17	4306.26	73.13%	849364	6000	11328	414430.4	766966.9	4.2
1.5	60	3552	156271	111.0	12	296	3203.31	4306.68	74.38%	899288	6000	11329	386484.7	780152.4	4.7
1.5	60	4448	195691	139.0	15	296	3241.83	4306.36	75.28%	938624	6000	11328	362805.1	789533.8	5.1
2	80	1184	52090	37.0	3	395	4054.62	5742.27	70.61%	940643	8000	15106	686871.9	987485.4	3.0
2	80	2368	104181	74.0	6	395	4192.92	5742.15	73.02%	1030837	8000	15105	652627	1021168	3.4
2	80	3552	156271	111.0	9	395	4283.76	5742.31	74.60%	1099288	8000	15106	620973.2	1043291	3.7
2	80	4736	208362	148.0	12	395	4343.62	5741.73	75.65%	1149251	8000	15104	595282.4	1057870	4.0
2	80	5920	260452	185.0	15	395	4379.65	5742.30	76.27%	1183984	8000	15106	575183.7	1066645	4.2
2.5	100	1472	64761	46.0	3	493	5091.82	7177.64	70.94%	1164759	10000	18882	880018.2	1240091	2.9
2.5	100	2976	130930	93.0	6	493	5339.04	7177.09	74.39%	1268498	10000	18880	875994.6	1300300	3.1
2.5	100	4448	195691	139.0	9	493	5457.04	7177.48	76.03%	1338624	10000	18881	853570.2	1329039	3.3
2.5	100	5920	260452	185.0	12	493	5504.49	7177.59	76.69%	1383984	10000	18881	827480.6	1340595	3.5
2.5	100	7392	325213	231.0	15	493	5548.69	7177.20	77.31%	1410835	10000	18880	818500.2	1351360	3.6
3	120	1792	78840	56.0	3	592	6187.33	8612.65	71.84%	1389876	12000	22656	1095561	1506898	2.8
3	120	3552	156271	111.0	6	592	6475.23	8612.97	75.18%	1499288	12000	22657	1102214	1577015	2.9
3	120	5344	235111	167.0	9	592	6595.88	8613.06	76.58%	1568784	12000	22658	1081479	1606398	3.1
3	120	7104	312543	222.0	12	592	6641.85	8613.47	77.11%	1606742	12000	22659	1062160	1617594	3.2
3	120	8896	391382	278.0	15	592	6708.39	8612.65	77.89%	1625663	12000	22656	1070031	1633800	3.3
3.5	140	2080	91510	65.0	3	691	7250.54	10047.87	72.16%	1611023	14000	26432	1302095	1765838	2.7
3.5	140	4160	183021	130.0	6	691	7551.59	10048.69	75.15%	1727049	14000	26434	1307445	1839157	2.9
3.5	140	6240	274531	195.0	9	691	7687.92	10048.26	76.51%	1791180	14000	26433	1298338	1872360	3.0
3.5	140	8320	366041	260.0	12	691	7780.04	10049.13	77.42%	1821071	14000	26435	1305558	1894795	3.0
3.5	140	10368	456143	324.0	15	691	7846.06	10048.74	78.08%	1834208	14000	26434	1318974	1910874	3.0
4	160	2368	104181	74.0	3	789	8391.1	11483.65	73.07%	1830837	16000	30209	1540987	2043617	2.6
4	160	4768	209770	149.0	6	789	8723.47	11484.29	75.96%	1950376	16000	30211	1555407	2124564	2.7
4	160	7136	313951	223.0	9	789	8821.3	11484.57	76.81%	2007222	16000	30211	1538102	2148390	2.8
4	160	9504	418131	297.0	12	789	8908.36	11484.29	77.57%	2029546	16000	30211	1550820	2169593	2.8
4	160	11872	522312	371.0	15	789	8976.55	11483.37	78.17%	2043398	16000	30208	1564396	2186200	2.8

Steam demanding temperature 170 °C															
Load [tons/h]	Number of PTCs	CTES capacity [kW_{th}]	CTES mass [kg]	CTES length [m]	Hours of storage [h]	SG capacity [kWh_{th}]	Solar production [tons/y]	Load [tons/y]	Solar Contribution [%]	PTC system cost [€]	Land [m^2]	Load [GJ/y]	Total Solar Savings [€]	Total CO_2 savings [$kgCO_2$]	Payback period [y]
1	40	589	25904	18.4	3	196	1981.05	2871.00	69.00%	486063	4000	7526	304393.5	480756	3.4
1	40	1184	52090	37.0	6	196	2140.58	2871.00	74.56%	540643	4000	7526	313909.1	519495.2	3.6
1	40	1760	77432	55.0	9	196	2229.77	2871.00	77.67%	587442	4000	7526	303045.6	541164	4.0
1	40	2349	103336	73.4	12	196	2273.92	2871.00	79.20%	629557	4000	7526	278708.9	551824.3	4.6
1	40	2944	129522	92.0	15	196	2319.88	2871.00	80.80%	666652	4000	7526	260168.9	562972.2	5.0
1.5	60	877	38575	27.4	3	294	2971.15	4306.64	68.99%	713288	6000	11289	474171.5	721052.7	3.2
1.5	60	1773	77995	55.4	6	294	3104.28	4306.71	72.08%	788418	6000	11289	452649.9	753361.3	3.7
1.5	60	2656	116852	83.0	9	294	3183.23	4306.32	73.92%	849364	6000	11288	423579.8	772521.3	4.1
1.5	60	3520	154864	110.0	12	294	3237.77	4306.69	75.18%	897695	6000	11289	397301.3	785757.3	4.6
1.5	60	4416	194283	138.0	15	294	3278.17	4306.58	76.12%	937386	6000	11289	373966.6	795561.7	4.9
2	80	1184	52090	37.0	3	392	4095.53	5741.67	71.33%	940643	8000	15051	697475.5	993922.5	2.9
2	80	2368	104181	74.0	6	392	4251.26	5739.52	74.07%	1030837	8000	15045	670002.3	1031716	3.3
2	80	3520	154864	110.0	9	392	4345.2	5742.30	75.67%	1097695	8000	15052	641043	1054514	3.6
2	80	4704	206954	147.0	12	392	4408.64	5741.91	76.78%	1148116	8000	15051	616244	1069910	3.9
2	80	5888	259044	184.0	15	392	4436.11	5741.79	77.26%	1183217	8000	15051	592305.3	1076576	4.1
2.5	100	1472	64761	46.0	3	490	5143.45	7177.57	71.66%	1164759	10000	18815	893436.2	1248237	2.8
2.5	100	2944	129522	92.0	6	490	5399.62	7177.48	75.23%	1266652	10000	18814	894476.6	1310405	3.1
2.5	100	4416	194283	138.0	9	490	5525.92	7177.45	76.99%	1337386	10000	18814	874598.2	1341056	3.3
2.5	100	5888	259044	184.0	12	490	5571.14	7177.45	77.62%	1383217	10000	18814	847080.4	1352030	3.5
2.5	100	7360	323806	230.0	15	490	5618.1	7177.85	78.27%	1410405	10000	18815	838806.6	1363427	3.6
3	120	1760	77432	55.0	3	588	6241.41	8612.41	72.47%	1387442	12000	22576	1110826	1514695	2.7
3	120	3552	156271	111.0	6	588	6529.91	8613.52	75.81%	1499288	12000	22579	1114890	1584709	2.9
3	120	5312	233703	166.0	9	588	6650.32	8613.29	77.21%	1567849	12000	22578	1094818	1613931	3.1
3	120	7040	309727	220.0	12	588	6697.07	8612.49	77.76%	1605764	12000	22576	1075788	1625276	3.2
3	120	8832	388567	276.0	15	588	6764.06	8613.35	78.53%	1625204	12000	22578	1083228	1641534	3.2
3.5	140	2080	91510	65.0	3	685	7325.86	10047.81	72.91%	1611023	14000	26338	1321922	1777874	2.7
3.5	140	4128	181613	129.0	6	685	7646.27	10048.98	76.09%	1725702	14000	26341	1335923	1855633	2.8
3.5	140	6176	271715	193.0	9	685	7786.56	10048.47	77.49%	1789808	14000	26340	1328232	1889679	2.9
3.5	140	8192	360410	256.0	12	685	7873.99	10049.76	78.35%	1819891	14000	26343	1333255	1910897	3.0
3.5	140	10304	453328	322.0	15	685	7942.86	10047.89	79.05%	1833874	14000	26339	1346876	1927611	2.9
4	160	2368	104181	74.0	3	783	8479.96	11484.24	73.84%	1830837	16000	30104	1564609	2057957	2.6
4	160	4736	208362	148.0	6	783	8819.75	11484.05	76.80%	1949251	16000	30103	1582642	2140418	2.7
4	160	7040	309727	220.0	9	783	8931.93	11483.58	77.78%	2005764	16000	30102	1571266	2167643	2.8
4	160	9408	413908	294.0	12	783	9046.25	11484.38	78.77%	2028981	16000	30104	1593870	2195387	2.8
4	160	11776	518089	368.0	15	783	9090.3	11483.45	79.16%	2042670	16000	30102	1597861	2206077	2.8

Steam demanding temperature 160 °C															
Load [tons/h]	Number of PTCs	CTES capacity [kW_{th}]	CTES mass [kg]	CTES length [m]	Hours of storage [h]	SG capacity [kWh_{th}]	Solar production [tons/y]	Load [tons/y]	Solar Contribution [%]	PTC system cost [€]	Land [m^2]	Load [GJ/y]	Total Solar Savings [€]	Total CO_2 savings [$kgCO_2$]	Payback period [y]
1	40	589	25904	18.4	3	194	2001.09	2871.00	69.70%	486063	4000	7496	309223.2	483687.9	3.4
1	40	1171	51527	36.6	6	194	2162.1	2871.00	75.31%	539537	4000	7496	320154.8	522618.9	3.6
1	40	1747	76869	54.6	9	194	2253.3	2871.00	78.48%	586464	4000	7496	309707.4	544617.4	3.9
1	40	2336	102773	73.0	12	194	2306.16	2871.00	80.33%	628700	4000	7496	288837.4	557455.6	4.4
1	40	2912	128114	91.0	15	194	2351.93	2871.00	81.92%	664791	4000	7496	271108.6	568489.5	4.9
1.5	60	877	38575	27.4	3	292	3002.31	4306.24	69.72%	713288	6000	11243	481820.4	725696.2	3.2
1.5	60	1760	77432	55.0	6	292	3142.46	4306.51	72.97%	787442	6000	11243	463851.4	759572.2	3.6
1.5	60	2624	115444	82.0	9	292	3226.29	4306.31	74.92%	847368	6000	11243	437613.4	779834.9	4.0
1.5	60	3488	153456	109.0	12	292	3283.8	4306.62	76.25%	896090	6000	11244	412041.5	793735.8	4.4
1.5	60	4384	192875	137.0	15	292	3326.86	4306.61	77.25%	936135	6000	11244	389347.5	804144	4.8
2	80	1184	52090	37.0	3	389	4142.34	5742.08	72.14%	940643	8000	14991	709555.2	1001256	2.9
2	80	2336	102773	73.0	6	389	4294.47	5742.04	74.79%	1028700	8000	14991	682525.4	1038028	3.2
2	80	3488	153456	109.0	9	389	4393.29	5742.11	76.51%	1096090	8000	14992	654830.1	1061914	3.5
2	80	4685	206109	146.4	12	389	4461.35	5741.76	77.70%	1147429	8000	14991	630854.5	1078365	3.8
2	80	5824	256229	182.0	15	389	4502.4	5742.12	78.41%	1181658	8000	14992	613147.4	1088287	4.0
2.5	100	1472	64761	46.0	3	486	5193.54	7177.36	72.36%	1164759	10000	18739	905143.8	1255344	2.8
2.5	100	2912	128114	91.0	6	486	5464.86	7177.38	76.14%	1264791	10000	18739	913657.6	1320926	3.0
2.5	100	4384	192875	137.0	9	486	5596.85	7177.29	77.98%	1336135	10000	18738	895234.8	1352829	3.2
2.5	100	5856	257637	183.0	12	486	5651.16	7177.90	78.73%	1382442	10000	18740	870791.5	1365957	3.4
2.5	100	7296	320990	228.0	15	486	5698.17	7177.44	79.39%	1409525	10000	18739	862565.6	1377319	3.5
3	120	1760	77432	55.0	3	583	6310.14	8613.35	73.26%	1387442	12000	22488	1128197	1525240	2.7
3	120	3520	154864	110.0	6	583	6637.22	8613.05	77.06%	1497695	12000	22487	1148744	1604300	2.8
3	120	5248	230887	164.0	9	583	6764.72	8613.09	78.54%	1565949	12000	22487	1131608	1635118	3.0
3	120	6976	306911	218.0	12	583	6810.34	8613.05	79.07%	1604760	12000	22487	1111162	1646145	3.1
3	120	8768	385751	274.0	15	583	6870.65	8613.08	79.77%	1624734	12000	22487	1115305	1660723	3.1
3.5	140	2048	90102	64.0	3	680	7394.76	10048.59	73.59%	1608740	14000	26235	1339895	1787407	2.6
3.5	140	4096	180205	128.0	6	680	7735.08	10048.17	76.98%	1724343	14000	26234	1360392	1869666	2.8
3.5	140	6144	270307	192.0	9	680	7873.51	10047.87	78.36%	1789109	14000	26233	1351078	1903127	2.9
3.5	140	8192	360410	256.0	12	680	7972.61	10048.66	79.34%	1819891	14000	26235	1359913	1927080	2.9
3.5	140	10240	450512	320.0	15	680	8057.35	10049.08	80.18%	1833539	14000	26236	1380075	1947563	2.9
4	160	2368	104181	74.0	3	778	8569.83	11484.63	74.62%	1830837	16000	29984	1586813	2071436	2.5
4	160	4704	206954	147.0	6	778	8918.03	11483.43	77.66%	1948116	16000	29981	1608779	2155600	2.6
4	160	6976	306911	218.0	9	778	9037.02	11484.33	78.69%	2004760	16000	29983	1599805	2184362	2.7
4	160	9344	411092	292.0	12	778	9148.5	11484.43	79.66%	2028596	16000	29984	1620479	2211308	2.7
4	160	11648	512457	364.0	15	778	9210.69	11484.65	80.20%	2041742	16000	29984	1632163	2226340	2.7

Steam demanding temperature 150 °C															
Load [tons/h]	Number of PTCs	CTES capacity [kW_{th}]	CTES mass [kg]	CTES length [m]	Hours of storage [h]	SG capacity [kWh_{th}]	Solar production [tons/y]	Load [tons/y]	Solar Contribution [%]	PTC system cost [€]	Land [m^2]	Load [GJ/y]	Total Solar Savings [€]	Total CO_2 savings [$kgCO_2$]	Payback period [y]
1	40	576	25341	18.0	3	193	2018.47	2871.00	70.31%	484817	4000	7463	313895.7	485771.9	3.3
1	40	1152	50683	36.0	6	193	2185.4	2871.00	76.12%	537873	4000	7463	327236.9	525913.2	3.5
1	40	1728	76024	54.0	9	193	2283.41	2871.00	79.53%	584991	4000	7463	319170.8	549472.9	3.8
1	40	2317	101928	72.4	12	193	2336.56	2871.00	81.39%	627410	4000	7463	298139.5	562323.6	4.3
1	40	2893	127270	90.4	15	193	2379.42	2871.00	82.88%	663667	4000	7463	279027.3	572618	4.7
1.5	60	877	38575	27.4	3	289	3035.86	4306.80	70.49%	713288	6000	11195	489854.4	730573.4	3.1
1.5	60	1728	76024	54.0	6	289	3183.17	4306.24	73.92%	784991	6000	11193	476916.3	766023.2	3.5
1.5	60	2592	114036	81.0	9	289	3273.21	4306.29	76.01%	845356	6000	11193	452556	787691.1	3.9
1.5	60	3469	152611	108.4	12	289	3335.32	4306.42	77.45%	895119	6000	11194	427670.3	802637.8	4.3
1.5	60	4352	191468	136.0	15	289	3382.24	4306.39	78.54%	934873	6000	11194	406721.3	813929	4.6
2	80	1152	50683	36.0	3	386	4183.63	5742.01	72.86%	937873	8000	14925	721413.6	1006782	2.8
2	80	2304	101365	72.0	6	386	4354.19	5742.04	75.83%	1026547	8000	14925	700809	1047827	3.2
2	80	3488	153456	109.0	9	386	4462.43	5741.68	77.72%	1096090	8000	14924	674532.7	1073874	3.5
2	80	4640	204138	145.0	12	386	4532.15	5741.99	78.93%	1145811	8000	14925	652705.3	1090652	3.7
2	80	5792	254821	181.0	15	386	4564.19	5741.84	79.49%	1180864	8000	14925	630534.2	1098363	3.9
2.5	100	1440	63353	45.0	3	482	5235.14	7177.32	72.94%	1162151	10000	18656	915120.3	1259826	2.8
2.5	100	2912	128114	91.0	6	482	5537.73	7177.87	77.15%	1264791	10000	18657	932959.4	1332643	2.9
2.5	100	4352	191468	136.0	9	482	5680.41	7177.67	79.14%	1334873	10000	18657	919798.3	1366979	3.1
2.5	100	5792	254821	181.0	12	482	5729.8	7177.50	79.83%	1380864	10000	18656	893623.3	1378864	3.3
2.5	100	7232	318174	226.0	15	482	5776	7177.83	80.47%	1408622	10000	18657	884322.9	1389982	3.4
3	120	1760	77432	55.0	3	579	6387.98	8612.62	74.17%	1387442	12000	22387	1147986	1537254	2.6
3	120	3488	153456	109.0	6	579	6727.38	8612.70	78.11%	1496090	12000	22387	1174441	1618930	2.8
3	120	5216	229480	163.0	9	579	6871.82	8613.46	79.78%	1564984	12000	22389	1163159	1653689	2.9
3	120	6944	305503	217.0	12	579	6918.07	8613.13	80.32%	1604248	12000	22388	1142432	1664819	3.0
3	120	8704	382935	272.0	15	579	6968.41	8612.54	80.91%	1624251	12000	22387	1142488	1676933	3.1
3.5	140	2048	90102	64.0	3	675	7479.19	10048.62	74.43%	1608740	14000	26119	1360395	1799851	2.6
3.5	140	4064	178797	127.0	6	675	7848.76	10048.34	78.11%	1722971	14000	26119	1393254	1888788	2.7
3.5	140	6112	268899	191.0	9	675	7989.7	10048.67	79.51%	1788402	14000	26120	1384031	1922705	2.8
3.5	140	8128	357594	254.0	12	675	8087.28	10048.81	80.48%	1819276	14000	26120	1391998	1946187	2.8
3.5	140	10112	444881	316.0	15	675	8138.12	10048.30	80.99%	1832869	14000	26119	1398628	1958422	2.8
4	160	2336	102773	73.0	3	772	8674.48	11483.29	75.54%	1828700	16000	29849	1615393	2087495	2.5
4	160	4640	204138	145.0	6	772	9035.33	11483.64	78.68%	1945811	16000	29849	1641930	2174333	2.6
4	160	6976	306911	218.0	9	772	9176.04	11484.41	79.90%	2004760	16000	29851	1639064	2208195	2.7
4	160	9280	408277	290.0	12	772	9289.4	11483.99	80.89%	2028204	16000	29850	1660678	2235475	2.7
4	160	11584	509642	362.0	15	772	9337.73	11484.11	81.31%	2041294	16000	29851	1666814	2247105	2.7

Steam demanding temperature 140 °C															
Load [tons/h]	Number of PTCs	CTES capacity [kW_{th}]	CTES mass [kg]	CTES length [m]	Hours of storage [h]	SG capacity [kWh_{th}]	Solar production [tons/y]	Load [tons/y]	Solar Contribution [%]	PTC system cost [€]	Land [m^2]	Load [GJ/y]	Total Solar Savings [€]	Total CO_2 savings [$kgCO_2$]	Payback period [y]
1	40	576	25341	18.0	3	192	2037.36	2871.00	70.96%	484817	4000	7427	317409.6	487905.1	3.3
1	40	1152	50683	36.0	6	192	2216.34	2871.00	77.20%	537873	4000	7427	335303	530809.9	3.4
1	40	1728	76024	54.0	9	192	2317.43	2871.00	80.72%	584991	4000	7427	328296.2	555012.7	3.7
1	40	2304	101365	72.0	12	192	2366.88	2871.00	82.44%	626547	4000	7427	306436.1	566839	4.2
1	40	2880	126707	90.0	15	192	2415.77	2871.00	84.14%	662915	4000	7427	289510.4	578527.8	4.6
1.5	60	877	38575	27.4	3	287	3074.09	4306.65	71.38%	713288	6000	11140	499148.8	736215.8	3.1
1.5	60	1728	76024	54.0	6	287	3233.47	4306.70	75.08%	784991	6000	11141	490691.6	774385.8	3.4
1.5	60	2592	114036	81.0	9	287	3329.44	4306.61	77.31%	845356	6000	11140	468499	797369.7	3.8
1.5	60	3456	152048	108.0	12	287	3396.04	4306.42	78.86%	894470	6000	11140	445912.2	813319.8	4.1
1.5	60	4320	190060	135.0	15	287	3443.12	4306.59	79.95%	933599	6000	11140	425558.3	824595	4.5
2	80	1152	50683	36.0	3	383	4236.33	5741.84	73.78%	937873	8000	14853	734228.4	1014561	2.8
2	80	2304	101365	72.0	6	383	4424.97	5742.24	77.06%	1026547	8000	14854	720431.3	1059739	3.1
2	80	3456	152048	108.0	9	383	4538.74	5742.33	79.04%	1094470	8000	14854	697741.3	1086986	3.3
2	80	4608	202730	144.0	12	383	4614.24	5741.96	80.36%	1144642	8000	14853	677613.3	1105067	3.6
2	80	5760	253413	180.0	15	383	4647.3	5741.66	80.94%	1180062	8000	14853	655418.4	1112985	3.8
2.5	100	1440	63353	45.0	3	479	5302.78	7177.56	73.88%	1162151	10000	18567	931824.5	1269966	2.7
2.5	100	2880	126707	90.0	6	479	5617.16	7177.56	78.26%	1262915	10000	18567	955604.1	1345257	2.9
2.5	100	4320	190060	135.0	9	479	5768.88	7177.90	80.37%	1333599	10000	18568	945138.5	1381593	3.0
2.5	100	5760	253413	180.0	12	479	5831.35	7177.93	81.24%	1380062	10000	18568	923560.1	1396554	3.2
2.5	100	7200	316766	225.0	15	479	5866.8	7177.39	81.74%	1408162	10000	18566	909591	1405044	3.3
3	120	1728	76024	54.0	3	575	6460.4	8612.72	75.01%	1384991	12000	22279	1166817	1547205	2.6
3	120	3456	152048	108.0	6	575	6825.21	8613.34	79.24%	1494470	12000	22281	1201822	1634574	2.7
3	120	5184	228072	162.0	9	575	6980.48	8612.56	81.05%	1564009	12000	22279	1193896	1671760	2.8
3	120	6912	304096	216.0	12	575	7027.6	8613.31	81.59%	1603730	12000	22281	1172970	1683044	3.0
3	120	8640	380120	270.0	15	575	7078.83	8612.76	82.19%	1623755	12000	22279	1173258	1695314	3.0
3.5	140	2016	88695	63.0	3	670	7556.6	10048.67	75.20%	1606441	14000	25994	1378963	1809735	2.5
3.5	140	4032	177389	126.0	6	670	7964.6	10048.70	79.26%	1721588	14000	25994	1425367	1907447	2.6
3.5	140	6048	266084	189.0	9	670	8117.79	10048.01	80.79%	1786964	14000	25992	1420763	1944135	2.7
3.5	140	8064	354778	252.0	12	670	8205.55	10048.43	81.66%	1818644	14000	25993	1423868	1965152	2.8
3.5	140	10080	443473	315.0	15	670	8270.2	10048.85	82.30%	1832701	14000	25994	1435387	1980635	2.8
4	160	2336	102773	73.0	3	766	8777.99	11483.50	76.44%	1828700	16000	29706	1639691	2102246	2.4
4	160	4608	202730	144.0	6	766	9174.46	11483.87	79.89%	1944642	16000	29706	1680756	2197197	2.5
4	160	6912	304096	216.0	9	766	9322.6	11483.86	81.18%	2003730	16000	29706	1680415	2232675	2.6
4	160	9216	405461	288.0	12	766	9438.12	11484.69	82.18%	2027803	16000	29709	1702038	2260341	2.6
4	160	11520	506826	360.0	15	766	9499.49	11483.91	82.72%	2040857	16000	29707	1713262	2275039	2.6

Steam demanding temperature 130 °C															
Load [tons/h]	Number of PTCs	CTES capacity [kW_{th}]	CTES mass [kg]	CTES length [m]	Hours of storage [h]	SG capacity [kWh_{th}]	Solar production [tons/y]	Load [tons/y]	Solar Contribution [%]	PTC system cost [€]	Land [m^2]	Load [GJ/y]	Total Solar Savings [€]	Total CO_2 savings [$kgCO_2$]	Payback period [y]
1	40	576	25341	18.0	3	190	2060.91	2871.00	71.78%	484817	4000	7389	322517	491005.7	3.2
1	40	1139	50119	35.6	6	190	2241.7	2871.00	78.08%	536760	4000	7389	341830.5	534100.3	3.4
1	40	1715	75461	53.6	9	190	2345.71	2871.00	81.70%	584006	4000	7389	335618.3	558862.7	3.7
1	40	2272	99957	71.0	12	190	2400.19	2871.00	83.60%	624378	4000	7389	316864	571859.5	4.1
1	40	2848	125299	89.0	15	190	2444.73	2871.00	85.15%	661024	4000	7389	297872.2	582462.1	4.5
1.5	60	864	38012	27.0	3	285	3104.29	4306.73	72.08%	712111	6000	11083	505937.3	739626	3.0
1.5	60	1715	75461	53.6	6	285	3277.19	4306.43	76.10%	784006	6000	11083	502272.1	780821	3.3
1.5	60	2579	113473	80.6	9	285	3379.14	4306.28	78.47%	844547	6000	11082	482056.6	805111.5	3.7
1.5	60	3424	150640	107.0	12	285	3446.47	4306.47	80.03%	892837	6000	11083	460441.1	821153.5	4.0
1.5	60	4288	188652	134.0	15	285	3496.23	4306.76	81.18%	932313	6000	11083	440698	833009.3	4.3
2	80	1152	50683	36.0	3	380	4291.29	5741.62	74.74%	937873	8000	14776	747206.1	1022440	2.7
2	80	2272	99957	71.0	6	380	4488.38	5741.82	78.17%	1024378	8000	14777	738500.6	1069398	3.0
2	80	3424	150640	107.0	9	380	4609.06	5741.95	80.27%	1092837	8000	14777	717758.7	1098151	3.3
2	80	4576	201323	143.0	12	380	4689.35	5741.83	81.67%	1143462	8000	14777	698907.2	1117281	3.5
2	80	5696	250597	178.0	15	380	4739.66	5742.26	82.54%	1178430	8000	14778	683864.3	1129268	3.6
2.5	100	1440	63353	45.0	3	475	5376.51	7177.29	74.91%	1162151	10000	18471	950005.7	1281004	2.7
2.5	100	2848	125299	89.0	6	475	5714.53	7177.25	79.62%	1261024	10000	18471	984306.7	1361540	2.8
2.5	100	4288	188652	134.0	9	475	5871.27	7177.59	81.80%	1332313	10000	18472	974901.8	1398885	3.0
2.5	100	5696	250597	178.0	12	475	5940.97	7177.69	82.77%	1378430	10000	18472	956378.3	1415491	3.1
2.5	100	7136	313951	223.0	15	475	5978.45	7177.87	83.29%	1407222	10000	18472	942445.9	1424421	3.2
3	120	1728	76024	54.0	3	570	6558.33	8613.51	76.14%	1384991	12000	22167	1192148	1562583	2.5
3	120	3424	150640	107.0	6	570	6940.16	8612.76	80.58%	1492837	12000	22165	1234717	1653558	2.6
3	120	5120	225256	160.0	9	570	7099.67	8612.97	82.43%	1562027	12000	22165	1228488	1691562	2.8
3	120	6848	301280	214.0	12	570	7134.86	8612.82	82.84%	1602672	12000	22165	1201864	1699947	2.9
3	120	8576	377304	268.0	15	570	7204.67	8612.88	83.65%	1623247	12000	22165	1208794	1716580	2.9
3.5	140	2016	88695	63.0	3	665	7668.98	10048.45	76.32%	1606441	14000	25860	1407742	1827206	2.5
3.5	140	4000	175981	125.0	6	665	8093.04	10048.47	80.54%	1720191	14000	25860	1461011	1928242	2.6
3.5	140	6016	264676	188.0	9	665	8264.74	10048.32	82.25%	1786232	14000	25859	1462699	1969151	2.7
3.5	140	8000	351963	250.0	12	665	8350.42	10048.64	83.10%	1817994	14000	25860	1464728	1989565	2.7
3.5	140	9984	439249	312.0	15	665	8424.14	10050.27	83.82%	1832194	14000	25864	1479534	2007130	2.7
4	160	2304	101365	72.0	3	760	8904.06	11484.66	77.53%	1826547	16000	29556	1673508	2121475	2.4
4	160	4576	201323	143.0	6	760	9343.41	11484.03	81.36%	1943462	16000	29554	1729630	2226154	2.5
4	160	6880	302688	215.0	9	760	9491.15	11483.55	82.65%	2003204	16000	29553	1728179	2261355	2.5
4	160	9152	402645	286.0	12	760	9602.71	11483.75	83.62%	2027394	16000	29553	1747899	2287935	2.5
4	160	11424	502602	357.0	15	760	9700.39	11483.83	84.47%	2040221	16000	29554	1773475	2311208	2.5

Steam demanding temperature 120 °C															
Load [tons/h]	Number of PTCs	CTES capacity [kW_{th}]	CTES mass [kg]	CTES length [m]	Hours of storage [h]	SG capacity [kWh_{th}]	Solar production [tons/y]	Load [tons/y]	Solar Contribution [%]	PTC system cost [€]	Land [m^2]	Load [GJ/y]	Total Solar Savings [€]	Total CO_2 savings [$kgCO_2$]	Payback period [y]
1	40	563	24778	17.6	3	189	2078.84	2871.00	72.41%	483568	4000	7348	326356.7	492582.1	3.2
1	40	1139	50119	35.6	6	189	2275.59	2871.00	79.26%	536760	4000	7348	350198.7	539180.5	3.3
1	40	1696	74616	53.0	9	189	2377.88	2871.00	82.82%	582523	4000	7348	344564.4	563398	3.6
1	40	2272	99957	71.0	12	189	2437.92	2871.00	84.92%	624378	4000	7348	326457.8	577683.6	4.0
1	40	2829	124454	88.4	15	189	2484.11	2871.00	86.52%	659882	4000	7348	309065.6	588567.9	4.4
1.5	60	851	37449	26.6	3	283	3140.84	4306.65	72.93%	710930	6000	11022	514654.5	744205.2	3.0
1.5	60	1696	74616	53.0	6	283	3323.44	4306.65	77.17%	782523	6000	11022	514702.1	787471.3	3.3
1.5	60	2560	112628	80.0	9	283	3433.7	4306.66	79.73%	843328	6000	11022	497245.8	813596.8	3.6
1.5	60	3392	149232	106.0	12	283	3502.36	4306.36	81.33%	891190	6000	11021	476430.2	829865.4	3.9
1.5	60	4256	187244	133.0	15	283	3556.18	4306.35	82.58%	931015	6000	11021	457816.8	842617.8	4.2
2	80	1120	49275	35.0	3	377	4342.54	5741.82	75.63%	935084	8000	14695	760690.1	1028942	2.7
2	80	2272	99957	71.0	6	377	4576.29	5741.89	79.70%	1024378	8000	14695	763092.5	1084327	2.9
2	80	3392	149232	106.0	9	377	4701.29	5741.68	81.88%	1091190	8000	14695	745413.8	1113945	3.1
2	80	4544	199915	142.0	12	377	4788.07	5741.78	83.39%	1142270	8000	14695	728469	1134508	3.3
2	80	5664	249189	177.0	15	377	4825.04	5742.04	84.03%	1177601	8000	14696	707749.9	1143267	3.5
2.5	100	1408	61945	44.0	3	472	5454.18	7177.50	75.99%	1159525	10000	18369	971289.7	1292339	2.6
2.5	100	2848	125299	89.0	6	472	5809.42	7177.44	80.94%	1261024	10000	18369	1008968	1376511	2.7
2.5	100	4256	187244	133.0	9	472	5972.15	7177.20	83.21%	1331015	10000	18369	1002853	1415069	2.9
2.5	100	5664	249189	177.0	12	472	6047.13	7177.60	84.25%	1377601	10000	18370	985773	1432835	3.0
2.5	100	7072	311135	221.0	15	472	6081.64	7177.67	84.73%	1406256	10000	18370	970735.1	1441012	3.1
3	120	1696	74616	53.0	3	566	6655.64	8613.49	77.27%	1382523	12000	22044	1218382	1577018	2.5
3	120	3392	149232	106.0	6	566	7052.97	8612.74	81.89%	1491190	12000	22043	1265357	1671163	2.6
3	120	5120	225256	160.0	9	566	7218.15	8612.52	83.81%	1562027	12000	22042	1259356	1710302	2.7
3	120	6816	299872	213.0	12	566	7266.05	8613.15	84.36%	1602133	12000	22044	1238153	1721652	2.8
3	120	8512	374488	266.0	15	566	7344.54	8613.28	85.27%	1622724	12000	22044	1248304	1740249	2.8
3.5	140	1984	87287	62.0	3	660	7774.75	10048.79	77.37%	1604125	14000	25718	1434721	1842185	2.4
3.5	140	3968	174573	124.0	6	660	8225.62	10048.40	81.86%	1718782	14000	25717	1496634	1949017	2.5
3.5	140	5952	261860	186.0	9	660	8414.86	10048.79	83.74%	1784742	14000	25718	1504876	1993856	2.6
3.5	140	7936	349147	248.0	12	660	8507.76	10048.14	84.67%	1817325	14000	25716	1508721	2015868	2.6
3.5	140	9920	436434	310.0	15	660	8581.37	10048.44	85.40%	1831853	14000	25717	1522998	2033310	2.6
4	160	2272	99957	71.0	3	755	9055.41	11484.35	78.85%	1824378	16000	29392	1715456	2145631	2.3
4	160	4544	199915	142.0	6	755	9504.91	11483.52	82.77%	1942270	16000	29390	1773616	2252137	2.4
4	160	6816	299872	213.0	9	755	9657.55	11483.41	84.10%	2002133	16000	29389	1773638	2288305	2.5
4	160	9088	399829	284.0	12	755	9781.73	11483.60	85.18%	2026976	16000	29390	1797392	2317728	2.5
4	160	11328	498379	354.0	15	755	9872.14	11484.57	85.96%	2039605	16000	29392	1820116	2339151	2.4

Steam demanding temperature 110 °C															
Load [tons/h]	Number of PTCs	CTES capacity [kW_{th}]	CTES mass [kg]	CTES length [m]	Hours of storage [h]	SG capacity [kWh_{th}]	Solar production [tons/y]	Load [tons/y]	Solar Contribution [%]	PTC system cost [€]	Land [m^2]	Load [GJ/y]	Total Solar Savings [€]	Total CO_2 savings [$kgCO_2$]	Payback period [y]
1	40	563	24778	17.6	3	187	2104.07	2870.88	73.29%	483568	4000	7305	331435	495665	3.1
1	40	1120	49275	35.0	6	187	2306.24	2870.96	80.33%	535084	4000	7305	358636	543291	3.2
1	40	1677	73771	52.4	9	187	2406.06	2870.85	83.81%	581033	4000	7305	351660	566806	3.5
1	40	2240	98550	70.0	12	187	2473.6	2870.94	86.16%	622192	4000	7305	336922	582716	3.9
1	40	2816	123891	88.0	15	187	2523.22	2870.88	87.89%	659118	4000	7305	319460	594417	4.2
1.5	60	851	37449	26.6	3	281	3190.96	4306.29	74.10%	710930	6000	10957	527014	751708	2.9
1.5	60	1696	74616	53.0	6	281	3391.76	4306.45	78.76%	782523	6000	10958	533712	799011	3.2
1.5	60	2528	111220	79.0	9	281	3503.92	4306.69	81.36%	841286	6000	10958	518776	825433	3.5
1.5	60	3360	147824	105.0	12	281	3576.09	4306.47	83.04%	889529	6000	10958	498788	842435	3.8
1.5	60	4224	185836	132.0	15	281	3631.46	4305.74	84.34%	929705	6000	10956	480305	855479	4.0
2	80	1120	49275	35.0	3	374	4420.89	5742.16	76.99%	935084	8000	14611	781292	1041449	2.6
2	80	2240	98550	70.0	6	374	4650.61	5742.20	80.99%	1022192	8000	14611	783777	1095565	2.8
2	80	3360	147824	105.0	9	374	4783.15	5742.08	83.30%	1089529	8000	14611	768221	1126788	3.1
2	80	4480	197099	140.0	12	374	4872.76	5742.12	84.86%	1139851	8000	14611	752932	1147898	3.2
2	80	5632	247782	176.0	15	374	4927.5	5742.34	85.81%	1176762	8000	14611	737454	1160793	3.4
2.5	100	1408	61945	44.0	3	468	5532.02	7177.92	77.07%	1159525	10000	18264	989184.9	1303202	2.6
2.5	100	2816	123891	88.0	6	468	5902.39	7177.90	82.23%	1259118	10000	18264	1033828	1390452	2.7
2.5	100	4224	185836	132.0	9	468	6084.14	7177.23	84.77%	1329705	10000	18262	1034134	1433268	2.8
2.5	100	5632	247782	176.0	12	468	6155.04	7177.89	85.75%	1376762	10000	18264	1014833	14499270	2.9
2.5	100	7040	309727	220.0	15	468	6240.33	7177.74	86.94%	1405764	10000	18264	1019078	1470062	3.0
3	120	1696	74616	53.0	3	562	6771.22	8612.59	78.62%	1382523	12000	21915	1248210	1595126	2.4
3	120	3392	149232	106.0	6	562	7186.84	8613.18	83.44%	1491190	12000	21916	1301386	1693036	2.5
3	120	5056	222440	158.0	9	562	7343.8	8613.42	85.26%	1560005	12000	21917	1293835	1730011	2.6
3	120	6752	297056	211.0	12	562	7411.62	8613.16	86.05%	1601034	12000	21916	1279335	1745988	2.7
3	120	8448	371672	264.0	15	562	7480.47	8613.09	86.85%	1622188	12000	21916	1285008	1762207	2.7
3.5	140	1984	87287	62.0	3	655	7922.6	10048.96	78.84%	1604125	14000	25570	1474546	1866362	2.4
3.5	140	3904	171758	122.0	6	655	8371.84	10049.02	83.31%	1715926	14000	25570	1537650	1972191	2.4
3.5	140	5888	259044	184.0	9	655	8569.03	10048.11	85.28%	1783217	14000	25567	1547225	2018644	2.5
3.5	140	7872	346331	246.0	12	655	8650.24	10049.07	86.08%	1816638	14000	25570	1545491	2037775	2.6
3.5	140	9856	433618	308.0	15	655	8733.29	10048.66	86.91%	1831510	14000	25569	1562924	2057340	2.6
4	160	2272	99957	71.0	3	749	9212.09	11483.53	80.22%	1824378	16000	29220	1755817	2170133	2.3
4	160	4480	197099	140.0	6	749	9687.08	11484.39	84.35%	1939851	16000	29222	1825260	2282028	2.3
4	160	6752	297056	211.0	9	749	9839.3	11483.78	85.68%	2001034	16000	29220	1823462	2317887	2.4
4	160	8960	394198	280.0	12	749	9962.93	11484.65	86.75%	2026111	16000	29223	1846489	2347012	2.4
4	160	11264	495563	352.0	15	749	10064.53	11483.95	87.64%	2039205	16000	29221	1872888	2370946	2.4

Appendix IV: Details about the suitable system depending on each design case in form of tables.

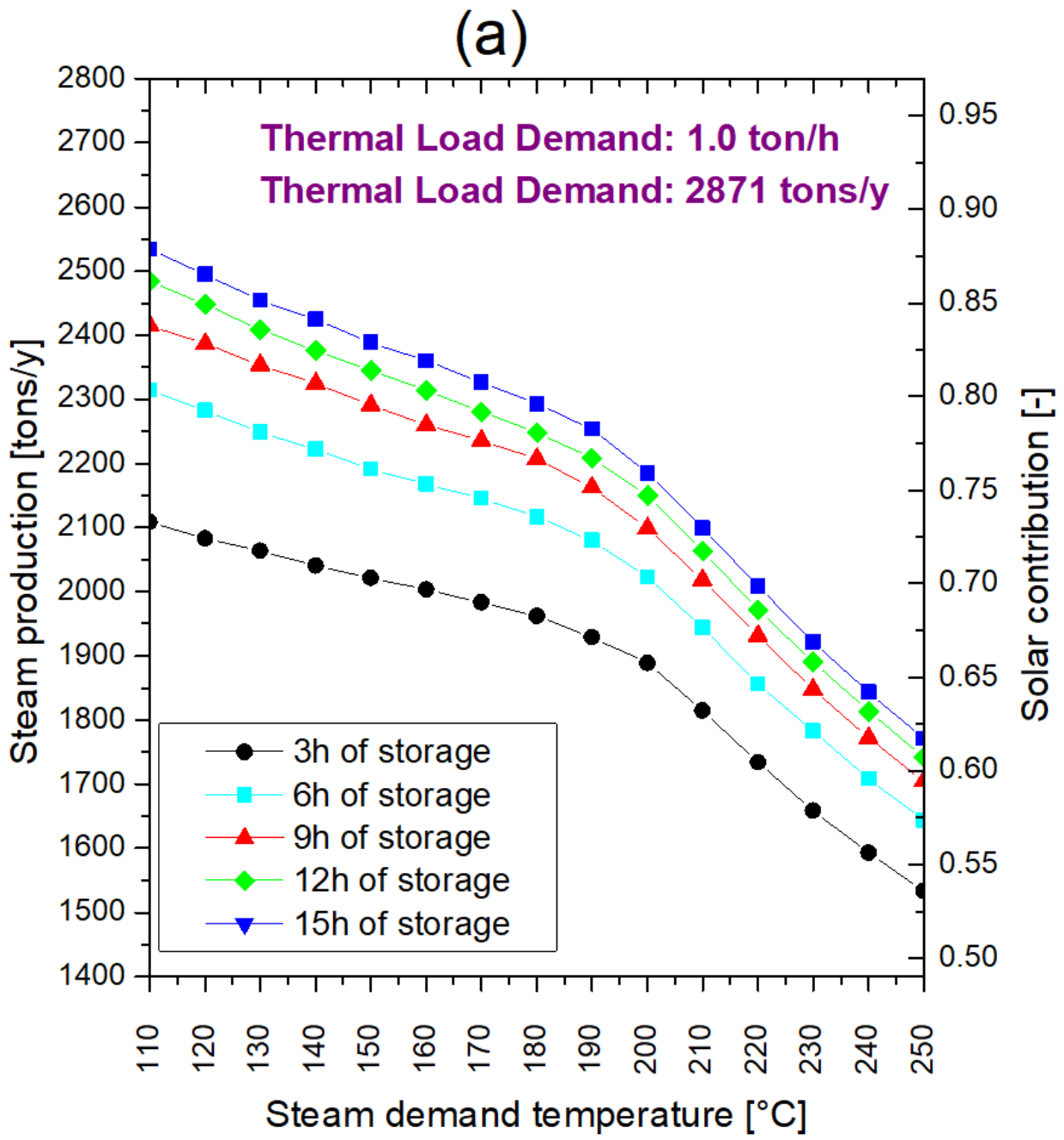

Figure 75a: The steam production, solar contribution for storage duration of 3h, 6h, 9h, 12h and 15h and steam demand temperature of 110 °C to 250 °C with step of 10 °C, for thermal loads demand of 1 ton/h.

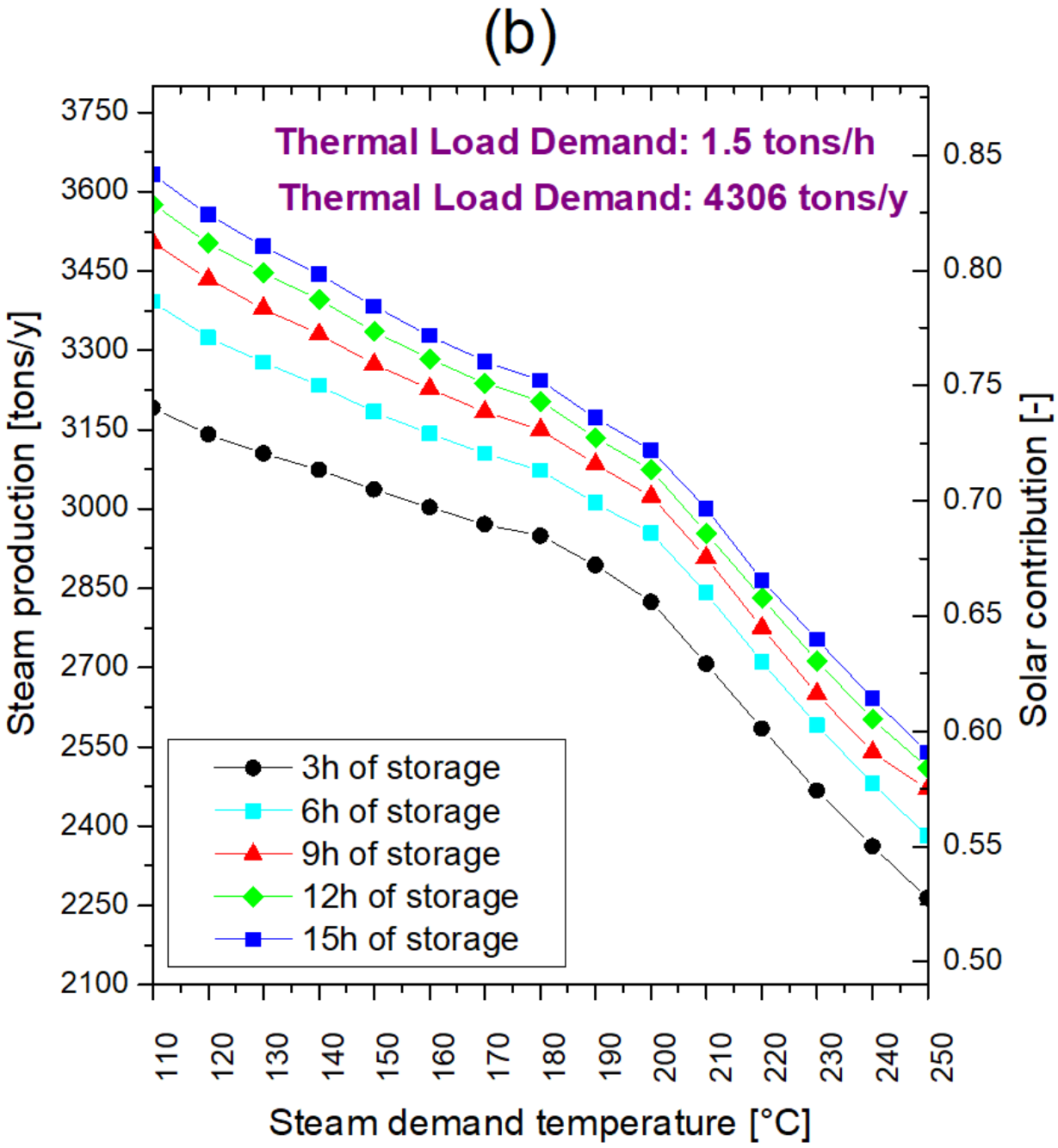

Figure 75b: The steam production, solar contribution for storage duration of 3h, 6h, 9h, 12h and 15h and steam demand temperature of 110 °C to 250 °C with step of 10 °C, for thermal loads demand of 1.5 tons/h.

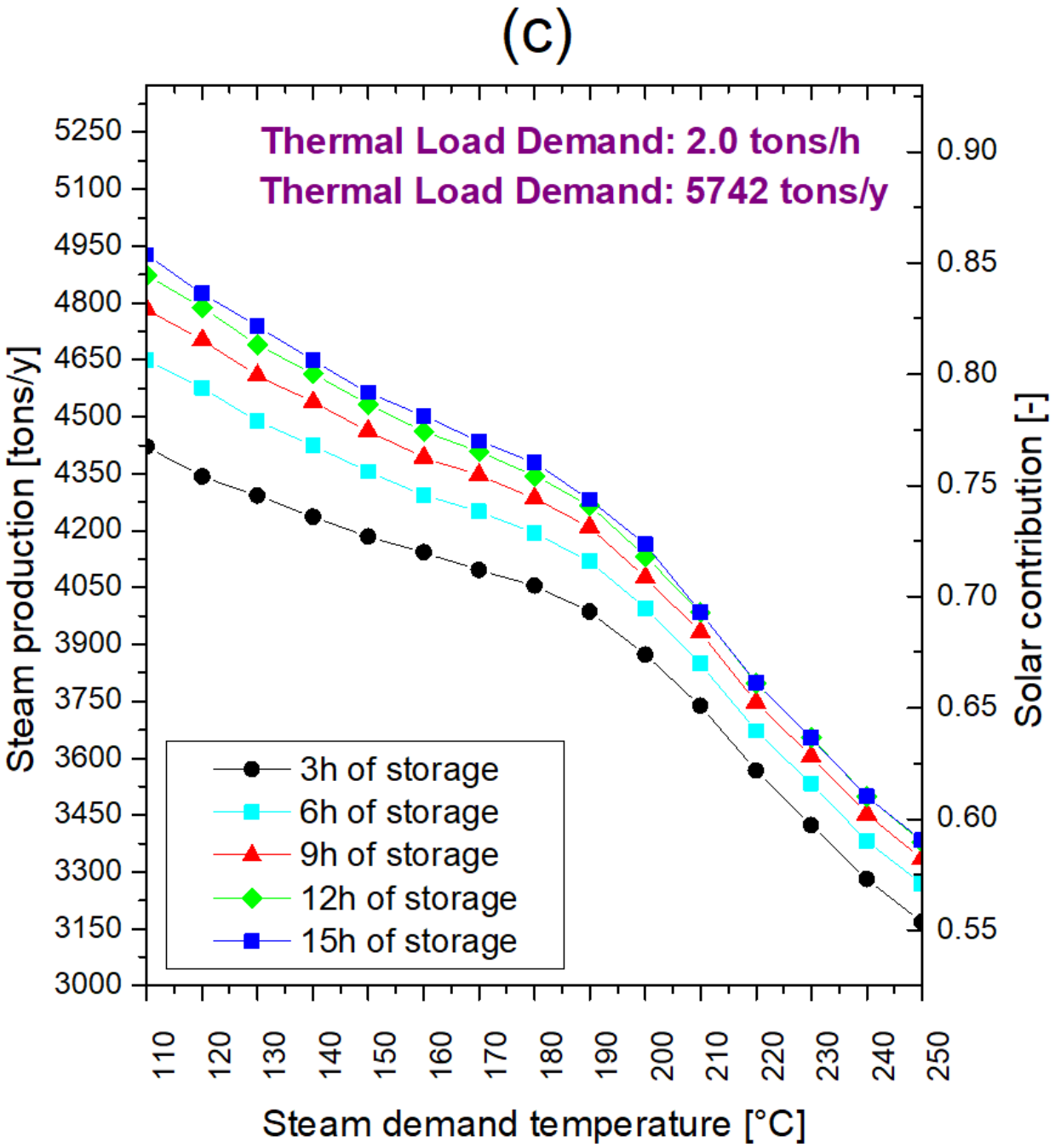

Figure 75c: The steam production, solar contribution for storage duration of 3h, 6h, 9h, 12h and 15h and steam demand temperature of 110 °C to 250 °C with step of 10 °C, for thermal loads demand of 2 tons/h.

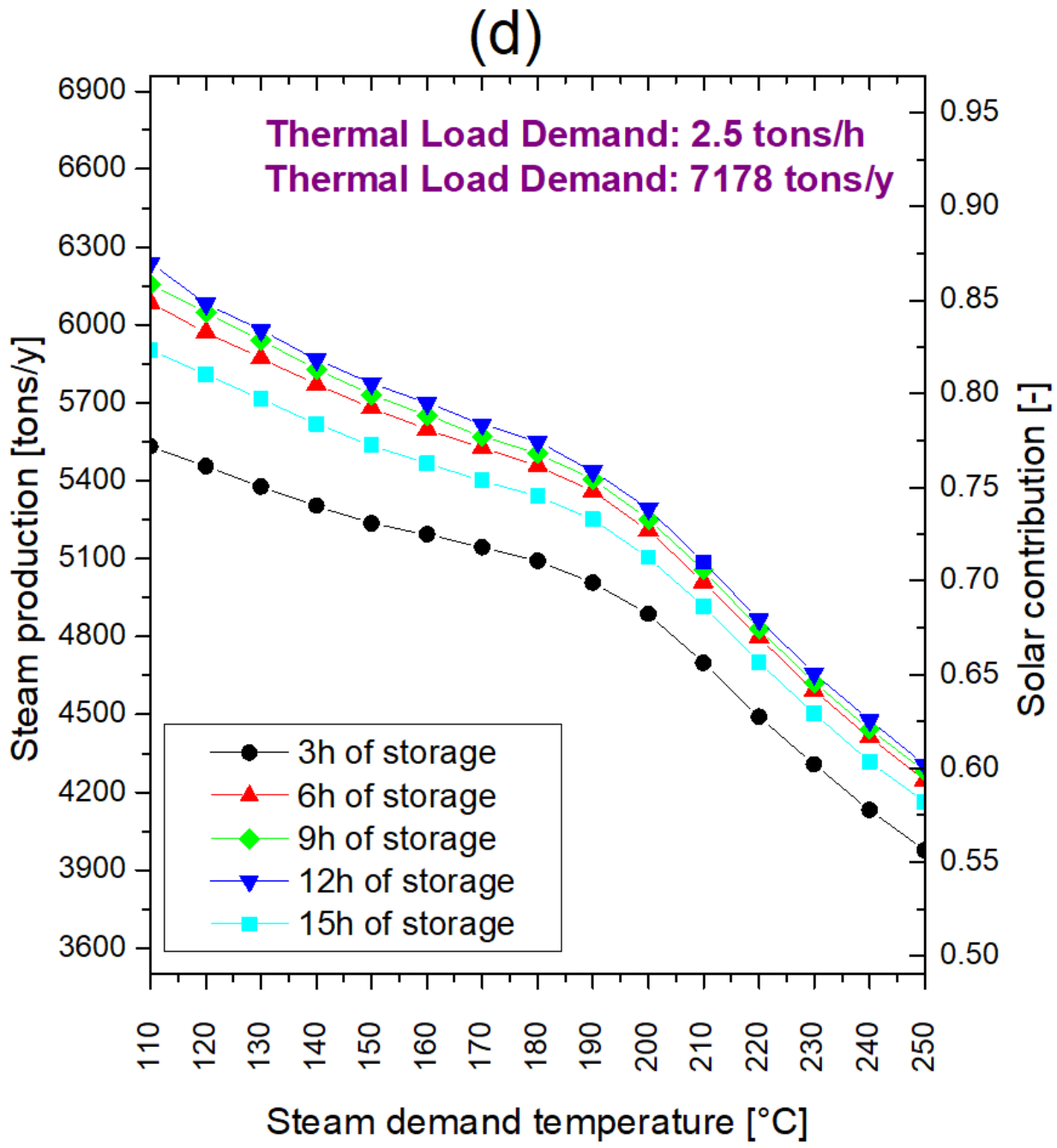

Figure 75d: The steam production, solar contribution for storage duration of 3h, 6h, 9h, 12h and 15h and steam demand temperature of 110 °C to 250 °C with step of 10 °C, for thermal loads demand of 2.5 tons/h.

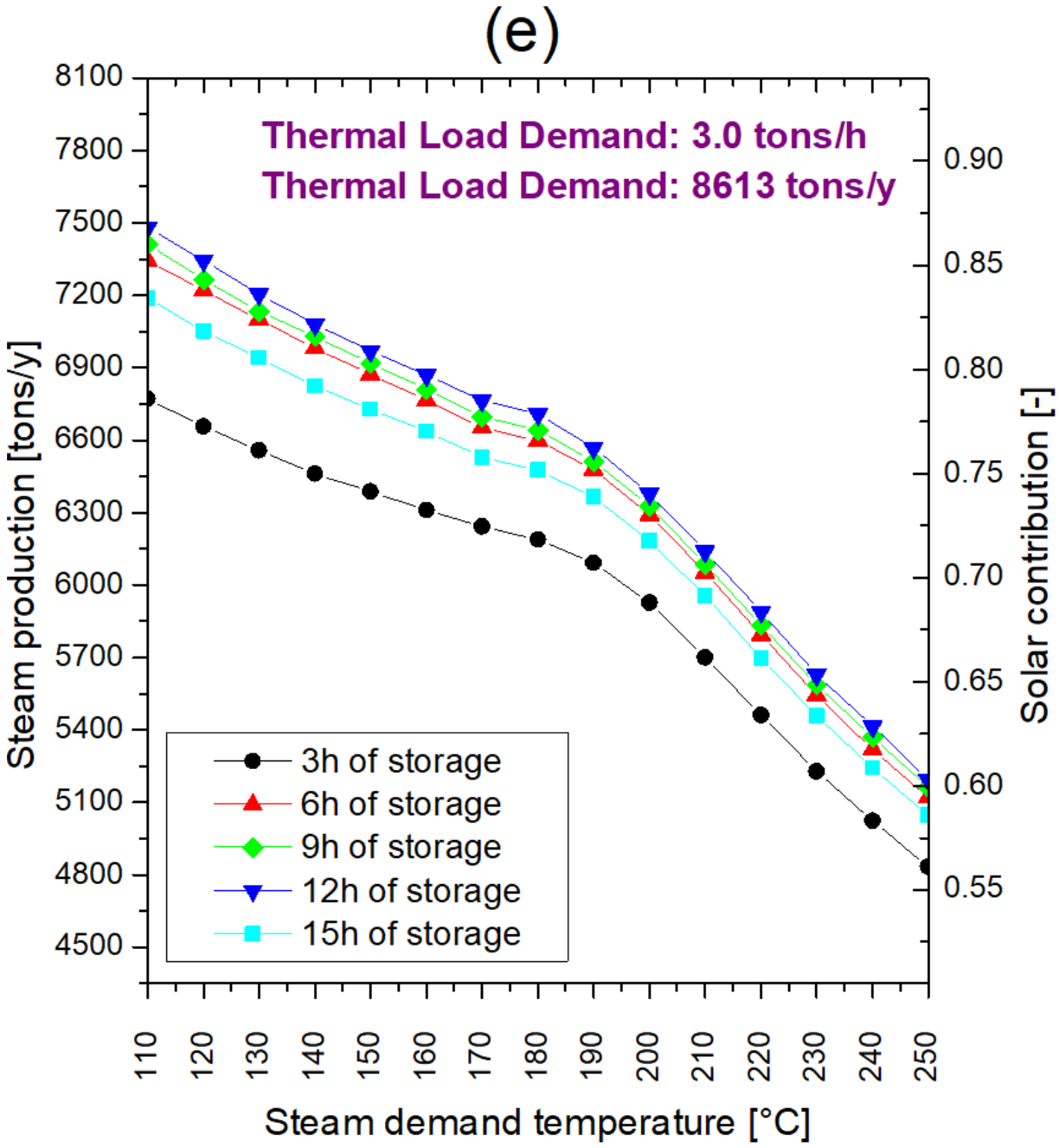

Figure 75e: The steam production, solar contribution for storage duration of 3h, 6h, 9h, 12h and 15h and steam demand temperature of 110 °C to 250 °C with step of 10 °C, for thermal loads demand of 3 tons/h.

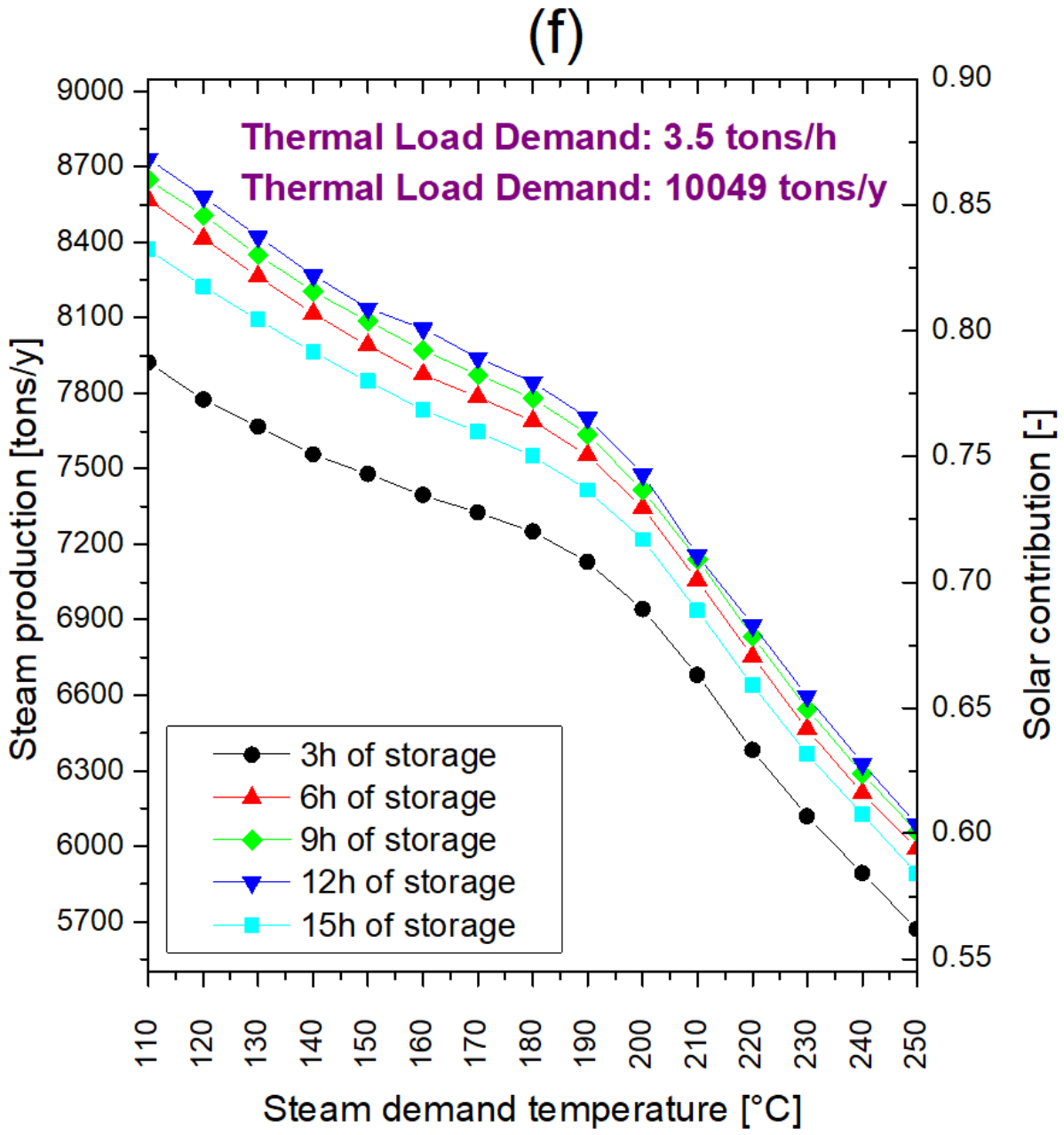

Figure 75f: The steam production, solar contribution for storage duration of 3h, 6h, 9h, 12h and 15h and steam demand temperature of 110 °C to 250 °C with step of 10 °C, for thermal loads demand of 3.5 tons/h.

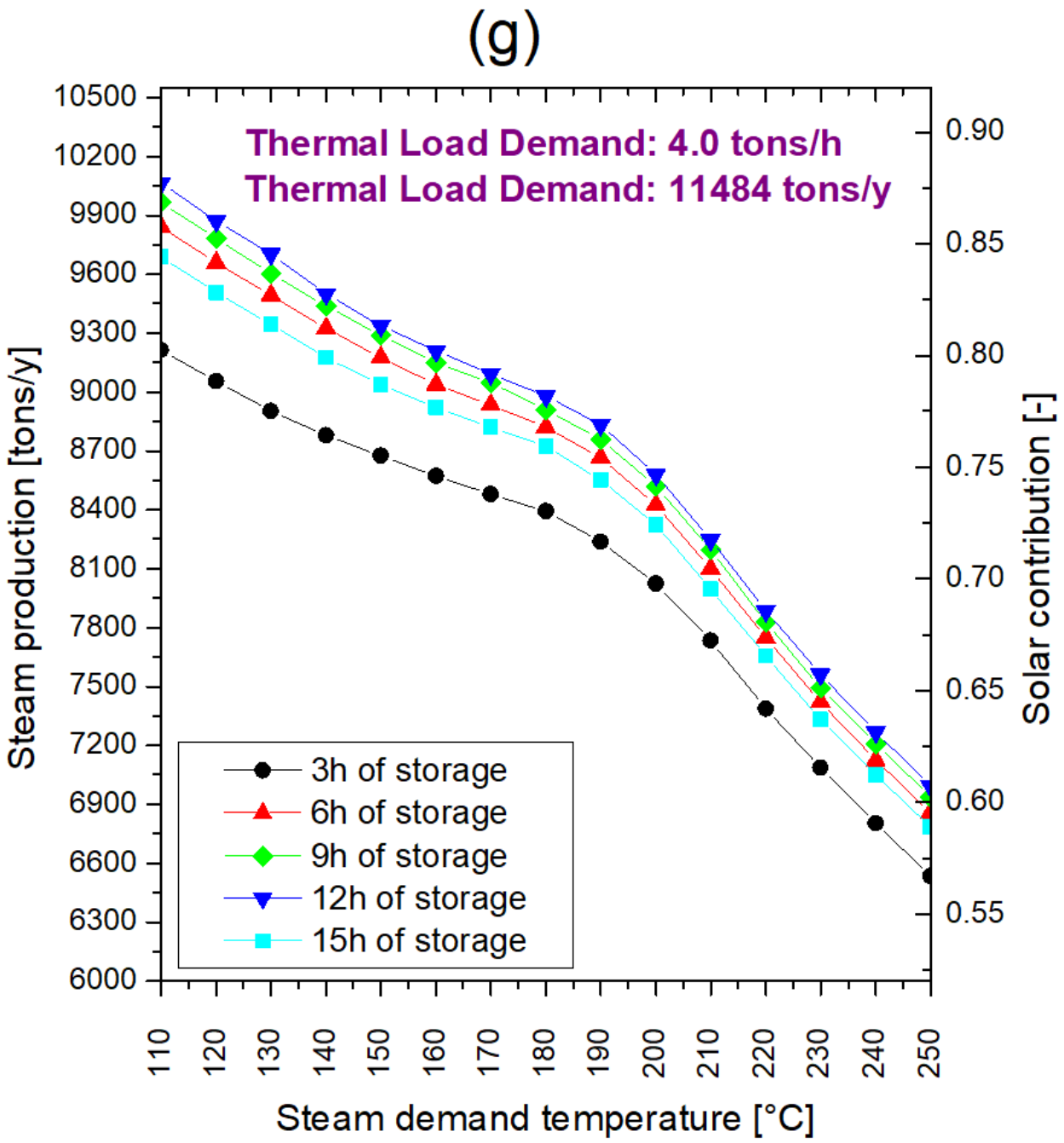

Figure 75g: The steam production, solar contribution for storage duration of 3h, 6h, 9h, 12h and 15h and steam demand temperature of 110 °C to 250 °C with step of 10 °C, for thermal loads demand of 4 tons/h.

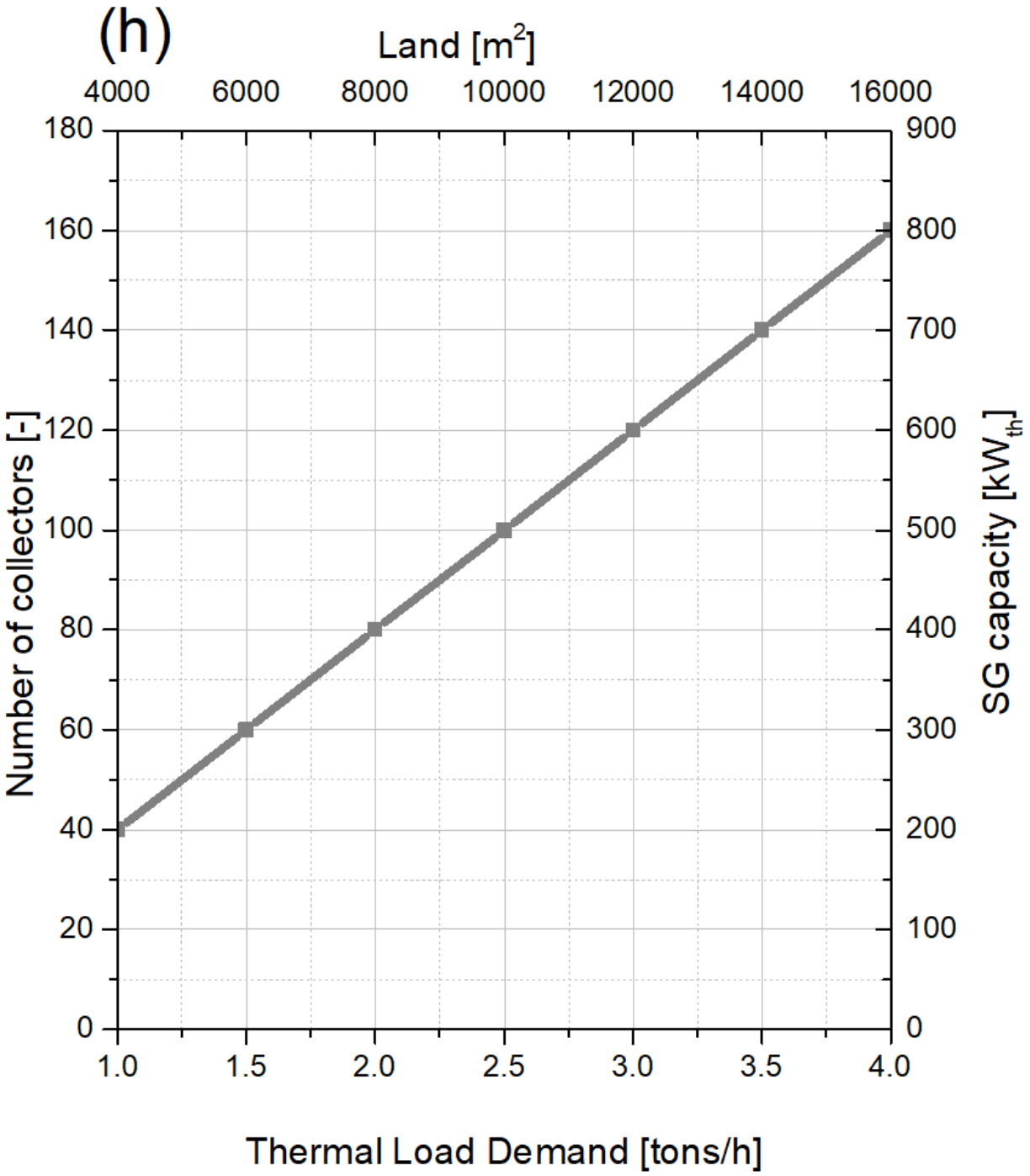

Figure 75h: The sizing of the system regarding area of the collectors, capacity of the SG and land requirements for thermal loads from 1 ton/h to 4 tons/h.

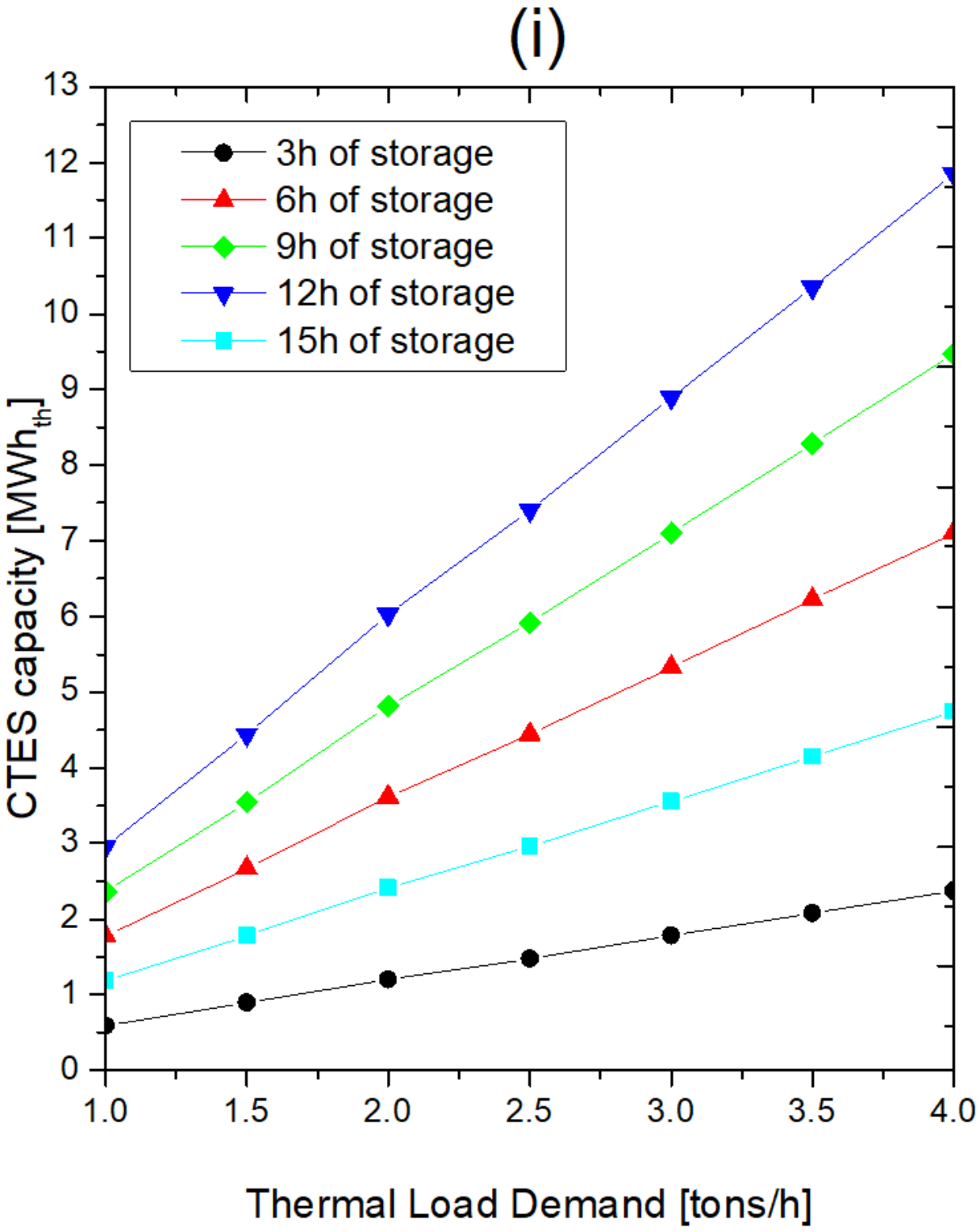

Figure 75i: The CTES capacity required for required storage duration of 3h, 6h, 9h, 12h and 15h, for thermal loads from 1 ton/h to 4 tons/h.

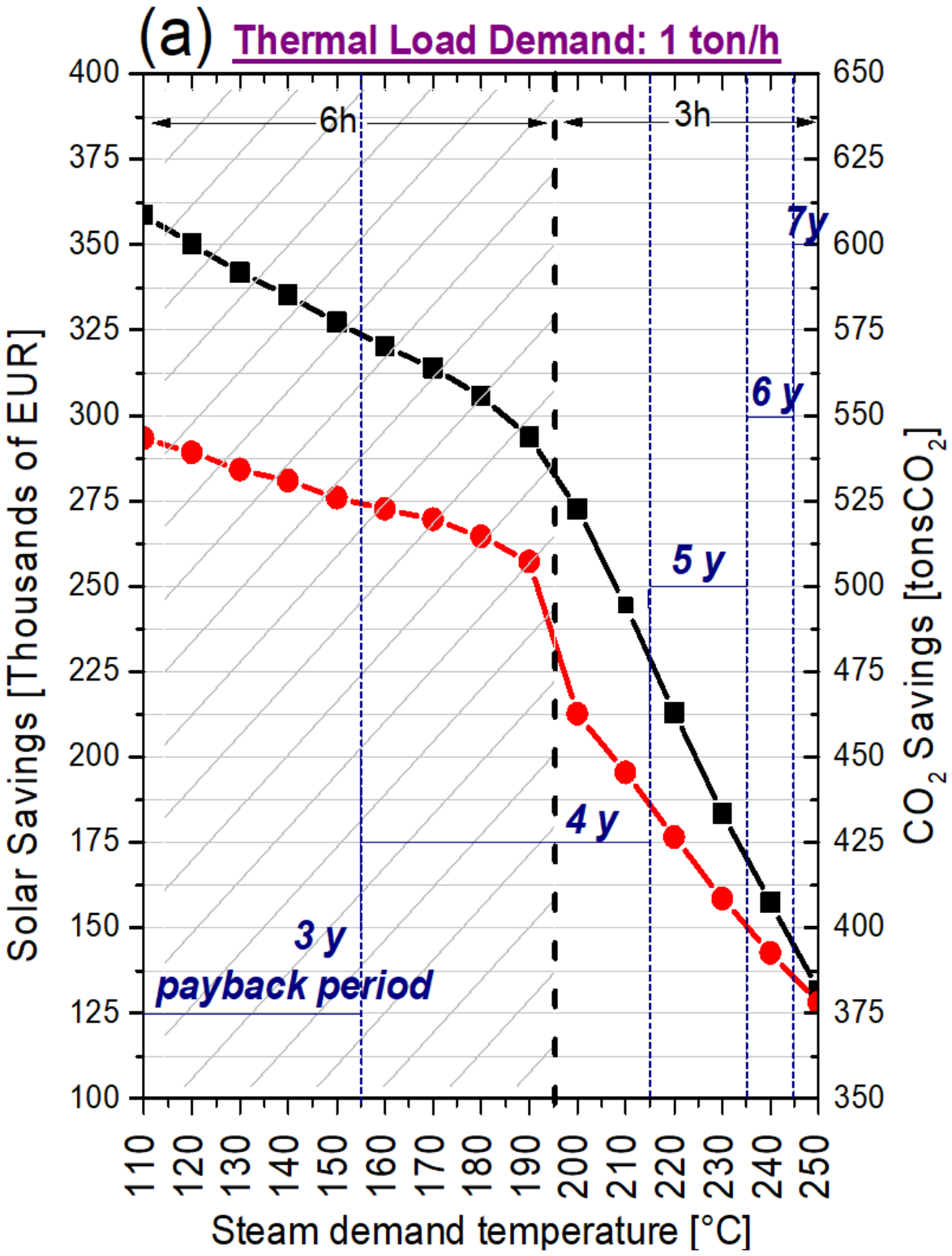

Figure 76a: The solar savings (Thousands of EUR), payback period and CO_2 savings, of the system at the end of its life cycle, for steam demand temperature of 110 °C to 250 °C for thermal load demand of 1 ton/h for the optimum storage capacity based on LCCA.

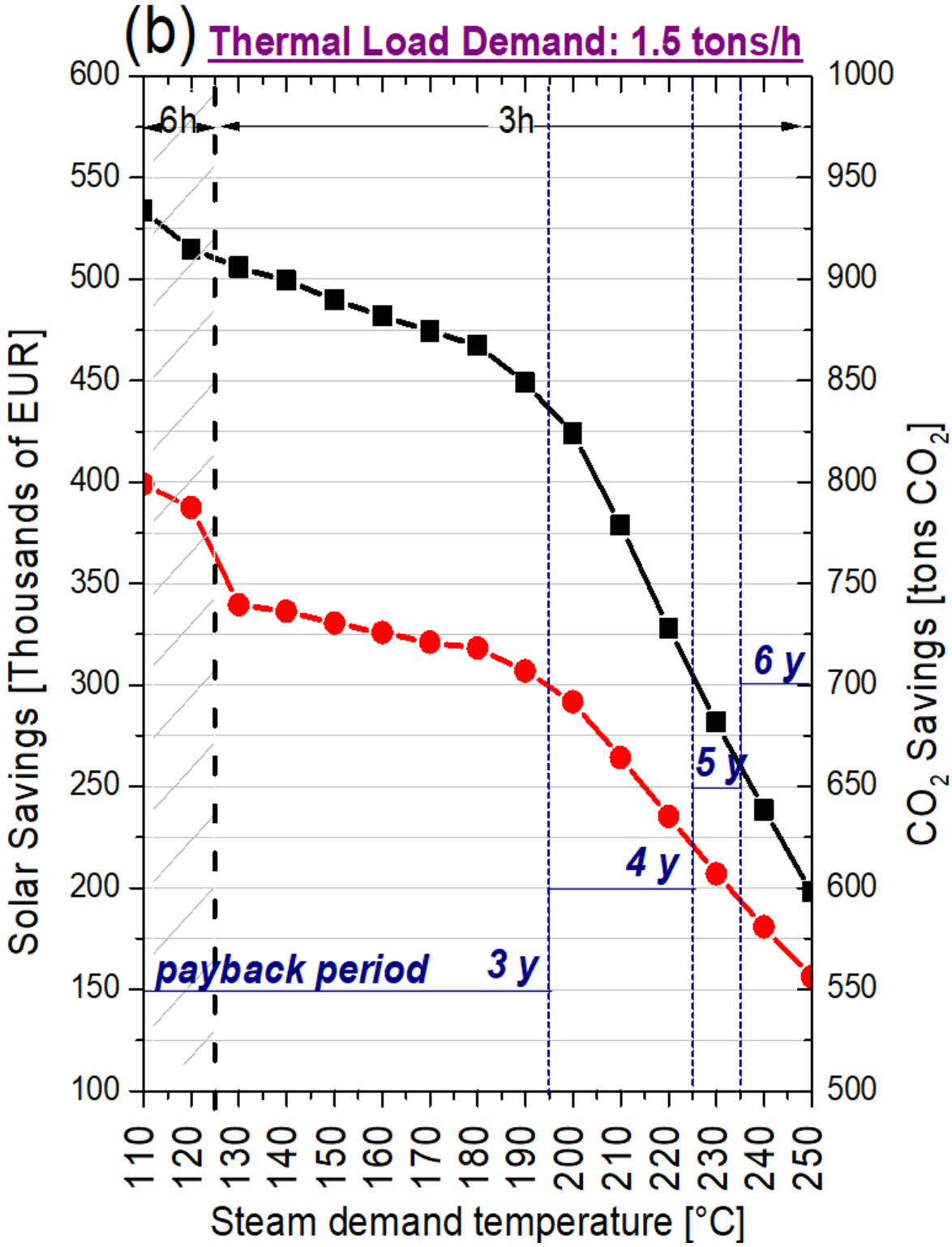

Figure 76b: The solar savings (Thousands of EUR), payback period and CO_2 savings, of the system at the end of its life cycle, for steam demand temperature of 110 °C to 250 °C for thermal load demand of 1.5 tons/h for the optimum storage capacity based on LCCA.

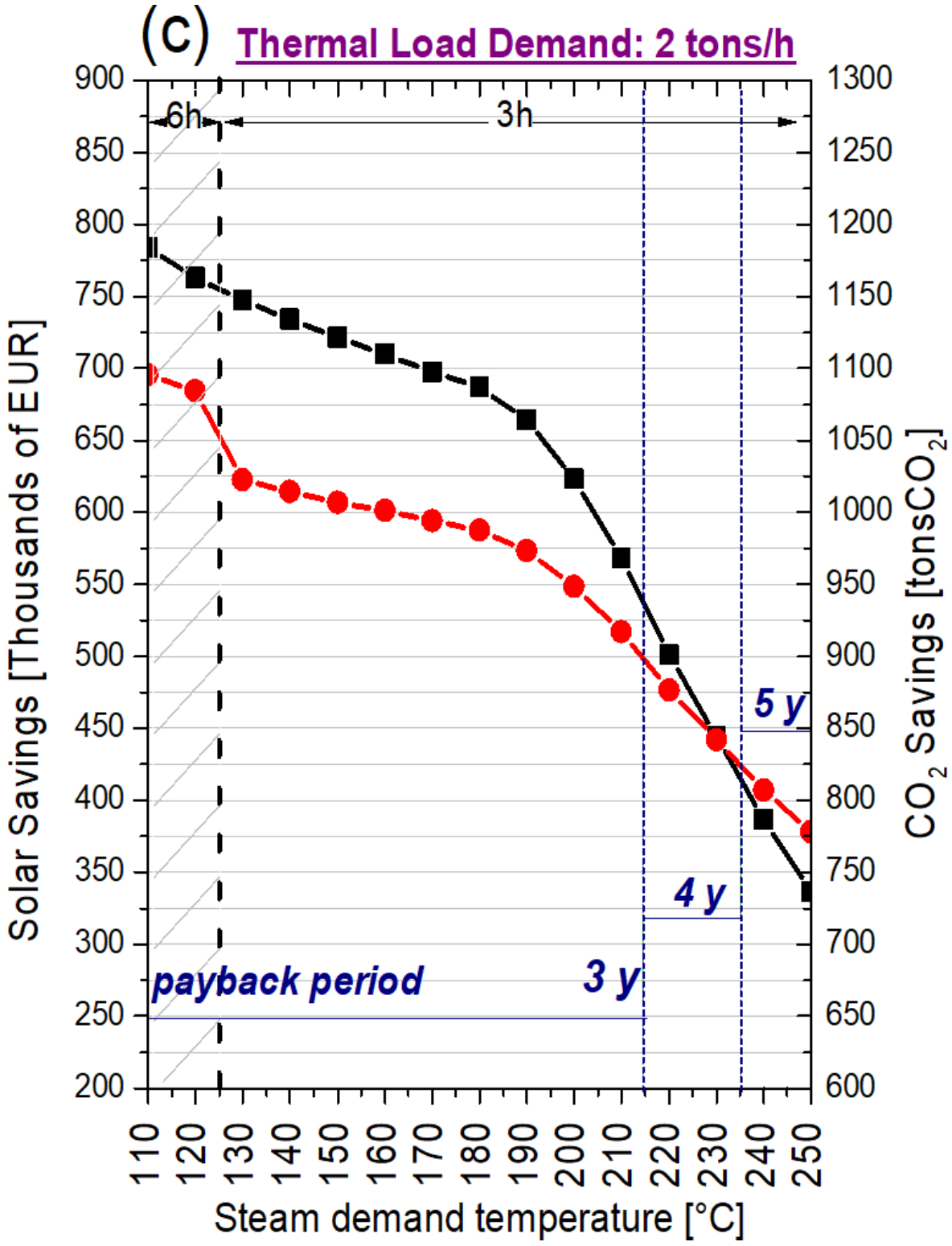

Figure 76c: The solar savings (Thousands of EUR), payback period and CO_2 savings, of the system at the end of its life cycle, for steam demand temperature of 110 °C to 250 °C for thermal load demand of 2 tons/h for the optimum storage capacity based on LCCA.

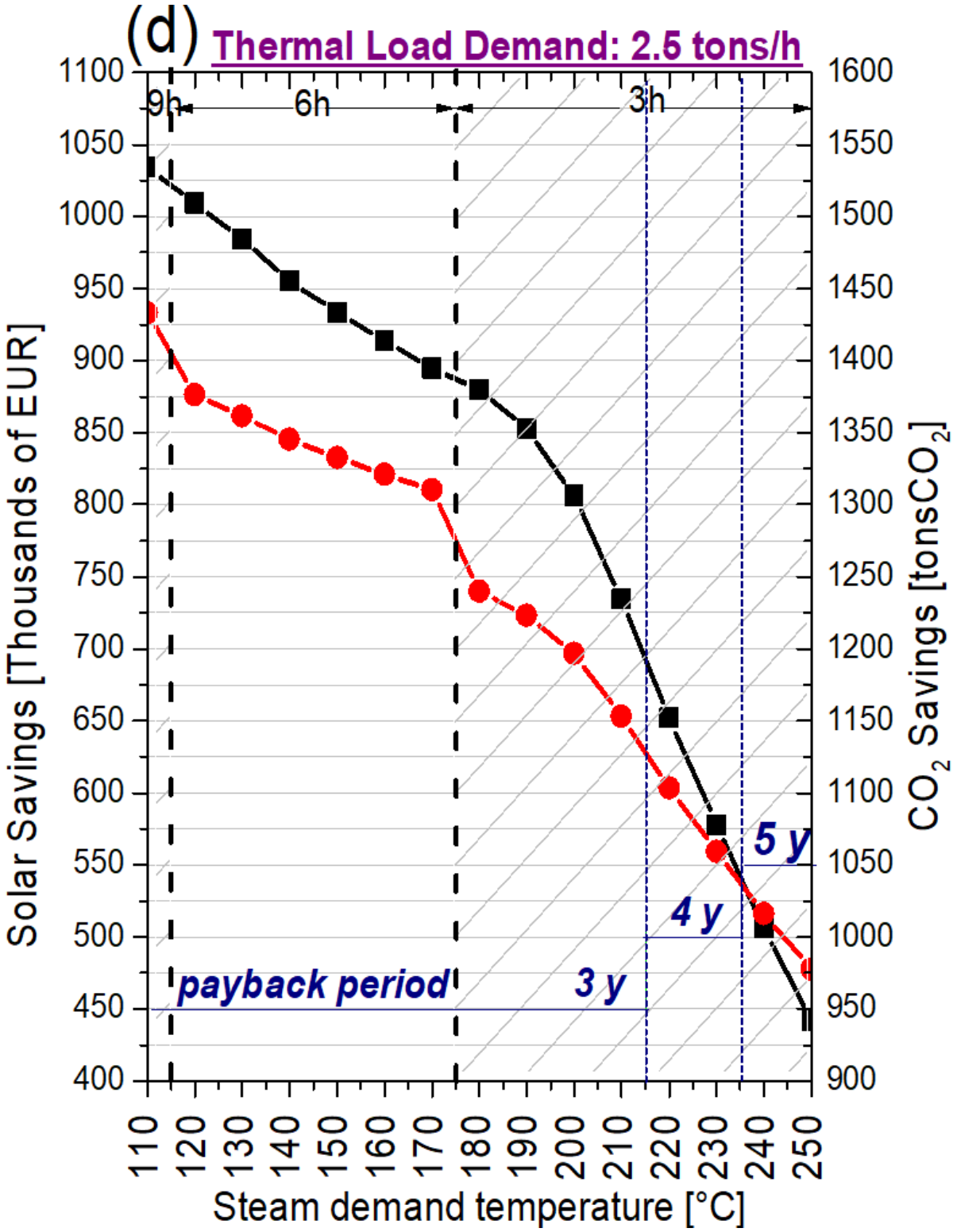

Figure 76d: The solar savings (Thousands of EUR), payback period and CO_2 savings, of the system at the end of its life cycle, for steam demand temperature of 110 °C to 250 °C for thermal load demand of 2.5 tons/h for the optimum storage capacity based on LCCA.

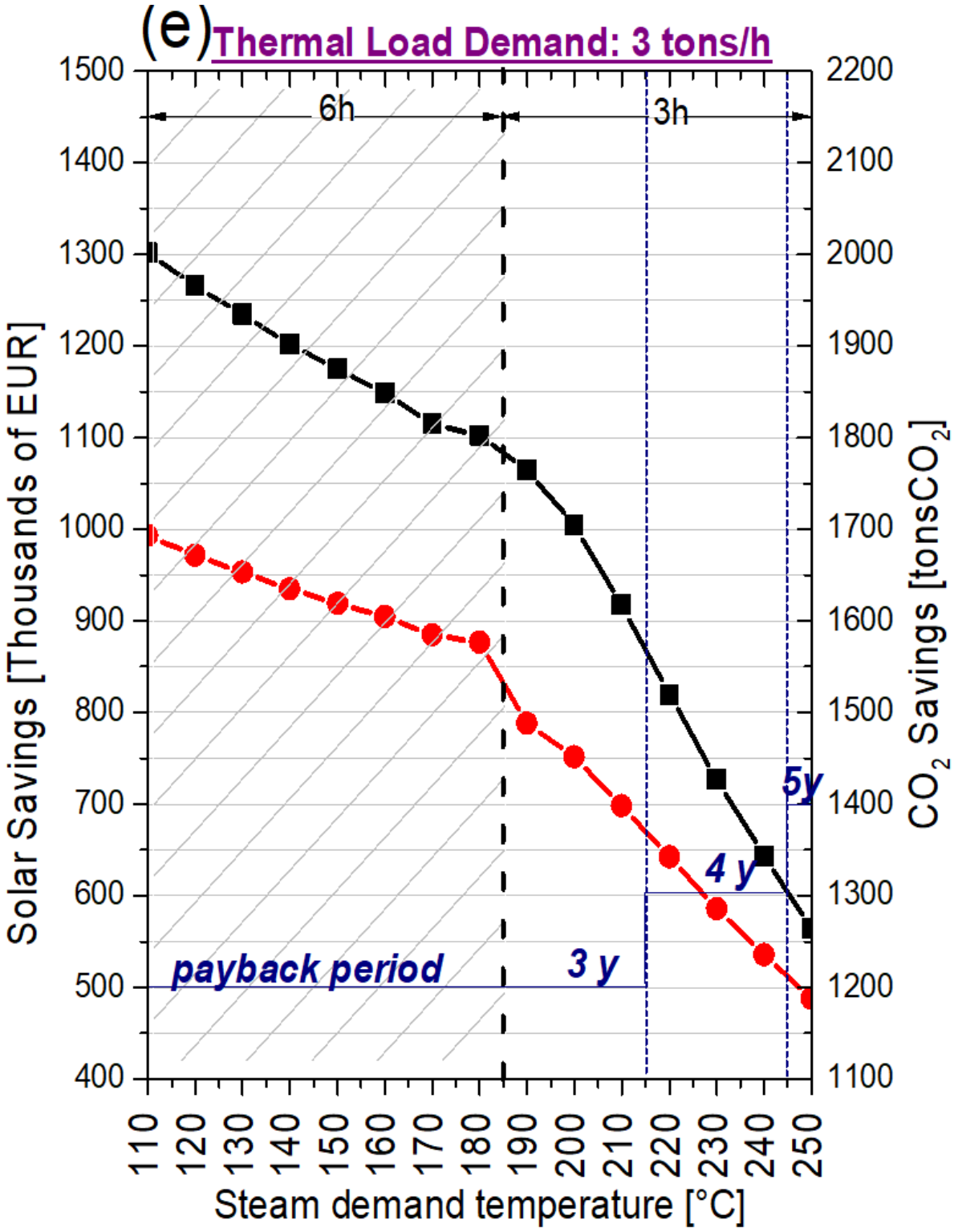

Figure 76e: The solar savings (Thousands of EUR), payback period and CO2 savings, of the system at the end of its life cycle, for steam demand temperature of 110 °C to 250 °C for thermal load demand of 3 tons/h for the optimum storage capacity based on LCCA.

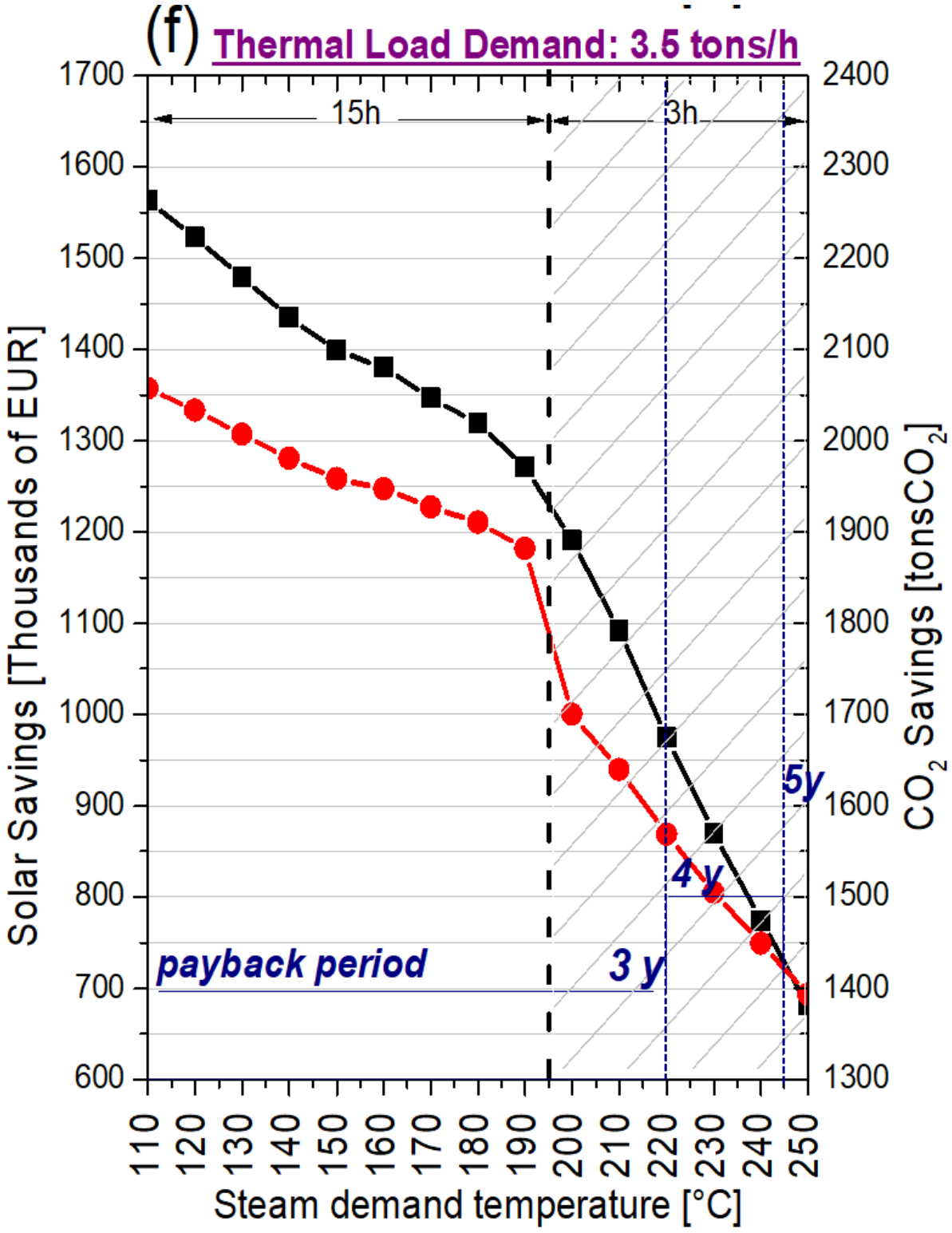

Figure 76f: The solar savings (Thousands of EUR), payback period and CO_2 savings, of the system at the end of its life cycle, for steam demand temperature of 110 °C to 250 °C for thermal load demand of 3.5 tons/h for the optimum storage capacity based on LCCA.

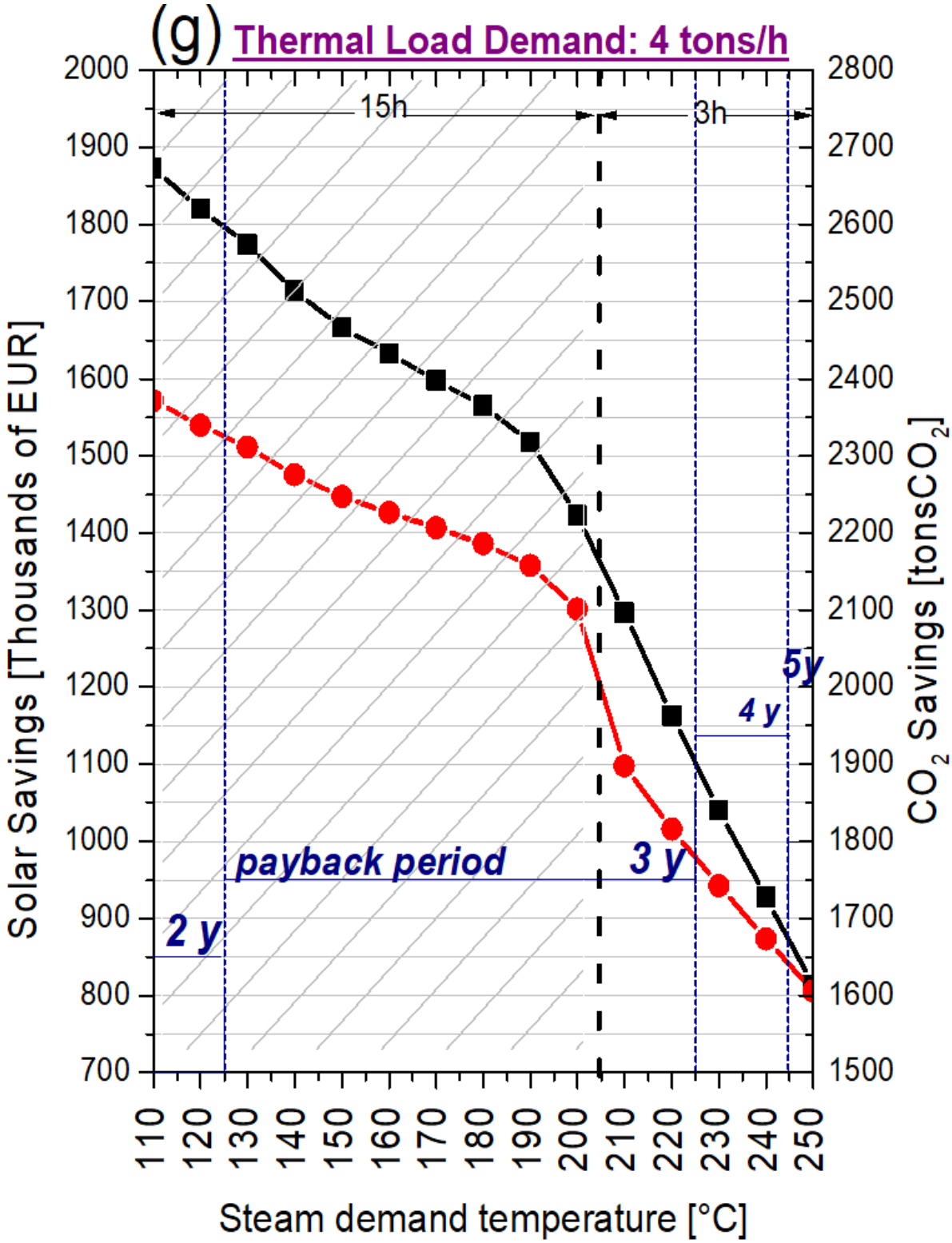

Figure 76g: The solar savings (Thousands of EUR), payback period and CO_2 savings, of the system at the end of its life cycle, for steam demand temperature of 110 °C to 250 °C for thermal load demand of 4 tons/h for the optimum storage capacity based on LCCA.